Theory and Simulation of Interfacial Effects and Phase Behavior of Nonionic Surfactants

Dissertation

zur Erlangung des Grades eines
Doktors der Naturwissenschaften
des Fachbereichs Chemie
der Universität Essen

von

Simeon Stoyanov

aus Sofia, Bulgaria

Essen 2002

Von Fachbereich Chemie (8) der Universität-GH Essen als Dissertation angenommen.

Referent:	Prof. Dr. H. Rehage
Korreferent:	Prof. Dr. F. Bandermann

Tag der Einreichung: 01.09.2002
Tag der Prüfung: 30.09.2002

Die vorliegende Dissertation wurde im Institut für Umweltanalytik und Angewandte Geochemie des Fascbereichs Chemie (8) der Universität-GH Essen unter der Leitung von Prof. Dr. H. Rehage angefertigt.

Many thanks to my scientific advisors and my colleagues from University of Essen and from Henkel KGaA for all their support.

To my daughter, Raya.

" *... a scientist must also be absolutely like a child. If he sees a thing, he must say that he sees it, whether it was what he thought he was going to see or not. See first, think later, then test. But always see first. Otherwise you will only see what you were expecting. Most scientist forget that. I'll show you something to demonstrate that latter ...*"

Wonko the Sane in "***So long and thanks for all the fish"***

Douglas Adams

CONTENTS

I. Introduction and motivation of the thesis

I.1. Surfactants

Surfactants are one of the main components in various colloidal systems[1-7]. They consist of two parts – hydrophilic and hydrophobic and their properties are result of the "fight" between them. The hydrophobic part is usually a long $(CH_2)_k$ chain, which is called tail, while the hydrophilic part usually is much shorter and is called head of surfactant. The hydrophobic chain could be also branched or contain different organic segments.

Depending their electric properties[8-9], surfactants could be nonionic (whole molecule is uncharged) and ionic (part of molecule is charged or it has distributed charges along it – which is called poly-electrolyte) or zwitter-ionic, where surfactant molecule is uncharged but has high dipolar moment. The charge of the surfactant molecule could change with the condition change like pH and ionic strength of solution, temperature, aggregation of surfactant molecule with other substances etc. Depending on the conditions one and the same molecule could be uncharged or charged or even can invert its charge[8].

The main subject of this study are nonionic surfactants, but later on, in the last part of the thesis we will show that some of the results, which are obtained for nonionics could also be applied for ionic surfactants as well.

I.2. Surfactants phase behavior

When the surfactant molecule is placed in water solution the hydrophilic part likes to be dissolved in water, while the hydrophobic part likes to minimize its contact with solvent. As a result, strong association of surfactant molecules can occur: several molecules can aggregate to form a micelle where oily (hydrophilic) part of surfactant is in oil core, surrounded by hydrophilic shell[1]. As a result the hydrophilic part is contacting with water and prevents the unfavorable water contact with hydrophobic part of the molecule. At low surfactant concentrations micelles have nearly spherical form. When the bulk surfactant concentration increases the micelles elongate and worm like structures (micelles) are formed, which in some cases could be very long – up to several hundreds of nanometers[5,7]. These worm like micelles could form rather complex networks, which are influencing the bulk properties (like

viscosity and diffusion transport) of solution. Depending on conditions these networks could be rather ordered and form a nice hexagonal phases. Further increase of concentration leads to formation of lamellas of surfactant layers (see Figure 1.1). At very high concentration of surfactant the inverse micelle phase could form (where water drops are surrounded by surfactant melt). The surfactant aggregation depends not from the concentration only, but also from the change of external conditions, like pressure and temperature, which are changing the interaction energies of different parts of surfactant molecule with solvent (water).

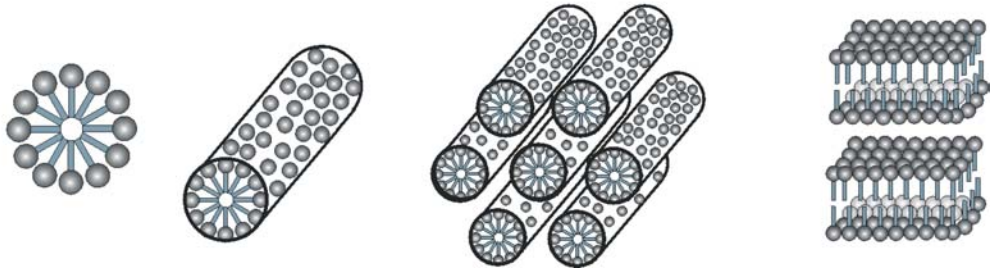

(a) (b) (c) (d)

Figure 1.1a. Sketch of different stages of surfactant association (phase behavior): (a) spherical micelles; (b) cylindrical worm like micelles; (c) hexagonal phase; (d) lamellar phase.

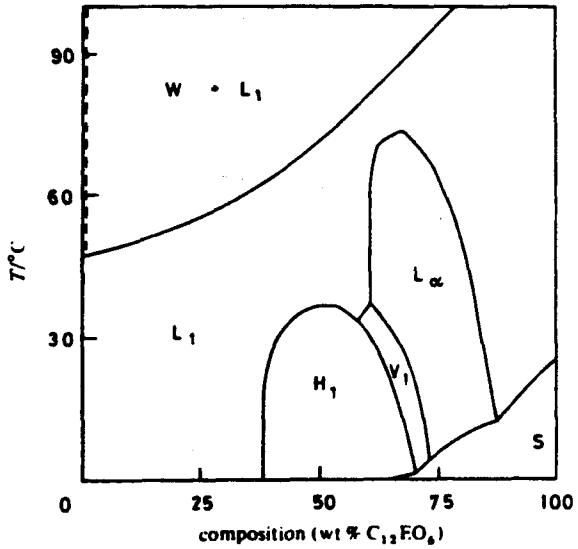

Figure 1.1b. Phase diagram of $C_{12}E_6$ taken from reference 5. L_1 represents homogeneous micellar solution region, L_α is lamellar phase, H_1 is hexagonal phase, V_1 is cubic phase and S is surfactant solid phase.

As an example of surfactant phase behavior in figure 1.1b we show a phase diagram of ethoxylated surfactant $C_{12}E_6$.

An additional way to control the phase behavior of surfactant system is to add other components into it: like other types of surfactants, polymers, salts or additional solvent (oil for example). The surfactant aggregation phenomena are known as phase behavior of the surfactant systems. If we have only water and surfactant – it is called binary phase behavior, while if we have water, oil and surfactant, it is called ternary phase behavior etc. The different phases formed by surfactant aggregates and solvent could have very different transport properties like bulk viscosity and diffusion transport of other substance trough them. The process of surfactant self-assembly usually is reversible and represents thermodynamic equilibrium, but additional structural changes could occur when system is a subject of external dynamic process like shear. The latter is very important for many applications such as washing and cleaning (detergency).

The ability to control surfactant phase behavior gives also possibility of very fine system property control. That is the reason why the phase behavior is a subject of intensive investigation of many experimental and theoretical studies. Understanding the phase behavior is very important for many industrial applications, where surfactants are used[1,2,7]. The surfactants play also an important role in many biological processes[1].

I.3. Surfactant interfacial properties

The name of surfactant is short for surface-active component and like the name suggests, surfactant molecules have very high surface affinity. Even at a very low bulk concentrations, the surfactants could strongly influence the interfacial properties of the system[2-3,11-14,]. When an interface is formed between two phases (like air and water or oil and water) one of the most energetically favorable state of the surfactant molecule is to be at the interface. In this case hydrophilic part is in water phase, while the hydrophilic part is in the other part of the interface (air or oil). As a result both parts of surfactant molecule are in contact with the phase, which they like (has lower energy) most.

When there is a weak interaction between the surfactant molecules at the interface one could consider them like two-dimensional gas and the same like in the case of three-dimensional

gas, when we increase the concentration (at constant temperature and volume) the pressure increases. Thus the increase of surfactant surface concentration (adsorption) increases the two-dimensional surface pressure. From the other side the definition surface tension is the energy needed to create a new interface per unit area and its dimension is force per unit length (the same is the dimension of two-dimensional pressure). But when the two-dimensional pressure increases the surface tension decreases, because higher pressure means that lower force per unit length is required creating the new interface, due to the fact that surface pressure acts against the surface tension. Thus an increase of surfactant surface concentration, leads to decrease of surface tension. This decrease could be very high and even at very low bulk concentrations – the surface tension could decrease several times (compared to the value of pure interface) and even it could become practically zero (or very low for certain oil/water interfaces).

It is well known that even a small changes of the surface tension have very impact to the properties of a whole colloidal system[10-14]. Lower surface tension means that we can create new interfaces much more easily. For instance one can create much easy (with less energy) foams – for the case of air/water systems or emulsions (for case of oil/water interface). But the effect of the surfactant is not limited only to the decrease of surface tension. The surfactant changes also other surface properties responsible for the stability of colloidal system – like surface charges and interfacial rheology[1-4,6,8-9]. For instance when we form a foam, which consists of highly packed air bubbles in water, there are a lot of foam films formed between the contacting bubbles[13]. Similar is the situation with concentrated emulsions, where the emulsion (oil/water/oil films is formed between every two adjacent oil or water drops. The stability of these films is the key factor, which determines the stability of the foams (emulsions). If the films are unstable, they could break and two bubbles (oil drops) could coalesce. If films break often then the colloid system is unstable: foam will disappear or emulsion will segregate into two fluids (see figure 1.2 form more details). The stability of these thin liquid films (which could be very thin in some cases – at about 10-20nm), is determined roughly by two factors: thermodynamic[1,6] and hydrodynamic[12-14], both of which are influenced by the presence of surfactant.

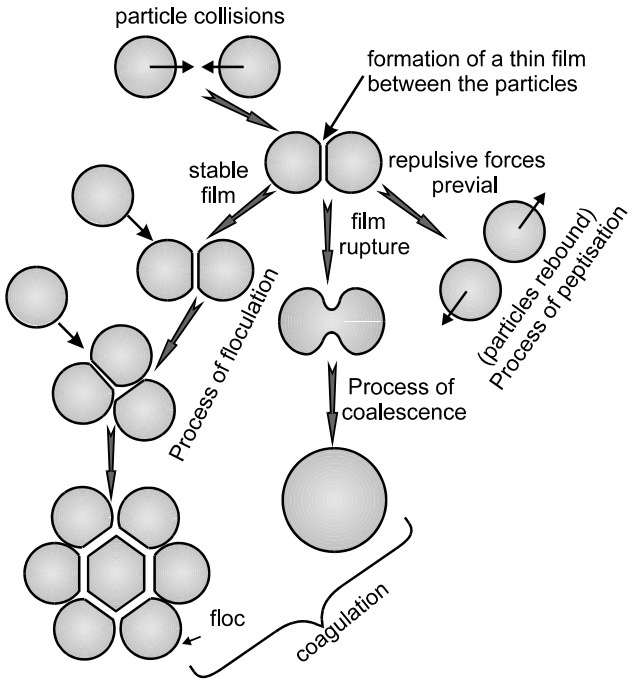

Figure 1.2. Behavior scenarios of colliding emulsion droplets. In all of the cases outcome is highly influenced by the presence of surfactant.

The hydrodynamic factors govern the drainage and stability of films during the process starting from their formation until they reach the equilibrium thickness. If during the time of the drainage process a hydrodynamic instability occurs one could expect that films will become unstable and rupture before they reach equilibrium conditions[†]. Due to the fact that films are very thin, the interfacial rheological properties[11-15] play an important role in this process. The main effect comes from the surface mobility. Lower surface mobility means slower film drainage and the opposite. If the interface has some surface velocity, then the adsorbed surfactant molecules should follow the surface motion, which will lead to redistribution of the surfactant molecules along the interface (convection) (see figure 1.3). As a result the concentration of surfactant will decrease in some places and increase in others. But due to the surface tension dependence from the local surfactant concentration, this redistribution will lead to a variation of surface tension along the interface. But as we have

[†] This is the same like a situation with a dieing patient in an ambulance: if the ambulance manage to reach the hospital the patient will probably survive, but if it breaks before reaching the hospital, the patient will probably die, though some could survive.

already discussed, the surface tension is connected with two-dimensional pressure. The same like in the three-dimensional case, where any variation of bulk pressure leads to an appearance of force acting on the fluid – the variations (gradients) of the surface pressure lead to surface force acting on the interface. The latter force is trying to oppose the motion of the interface and to restore the surfactant equilibrium distribution. The appearance of the force due to the gradients of the surface tension is known as Marangonni effect[12-14] (see Figure I.3).

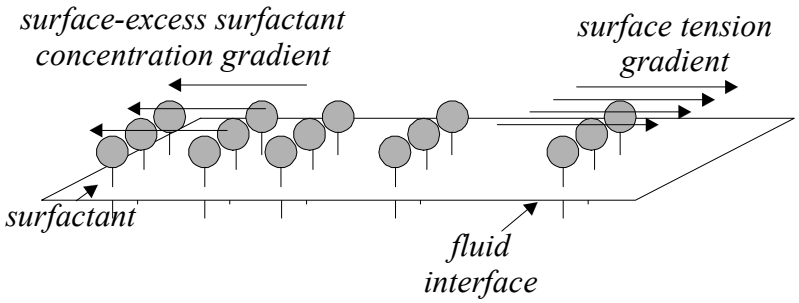

Figure 1.3. Sketch of the Marangonni effect.

The interplay between surface convection and surface and bulk diffusion determines, which effect will prevail and what is the actual value of the surface velocity. The bulk diffusion decreases with the decrease of the film thickens, while the surface diffusion is not strong enough to compensate any even very low surface convection, thus as a result the surface velocity (mobility) of the interface is strongly decreased (and could become practically zero) even at very low surfactant concentrations[12-13]. Thus surfactants could strongly influence the thin film drainage behavior and stability. The decreased surface mobility motivates so-called Bancroft's rule[13], which determines what type of emulsion (oil in water or water in oil) we get if we shake water and oil. Based on the theory of hydrodynamic drainage and stability of thin films in the presence of surfactant the Bancroft rule says that the emulsion type is determined by the surfactant solubility (in both phases) – the more stable will be the emulsion where surfactant is predominantly soluble in the continuous phase.

One of the most famous examples for the effect of surfactant on the surface mobility is the experiment for determination of sedimentation velocity of small oil drops in water. Rybczynski[17] and Hadamar[18] have obtained the generalization of the Stokes formula for the hydrodynamic drag force acting on a small spherical drop, when it moves in second fluid.

When the viscosity of the drop goes to infinity the formula restores well known Stokes result for the drag force of a solid sphere. When the viscosity of the drop is finite where the drag force depends on viscosity of both phases. When the experiments were performed in order to check the Rybczynski–Hadamar[12] formula, it was found that in many experimental cases the drops are moving like a solid spheres according Stokes[14] formula, though their bulk viscosity was quite small. The explanation was found latter by realization that presence of small amount impurities in water system could act like surfactants, which are making the droplet interface practically immobile. Thus from the hydrodynamic point of view the interior of the drop is isolated from the flow of the surrounding fluid and drop is moving like a solid sphere.

Another influence of the surfactant to the stability of thin films comes trough the modification of the forces acting between the interfaces. If we have an ionic surfactant, any change of surfactant surface concentration leads to a change in the total surface charge, which determines the electrostatic interaction between interfaces. For the case of symmetric films the electrostatic interactions lead to repulsion between the interfaces, which could oppose the van der Waals attraction between the interfaces (DLVO theory[1,6]). Thus the ability of surfactants to modify the surface charge of the interfaces is giving us an ability to control the stability of the films trough the control of the forces acting between the interfaces.

The main physico-chemical properties, which determine the surfactant influence, are the values of surface tension and the amount of the surfactant adsorbed at the interface (adsorption)[15]. So the determination of their values is very important for the understanding and predicting the properties of thin films, foams and emulsions. The results obtained in the chapter VI of the thesis are actually aimed to give a better practical determination of the surface tension and adsorption of the surfactant systems.

An additional influence of surfactants to the surface forces comes from so called structural forces[1]. At higher surfactant concentrations we have micelles formation in the bulk of the film. When the film thickness becomes of order of several micelle diameters they start to feel the presence of the interface and start to form an ordered structures. Depending on the film thickness, the force needed to order/disorder those structures could be either attractive or repulsive – and oscillate with an increasing magnitude when film thickness decreases. The presence of structural forces gives rise to a stratification effects in the thin films – were stepwise drainage (with constant step height, roughly corresponding to one micelle diameter)

is observed. Nearly the same effects occur at higher concentrations where other surfactant phases are present.

When thin film thickness becomes comparable with the length of the corresponding part of the surfactant (which is dissolved into the film), two surfactant layers start to interact and give rise to so called steric (overlapping) forces[1], which are also influencing the thin film stability. The latter effect is highly pronounced for surfactant with very long chains like di-block polymers.

Thus the presence of the surfactants is very important for the stability of films formed between various colloidal objects and the surfactants are one of the main tools giving us the ability to tailor the stability of the system as a whole. One of the most important properties which one needs to consider in order to estimate the effect of surfactant are values of the surface tension and surfactant adsorption[15].

I.4. Static and dynamic properties – "effective" concentration concept

Though throughout the thesis we will be interested mainly on equilibrium properties of surfactants (all the theories and most of the simulations are targeted to study the equilibrium behavior of the system), were we would like to point that in some cases one could also use the equilibrium values for the characterization of the system behavior even in high nondelirium regime.

In the previous section we have limited our considerations only on the equilibrium properties of the surfactant systems – like equilibrium values of the adsorption surface tension as a factors determining surfactant influence on the system. The reason why we are interested in the equilibrium properties is very simple: the equilibrium theories are much more simple and equilibrium experiments are much more easy to carry! We have discussed that surface tension and adsorption are important even when we have some dynamical process into the system like film drainage. Of course if we have some dynamical process, the system is not in equilibrium and the values of the interfacial tension and adsorption are different from the respective equilibrium values[11]. In some cases when the specific rate of the dynamical process is much lower than the time needed to equilibrate the interface and provided that system is close to the equilibrium, we can consider that equilibrium values

could give us a very close estimate of the dynamical values of the adsorption and surface tension[12-15]. In this case we say that the process is quasi-equilibrium and any small deviations from the equilibrium could be treated in terms of small (linear) perturbations of the equilibrium values. But in many other cases the rate of the process is comparable (or even faster) to the equilibration rate of the interface. In this case, the mechanical mapping of the equilibrium to the dynamic properties of the system could be very misleading. For instance during the initial stages of foam (emulsion) formation we have highly non-equilibrium process, where a huge amount new interface is created for a very short time period. During this time interval, the interfaces are far from equilibrium and the adsorption of surfactant is much lower compared to the equilibrium value corresponding to specific bulk concentration of surfactant. If the time scale we are interested in is within this initial (highly non-equilibrium) stage then the use of equilibrium values could lead us to completely wrong conclusions. For example it could happen that equilibrium thin liquid films formed in the Scheludko cell are very stable, while the same films (with the same bulk concentration of surfactant) in non-equilibrium system are unstable. Or another example: consider that we have two different surfactants with nearly the same equilibrium values of surface tension and adsorption, having nearly the same charges per molecule. If we perform the equilibrium experiments with these two surfactants we observe nearly the same stability of the films, but the dynamic experiments could show very drastic difference: system containing one of the surfactant is very stable while the same system with second surfactant is completely unstable. Note that this is not some imaginary case, this is quite realistic behavior of surfactants and one could find many real examples in many books about emulsion and foam stability[4,10,16-17]. The main reason why our surfactants perform differently in dynamic conditions is due the difference in their dynamical properties[11]. In our specific example one of the surfactants is very “fast” and within the time scale of the process the interfaces manage to equilibrate – and the surface tension and adsorption (e.g. surface charge) for the dynamic and equilibrium system are very close, so both equilibrium and dynamic experiments give nearly the same results. The other surfactant is very “slow” and during the time of the experiment the system is far from the equilibrium – the adsorption is much lower than the equilibrium value – the surface charge is lower and the electrostatic repulsion between interfaces is lower. This

explains the big difference in thin film (foam or emulsion) stability for the case of second surfactant[16-17].

So what we can do in the case when we have fast dynamic process: How we could find some equilibrium properties, which could be mapped more realistically to the non-equilibrium case? One of the possible ways to find such a mapping is using so called "effective" bulk concentration concept: We consider a system, which has much lower bulk concentration, whose equilibrium values of surface tension and adsorption are close to the typical values in the dynamic experiment of system with real concentration. We could speculate than that the equilibrium properties of system with an effective concentration are much closer to the properties of the real system in the dynamic conditions. Thus one way to map the properties of the equilibrium system to the dynamic one is to perform an equilibrium experiments at lower concentration. The faster is the process the bigger will be difference between real and effective concentration, which means that the amount of the surfactant, which is not operative (from the stabilization point of view) is increasing with the decrease of the process time scale. Thus one way to determine an effective concentration is:

a) from the dynamic surface tension curve, we determine the typical value of the surface tension characterizing the dynamic process;
b) using the equilibrium surface tension isotherm, we determine the value of equilibrium bulk concentration, which correspond to the dynamical value of the surface tension.

Same could be obtained directly if we combine the dynamic surface tension (at given bulk concentration) curve, $\gamma(t,c_0)$ and equilibrium surface tension isotherm curve, $\gamma(c)->c(\gamma)$, to get a new curve excluding the surface tension from both, $c(\gamma(t,c_0))$, which directly gives effective concentration vs. time.

All this was to show that knowledge of the surface properties of the surfactant system is the key step for understanding the properties of much more complicated colloidal systems.

I.5. Self Consistent Field Theory of Polymers – Is it anything to do with surfactants?

In the present thesis we will focus our attention on some theoretical and computer modeling aspects of the surfactant systems. This will be achieved by applying a theory, which originally was developed for very long polymers[20-26]. From the other point of view we will try to apply this theory for surfactants, which in most cases are quite short – or definitely much shorter than the polymers considered in the theory. So it is quite natural to ask: Is such a theory has anything to do with surfactant systems? The aim of the current paragraph should be considered more or less as a try to motivate such an application.

There are huge variety of theories, which allow property prediction of a single atom (particle) gases and fluids. Knowing the exact form of inter-particle potential one could use many approximate expressions, which allow determination of the pair correlation function of the system, wherefrom all the thermodynamic properties could be calculated. But if our system consists not only from a single atoms (particles) and we have some molecules, where several atoms (particles) are connected to form a molecule then the situation becomes much more complicated. We can still calculate with a sufficient accuracy properties of the two atom systems, but for three or more atom systems the situation is practically out of control and only numerical or computer modeling could give an information about the system with a sufficient accuracy. The problem is that if we have a complex molecules into the system we must also to take into account the all-possible conformations of the molecules, and not only their positions. For the case of di-atom molecule we need to know the position of one of them and the direction, where molecule is oriented. For the case of ternary molecule we need to specify the position of one of atoms (or center of mass), plane where molecule resides and the angle between the bonds, etc. So one could get an impression that the bigger the molecule is, the more complicated the considerations are. But there is a limiting case of infinitely long molecules where one could again calculate many properties of the system[21-23]. Infinitely long molecules are very close to polymers, which consists of many similar (or several types) of segments, connected into a long molecule – in some cases single polymer molecule could

have tens or hundred thousands of segments connected. The reason why we have a possibility to calculate the properties of polymer systems is that the probability that a randomly chosen segment to be part of the end of polymer molecule is extremely low – thus each segment could be considered as being situated somewhere in the middle of the chain. By making this important step one gains an access to a powerful mean field treatment, which considers an average segment in the potential field of all other segments.

The main assumption wherefrom practically all of the mean field polymer theories start with is to assume a certain distribution of the polymer conformations in a phase-space, wherefrom the statistical weight of each state (conformation) of the chain could be extracted. One of the most realistic distributions is the Gaussian one. The reasoning for using it is motivated by the Gaussian central limit theorem, saying that all the possible positions of any given segment are independent from the positions of the others, with only limitation that consecutive segments lay within a given distance from each other, determined from the length of the chemical bond, which connects them. Thus the whole chain on average will have a form like a random walk path, with a fixed distance between the steps. Thus the conformations of the polymer chains are similar to random walk trajectory with fixed number of steps[21], or a drunk person trajectory, who is trying to find his way back home. The longer the chain is, the better is satisfied this assumption and better is the agreement between the properties of the real system and theoretical predictions. It was shown that the polymer theory is working very well for the chains having more than 20 segments[26]. For shorter chains there is a deviation from the predictions of the theory due to the fact that when we decrease the chain length we increase probability to find a segment, which part of the molecule end. Which brings an asymmetry and the assumption that all of the segments are nearly similar and are situated in the middle of the chain is less and less motivated. The longer is the chain lower is the memory in the molecule where it starts and where it ends. For shorter chains the system could still remember very well where the ends are and it is much more difficult to cheat it that each of the segments has nothing to do with the end. Nevertheless there are many successful applications of the polymer theory to the case of shorter molecules[28-33]. The reason why this is possible is due to the fact that most of the thermodynamic properties are integrals over all the conformations of the chain and it is possible to get a proper value of integral with a different integrand function. Thus for the case of shorter chains the polymer theory could be used like

a quantitative theory, which could give a rough estimate for the properties of the system and their scaling laws. When and why it is possible to apply the predictions from the polymer theory to the case of shorter chains is very difficult question and usually only the comparison between theory and experiment or computer modeling could give justification for such an use. The detailed theoretical analysis is very complicated – even it could be more difficult than to solve the problem for the case of short chains itself.

So we could find a good theoretical solutions and predictions for two limiting cases: (a) single atom systems or (b) systems containing very long chains. The question is where are the surfactants situated? The answer is: most of the surfactants which are interesting and have found a huge industrial application are somewhere in between: usually neither hydrophilic nor hydrophobic parts are long enough to be considered as polymers. From the other point of view they are too long be considered as a single atoms. What we should do then? The answer is that we can use both extremes: in some cases we could consider surfactants like a point like particles and in some case we could consider them being long enough and we can use a results from polymer theory. There is no universal recipe which of the extremes to use - the only justification usually is the comparison with an experiment in order to check the predictions out of the theory.

The case when surfactants are considered like single particles is called coarse – graining: one forgets about all the internal structure of the surfactant molecule and assumes that it behaves like a solid particle with a given shape and volume. There are many theories and computer modeling methods where this concept is used. The case when we artificially extend surfactant molecules (assuming an additional internal degrees of freedom which allow us to consider them like a long polymers) is exactly the opposite case of coarse graining. There are also many considerations where a combination of both methods is used, i.e. some part of the surfactant molecules are coarse – grained and some are expanded in order to use a predictions from polymer theories. The limiting cases where “simple” theories exists (single particles and very long chains) provide us very useful relations, which bridge the corresponding properties of the system into a new level of consideration (coarse-graining or expansion). Here we give a simple example: Coarse-graining (renormalization) is used for the case of polymer systems also. If we like to decrease the number of segments in the system (especially important for

the molecular modeling – where any decrease of the complexity of the system could give a significant performance boost), we could renormalize the polymer chain (see Figure 1.4.).

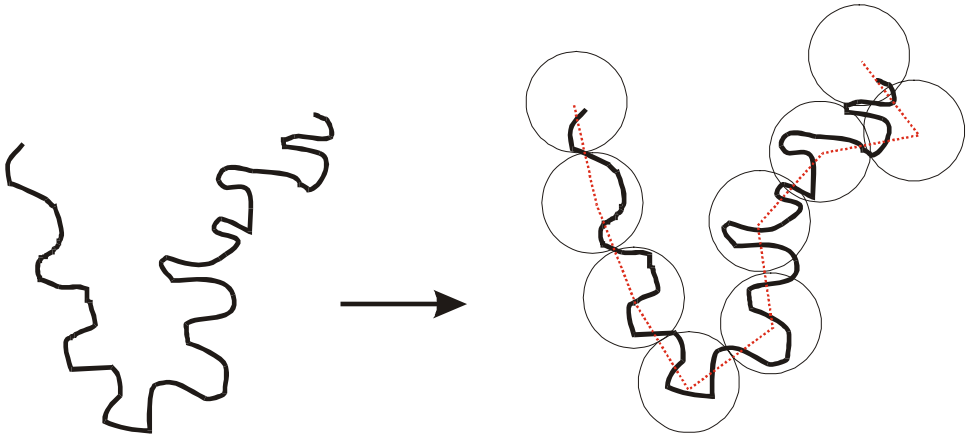

Figure 1.4. Coarse-graining (renormalization) of polymer chain.

Consider a homo-polymer with 2000 segments, which we like to coarse-grain to a shorter one with 20 segments only (where polymer theory is still working) i.e. e will combine every 100 segments into one segment. If we would like that our course-grained polymer has the same radius of gyration or end to end distance like the original one, then we must increase also the length, l, (Kuhn lenght) between the segments. We do the renormalization in this case using results from polymer theory[21]: which says that the squared gyration radius of free polymer chain is proportional to squared length of segment as well as to the number of segments. Thus in order to have a polymer with same radius of gyration we need to increase the length of the segment 10 times – which is not 100 times like one could assume without the knowledge of the polymer theory: one could say that decreasing the number of segments 100 times each having length l will increase length of the segment of new polymer 100 times in order to have the same distance of stretched polymer. This is simply wrong due to the fact that the conformation of highly extended polymer molecules is very unlikely to happened in real solution. The most probable conformation of the polymer has a structure of Gaussian core. The obvious similarity between the bulk diffusion and radius of gyration of polymers is due to the fact that in both cases we have one and the same physics and the outcome is determined from the central limit theorem.

In this thesis we will use the analytical form of self consistent mean field theory for polymer brushes grafted on the solid interface. The self consistent mean field theory (SCF) was originally developed more than 15 years ago, starting from deGennes[21,25] and Alexander[24] scaling concepts for polymer systems. The scaling concepts give many useful relations between various polymer chain properties and system properties of interest. But main drawback is that scaling concepts give usually a power laws but not the pre-factors of these laws. So they could be used as a powerful tool for check a dependences, but not for a quantitative predictions. Latter Semonov[26] and Milner[30-31] developed more sophisticated quantitative theories, which allows prediction of various properties of polymer systems on the quantitative level. In the present thesis we will use a SCF, which was developed for the case of very long polymer brushes grafted at the solid interface and later generalized for the case of di-block polymers adsorbed on the liquid/liquid interface[28-32]. As in any polymer theory one should take into account the conformation of the polymer chains - polymer chain could have many different conformations at the interface, each with its own statistical weight. In order properly to calculate the thermodynamic properties of the system one should extract most probable states and based on the statistical weight distribution. Then the thermodynamic properties of the system could be calculated taking into account only most probable states and their weights again. This is exactly what Self Consistent theory does: it gives us an estimate of the statistical weight distribution of the possible states of the chain, and also gives us procedure to calculate the thermodynamic properties of the system. Thus in his nature the SCF is statistical theory. It is equilibrium theory because it gives the distribution of states of the system in equilibrium, though there are generalizations of the SCF for the quasi equilibrium case, when the system is close to equilibrium[35]. SCF is mean field theory because it is working with an average (most probable) chain using a mean field representation of the statistical system: main object which theory is working with is the segment density distribution of the most probable chain as a function of the distance from the solid interface. Theory is called self consistent due to the fact it self consistently determines the mean field potential of the segment in the field of other segments as well the segment density distribution, which are not independent.

SCF assumes that there are two main contributions to the free energy of the system (polymer brush): (i) pure osmotic one, which takes into account the fact that increased local

concentration of the segments changes the local pressure; (ii) pure entropic contribution of the conformational energy of the chain. The first contribution makes a finite volume correction (each chain occupies some volume and due to the fact that the whole system is incompressible the solvent should be expelled out from that region), but it does not account for the fact that some of the segments are connected together to form a chain, which was accounted with the second term. Theory assumes that the averaged conformation of the chain is like a Gaussian random walk path with a given length. So the statistical weight factors of different states are extracted from the Gaussian distribution. Additional simplification, which is used, assumes that chains are strongly stretched so from all-possible states of the chain only those, which do not have loops and knots, are taken into account. The latter is fulfilled for the case of high grafting densities at the interface. These assumptions allow us to write the free energy of the system in the form of Density Functional (DF) for the local segment volume fraction, which after minimization of the free energy allows determination of the equilibrium segment volume fraction near the interface, wherefrom all the thermodynamic properties of the system could be calculated.

There are very close analogy between the theories for calculation of a pair correlation distribution of the systems consisting of many molecules and SCF: the equilibrium volume fraction is analogy of pair correlation function, while the field potential acting on the segment is equivalent to the potential of the mean force.

Originally the theory was developed for very long chains. Latter with the use of the computer modeling methods it was shown that the predictions from the theory could be applied for rather short chains having at about 20 segments[27]. Pushing the application of the theory to even higher extend there are applications for the case of surfactant systems where the chains are even shorter[29,30,32,35] – and astonishingly the predictions of the theory rather well describe the properties of the real system. Of course in this case the predictions are more qualitative (in sense that they give scaling lows and tendencies), rather than being quantitative. Thus the application of SCF for the case of shorter chains is mostly for getting the scaling behavior of the system, rather than precise qualitative predictions. The use of SCF in those cases is simply motivated by the fact that other theories are very complicated and in many cases they do not allow analytical solution. Thus SCF could give us an initial starting information about system behavior.

The application of the SCF for the case of short surfactant molecules could be expanded in many directions. It was successfully used for predicting the surface elastic properties of non ionic surfactant layers adsorbed at oil/water interface, which gives very interesting and powerful applications for understanding the phase behavior ternary surfactant systems and microemulsions[29,32]. There are other applications where the interaction between surfactant molecules adsorbed at the interface and micelles was taken into account – the latter is very important for understanding both static and dynamic properties of the surface tension of micellar solutions[36]. Some of these applications are subject of the present the thesis.

I.6. Aim of the thesis

The thesis has two aims: scientific one and prosaic one. The latter is simple and obvious, but the first one (scientific) is much more important for the author and probably for a possible reader. The scientific aim is the following: *Application of the self consistent field theory for predicting surface properties of surfactant systems*.

The properties, which we are interested in and which are investigated in the thesis, are:

- surface elastic properties of surfactant mono layers: spontaneous curvature, benign and splay (saddle) modulus
- surface and interfacial tension of surfactant systems.

Both of them are studied and investigated with one and the same theory using one and the same approach. For the case of surface and interfacial tension the theoretical predictions of the theory are also checked using a computer modeling. The latter statement could also be inverted to say that the computer modeling algorithm (Dissipative Particle Dynamics) was checked against the prediction of the theory.

The main new results, which are obtained in order to fulfill the thesis aims are:

- new general relations, which allow determination of the surface elastic constants of *any* local density functional theory (SCF for example) using *only* few moments of the *flat* solution of the theory.
- new theoretical surface and interfacial tension isotherm of surfactants systems. The scaling predictions of the latter are checked with a huge variety of surfactants types – non-ionics, ionics and amphoterics.

I.7. Outline of the thesis

The thesis is structured as follows:

In Chapter II could be considered as a part of the introduction, and it describes the method, which we are going to use later on in the thesis. Thus there are no new results in this chapter, and it simply outlines the self consistent field theory of the polymer brushes for the case of flat and curved interfaces. But despite of the fact that the results in this chapter are known and published, one could hardly find in literature many of the details given in this chapter (some of which are of critical importance if one needs to use and apply the SCF in other new areas). Thus this chapter could be considered as a done homework and by no means is a cut and paste from the literature articles.

In Chapter III we present a general method for the calculation of surface elastic properties (bending and splay modulus and spontaneous curvature) of a mono and di-block polymers and surfactants. There we managed to derive general formulas for the surface elastic constants in terms of the flat solution of the theory. The main breakthrough here is the observation that for certain class of density functional theories (SCF also belongs to this class) the curvature expansion of the free energy could be obtained in a closed analytical form without necessity to know any specific solution of the problem. This is rather different from known literature results, where the elastic constants are given in terms of moments of flat profile and its first curvature series expansion in spherical or cylindrical geometry. Different cases of brushes and solvents are considered and the elastic constants are calculated for each of them. Combination of those results for the case of di-block polymers and surfactants allows determination of a new variety of the practical relationships, which could find an application in surfactant ternary phase behavior prediction as well as in modeling and microemulsions property prediction.

In Chapter IV we describe the Dissipative Particle Dynamics (DPD) computational method and discus its application for the case of surfactant systems. Many applications are given, but the results, which are discussed there, remain on the qualitative level.

In Chapter V we give a comparison between the predictions of SCF and DPD, both for the case of solid/liquid and liquid/liquid interfaces. We show that there is an excellent agreement between both methods and we believe that the results presented in this chapter are the first systematic and quantitative comparison of the predictions from DPD and SCF. This is very important motivation for the quantitative predicting power of DPD method, which is rather new one and still is subject of intensive investigations.

In Chapter VI we derive a new surface tension isotherm based on the SCF. We show the comparison between the scaling predictions of SCF-isotherm and surface tension experiments for various surfactant systems. We show that a huge variety of surfactant systems follow the scale behavior of this isotherm starting from very low concentrations up to the critical micelle concentration (CMC). According to our knowledge this is one of the best performing general-purpose isotherm, which works for non-ionic, ionic and amphoteric surfactants both for air/water and oil/water interfaces. In this chapter, we have also outlined a new method, which allows bridging of the surface tension results obtained from DPD to those for real systems. The interfacial tension mapping procedure between real and DPD systems could be used for an estimation of the DPD interactive parameters as well.

Thesis finishes with the summary of the main results in Chapter VII.

II. Introduction to Self Consistent Field Theory of Polymer Brushes

II.1. Polymer Brushes at flat interface

Polymer chains grafted at the impenetrable interface with their one end, form a good model for the analysis of numerous systems, such as sterically stabilized colloidal dispersion, block polymer surfactants at solid –liquid and liquid-liquid interfaces, solutions and melts of block copolymers under the conditions, in which microphases are formed etc. Theoretical analysis of grafted chain layers was initiated by pioneering work of Alexander[24]. Using scaling arguments the main features of grafted chains were established. Further progress in the analytical theory of grafted layers using the self consisted field (SCF) approach proposed by Simeonov[26]. In this chapter we will briefly outline main assumptions of the theory as well as the results, which we will need in next chapters.

We will consider mono disperse chains grafted on the solid interface[24-27,37-40,] . In the Self Consistent Mean Field theory (SCF)[26,37-38] the free energy of the system is written in terms of density functional of the monomer concentration. For long grafted chains the free energy could be written as:

$$F = F_{ent} + F_{conf} + F_{solvent\_bulk} \tag{2.1}$$

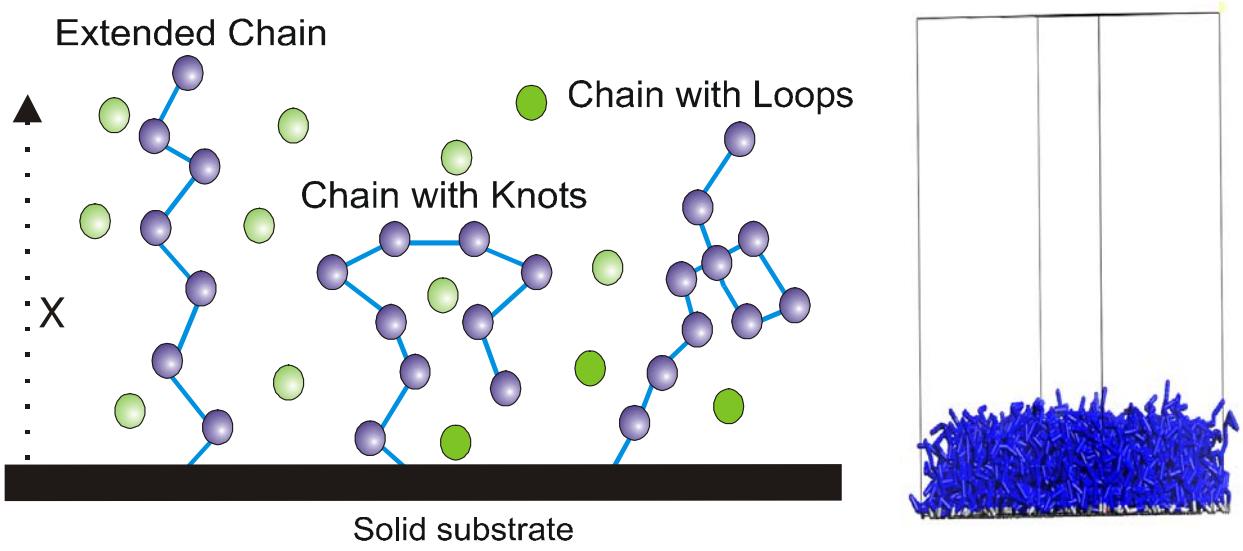

Figure 2.1. Polymer chains grafted on the solid interface. (a) various chains conformations are depicted; (b) snapshot of DPD simulations.

The first term in eq 2.1 is pure osmotic contribution of the monomer segments, which does not account for the connections in the polymer chain. The second term is the conformational entropy of a long chain and the last one is the bulk free energy of the bulk solvent. The latter contribution will be omitted latter on, because it is of no interest to our considerations.

The conformational entropy of brush having long extended chains could be written in a continuous limit to have pure Gaussian[27,37] form

$$F_{conf} = \frac{3kT}{2l^2}\sum_{i=1}^{M}\int_0^N \left(\frac{ds_i(n)}{dn}\right)^2 dn \qquad (2.2)$$

where, k is Boltzman constant, T is thermodynamic temperature, s, is the arc length (measured from the grafted end) of polymer chain and, $n(s)$ is number of segments in a part of polymer chain between grafted end and position s, $s_i(n)$ is the inverse function and has the meaning of the most probable path of the i-th polymer chain, l is the Kuhn length of the segment, M is the total number of polymers at the interface‡. Note that the integral in eq 2.2 is contour integral along the most probable path. The above expression is nothing more than an conformational entropy calculated assuming a Gaussian distribution of the segments of the chain, which describes correctly only a long scale of the chains and smears out all the local structure. It was firstly realized by Semonov[26] (and letter derived independently by Millner et. al[38].) that the contour integral could be changed to a normal integral (arc length of the chain is

‡ Different authors use different numerical coefficients in front of F_{conf}. In his work Semonov[26] uses the same expression like the one given with eq 2.2. while Milner et. al.[31] and Safran et. al.[32] are working without the factor 3 in front of eq. 2.2. The reason for this difference is due to the fact that the form of free energy written above is valid for isotropic 3D system. In general case in eq 2.2 we must have a scalar product of $\left(\frac{d\mathbf{s}_i(n)}{dn}\right)^2$, which for the case of purely isotropic 3D system gives $3\left(\frac{ds_i(n)}{dn}\right)^2$ (assuming independence of the chain distribution in each direction). In our case we consider conformations of the chains only in one direction and one could argue that the factor 3 should be omitted, while from the other point of view we consider very long chains and far away from the interface the system is nearly isotropic and factor 3 should remain. Thus there is no a strict theoretical arguments whether one should use this factor 3 or not. The simulations of Lai et. al.[27] using a Monte Carlo bond fluctuation model agree numerically well with the factor 3 in front of the free energy. Our simulation results with DPD agree also very well.

substituted with the distance from the interface) for the case of extended chains (see figure 2.1):

$$F_{conf} = \frac{3kTM}{2l^2}\int_0^H P(y)\int_0^H \varepsilon(x,y)\theta(y-x)dxdy \tag{2.3}$$

where, $\varepsilon(x,y)=\frac{dx}{dn}$ is the local stretching of the chain: $dn=\frac{dx}{\varepsilon(x,y)}$ is the number of segments in the interval, dx, of the chain having an end at y, $P(y)$ is the density probability for finding an end of a polymer chain at y, while H is the brush thickness, and $\theta(y-x)$ is a step function, which is 1 when y>x and zero otherwise. We need strong stretching approximation because only for extended chain one could map one to one length of the chain to the distance from the interface. If chain has knots or loops the latter mapping is not bijective (see figure 2.1) and the contour integral must be split in several integrals with respect of the distance from the interface. One could argue that the latter assumption is motivated for the case of comparatively high surface coverage, because the higher the adsorption is the higher is the repulsion between the segments, which leads to a strong stretching of the chains.

From the definition of the local stretching and the probability it follows that

$$\int_0^y \frac{dx}{\varepsilon(x,y)} = \int_0^H \frac{\theta(y-x)dx}{\varepsilon(x,y)} = N \text{ for any } y\in[0,H] \text{ and } \int_0^H P(y)dy = 1 \tag{2.4}$$

where, N is the number of segments in the polymer chain.

The entropy part (in the mean field Flory type of approach) could be written as

$$F_{ent} = \frac{kTA}{v_0}\int_0^H Q(\varphi(x))dx \tag{2.5}$$

where, $\varphi(x)$ is the volume fraction of the polymer segments, which is dependent from the density of end chains P, and local extension ε, A is the total system area and v_0 is the volume of the monomer segment. Here with $Q(\varphi)$ we denote the osmotic free energy density. By definition if we have free segments in a homogeneous continuum with a constant volume fraction φ_0, the pressure, P, of the system is connected with Q as $P=\frac{kT}{v_0}\left(\varphi_0\frac{\partial Q}{\partial\varphi_0}-Q\right)$.

Note also that in the last expression we have explicitly assumed that the solvent and segments have one and the same volume molecular volume, i.e. segments are from the same type like solvent molecules, and the polymer chain was constructed by connecting several solvent

molecules into a long chain. For the case when solvent and segments have different volumes the eq 2.5 should be corrected by factor v_0 / v_w, where v_w is the volume of the solvent molecule.

The local volume fraction at position *x* could be expressed as:

$$\varphi(x) = \frac{v_0}{\sigma}\int_0^H \frac{P(y)\theta(y-x)dy}{\varepsilon(x,y)} \tag{2.6}$$

which, is nothing more that we count for the contribution to the local volume fraction of all chains, which are extended to a distance more than *x*. The brush thickness is defined from, $\varphi(H) = 0$. We have introduced, $\sigma = A/M$, which is the area per polymer chain and the adsorption is $\Gamma = 1/\sigma$. The straightforward integration of the last equation with respect of *x* from 0 to *H* (using eq 2.4) gives following normalizing condition for the segment volume fraction

$$\int_0^H \varphi(x)dx = Nv_0/\sigma\,. \tag{2.7}$$

In order to find a physical solution of the problem one should minimize the free energy (eq 2.1) by all independent functions. The easiest way to get the final result is to minimize the functional with respect of, ε, while keeping, *P*, constant and taking into account the connection between volume fraction and ε (at constant P) and using a normalizing condition for ε (eq 2.4), with an unknown Lagrange multiplier *f*. Thus we should minimize:

$$\tilde{F}/(kTA) = \frac{1}{v_0}\int_0^H Q(\varphi(x))dx + \frac{3}{2l^2\sigma}\int_0^H P(y)\int_0^H \varepsilon(x,y)\theta(y-x)dxdy + \int_0^H f(y)\int_0^H \frac{\theta(y-x)dx}{\varepsilon(x,y)}dy$$

using that $\delta\varphi(x) = -\frac{v_0}{\sigma}\int_0^H \frac{\delta\varepsilon(x,y)P(y)\theta(y-x)dy}{\varepsilon(x,y)^2}$. The result is straight forward and gives that

$$-\frac{\delta Q}{\delta\varphi(x)} + \frac{3}{2l^2}\varepsilon(x,y)^2 = \frac{f(y)}{P(y)} \tag{2.8}$$

for every *x* and *y*. Setting *x*=*y* and using that $\varepsilon(y,y) = 0$ (the latter is directly seen from the normalizing condition of, ε, which should be valid also when $y \to 0$. In this case if there is no singularity of, $1/\varepsilon(x,y)$, when $x->y->0$, the integral should vanish instead of being constant), we get that

$$\varepsilon(x,y)=\sqrt{\frac{2l^2}{3}}\sqrt{\bar{\mu}(x)-\bar{\mu}(y)} \tag{2.9}$$

where, $\bar{\mu}(x)=\dfrac{\delta Q}{\delta\varphi(x)}$ is proportional to the partial chemical potential due to the entropy contribution. It follows immediately that in order to have physical solution we should have that, $\bar{\mu}(x)>\bar{\mu}(y)$ when for any $y>x$, thus $\mu(x)$ is monotonic decreasing function. Then we can substitute this result into the normalizing condition for ε (eq 2.4) and solve it like an integral equation for unknown function $\bar{\mu}(x)$:

$$\int_0^y \frac{dx}{\sqrt{\bar{\mu}(x)-\bar{\mu}(y)}}=Nl\sqrt{\frac{2}{3}}\,. \tag{2.10}$$

The latter is Voltera integral equation of the second type, which has an Abelian form. The solution can be obtained by multiplying both sides of the equation with $\dfrac{\bar{\mu}'(y)}{\sqrt{\bar{\mu}(y)-\bar{\mu}(z)}}$ and integration by y from 0 to z. The RHS of eq 2.10 integrates immediately to $-2Nl\sqrt{\dfrac{2}{3}}\sqrt{\bar{\mu}(0)-\bar{\mu}(z)}$. The LHS of eq 2.10 after the change of integration order gives

$$\int_0^z dx\int_x^z \frac{d\bar{\mu}(y)}{\sqrt{\big(\bar{\mu}(y)-\bar{\mu}(z)\big)\big(\mu(x)-\mu(y)\big)}}=\int_0^z dx\int_{\bar{\mu}(x)}^{\bar{\mu}(z)} \frac{du}{\sqrt{\big(u-\bar{\mu}(z)\big)\big(\bar{\mu}(x)-u\big)}}\,. \tag{2.11}$$

Using that

$$\int_a^b \frac{dx}{\sqrt{(x-a)(b-x)}}=\begin{cases}-\pi & b>a\\ \pi & b<a\end{cases}. \tag{2.12}$$

and taking into account properties of $\bar{\mu}(x)$ we see that LHS of eq 2.10 is $-\pi z$, which gives final solution for

$$\bar{\mu}(x)=\frac{\delta Q}{\delta\varphi(x)}=\bar{\mu}(0)-\frac{3\pi^2}{8N^2l^2}x^2\text{, and for }\varepsilon(x,y)=\frac{\pi}{2N}\sqrt{y^2-x^2}\,\theta(y-x)\ ^{37\text{-}38}. \tag{2.13}$$

The latter is very important result, which shows that the local stretching depends only on the polymerization index N and is completely independent from all other properties of the system, and is universal function from the distance from the interface. This is direct consequence from the strong stretching approximation and normalizing condition that all polymers should have given length. The straightforward integration shows that

$\int_0^y \varepsilon(x,y)dx = \frac{\pi^2}{8N} y^2$. One can also substitute ε in the relation between volume fraction and $P(y)$ and integrate the equation by x from zero to H to show that

$$\int_0^H \varphi(x)x^2dx = \frac{2Nv_0}{\sigma\pi}\int_0^H P(y)y^2dy\int_0^1 \frac{z^2dz}{\sqrt{1-z^2}} = \frac{Nv_0}{2\sigma}\int_0^H P(y)y^2dy \qquad (2.14)$$

(where we have changed variable x to $z = y/x$).

The end chain probability distribution could be calculated very easy if we knew the solution for $\varphi(x)$ also: taking the form for ε and multiplying the connection between volume fraction and P by $\frac{xdx}{\sqrt{x^2-z^2}}$ and integrating by x from z to H and after some simple manipulations one gets that

$$P(z) = -\frac{\sigma z}{v_0 N}\int_z^H \frac{\varphi'(x)dx}{\sqrt{x^2-z^2}}\ ^{38}. \qquad (2.15)$$

Thus after the minimization of the free energy with respect of ε we obtain a form of the free energy, which depends only on the volume fraction of the segments

$$F_{conf} = \frac{kTAK_S}{v_0}\int_0^H \varphi(x)x^2dx \qquad (2.16)$$

where, $K_S = \frac{3\pi^2}{8N^2l^2}$ is the string constant of the mean field spring potential of the chains – i.e. $K_s x^2/2$ is a mean potential of all surrounding chains that are acting on the specific segment of polymer. Latter equation allows us to write the free energy of the system in the form of a density functional (DF) containing only the segment volume fraction.

For the case of long polymer chains it was shown by Flory[22,74] that osmotic part of the free energy (or free energy of mixing a polymer chains with solvent), could be expressed as

$$Q(\varphi(x)) = \frac{v_0}{v_w}\left[(1-\varphi(x))\ln(1-\varphi(x)) + \chi\varphi(x)(1-\varphi(x))\right] \qquad (2.17)$$

where, χ is the Flory-Huggins parameter, which accounts for the interaction between the monomers and solvent, v_w is solvent molecular volume.

For the case of moderate volume fraction one can use a virial expansion (up to the quadratic term, with respect of the volume fraction) of the latter equation to get.

$$Q = \frac{w}{2}\varphi^2(x) \tag{2.18}$$

w is the second virial coefficient of the pressure expansion (of like solvent and polymer segments) $w = (1-2\chi)\frac{v_0}{v_w}$. The linear terms with respect of volume fraction could be omitted, because they integrate to constant (due to normalizing condition for the volume fraction eq. 2.7) and change the reference state of the system only, but not the pressure. One could also directly write eq 2.18, provided that the virial coefficient is known a priory. We will use the latter approach for the case of DPD simulation, where the main predictions out of the theory are compared with the simulations.

Note also that the virial expansion given with eq. 2.18 is valid for the case of moderate volume fractions and providing that second virial coefficient differs from zero. We will illustrate this in the next chapter for the case of Θ solvent ($\chi = 1/2$), where the second virial coefficient is zero and higher order expansion should be used. More cases are discussed in the next chapter, here we will give the results only for the simple case of moderate volume fractions providing that we are away from Θ point.

Thus for the case of moderate volume fractions the density functional of polymer brush reduces to

$$F/A = \int_0^H \Phi(\varphi(x))dx = \frac{kT}{v_0}\int_0^H \left\{\frac{w}{2}\varphi(x)^2 + K_S\varphi(x)x^2\right\}dx\,. \tag{2.19}$$

In order to find a real solution the free energy should be minimized with respect of the segment volume fraction taking into account the normalizing condition eq 2.7. The solution is straight forward:

$$kT\left(w\varphi(x) + K_S x^2\right) = \mu_C = kTK_s H^2 \qquad \varphi(x) = \frac{K_S H^2}{w}(1-(x/H)^2) \tag{2.20}$$

where, we have used that the volume fraction vanishes at the x=H, and $\mu_C = v_0\frac{\delta\Phi}{\delta\varphi}$ is the chemical potential of the segment, which is independent of x. Substituting the last equation in the normalization condition for the volume fraction, gives the expression for the brush thickness,

$$\left(\frac{H}{N}\right)^3 = \frac{3wv_0}{2K_s\sigma} = \frac{4wv_0l^2}{\pi^2\sigma}. \qquad (2.21)$$

Substituting the solution for the brush thickness in the volume profile one can see that $\varphi(x)\sigma^{2/3}$ is an universal function of $x\sigma^{1/3}$, for any area per polymer σ, thus all the density profiles (when keeping all other properties of the polymer constant, while varying the surface coverage) should collapse at master curve[27]. One can also show that[26,27,37]

$$\langle x\rangle = \frac{\int_0^H \varphi(x)xdx}{\int_0^H \varphi(x)dx} = \frac{3}{8}H. \qquad (2.22)$$

II.2. Brush at Curved interface

Consider now that we have a polymer brush grafted at the interface, which has a small curvature. Depending on which side of the interface the brush is grafted – the presence of curvature either lowers segment volume fraction or increases it. Thus the curvature presence will influence the monomer density distributions, wherefrom it will change the total energy of the system.

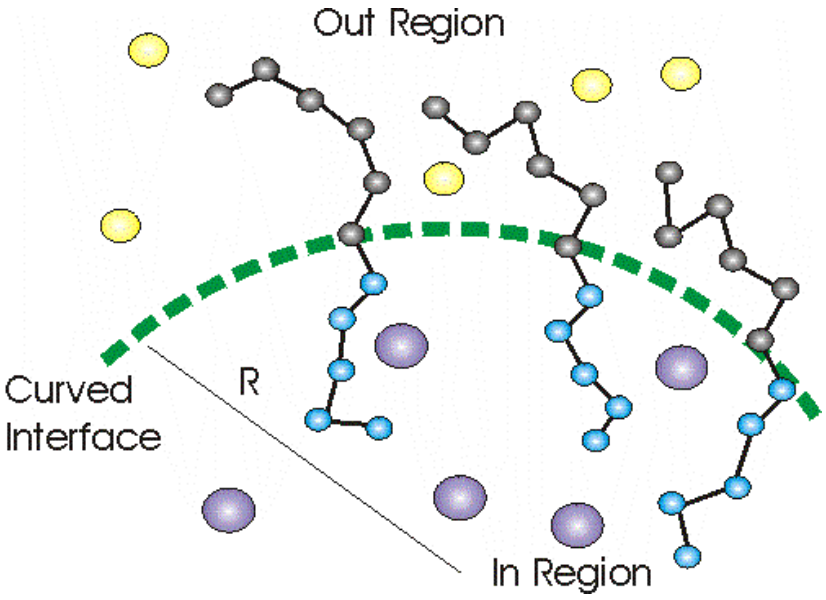

Figure 2.2. The polymer brush grafted on the interface: brush could be grafted on both sides of the interface, and depending on the curvature sign, brush is either compressed or expanded.

The latter is very important, and after corresponding expansion of the free energy with respect of the curvature rather important characteristic of the brush layer could be calculated. We will discuss this in more details in the next chapter. Here we will give very short outline of the SCF theory of the brush grafted at the interface with very small curvature. Small curvature means that we can still use the strong stretching approximation, like in the previous section. In this case we could write the free energy of the system again as

$$F = F_{ent} + F_{conf} \tag{2.23}$$

Due to the small curvature of the interface we still have that

$$F_{conf} = \frac{3kTM}{2l^2}\int_0^H P(y)\int_0^H \varepsilon(x,y)\theta(y-x)dxdy \tag{2.24}$$

and again x and y are distances measured from the interface, while the distance measured from the center of curvature are $R+x$ and $R+y$, respectively. We will assume that we have the same conditions for the local stretching and the end probability i.e.

$$\int_0^y \frac{dx}{\varepsilon(x,y)} = \int_0^H \frac{\theta(y-x)dx}{\varepsilon(x,y)} = N \text{ and } \int_0^H P(y)dy = 1. \tag{2.25}$$

Note that we work again with the linear density of end chain distribution of the polymer. One could work also with the volume density of this distribution but the results should not depend on the choice. The reason, which allows us to do this, is that the conformation free energy is in the form of path integral over the most probable chain conformation. While for the osmotic part (which has the form $P\mathrm{d}V$) we must work with the volume densities. The above formulas are true for any type of interface with a small curvature! The entropic part (in the mean field Flory type of approach) could be written as

$$F_{ent} = \frac{kTA}{v_0}\int_0^H Q(\varphi(x))\left(\frac{R+x}{R}\right)^{\alpha} dx \tag{2.26}$$

Here $A = \beta R^{\alpha}$ is the total system area. Note the volume correction due to the curvature is taken explicitly into account in the above formula. Here α is the topological index of the interface: $\alpha = 1$ corresponds to cylindrical interface, while $\alpha = 2$, corresponds to spherical one. The normalizing volume factor β is $\beta = 2\pi L$ for the case of cylindrical interface (L is

the length of the cylinder) and $\beta = 4\pi$ for the case of spherical one. The local volume fraction at a position x could be expressed like[§]:

$$\varphi(x)\left(\frac{R+x}{R}\right)^{\alpha} = \frac{v_0}{\sigma}\int_0^H \frac{P(y)\theta(y-x)dy}{\varepsilon(x,y)} \tag{2.27}$$

And again as in the previous part of this chapter, the free energy of the system could be calculated directly by minimizing the functional with respect of ε, while keeping P constant and taking into account the connection between volume fraction and ε (at constant P) and using a normalizing condition for ε with a unknown Lagrange multiplier f. Thus we will minimize:

$$F/(kTA) = \frac{1}{v_0}\int_0^H Q(\varphi(x))\left(\frac{R+x}{R}\right)^{\alpha} dx + \frac{3}{2l^2\sigma}\int_0^H P(y)\int_0^H \varepsilon(x,y)\theta(y-x)dxdy + \int_0^H f(y)\int_0^H \frac{\theta(y-x)dx}{\varepsilon(x,y)}dy \tag{2.28}$$

using that $\delta\varphi(x)\left(\frac{R+x}{R}\right)^{\alpha} dx = -\frac{v_0}{\sigma}\int_0^H \frac{\delta\varepsilon(x,y)P(y)\theta(y-x)dy}{\varepsilon(x,y)^2}$. The result is straight forward and gives again that

$$-\frac{\delta Q}{\delta\varphi(x)} + \frac{3}{2l^2}\varepsilon(x,y)^2 = \frac{f(y)}{P(y)}. \tag{2.29}$$

Wherefrom we get that $\varepsilon(x,y) = \sqrt{\frac{2l^2}{3}}\sqrt{\mu(x)-\mu(y)}$. Again the definition of μ is similar like the previous section. One can also substitute ε in the relation between volume fraction and P(y) and integrate the equation by x from zero to H to show that

$$\int_0^H \varphi(x)\left(\frac{R+x}{R}\right)^{\alpha} x^2 dx = \frac{2Nv_0}{\sigma\pi}\int_0^H P(y)y^2 dy \int_0^1 \frac{z^2 dz}{\sqrt{1-z^2}} = \frac{Nv_0}{2\sigma}\int_0^H P(y)y^2 dy \tag{2.30}$$

[§] The local volume fraction at a position x could be expressed like: $\varphi(x)\beta\left(R+x\right)^{\alpha} dx = v_0 M\int_x^H \frac{P(y)dy}{\varepsilon(x,y)}dx$

which is nothing more that we count the contribution to the local volume fraction of all chins, which are extended to a distance more than x by explicitly taking into account that P and ε are properties defined per unit length, while φ is property per unit volume.

(where we have changed variable x to $z = y/x$). This immediately gives the final form of conformation free energy:

$$\frac{3}{2l^2\sigma}\int_0^H P(y)\int_0^H \varepsilon(x,y)\theta(y-x)dxdy = \frac{3\pi^2}{8N_2l^2v_0}\int_0^H \varphi(x)\left(\frac{R+x}{R}\right)^{\alpha} x^2dx \qquad (2.31)$$

The end probability distribution it could be also calculated very easy if we knew the solution for $\varphi(x)$. Taking the form for ε and multiplying the connection between volume fraction and P by $\frac{xdx}{\sqrt{x^2-z^2}}$ and integrating by x from z to H and after some simple manipulations one gets that

$$P(z) = -\frac{\sigma z}{v_0 N}\int_z^H \frac{f'(x)dx}{\sqrt{x^2-z^2}} \qquad (2.32)$$

where $f(x) = \varphi(x)\left(\frac{R+x}{R}\right)^{\alpha}$. The latter equation could be used if one need expansion of P in powers of 1/R.

Thus the final form of density functional of the chain grafted at curved interface has the form

$$F/A = \frac{kT}{v_0}\int_0^H \left\{\frac{w}{2}\varphi(x)^2 + K_S\varphi(x)x^2\right\}\left(\frac{R+x}{R}\right)^{\alpha} dx \qquad (2.33)$$

which should be solved using the normalizing conditions for segment volume fraction (obtained by direct integration from eqs 2.25 and 2.27)

$$\sigma\int_0^H \varphi(x)\left(\frac{R+x}{R}\right)^{\alpha} dx = C = Nv_0 \qquad (2.34)$$

The most important fact coming out of the last consideration is that the DF of the free energy and normalizing condition have an explicit dependence from the radius of curvature R only in the Jacobian of the integral and an implicit curvature dependence coming out from the dependence of the brush thickness and a local volume fraction from the curvature. We will exploit this result in the next section where the bending properties of grafted chains and di-block polymers will be calculated.

III. Bending constants of interfaces containing surfactants or polymers

Abstract

Here we present a general method for calculating the spontaneous curvature and bending modulus of surfactant monolayers or grafted polymer brushes, which is based on a density functional theory. The free energy functional is represented in series of the curvature in sphero-cylindrical geometry and the bending parameters and the spontaneous curvature are represented in terms of integral moments of the solution for the flat geometry. The problem is solved for an arbitrary form of the free energy density function with the only requirement that the energy functional is local. This approach enables a variety of problems involving polymer brushes, surfactants and amphiphilic diblock copolymers to be treated directly and would be very useful for studying the phase behavior of microemulsions and surfactant solutions. Although the derivations are done for local functional, which does not contain derivatives of the density function, we believe that the generalization for that case non-local (e.g. Van der Waals theory) is possible. A particular example is given for a low-density polymer brush where the method reproduces know results.

III.1. Introduction and Motivation

The properties of microemulsions are determined by the bending energy and the entropic contributions. At a microscopic level, these thermodynamically stable mixtures of oil, water and amphiphiles are structured into water and oil domains separated by an amphiphilic monolayer. It has long ago[42] been recognized that the properties of the microscopic surfactant film control in a great extent the type of the microstructure formed. The phenomenological model of Helfrich[43] for the curvature energy of amphiphilic structures proved quite successful in reducing the number of natural parameters used to describe the phase behavior and micro-structural characteristics of complex systems like microemulsions, vesicles, mixtures of surfactants and polymers, and biological membranes. Helfrich introduced the concepts of a natural radius of curvature and bending constants (mean and

saddle splay moduli). A variety of molecular models have been developed in order to relate these mechanical quantities to the molecular properties of the surfactant molecules and the oils used. A comprehensive review of curvature and elastic properties of monolayers and membranes is given by Petrov *et al.*[44,45] Huh[46] used the ideas, proposed by Mejer[47], Hesselink[48], and Dollan and Edwards[49], combined with "electrostatic" bending energy to derive an approximate expression for the interfacial bending stress of weakly charged surfactant monolayers. The statistical mechanics approach of Ben-Shaul et al.[50] was used by Szleifer et al.[51,52] to develop a molecular theory of the curvature elasticity in surfactant films and monolayers. Barneveld *et al.*[53-55] have applied the self-consistent field lattice approach of Scheutjens and Fleer[56] to develop a numerical scheme for evaluating the spontaneous curvature and the bending elasticity parameters for both bilayers and monolayers of alkyl polyethylene-glycols. Safran[28] developed a simple model for low-density grafted polymer brushes based on stretching and osmotic contributions which was used latter by Paunov *et al*[29] for C_iE_j monolayers at the interface between oil and water. Milner and Witten[30] used SCF to represent the stretching contribution in the energy functional of grafted polymer brushes. Milner[31] and Safran[32] applied this approach with an optimization with respect to the area per molecule at the surface. Clement et.al.[33] has used non local form of density functional to calculate the bending constants of adsorbed polymer layer which gives a different results compared to ref 31 and 32 due to the difference in the density functional form.

Our purpose in this study is to develop a general method for calculation of the spontaneous curvature of amphiphilic diblock copolymers and surfactants, consisting of hydrophilic and hydrophobic blocks, each in contact with the favorable solvent. This is done for an arbitrary form of the free energy density and two different cases: (i) fixed area per molecule at the interface, and (ii) by optimizing the free energy with respect to the area per molecule. We derive general expressions for the bending rigidity, κ, the saddle splay modulus, $\bar{\kappa}$ and the spontaneous curvature H_0 are derived in terms of integral moments of the segments distribution function for a flat interface. We demonstrate that results obtained by other authors can be obtained directly by using this approach.

The known approach given in literature (see ref 34 for more detailed comments and review of the literature) also calculates the bending constants starting from density functional of the theory, but that the results for bending constants are given in terms of moments of flat solution profile and its first curvature expansion in a curved geometry (cylindrical or spherical), thus in order to calculate the bending constants one need to solve the problem in two geometries – flat and curved. This is rather inconvenient for the calculation purpose, because if the analytical flat solution does not exist the curved solution probably also does not exists and making a curvature expansion of this solution is very complicated and must be done for any particular case. What we will show in this chapter is that the first curvature expansion of the density profile could be calculated for **any** *local* density functional in the ***evident*** form provided that this functional satisfies certain boundary conditions and normalization, which leads to expressions for the elastic modulus expressed in the terms of flat solution of the density functional ***only***. Thus for the calculation of the bending constants one needs only flat solution in this case and several moments of it: thus even if we do not know in analytical form the solution we can still calculate numerical one and also to calculate certain moments of it, which immediately will give the values of bending constants.

III.2. Bending constants for the case of constant area per molecule

We assume that we have a system, which has a solid interface (flat or curved), and that we have some property with non-even distribution near the interface (see figure 3.1). We assume that the free energy density functional (DF) of our system has the following form for the case of planar geometry:

$$F = A\int_0^H \Phi(\varphi(x), x)dx \tag{3.1}$$

with following normalizing condition (mass conservation)

$$A\int_0^H \varphi(x)dx = CM \tag{3.2}$$

where, A is total area of the system, C is a constant, Φ is the density of the free energy functional, and $\varphi(x)$ is some local density function, which describes the distribution of the

property of interest, which determines the free energy (e.g. segment density for the case of polymer brush), x is the distance from the interface, where $x=0$, corresponds to flat interface, while H gives the thickness of the layer, M is the total number of "molecules", which density is given with $\varphi(x)$. Thus the last equation is nothing more that mass conservation requirement.

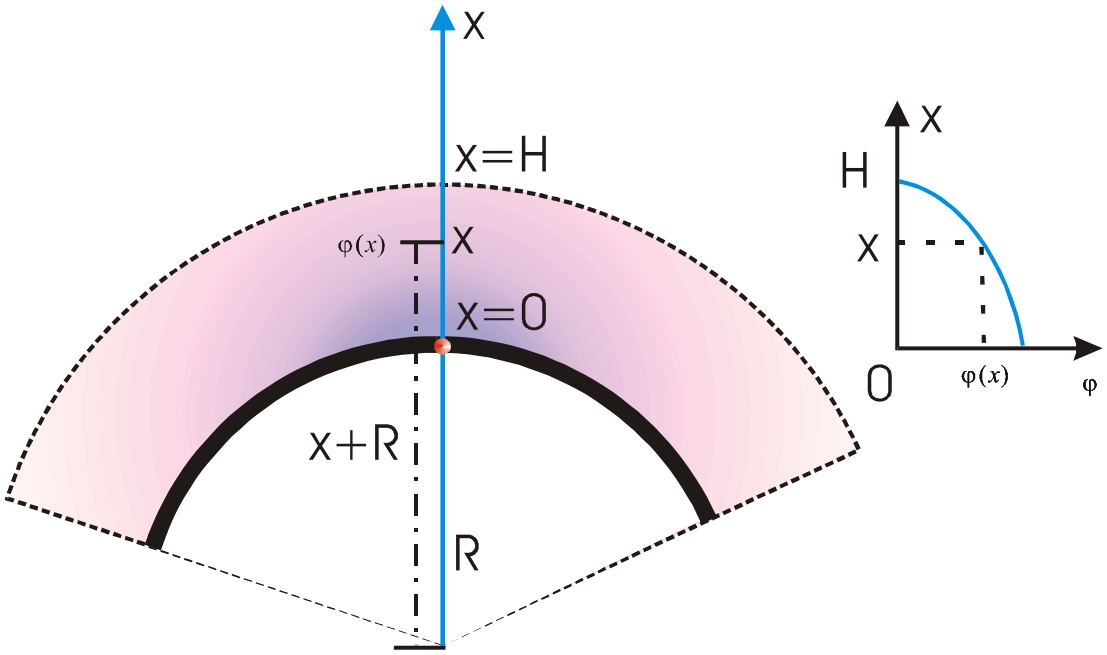

Figure 3.1. Sketch of the system under consideration.

Here we will explicitly assume that our density functional, Φ, is *local*. Which means that at every point (x) the values of the free energy density are determined from the local value of the density distribution $\varphi(x)$, and it does not depend on local derivatives of the density distribution or from the values of the density distribution within surrounding of the point x. We have shown in previous section that the polymer brushes obey this requirement, but the consideration in this part are rather general and they are not restricted only for the case of polymer brushes. They could be applied for *any local* density functional having an *arbitrary form*.

In order to find physical solution the DF given with eq. 3.1 should be minimized taking into account the normalizing condition eq 3.2. The solution of the problem is straightforward

$$\frac{\delta\Phi(\varphi,x)}{\delta\varphi}=\mu=const \tag{3.3}$$

where, μ is the Lagrange multiplier.

Additionally will assume that both free energy density for Φ and density distribution function φ vanish at the end (x=H), i.e.

$$\Phi(\varphi(H), H) = 0 \text{ and we require that } \varphi(H) = 0. \tag{3.4}$$

In the case when both Φ and φ are non zero at the end but are some *given* constants, Φ_0 and φ_0 the problem could be converted to our case by simple introducing an excess properties $\bar{\Phi} = \Phi - \Phi_0$ and $\bar{\varphi} = \varphi - \varphi_0$. Thus the vanishing assumption at the end of the layer of interest is not a restriction provided that we knew the values of the functions and if they do not depend on curvature, which is the most important condition.

Let us now consider the case when we have curved the interface with a given very small radius of curvature R. Then for this case we will assume that the form of the functional Φ does not depend explicitly on the curvature and that the implicit curvature dependence comes from the dependence of the density distribution φ. We have shown that for the case of polymer brushes this is justified assumption for the case of small curvatures. Thus we consider a DF, which has the following form:

$$F = \beta R^{\alpha} \int_0^H \Phi(\varphi(x), x) \left(\frac{R + x}{R} \right)^{\alpha} dx \tag{3.5}$$

with following normalizing condition

$$\beta R^{\alpha} \int_0^H \varphi(x) \left(\frac{R + x}{R} \right)^{\alpha} dx = MC = const \tag{3.6}$$

where, α is the topological index of the interface defined us: $\alpha = 1$, and $\beta = 2\pi L$ for the case of cylindrical interface, while $\alpha = 2$, and $\beta = 4\pi$ for the case of spherical interface. The case when $\alpha = 0$ and $\beta = A$ corresponds to flat solution. By introducing an area per molecule $\sigma = \beta R^{\alpha} / M$ we can rewrite last equation as

$$\sigma \int_0^H \varphi(x) \left(\frac{R + x}{R} \right)^{\alpha} dx = C \tag{3.6b}$$

In this section we will assume that the area per molecule σ is constant with respect of the curvature. In the next section case with varying area per molecule will be considered.

What we like to do now is to make a series expansion of the free energy F per unit area around the point of zero curvature ($1/R \to 0$ i.e. $R \to \infty$):

$$F/\beta R^{\alpha} = \gamma(1/R) = \int_0^{H(1/R)} \Phi(\varphi(x,1/R),x)\left(\frac{R+x}{R}\right)^{\alpha} dx = \gamma(0) + \gamma'(0)/R + \gamma''(0)/(2R^2) \qquad (3.7)$$

in terms of moments of the equilibrium distribution of the density for the case of **flat** interface only! For this reason we will need to perform the differentiation with respect of 1/R for the free energy in order to make a Taylor expansion around the point of zero curvature. We can calculate the first derivative straightforward by taking all implicit and explicit dependences from the curvature:

$$\frac{d\gamma}{d1/R} = \Phi(\varphi(H),H)\frac{dH}{d1/R}\left(\frac{R+H}{R}\right)^{\alpha} + \alpha\int_0^H \Phi(\varphi(x),x)\left(\frac{R+x}{R}\right)^{\alpha-1} xdx + \int_0^H \frac{\delta\Phi}{\delta\varphi}\frac{\partial\varphi}{\partial 1/R}\left(\frac{R+x}{R}\right)^{\alpha} dx \quad (3.8)$$

The first term if RHS of eq. 3.8 is zero due to eq. 3.4. But we are interested to calculate the value of this derivative for the equilibrium profile where we have that $\frac{\delta\Phi}{\delta\varphi} = \mu = const$.

Assuming the density profile is equilibrium, we get:

$$\frac{d\gamma}{d1/R} = \alpha\int_0^H \Phi(\varphi(x),x)\left(\frac{R+x}{R}\right)^{\alpha-1} xdx + \mu\int_0^H \frac{\partial\varphi}{\partial 1/R}\left(\frac{R+x}{R}\right)^{\alpha} dx \qquad (3.9)$$

Where in the last equation we have taken into account that the Lagrange multiplayer μ is independent from the position. The physics here is that Lagrange multiplayer is proportional to the chemical potential of the system, which in equilibrium must be constant throughout the system, thus it could be taken out of the integration routes. Note that the chemical potential depends on the curvature and we will come on this point shortly after.

In order to calculate the implicit dependence of the density profile from the curvature we can differentiate the normalizing condition (eq. 3.6), which gives:

$$\int_0^H \frac{\partial\varphi}{\partial 1/R}\left(\frac{R+x}{R}\right)^{\alpha} dx = -\alpha\int_0^H \varphi\left(\frac{R+x}{R}\right)^{\alpha-1} xdx \qquad (3.10)$$

Where in the last equation we have explicitly assumed that the area per molecule is constant and does not depend on curvature. This is justified for the case of brushes, which are strongly attached at the interface. For the case of liquid/liquid interface this is not true and the variation of the area per molecule should be taken into account. The reason the dependence of

the area per molecule with respect of curvature is due to the fact that the brushes could also be dissolved into the bulk solution and always (curved interface or not) there should exists equilibrium between the interface and the bulk. We will consider in details this case in the next section.

Substituting the last equation in eq 3.9 we finally obtain the first derivative of the free energy:

$$\frac{d\gamma}{d1/R} = \alpha \int_0^H \left(\Phi(\varphi(x), x) - \mu\varphi(x)\right)\left(\frac{R+x}{R}\right)^{\alpha-1} x dx \tag{3.11}$$

The limit of vanishing curvature gives:

$$\gamma'(0) = \alpha \int_0^H \left(\Phi(\varphi(x), x) - \mu\varphi(x)\right) x dx \tag{3.12}$$

Now we can use eq 3.11 to get the expression for the second derivative of the free energy with respect of the curvature. Again all the implicit and explicit dependences of the curvature should be taken into account. Straightforward differentiation of eq 3.11 gives (again we have used that the free energy density vanish at the end of layer and that we have equilibrium profile):

$$\frac{d^2\gamma}{d(1/R)^2} = \alpha(\alpha-1)\int_0^H \left(\Phi(\varphi(x), x) - \mu\varphi(x)\right)\left(\frac{R+x}{R}\right)^{\alpha-2} x^2 dx - \alpha\frac{\partial\mu}{\partial 1/R}\int_0^H \varphi(x)\left(\frac{R+x}{R}\right)^{\alpha-1} x dx . \tag{3.13}$$

In the last equation we have a derivative of the Lagrange multiplier with respect of the curvature. Again we have used that it do not depend on distance from the interface, so its curvature derivative is constant also and could be taken out of the integral. In order to calculate the closed formulas for the free energy expansion we must calculate the derivative of the chemical potential in explicit form. We can do this by differentiating the Lagrange equation for the equilibrium profile (eq. 3.3), which gives, $\frac{\partial\mu}{\partial 1/R} = \frac{\delta^2\Phi}{\delta\varphi^2}\frac{\partial\varphi}{\partial 1/R}$. Where we have used the fact that free energy density implicitly dependent from the curvature, due to explicit dependence of the equilibrium density profile. The last expression could be integrated out in order to have an expression for the chemical potential derivative in terms of the integrals of the equilibrium solution (again the most important was that chemical potential and its derivative are independent on the space coordinate),

$$\frac{\partial\mu}{\partial 1/R}=\frac{\int_0^H\frac{\partial\varphi}{\partial 1/R}\left(\frac{R+x}{R}\right)^{\alpha}dx}{\int_0^H\left(\frac{\delta^2\Phi}{\delta\varphi^2}\right)^{-1}\left(\frac{R+x}{R}\right)^{\alpha}dx}=-\frac{\alpha\int_0^H\varphi\left(\frac{R+x}{R}\right)^{\alpha-1}xdx}{\int_0^H\left(\frac{\delta^2\Phi}{\delta\varphi^2}\right)^{-1}\left(\frac{R+x}{R}\right)^{\alpha}dx} \tag{3.14}$$

This is the main "trick" in this work, which allows us to obtain the closed formulas for the bending constants of the system. Other authors have obtained similar expressions but the implicit expression for the derivative of chemical potential was not presented – and formulas are expressed in terms of the second order expansion of the equilibrium density profile with respect of curvature. What we have demonstrated hire is that this dependence for the case of local DF could be calculated in explicit form. The same trick we will use also in the next section where we will need also a derivatives of the chemical potential with respect of the area per molecule.

Finally substituting the last equation of in the Eq. 3.13 and taking zero curvature limit allows us to obtain the expression for the second curvature expansion:

$$\frac{d^2\gamma}{d(1/R)^2}=\alpha(\alpha-1)\int_0^H\left(\Phi(\varphi(x),x)-\mu\varphi(x)\right)x^2dx+\alpha^2\frac{\left(\int_0^H\varphi xdx\right)^2}{\int_0^H\left(\frac{\delta^2\Phi}{\delta\varphi^2}\right)^{-1}dx} \tag{3.15}$$

Now we have all the expressions, which will allow us to calculate elastic constants of our system. We will use well-known Helfrich[43] expression for the free energy of the system expanded in power of curvature. We would like to note that the correct Helfrich[43] expression is given not for the free energy per unit area, but for the free energy per molecule, which differ by factor of area per molecule. For the case of constant area per molecules this is not important difference, but when the area per molecule varies with curvature, the expansions of free energy per molecule and free energy per unit are differ in the second term containing the curvature (assuming that factor area per molecule is already taken into account). This will be considered in details in the next paragraph. Here we will use the Helfrich expression for the case of constant area per molecule, which in this case is:

$$f=f_0-\alpha H\kappa/R+\alpha\left(2(\alpha-1)\bar{\kappa}+\alpha\kappa\right)/(2R^2) \tag{3.16}$$

where, H_0 is spontaneous curvature, κ is bending (or Gaussian) elasticity modulus, which determines the free energy cost for bending the interface, and $\bar{\kappa}$, is so called saddle- splay modulus determining the cost of saddle like deformations (torsions) (see figure 3.2). Spontaneous curvature could be either positive or negative and describes the tendency of the interface to bend in a given direction. For the case of di-block polymer (surfactant) in oil/water solution spontaneous curvature determines a tendency of the interface bends either to water or to oil phase (see figure 3.2). This is extremely important for the properties of microemulsion and determines which type of emulsion will form – either oil in water or water in oil.

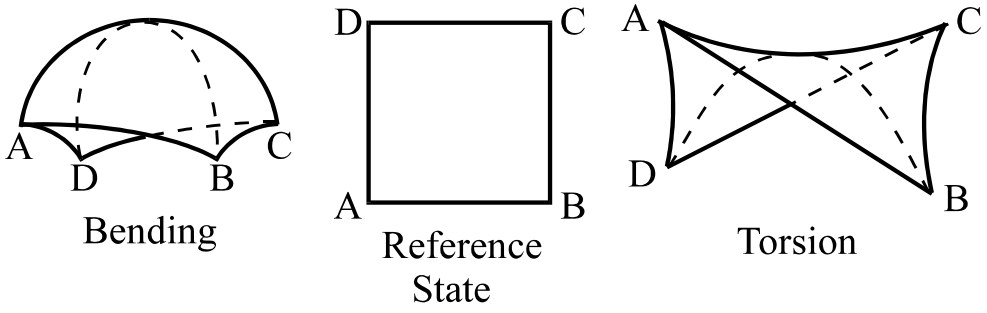

Figure 3.2. Different types of deformation of the interface.

By direct comparison of eq. 3.16 with eq. 3.7 with use of eq. 3.12 and 3.15 we immediately could recognize corresponding elastic constant of the system:

$$\kappa = I_1 = \frac{\left(\int_0^H \varphi x dx\right)^2}{\int_0^H \left(\frac{\delta^2 \Phi}{\delta \varphi^2}\right)^{-1} dx} \tag{3.17}$$

$$H_0 = \frac{1}{2}\frac{I_2}{I_1} = \frac{1}{2}\frac{\int_0^H \left(\frac{\delta^2 \Phi}{\delta \varphi^2}\right)^{-1} dx}{\left(\int_0^H \varphi x dx\right)^2} \int_0^H \left(\mu\varphi(x) - \Phi(\varphi(x), x)\right) x dx \tag{3.18}$$

where,

$$I_2 = \int_0^H \left(\mu\varphi(x) - \Phi(\varphi(x), x)\right) x dx\,. \tag{3.19}$$

It could be shown that in order that we have a physical solution of our system we must have $I_2 > 0$, which means that for the case of single brush the spontaneous curvature is always positive, thus the system will try to bend in the opposite direction to the brush in order to lower the segment volume fraction. For splay modulus we have:

$$\bar{\kappa} = I_3 = \int_0^H \left(\Phi(\varphi(x), x) - \mu\varphi(x)\right) x^2 dx \,. \tag{3.20}$$

The usefulness of Eq. 3.17,3.18 and 3.20 is that we have expressed the curvature, and elastic moduli of the system as a moments of the flat profile distribution: thus we will do not need to solve the DFT in different geometries in order to calculate the respective moduli and spontaneous curvature.

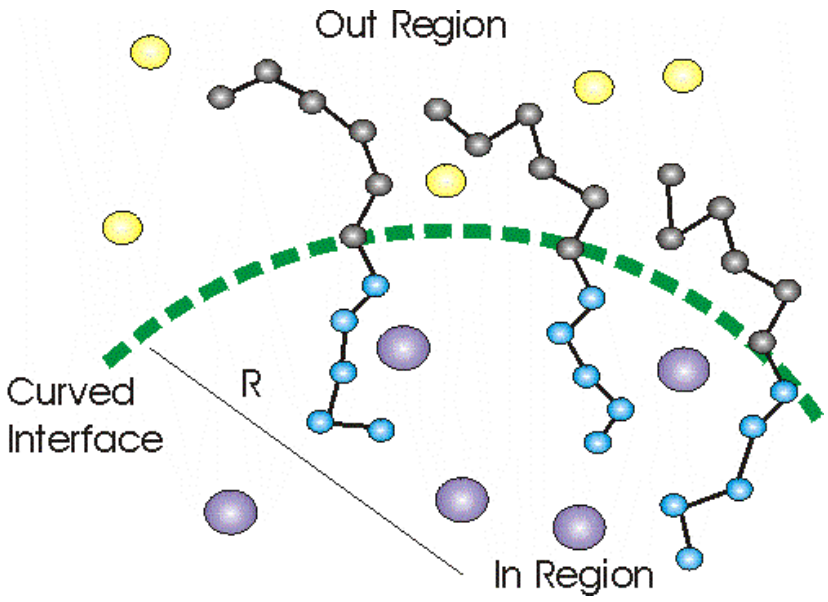

Figure 3.3. Di-block polymer brush (surfactant) adsorbed on the curved interface. The outer brush is expanded due to the curvature while the inner one is compressed.

Consider now that we have two distributions (φ^{out}, φ^{in}) on the both sides of the interface (see figure 3.3) determined from two functionals Q^{out} and Q^{in} having the same properties like the previous part. This case corresponds to a strongly adsorbed (in order that the area per molecule do not change with curvature) di-block polymer or surfactant. In this case hen we can very easy to get the formulas for the corresponding moduli of the interface, by simply summing the contributions from both layers. The only thing one should do is to replace *x* by –

x in all the space integrals for the inner layer. It could be easily shown that the latter change is equivalent to change of the curvature sign in inner layer. So the even powers of free energy expanding by $1/R$ will remain intact and the contributions from both layers should be summed in the final expression of the system free energy, while the odd powers will change their sign and should be subtracted. Then it is straightforward to shown that we will have following expression for the elastic constants of the system containing di-block polymer (surfactant):

$$\kappa = I_1^{out} + I_1^{in}$$
$$\overline{\kappa} = I_3^{out} + I_3^{in} \qquad (3.21)$$
$$H_0 = \frac{1}{2}\frac{I_2^{out} - I_2^{in}}{I_1^{out} + I_1^{in}}$$

Where we have assumed the spontaneous curvature is positive when the interface is curved to the inner part. The main difference compared to the case of single brush is that in this case the spontaneous curvature could change its sign, depending on the values of I_2^{out} and I_2^{in}. Thus depending on the properties of both parts of surfactant one could have either oil in water or water in oil emulsion. We can also get a very simple expression for the "lamellar" condition (zero spontaneous curvature) of the layer, which is:

$$I_2^{out} = I_2^{in}. \qquad (3.22)$$

III.2. Variation of the surface area with respect of the curvature

In the previous section we have done the free energy expansion with respect of the curvature assuming that the area per molecule remains constant when curvature changes. The last is true only for the case of very strongly attached molecules. But in many cases the area per molecule varies with curvature and this variation should be taken into account in energy expansion. The reason for this variation is that our system also trying to minimize the total free energy, with respect of the total interfacial area. Thus for a given curvature the area per molecule will be one, which minimizes the free energy. Physically this change occurs by adsorption or desorption of the molecules from the interface. Thus the interfacial area is also

parameter, which must be taken into account when the free energy of the system is minimized.

When we have a liquid/liquid interface total free energy could be written as:

$$F = \gamma_L A + AF_{molecules} + F_{surface\_translation} \tag{3.23}$$

where, γ_L is the interfacial surface tension of the bare liquid-liquid interface, $F_{molecules}$ is the free energy of the molecules given with eq. 3.23, and $F_{surface\_translation} / M = kT \ln A_d / \sigma$ - is the translation entropy of per molecule, and A_d is the area per junction group. The last term does not account for internal degrees of freedom of molecules, which are taken into account in the second term. We will assume that the latter term could be neglected with respect of first two. As we will show in the chapter V and VI of the thesis the latter assumption is equivalent to assume that total interfacial tension of the system is very low i.e. we are in micro-emulsion region. For the general case when the total interfacial tension is non-zero one can still use this approach, and have same formulas for the bending constants, but the expression for the area per molecule of flat interface should be corrected. We will come to this point later.

Minimizing the total free energy with respect of total area A is equivalent to minimize the free energy per molecule with respect of the area per molecule (while the total number of molecules is kept constant). For the sake of convenience we will work with free energy per molecule. Assuming that we have done already the expansion of the free energy with respect of curvature (at constant area per molecule), now we should additionally minimize the free energy with respect of area per molecule, while keeping the curvature constant in order to find a total minimum of the free energy of the system. The latter is possible due to the independence of the equilibrium state from the way it is reached. Taking the form of the free energy per molecule abstained in previous section (we simply should divide free energy expression by total number of molecules M at the interface) we have that

$$f = \gamma_0(\sigma) + \gamma_1(\sigma)/R + \gamma_2(\sigma)/R^2 \tag{3.24}$$

where, $\gamma_0(\sigma) = \gamma_L \sigma + \gamma(0,\sigma)\sigma$, $\gamma_1(\sigma) = \gamma'(0,\sigma)\sigma$, $\gamma_2(\sigma) = \gamma''(0,\sigma)\sigma/2$ are the energy expansion derived in the last section. We have added the symbol σ in order to stress that the latter expansion was done while keeping total area per molecule constant. What we would like to do now is to minimize the expanded form of free energy with respect of the area per

molecule. The minimum condition is, $\left.\frac{\partial f}{\partial \sigma}\right|_{\sigma_o^R} = 0$, wherefrom by solving this equation, the value σ_0^R of the area per molecule, which minimizes the energy, could be obtained. Note that the latter value depends from the curvature of the interface. We can also introduce, σ_0 which is the value of the area per molecule, which minimizes the free energy for the case of flat interface, and we could expand $\sigma_o^R = \sigma_0 + \Delta / R + O(1/R^2) \approx \sigma_0 + \Delta / R$ up to the first order terms. Substituting the last equation into the minimum conditions gives[28,32]:

$$\left.\frac{\partial \gamma_0}{\partial \sigma}\right|_{\sigma_0^R} + \left.\frac{\partial \gamma_1}{\partial \sigma}\right|_{\sigma_0^R} \frac{1}{R} + \left.\frac{\partial \gamma_2}{\partial \sigma}\right|_{\sigma_0^R} \frac{1}{R^2} \approx \left.\frac{\partial \gamma_0}{\partial \sigma}\right|_{\sigma_0} + \left(\left.\frac{\partial \gamma_1}{\partial \sigma}\right|_{\sigma_0} + \left.\frac{\partial^2 \gamma_0}{\partial \sigma^2}\right|_{\sigma_0} \Delta \right) \frac{1}{R} + O(1/R^2) = 0 . \qquad (3.25)$$

The letter equation gives the minimizing condition expanded around flat interface keeping the only the first order term with respect of 1/*R*. The last equation could be regarded as a polynomial of powers of 1/*R* and in order that this polynomial is zero for any value of *R*, all its coefficients must be zero, thus we must have (up to the first orders of expansion):

$$\left.\frac{\partial \gamma_0}{\partial \sigma}\right|_{\sigma_0^R} = \gamma_L + \gamma(0,\sigma_0) + \sigma_0 \left.\frac{\partial \gamma(\sigma,0)}{\partial \sigma}\right|_{\sigma_0} = 0 \text{ and } \Delta = -\left.\frac{\partial \gamma_1}{\partial \sigma}\right|_{\sigma_0} \left(\left.\frac{\partial^2 \gamma_0}{\partial \sigma^2}\right|_{\sigma_0} \right)^{-1} . \qquad (3.26)$$

Again like in the previous case we can immediately calculate all the derivatives of the respective functional, which enter in the equations:

$$\gamma(0,\sigma_0) = \int_0^H \Phi(\varphi(x),x)dx \,,\; \sigma_0 \left.\frac{\partial \gamma(\sigma,0)}{\partial \sigma}\right|_{\sigma_0} = \sigma_0 \int_0^H \frac{\delta \Phi}{\delta \varphi} \frac{\partial \varphi}{\partial \sigma} dx = \mu \sigma_0 \int_0^H \frac{\partial \varphi}{\partial \sigma} dx . \qquad (3.27)$$

Where we have used that:

(i) all the values are calculated for the case of the equilibrium density profile, which is solution of the Lagrange equation

(ii) the free energy density, Φ, has no explicit dependence from area per molecule and the implicit dependence comes form the density distribution φ

(iii) both free energy density and density distributions vanish at the end of the layer at *x*=*H*.

The straightforward differentiation of eq. 3.6b with respect of σ (while setting R to infinity) gives that $\sigma\int_0^H \frac{\partial\varphi}{\partial\sigma}dx = -\int_0^H \varphi dx$, which substituted back into eq. 3.27 gives $\left.\frac{\partial\gamma(\sigma,0)}{\partial\sigma}\right|_{\sigma_0} = -\mu\int_0^H \varphi dx$. If we substitute the last expression into eq. 3.26 we get an expression for the surface tension of the flat interface:

$$\left.\frac{\partial\gamma_0}{\partial\sigma}\right|_{\sigma_0^R} = \gamma_L + \int_0^H \left[\Phi(\varphi(x),x) - \mu\varphi(x)\right]dx = 0 \ . \tag{3.28a}$$

Wherefrom we can calculate the value of the area per molecule, which minimizes the free energy, by simply inverting the last equation. The last equation actually says that the total surface tension of the system is zero, which is consequence from the fact that we have neglected the translation degrees of the polymer chain. If we would like to have a non- zero interfacial tension, one should substitute the value of the interfacial tension into the left side of eq 3.28, provided that this value corresponds to the equilibrium values of adsorption and bulk concentration of surfactant. We will discuss this point in more details into the next chapter. The last equation could be also rearranged into the following manner

$$\gamma_0(\sigma_0) = \sigma_0\gamma_L + \sigma_0\int_0^H \Phi(\varphi(x),x)dx = \sigma_0\mu\int_0^H \varphi(x)dx \ . \tag{3.28b}$$

The second derivative of the zero order expansion of the free energy could be calculated also straightforward:

$$\left.\frac{\partial^2\gamma_0}{\partial\sigma^2}\right|_{\sigma_0} = \frac{\partial}{\partial\sigma}\left[\gamma_L + \int_0^H \left[\Phi(\varphi(x),x) - \mu\varphi(x)\right]dx\right] = -\frac{\partial\mu}{\partial\sigma}\int_0^H \varphi(x)dx \tag{3.29}$$

The derivative of the Lagrange multiplier with respect of the area per molecule could be calculated in the same manner like in the previous section:

$$\frac{\partial\mu}{\partial\sigma} = \frac{\int_0^H \frac{\partial\varphi}{\partial\sigma}dx}{\int_0^H \left(\frac{\delta^2\Phi}{\delta\varphi^2}\right)^{-1}dx} = -\frac{\int_0^H \varphi dx}{\sigma_0\int_0^H \left(\frac{\delta^2\Phi}{\delta\varphi^2}\right)^{-1}dx} \ . \tag{3.30}$$

Which allows us to get the closed form for second derivative of the zero order term of the free energy,

$$\left.\frac{\partial^2\gamma_0}{\partial\sigma^2}\right|_{\sigma_0} = \frac{\left[\int_0^H \varphi dx\right]^2}{\sigma_0\int_0^H\left(\frac{\delta^2\Phi}{\delta\varphi^2}\right)^{-1}dx} \tag{3.31}$$

The first derivative with respect of the area per molecule of the first order free energy expansion could be calculated also directly using the same procedure

$$\left.\frac{\partial\gamma_1}{\partial\sigma}\right|_{\sigma_0} = \frac{\partial}{\partial\sigma}\left(\sigma\alpha\int_0^H\left(\Phi(\varphi(x),x)-\mu\varphi(x)\right)xdx\right) = \alpha\int_0^H\left(\Phi(\varphi(x),x)-\mu\varphi(x)\right)xdx - \sigma\alpha\frac{\partial\mu}{\partial\sigma}\int_0^H\varphi(x)xdx \tag{3.32}$$

Note how important is that the structure of the last equation is such, that cancels out all the terms, which contain σ derivatives of Φ and φ, integrated with respect of xdx. The latter is extremely important because such an integrals could be not expressed as moments of the equilibrium flat distribution in a general form, rather one should keep them and evaluate them knowing the real solution! But as we could see those terms are exactly compensating each so they cancel into the final form of equation. Substituting again the derivate of Lagrange multiplier we get that:

$$\left.\frac{\partial\gamma_1}{\partial\sigma}\right|_{\sigma_0} = \alpha\int_0^H\left(\Phi(\varphi(x),x)-\mu\varphi(x)\right)xdx + \alpha\frac{\left[\int_0^H\varphi dx\right]\left[\int_0^H\varphi(x)xdx\right]}{\int_0^H\left(\frac{\delta^2\Phi}{\delta\varphi^2}\right)^{-1}dx} \tag{3.33}$$

Substituting this back gives expression for the expansion of the area per molecule

$$\Delta = -\alpha\sigma_0\left\{\frac{\int_0^H\left(\frac{\delta^2\Phi}{\delta\varphi^2}\right)^{-1}dx}{\left[\int_0^H\varphi dx\right]^2}\int_0^H\left(\Phi(\varphi(x),x)-\mu\varphi(x)\right)xdx + \frac{\int_0^H\varphi(x)xdx}{\int_0^H\varphi dx}\right\} \tag{3.34}$$

The later could be substituted back into the free energy expansion to get final form of the minimized free energy per molecule, wherefrom all the elastic constants could be calculated:

$$\begin{aligned} f &= \gamma_0(\sigma_0^R)+\gamma_1(\sigma_0^R)/R+\gamma_2(\sigma_0^R)/R^2 = \\ &= \gamma_0(\sigma_0)+\left\{\gamma_1(\sigma_0)+\Delta\left.\frac{\partial\gamma_0(\sigma)}{\partial\sigma}\right|_{\sigma_0}\right\}/R+\left\{\gamma_2(\sigma_0)+\Delta\left.\frac{\partial\gamma_1(\sigma)}{\partial\sigma}\right|_{\sigma_0}+\frac{\Delta^2}{2}\left.\frac{\partial\gamma_0(\sigma)}{\partial\sigma}\right|_{\sigma_0}\right\}/R^2 \end{aligned} \tag{3.35}$$

By substituting the value for Δ given with eq 3.34 we get:

$$f = \gamma_0(\sigma_0) + \gamma_1(\sigma_0)/R + \left\{ \gamma_2(\sigma_0) - \frac{\Delta^2}{2} \frac{\partial \gamma_0(\sigma)}{\partial \sigma}\bigg|_{\sigma_0} \right\} / R^2 \tag{3.36}$$

Expressing everything with terms of integrals defined in the previous section we finally have that:

$$f = \mu C - \alpha \sigma_0 I_2 / R + \alpha \sigma_0 \left\{ (\alpha - 1) I_3 + \alpha I_1 - \alpha I_1 \left(1 - \frac{I_2 I_4 \sigma_0}{C I_1} \right)^2 \right\} / (2R^2) \tag{3.37}$$

where the area per molecule which is minimizing the free energy is determined from the condition;

$$\gamma_L = I_0 = \int_0^H \left[\mu \varphi(x) - \Phi(\varphi(x), x) \right] dx \tag{3.38}$$

The direct comparison with the Helfich formula (eq. 3.16) immediately gives the closed forms of for all tree elastic constants.

$$\kappa = I_1 \left\{ 1 - \left(1 - \frac{I_2 I_4 \sigma_0}{C I_1} \right)^2 \right\} = \frac{I_2 I_4 \sigma_0}{C} \left(2 - \frac{I_2 I_4 \sigma_0}{C I_1} \right) \tag{3.39}$$

$$H_0 = \frac{C}{2 I_4 \sigma_0 \left(2 - \frac{I_2 I_4 \sigma_0}{I_1 C} \right)}$$

$$\bar{\kappa} = I_3$$

We have also introduced the notation:

$$I_4 = \int_0^H \varphi(x) x dx \,.\; \bar{\kappa} = I_3 \tag{3.40}$$

The generalization for the case of di-block polymer adsorbed on both sides of the interface is straightforward using the same motivation like in the previous section. Here we will give only the final results for the free energy:

$$\frac{\partial^2 \gamma^{tot}_0}{\partial \sigma^2}\bigg|_{\sigma_0} = \frac{1}{\sigma^3_0} \left\{ \frac{C_{in}^2 I_1^{in}}{\left(I_4^{in} \right)^2} + \frac{C_{out}^2 I_1^{out}}{\left(I_4^{out} \right)^2} \right\}, \quad \frac{1}{\alpha} \frac{\partial \gamma^{tot}_1}{\partial \sigma}\bigg|_{\sigma_0} = I_2^{in} - I_2^{out} + \frac{1}{\sigma_0} \left(\frac{C_{out} I_1^{out}}{I_4^{out}} - \frac{C_{in} I_1^{in}}{I_4^{in}} \right) \tag{3.41}$$

$$\frac{\left.\frac{\partial \gamma^{tot}{}_1}{\partial \sigma}\right|_{\sigma_0}}{2\left.\frac{\partial^2 \gamma^{tot}{}_0}{\partial \sigma^2}\right|_{\sigma_0}} = \frac{\alpha^2 \sigma_0 \left\{\left[I_2^{out} - I_2^{in}\right] I_4^{out} I_4^{in} \sigma_0 + \left(C_{in} I_1^{in} I_4^{out} - C_{out} I_1^{out} I_4^{in}\right)\right\}^2}{2\left\{C_{in}^2 I_1^{in} \left(I_4^{out}\right)^2 + C_{out}^2 I_1^{out} \left(I_4^{in}\right)^2\right\}} \tag{3.42}$$

$$f = \mu_{out} C_{out} + \mu_{in} C_{in} - \alpha\sigma_0 \left(I_2^{out} - I_2^{in}\right)/R +$$

$$+\alpha\sigma_0 \left\{(\alpha - 1)(I_3^{out} + I_3^{in}) + \alpha\left[(I_1^{out} + I_1^{in}) - \frac{\left\{\left[I_2^{out} - I_2^{in}\right] I_4^{out} I_4^{in} \sigma_0 + \left(C_{in} I_1^{in} I_4^{out} - C_{out} I_1^{out} I_4^{in}\right)\right\}^2}{\left\{C_{in}^2 I_1^{in} \left(I_4^{out}\right)^2 + C_{out}^2 I_1^{out} \left(I_4^{in}\right)^2\right\}}\right]\right\}/(2R^2) \tag{3.43}$$

Which give immediately the values for all modulus:

$$\kappa = \frac{(C_{out}/I_4^{out} + C_{in}/I_4^{in})^2 I_1^{in} I_1^{out} + \sigma_0\left[I_2^{out} - I_2^{in}\right]\left\{2\left(I_1^{out} C_{out}/I_4^{out} - I_1^{in} C_{in}/I_4^{in}\right) - \sigma_0\left[I_2^{out} - I_2^{in}\right]\right\}}{\left\{I_1^{in}\left(C_{in}/I_4^{in}\right)^2 + I_1^{out}\left(C_{out}/I_4^{out}\right)^2\right\}}$$

$$\bar{\kappa} = I_3^{out} + I_3^{in} \tag{3.44}$$

$$H_0 = \frac{1}{2}\frac{I_2^{out} - I_2^{in}}{\kappa}$$

where equilibrium area per molecule is given with $\gamma_L = I_0^{in} + I_0^{out}$

After some rearrangements we can get another expression for

$$\kappa = \frac{\left[P^{out} I_2^{out}/I_1^{out} + P^{in} I_2^{in}/I_1^{in}\right]^2 I_1^{in} I_1^{out} + \left[I_2^{out} - I_2^{in}\right]\left[(2P^{out} - 1) I_2^{out} - (2P^{in} - 1) I_2^{in}\right]}{\left[(I_2^{in} P^{in})^2/I_1^{in} + (I_2^{out} P^{out})^2/I_1^{out}\right]} \tag{3.45}$$

The reason for writhing terms in this form is that $P^s = C^s I^s{}_1/(\sigma_0 I^s{}_4 I^s{}_2)$ (where $s \in \{in, out\}$) is dimensionless constant!

Note that similar approach could be applied for non-local DF, which depends also on the derivatives of the volume fraction (like Guinsburg Landau type of functionals). One should take into account that in this case the DF will have an explicit dependence of the curvature, which makes the considerations more difficult. In this case the equations obtained in this part could be used like a first rough estimate of the elastic constants of non local DF theories. Provided that following functional derivative replacement is done

$$\frac{\delta\Phi(\varphi(x), x, \varphi^k(x))}{\delta\varphi(x)} \rightarrow \frac{\delta\Phi(\varphi(x), x, \varphi^k(x))}{\delta\varphi(x)} + (-1)^k \frac{\partial^k}{\partial x^k}\frac{\delta\Phi(\varphi(x), x, \varphi^k(x))}{\delta\varphi^k}. \tag{4.46}$$

Another necessary restrictions are: (i) the density functional must vanish in the same point where the density function vanish, and (ii) we must have corresponding conservation of matter condition. The detailed investigation of the surface elastic properties of non-local DF theories is out of scope of current research. One could find more details for this case in the works of Oversteegen[55].

The main advantage of the above outlined approach is that it is extremely useful for the case when one could not find an analytic solution of his problem, but numerical one still exists. In this case the above formulas are providing necessary moments of density distributions, which are needed to calculate numerically the values of all curvature modulus.

Although we do not needed in this part the derivative of the layer thickness with respect of the curvature, $\frac{\partial H}{\partial 1/R}$, we could also very easy calculate it. We start with the vanishing condition for the density distribution at the end of the layer:

$$\varphi(H(1/R),1/R)=0 \tag{3.47}$$

which should be true for any value of curvature $1/R$. By taking the derivative with respect of $1/R$ we get:

$$\left.\frac{\partial\varphi}{\partial x}\right|_{x=H}\frac{\partial H}{\partial 1/R}+\left.\frac{\partial\varphi}{\partial 1/R}\right|_{x=H}=0 \tag{3.48}$$

Note that strictly speaking both terms could be singular (and they actually are in all of the cases when polymer brushes are considered) but this singularity will be removed latter on. We can differentiate also Lagrange equation of DFT with respect of x and calculate its value at $x=H$.

$$\frac{\delta\Phi^2}{\delta\varphi^2}\frac{\partial\varphi}{\partial x}+\frac{\delta}{\delta\varphi}\frac{\partial\Phi}{\partial x}=0\ . \tag{3.49}$$

By multiplying the last equation by $\frac{\partial\varphi}{\partial 1/R}$ and recognizing that $\frac{\partial\mu}{\partial 1/R}=\frac{\delta^2\Phi}{\delta\varphi^2}\frac{\partial\varphi}{\partial 1/R}$ we get: $\frac{\partial\mu}{\partial 1/R}\frac{\partial\varphi}{\partial x}+\frac{\partial\varphi}{\partial 1/R}\frac{\delta}{\delta\varphi}\frac{\partial\Phi}{\partial x}=0$, which substituted back in the first equation gives (after multiplication by $\frac{\partial\mu}{\partial 1/R}$) :

$$\left.\frac{\partial\varphi}{\partial x}\right|_{x=H}\left(-\frac{\delta}{\delta\varphi}\left.\frac{\partial\Phi}{\partial x}\right|_{x=H}\frac{\partial H}{\partial 1/R}+\frac{\partial\mu}{\partial 1/R}\right)=0\,. \tag{3.50}$$

So we manage to factor the singularity out, which finally gives

$$\left.\frac{\delta}{\delta\varphi}\frac{\partial\Phi}{\partial x}\right|_{x=H}\left.\frac{\partial H}{\partial 1/R}\right|_{1/R=0}=-\frac{\alpha\int_0^H\varphi x dx}{\int_0^H\left(\frac{\delta^2\Phi}{\delta\varphi^2}\right)^{-1}dx}\,. \tag{3.51}$$

The latter equation is valid for the case of constant area per molecule. Similar approach could be applied for calculating the curvature dependence of the layer thickness when the area per molecule is function of the curvature.

III.3. Same simple applications – Grafted polymer brushes

We have shown in previous chapter that for the case of polymer brushes grafted on the flat interface the SCF theory gives:

$$\Phi(\varphi(x),x)=\frac{kT}{v_0}\left\{\frac{v_0}{v_w}\left[(1-\varphi(x))\ln(1-\varphi(x))+\chi\varphi(x)(1-\varphi(x))\right]+K_s x^2\varphi(x)\right\} \tag{3.52}$$

where $K_s=\frac{3\pi^2}{8N^2l^2}$ is the elastic constant, N is degree of polymerization, v_0 is the volume of the polymer segment, v_w is the volume of the solvent molecule, χ is the Flory – Huggins parameter of interaction between polymer monomer and solvent molecule, l is the Kuhn length of polymer segment and φ is the volume fraction of polymer segments. We have also a normalizing conditions which is:

$$\sigma\int_0^H\varphi(x)dx=C=Nv_0 \tag{3.53}$$

where, $\sigma=A/M$ is the area per polymer molecules and M is the total number of polymers in the system while A is the total area of the layer. We will use the approach described in the previous section to calculate the bending elasticity moduli and spontaneous curvature of the system.

We have also shown that for the case of curved interface the free energy density does not have explicit dependence on the curvature. So we see that the outlined approach in the previous section could be directly applied for the case of polymer brushes.

III.3.1 Very low volume fractions case

For the case of small volume fractions the logarithmic term in eq. 3.52 could be expanded in series of φ up to the second order. In this case DFT could be expressed as:

$$\Phi(\varphi(x),x)=\frac{kT}{v_0}\left\{\frac{1}{2}w\varphi(x)^2+K_s x^2\varphi(x)\right\} \tag{3.54}$$

where, $w=\frac{v_0}{v_m}(1-2\chi)$ is the second virial coefficient. Note that this quantity is dimensionless, in some cases it is more convent to work with dimensional viral coefficient which is defined as $B=wv_0=\frac{v_0^2}{v_m}(1-2\chi)$. Note also that there is a linear term in the DF, $\frac{v_0}{v_m}(\chi-1)\varphi(x)$, which could be omitted due to the normalizing condition, because it integrates to and does not contribute to the elastic constants of the interface.

The solution of DFT in this case is straightforward:

$$\frac{\delta\Phi}{\delta\varphi}=\frac{kT}{v_0}\left(w\varphi(x)+K_s x^2\right)=\mu=\frac{kT}{v_0}K_s H^2,\ \varphi(x)=K_s(H^2-x^2)/w \tag{3.55a}$$

Wherefrom we can calculate all moments, which we need for the calculation of the elastic constants:

$$\int_0^H\varphi(x)dx=\frac{2K_sH^3}{3w}=\frac{Nv_0}{\sigma} \tag{3.55b}$$

and the brush thickness

$$H=\left(\frac{3wv_0N}{2K_s\sigma}\right)^{1/3}. \tag{3.55c}$$

Then the calculation of the moments is also matter of pure algebra

$$,\left(\int_0^H\varphi(x)xdx\right)^2=\left(\frac{K_sH^4}{4w}\right)^2=\frac{K_s{}^2H^8}{16w^2}$$

$$\mu\varphi(x)-\Phi(\varphi(x),x)=\frac{kT}{v_0}B\varphi(x)^2/2\,,\ \frac{\delta^2\Phi}{\delta\varphi^2}=\frac{kT}{v_0}w\,,\ \int_0^H\left(\frac{\delta^2\Phi}{\delta\varphi^2}\right)^{-1}dx=\frac{v_0H}{kTw}$$

$$I_0=\frac{4kTK_s^{\,2}H^5}{15v_0w}=\gamma_L$$

$$I_1=\frac{kTK_s^{\,2}H^7}{16v_0w}$$

$$I_2=\int_0^H\left(\mu\varphi(x)-\Phi(\varphi(x),x)\right)xdx=\frac{kTK_s^{\,2}H^6}{12v_0w}$$

$$I_3=-\int_0^H\left(\mu\varphi(x)-\Phi(\varphi(x),x)\right)x^2dx=-\frac{4kTK_s^{\,2}H^7}{105v_0w}$$

$$I_4=\frac{K_sH^4}{4w}\,. \qquad (3.55d)$$

After substitution of these algebraic expressions into eqs. 3.21, we get the values of the elastic constants of a single polymer brush having constant area per molecule:

$$\kappa=\frac{kTK_s^{\,2}H^7}{16v_0w}\,,\ \bar{\kappa}=-\frac{4kTK_s^{\,2}H^7}{105v_0w}\,,\ \kappa/\bar{\kappa}=-105/64\,,\ H_0=\frac{2}{3H}\,. \qquad (3.56)$$

One can substitute expression for H in order to get all moduli in terms of the parameters of the model as well.

For the case when area per molecule is adjusted (eqs 3.44) we have $\frac{CI_1}{I_2I_4\sigma_0}=\frac{v_0NI_1}{I_2I_4\sigma_0}=2$ thus one gets a correction for $\kappa_{adj}=\frac{3}{4}\kappa_{non\_adjust}$. The latter result is obtained by Milner et. al.[31] and Safran et. al.[32] For the case of mixtures we have

$$\kappa=\frac{4(I_2^{out}/I_1^{out}+I_2^{in}/I_1^{in})^2I_1^{in}I_1^{out}+3\left[I_2^{out}-I_2^{in}\right]^2}{4\left\{(I_2^{in})^2/I_1^{in}+(I_2^{out})^2/I_1^{out}\right\}} \qquad (3.57)$$

For the case of one chain grafted on the interface, with adjusted area per molecule we have, $I_0=\frac{4kTK_s^{\,2}H^5}{15v_0w}$. By using eq. 3.55c we can remove H in order to we have

$$I_0=\frac{kT}{5}\left(\frac{\sqrt{2K_s}\,3N^{5/2}v_0w}{\sigma_0^{\,5/2}}\right)^{2/3}=\frac{3kTN}{5\sigma_0^{\,5/3}}\left(\frac{\pi v_0^{\,2}(1-2\chi)}{2lv_m}\right)^{2/3}=\gamma_L \qquad (3.58)$$

Where from we could derive the following expression for the area per molecule:

$$\sigma_0 = \left(\frac{3kT}{5\gamma_L}\right)^{3/5} \left(\frac{\pi v_0^{\,2} N^{3/2}(1-2\chi)}{2lv_m}\right)^{2/5} \tag{3.59}$$

If we assume that we have a system with two type of brushes grafted on both side of the interface, by using eq. 3.22 (after substituting the expression for *H*, eq 3.55c) we get the condition for the "lamellar" regime (zero spontaneous curvature):

$$w_{out} N^2{}_{out} = w_{in} N^2{}_{in} \tag{3.60}$$

A similar result was obtained also by Paunov et. al.[29] , but due to the different value of brush elastic constant K_s, which was used in ref 29 (instead of SCF value $K_s = \frac{3\pi^2}{8N^2l^2}$ they have used value proposed by deGennes[21] and Safran[28] $K_s = \frac{1}{2N^2l^2}$), there is numerical differences between our and their expression. In order to correct their results, one must multiply the expressions for κ and $\bar{\kappa}$ obtained in their article by factor $2/\sqrt[3]{3\pi^2} \approx 0.65$, while the spontaneous curvature should be dived by this value, which gives about 1.5 higher values. Their criteria for zero spontaneous curvature (or Phase Inversion Temperature (PIT)) does not depend on the definition of the elastic constant of the brush, K_s, because numerical factor cancels out when spontaneous curvature is 0.

Another interesting conclusion from Eq. 3.60 is that within this model the PIT criteria does not depend on the area per molecule (adsorption), and it depends only on the interaction between chain and solvent (*w*) and on the chain length (*N*).

III.3.2. Θ solvent ($\chi = 1/2$) and low volume fractions

In this case $\chi = 1/2$ and $w = \frac{v_0}{v_m}(1-2\chi) = 0$, so the quadratic part of the DFT is zero and one needs to take into account higher order term in the expansion of logarithmic term. So the DF has the following form:

$$\Phi(\varphi(x), x) = \frac{kT}{v_0}\left\{\frac{1}{3}w_1\varphi(x)^3 + K_s x^2 \varphi(x)\right\} \tag{3.61}$$

where, $w_1 = \frac{1}{2}\frac{v_0}{v_w}$. Linear term with respect of volume fraction again could be neglected. The solution of DF in this case is:

$$\frac{\delta\Phi}{\delta\varphi} = \frac{kT}{v_0}\left(w_1\varphi(x)^2 + K_s x^2\right) = \mu = \frac{kT}{v_0}K_s H^2,\ \varphi(x) = \sqrt{K_s(H^2 - x^2)/w_1} \qquad (3.62a)$$

Using the solution we can calculate all the moments we need for the calculation of the elastic constants:

$$\int_0^H \varphi(x)dx = \sqrt{\frac{K_s}{w_1}}\frac{\pi H^2}{4} = \frac{Nv_0}{\sigma},\ H = 2\left(\frac{w_1}{K_s}\right)^{1/4}\left(\frac{Nv_0}{\pi\sigma}\right)^{1/2},\left(\int_0^H \varphi(x)xdx\right)^2 = \frac{K_s H^6}{9w_1}$$

$$\mu\varphi(x) - \Phi(\varphi(x),x) = \frac{2kT}{3v_0}w_1\varphi(x)^3,\ \frac{\delta^2\Phi}{\delta\varphi^2} = \frac{2kTw_1}{v_0}\varphi(x),\ \int_0^H\left(\frac{\delta^2\Phi}{\delta\varphi^2}\right)^{-1}dx = \frac{\pi v_0}{4kTw_1}\sqrt{\frac{w_1}{K_s}}$$

$$I_1 = \frac{4kTH^6}{9\pi v_0}\sqrt{\frac{K_s^3}{w_1}}$$

$$I_2 = \int_0^H\left(\mu\varphi(x) - \Phi(\varphi(x),x)\right)xdx = \frac{2kTH^5}{15v_0}\sqrt{\frac{K_s^3}{w_1}}$$

$$I_3 = -\int_0^H\left(\mu\varphi(x) - \Phi(\varphi(x),x)\right)x^2dx = -\frac{\pi kTH^6}{48v_0}\sqrt{\frac{K_s^3}{w_1}} \qquad (3.62b)$$

Thus for the bending moduli for the case of single brush (constant area per molecule) we have following expressions

$$\kappa = \frac{4kTH^6}{9\pi v_0}\sqrt{\frac{K_s^3}{w_1}},\ \bar{\kappa} = -\frac{\pi kTH^6}{48v_0}\sqrt{\frac{K_s^3}{w_1}},\ \kappa/\bar{\kappa} = -64/(3\pi^2),\ H_0 = \frac{3\pi}{20H}. \qquad (3.62c)$$

For the case when area per molecule changes with curvature the result could be also calculated straightforward using a simple algebra.

III.3.3. Intermediate case of small volume fractions (cubic DFT)

Here is the general case, which combines the results form both previous ones. We expand the DF to the cubic terms:

$$\Phi(\varphi(x),x) = \frac{kT}{v_0}\left\{\frac{1}{2}w\varphi(x)^2 + \frac{1}{3}w_1\varphi(x)^3 + K_s x^2\varphi(x)\right\} \qquad (3.63)$$

where, w and B a given above. The solution in this case is:

$$\frac{\delta\Phi}{\delta\varphi}=\frac{kT}{v_0}\left(w_1\varphi(x)^2+w\varphi(x)+K_s x^2\right)=\mu=\frac{kT}{v_0}K_s H^2,\ \varphi(x)=\sqrt{C^2+\varphi_\Theta^2(x)}-C \qquad (3.64)$$

where, $\varphi_\Theta=\sqrt{\frac{K_s}{w_1}(H^2-x^2)}=D\sqrt{1-x^2/H^2}$ is the solution for the case of Θ solvent given in previous section, while $C=\frac{w}{2w_1}=1-2\chi$, $D=H\sqrt{K_s/w_1}$. In order to calculate all the moments of the distributions we need to solve following transcendental equation:

$$\int_0^H\varphi(x)dx=\frac{H}{2D}\left(\left[C^2+D^2\right]\arctan\left[\frac{D}{C}\right]-CD\right)=\frac{Nv_0}{\sigma}. \qquad (3.65)$$

Introducing $z=D/C$ we can rearrange the latter one into more simple form:

$$\left(\left[z^2+1\right]\arctan(z)-z\right)=\frac{2Nv_0}{\sigma C^2}\sqrt{\frac{K_s}{w_1}}=\frac{\pi\sqrt{3v_0v_w}}{\sigma l C^2}=\frac{A}{C^2} \qquad (3.66)$$

where, $A=\frac{\pi\sqrt{3v_0v_w}}{\sigma l}$. The latter transcendent equation does not depend on length of the polymer. One can calculate z and H numerically for a given parameters of polymer brush. For small values of C (close to the Θ point) the RHS of the last equation is very big, which means that we must take asymptotic of the equation for large z, $\left[z^2+1\right]\arctan(z)-2z\approx\frac{\pi}{2}z^2-2z+O((1/z)^0)$. Setting C=0, (keeping only the first term in the expansion) we immediately get previous case solution. For small non-zero values of C we get:

$$z=\frac{1}{C}\sqrt{\frac{2A}{\pi}}+\frac{2}{\pi}+O(C)\approx\frac{1}{C}\sqrt{\frac{2\pi\sqrt{3v_0v_w}}{\sigma l}}+\frac{2}{\pi},\ D=zC=\sqrt{\frac{2A}{\pi}}+\frac{2C}{\pi}+O(C^2)\approx\sqrt{\frac{2\pi\sqrt{3v_0v_w}}{\sigma l}}+\frac{2C}{\pi}$$

$$H=zC\sqrt{\frac{w_1}{K_s}}=2Nl\sqrt{\frac{2\sqrt{v^3{}_0}}{\pi\sigma l\sqrt{3v_w}}}+\frac{4NlC}{\pi^2}\sqrt{\frac{v_0}{3v_w}}+O(C^2)$$

$$\left(\int_0^H\varphi(x)xdx\right)^2=\frac{(DH)^2H^2}{36z^6}\left(3z^2+2-2\left[\sqrt{z^2+1}\right]^3\right)^2$$

$$\mu\varphi(x)-\Phi(\varphi(x),x)=\frac{kTw_1}{v_0}\left(\frac{2}{3}\varphi(x)^3+C\varphi(x)^2\right)$$

$$\frac{\delta^2\Phi}{\delta\varphi^2}=\frac{2kTw_1}{v_0}(\varphi(x)+C)\,,\ \int_0^H\left(\frac{\delta^2\Phi}{\delta\varphi^2}\right)^{-1}dx=\frac{v_0H^2}{2kTw_1DH}\arctan(z)$$

$$I_1=\frac{kTw_1(DH)^3}{18v_0}\frac{\left(3z^2+2-2\left[\sqrt{z^2+1}\right]^3\right)^2}{z^6\arctan(z)}$$

$$I_2=\int_0^H\left(\mu\varphi(x)-\Phi(\varphi(x),x)\right)xdx=\frac{kTw_1(DH)^3}{60v_0Hz^5}\left(8\left[\sqrt{z^2+1}\right]^5-15z^4-2z^2-8\right)$$

$$I_3=-\int_0^H\left(\mu\varphi(x)-\Phi(\varphi(x),x)\right)x^2dx=\frac{kTw_1(DH)^3}{360v_oz^6}\left\{33z^5+40z^3+15z-15\left(z^6+3z^4+3z^2+1\right)\arctan(z)\right\}$$

$$\kappa=\frac{kTw_1(DH)^3}{18v_0}\frac{\left(3z^2+2-2\left[\sqrt{z^2+1}\right]^3\right)^2}{z^6\arctan(z)} \tag{3.67}$$

For small values of C (large z) we have;

$$\kappa\approx\frac{kTw_1(DH)^3}{18v_0}\left(\frac{8}{\pi}+\frac{8(2-3\pi)}{\pi^2}\frac{1}{z}\right) \tag{3.68}$$

$$\bar{\kappa}=\frac{kTw_1(HD)^3}{360v_oz^6}\left\{33z^5+40z^3+15z-15\left(z^6+3z^4+3z^2+1\right)\arctan(z)\right\}$$

$$\bar{\kappa}\approx-\frac{kTw_1(HD)^3}{360v_o}\left\{\frac{15\pi}{2}-\frac{48}{z}\right\}$$

$$H_0=\frac{3z\left(8\left[\sqrt{z^2+1}\right]^5-15z^4-2z^2-8\right)\arctan(z)}{20H\left(3z^2+2-2\left[\sqrt{z^2+1}\right]^3\right)^2}$$

$$H_0\approx\frac{3\pi}{20H}\left(1+\frac{9\pi-16}{8\pi}\frac{1}{z}\right)$$

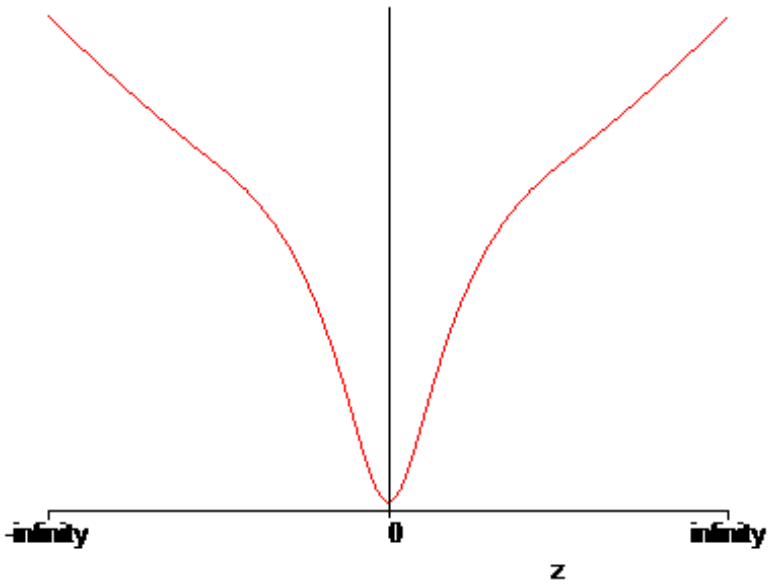

Figure 3.4. $-\frac{3\pi^2\kappa}{64\bar{\kappa}} = -\frac{15\pi^2\left(3z^2+2-2\left[\sqrt{z^2+1}\right]^3\right)^2}{16\left\{33z^5+40z^3+15z-15\left(z^6+3z^4+3z^2+1\right)\arctan(z)\right\}\arctan(z)}$ as a function of z. The value at z=0 ($C >> D$, i.e. the case when elastic contribution is dominating one) is $315\pi^2/4096$

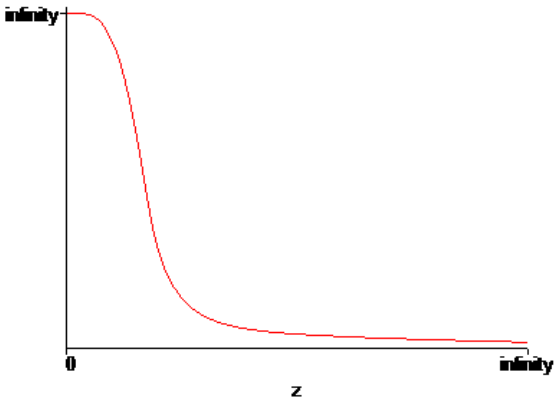

Figure 3.5. $\frac{20HH_0}{3\pi} = \frac{z\left(8\left[\sqrt{z^2+1}\right]^5-15z^4-2z^2-8\right)\arctan(z)}{\pi\left(3z^2+2-2\left[\sqrt{z^2+1}\right]^3\right)^2}$ as a function of z.

The last dependences ($k/\bar{k}$ and H_0H) as a function of parameter z are illustrated in figures 3.4 and 3.5. For the case of di-block polymers one could also calculate the elastic constants, but the results are omitted for the sake of simplicity.

III.3.4. Case for $\chi = 0$, arbitrary volume fractions

In this case we will assume that we have a good solvent ($\chi = 0$), which gives the following functional for DF of SCF[37]

$$\Phi(\varphi(x),x) = \frac{kT}{v_0}\left\{\frac{v_0}{v_w}(1-\varphi(x))\ln(1-\varphi(x)) + K_s x^2\varphi(x)\right\} \tag{3.69}$$

The solution of this problem is:

$$\frac{\delta\Phi}{\delta\varphi} = \frac{kT}{v_0}\left(-\frac{v_0}{v_w}(\ln(1-\varphi(x))+1) + K_s x^2\right) = \mu = \frac{kT}{v_0}\left(-\frac{v_0}{v_w} + K_s H^2\right) \tag{3.70}$$

$$\varphi(x) = 1 - \exp\left[-\alpha^2(1-x^2/H^2)\right]$$

where, $\alpha = H\sqrt{\frac{v_w K_s}{v_0}}$.

$$\int_0^H \varphi(x)dx = H(1-D(\alpha)/\alpha) = \frac{Nv_0}{\sigma},\ \left(\int_0^H \varphi(x)xdx\right)^2 = \frac{H^4}{4\alpha^4}\left(e^{-\alpha^2}+\alpha^2-1\right)^2 \tag{3.71}$$

where, $D(x) = e^{-x^2}\int_0^x e^{t^2}dt$ is the Dawson integral. For the case of small coverage ($\alpha \approx H/Nl << 1$) we have $D(x) \approx x - 2x^3/3 + O(x^5)$, ($x<<1$), which substituted back into the last equation gives the result from eq. 3.62, after substitution, $w = \frac{v_0}{v_m}$. For another case when we have high coverage $H/Nl \approx 1$ the Dawson integral could be expanded for the case of high values: $D(x) \approx 1/2x + 1/4x^3 + O(1/x^5)$, (x>>1) thus the first estimate for H is $H = Nv_0/\sigma$.

$$\mu\varphi(x) - \Phi(\varphi(x),x) = -\frac{kT}{v_w}\left(\varphi(x) + \ln\left(1-\varphi(x)\right)\right) \tag{3.72}$$

$$I_2 = \int_0^H \left(\mu\varphi(x) - \Phi(\varphi(x),x)\right)xdx = \frac{kTH^2}{4v_w\alpha^2}\left(2(1-e^{-\alpha^2}) + \alpha^2(\alpha^2-2)\right)$$

$$\frac{\delta^2\Phi}{\delta\varphi^2} = \frac{kT}{v_w}\frac{1}{1-\varphi(x)},\ \int_0^H\left(\frac{\delta^2\Phi}{\delta\varphi^2}\right)^{-1}dx = \frac{v_w}{kT}\int_0^H(1-\varphi(x))dx = \frac{v_w}{kT}\left(H - \frac{Nv_0}{\sigma}\right) = \frac{v_w HD(\alpha)}{kT\alpha},$$

$$\kappa = I_1 = \frac{kTH^3}{4v_w\alpha^3}\frac{\left(e^{-\alpha^2}+\alpha^2-1\right)^2}{D(\alpha)},\ H_0 = \frac{I_2}{2I_1} = \frac{\alpha}{2H}\frac{\left(2(1-e^{-\alpha^2})+\alpha^2(\alpha^2-2)\right)D(\alpha)}{\left(e^{-\alpha^2}+\alpha^2-1\right)^2}$$

$$\bar{\kappa} = I_3 = -\int_0^H \left(\mu\varphi(x) - \Phi(\varphi(x), x)\right) x^2 dx = \frac{kTH^3}{v_w}\left(\frac{D(\alpha)}{2\alpha^3} + \frac{1}{3} - \frac{2\alpha^2}{15} - \frac{1}{2\alpha^2}\right)$$

$$\kappa / \bar{\kappa} = \frac{\left(e^{-\alpha^2} + \alpha^2 - 1\right)^2}{4\alpha^3\left(\frac{D(\alpha)}{2\alpha^3} + \frac{1}{3} - \frac{2\alpha^2}{15} - \frac{1}{2\alpha^2}\right)D(\alpha)}$$

For small values of α the results reproduces the results from section (III.3.1) with the substitution, $w = \frac{v_0}{v_m}$. For large values some of the asymptotic are, $\kappa = \frac{kTH^3\alpha^2}{2v_w}$, $\bar{\kappa} = -\frac{2kTH^3\alpha^2}{15v_w}$, while intermediate cases are depicted in figure 3.5 and 3.6.

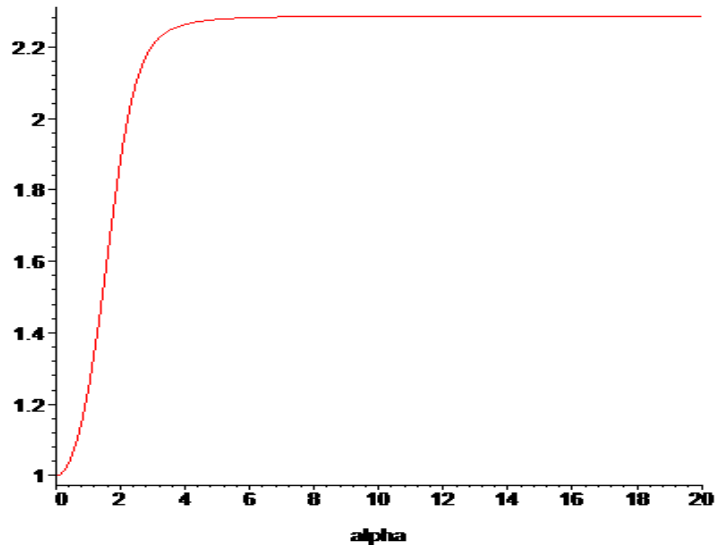

Figure 3.5. $-64\kappa/105\bar{\kappa} = \frac{32\left(e^{-\alpha^2} + \alpha^2 - 1\right)^2}{7\left(4\alpha^5 + 15(\alpha - D(\alpha)) - 10\alpha^3\right)D(\alpha)}$ as a function of α. For small α this function has limit 1 while for big values ($\alpha > 4$) the limit is 16/7.

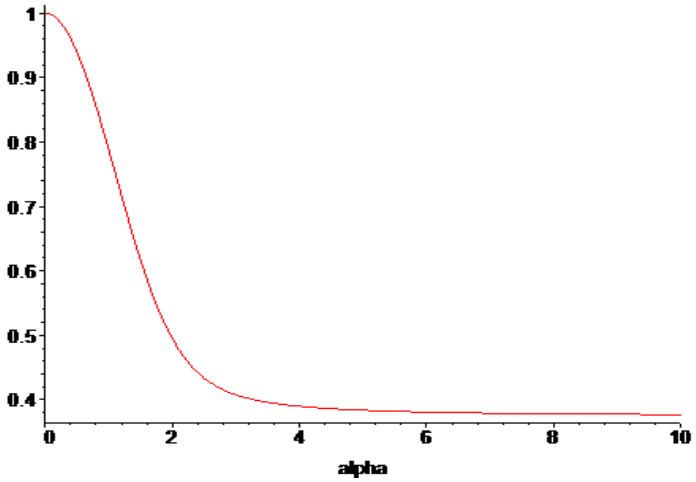

Figure 3.6. $\frac{3H_0H}{2}=\frac{3\alpha}{4}\frac{\left(2(1-e^{-\alpha^2})+\alpha^2(\alpha^2-2)\right)D(\alpha)}{\left(e^{-\alpha^2}+\alpha^2-1\right)^2}$, as a function of α. For small values function is 1 and for large values it goes to 3/8.

III.3.5. Some remarks on the general case

Finally we would like to make some comments concerning the most general case, wherefrom all other cases could be extracted. The problem in the general case is that the solution is very simple but it is given with a transcendental equation:

$$\frac{v_0}{v_w}\left[-\ln(1-\varphi(x))+2\chi\varphi(x)\right]+K_sx^2=K_sH^2=\frac{v_0}{v_w}\left[-\ln(1-\varphi(0))+2\chi\varphi(0)\right] \qquad (3.73)$$

which could be expressed also as

$$\ln\left[\frac{1-\varphi(x)}{1-\varphi_0}\right]+2\chi(\varphi_0-\varphi(x))=\frac{v_w}{v_0}K_sx^2\text{, or }\quad x=\sqrt{\frac{v_0}{v_wK_s}}\sqrt{\ln\left[\frac{1-\varphi(x)}{1-\varphi_0}\right]+2\chi(\varphi_0-\varphi(x))} \qquad (3.74)$$

where, $\varphi_0=\varphi(0)$. Then the normalizing condition reads:

$$\frac{Nv_0}{\sigma}=\int_0^H\varphi(x)dx=-\int_0^H xd\varphi(x)=\sqrt{\frac{v_0}{v_wK_s}}\int_0^{\varphi_0}\sqrt{\ln\left[\frac{1-u}{1-\varphi_0}\right]+2\chi(\varphi_0-u)}du \qquad (3.75)$$

The latter should be considered as an equation for φ_0, which is independent on *N*. The ability to solve this equation actually will solve the problem. If we knew φ_0 than we could immediately calculate *H* from eq. 3.73.

A more convenient form of last equation could by obtained by changing the variables: $z = \ln\left[\frac{1-u}{1-\varphi_0}\right]$ with $z_0 = -\ln(1-\varphi_0)$, which gives

$$\frac{Nv_0}{\sigma} = \sqrt{\frac{v_0}{v_w K_s}} \int_0^{z_0} \sqrt{z + 2\chi e^{z-z_0}}\, e^{z-z_0} dz \,. \tag{3.76}$$

For the calculation of bending modulus we need to solve integrals of a type: $\int_0^H \varphi(x) x^k dx$. The integrals containing odd powers of k could be calculated analytically in terms of φ_0, by simple partial integration, while for the even powers integrals it could be shown they could expressed in terms of the normalizing integral (eq. 3.75). Thus if we have a good approximation for the equation 3.76 we can get a good guess for bending constants. For the case of small z_0 the estimation is straightforward and gives well-known result. For the case when $\chi = 0$ one can take the integral analytically in terms of Dawson functions. More problematic is calculation of the integral for big z_0. In this case the integral could be expanded by two parts: one close to z_0 (end of the chain) and one close to the wall z=0. Which is the same as to look for a solution of transcendental equation 3.73 in terms of two solutions inner (close to the wall) and outer one (close to H) and a proper matching between the in the intermediate region. The latter is a subject of a future work.

III.4. Conclusions and perspectives

We have demonstrated that there is a simple method for calculation of the bending constants of grafted copolymer brushes, both for mono-block and di-block polymers (surfactants). The main advantage of the method described in the present chapter is that we have expressed in closed analytical form all the elastic constants in terms of moments of the *flat solution only*. In order to illustrate the method, we have calculated the bending moduili of mono and di block polymers (surfactants) in several different conditions. For the cases when there are literature data we have compared our calculations (see part 3.3.1) with literature[28,29,32] and have demonstrated the applicability of the method. We have also calculated several cases

(3.3.2-3.3.4), which according to our knowledge are new results. For the case of di-block polymers and surfactants we derive a simple algebraic expressions for the bending constants as functions of the corresponding moments of the single blocks. By making all possible combinations from the cases studied in this part one can get plenty of a new results for the case of di-block polymers. These results obtained in this chapter could be used for better prediction of phase behavior of non-ionic surfactants[29]. For example for the case of C_nE_k surfactants in ternary water/oil (hexadecanes) the Flory parameter is practically zero for oily part of surfactant and one can use results from case 3.3.4, while for ethoxylated part dissolved in water one could assume that it is close to Θ point and use results from cases 3.3.2 and 3.3.3. The resulting formulas should give better description of microemulsion properties in this case than one proposed by Safran[32], Milner[31], Paunov[29].

IV. Dissipative Particle Dynamics – method and its applications for studying properties of colloidal systems

IV.1. Introduction

The Dissipative Particle Dynamics (DPD) computer model has been initially devised by Hoogerbrugge and Koelman[57-58] as a simulation method to avoid the lattice artifacts of Lattice Gas Automata and yet capturing hydrodynamic time and space scales much larger than those available with Molecular Dynamics[57]. The DPD model consists of a set of point particles that move off-lattice, interacting with each other through a set of prescribed forces[57-59]. These forces are of three types: a purely repulsive conservative force, a dissipative force set to reduce velocity differences between the particles, and a further stochastic force directed along the line joining the centers of the particles. The amplitudes of these forces are tuned to satisfy the Fluctuation-Dissipation theorem[59]. The forces are modulated with a weight function that specifies the range of interaction between dissipative particles, which makes the interaction purely local. The distinguishing feature of the DPD forces is that they conserve momentum and, therefore, the DPD model captures the essentials of mass and momentum conservation, which are the responsible for the hydrodynamic behavior of a complex fluids at large scales[59-73]. From a physical point of view, each dissipative particle is regarded not as a single molecule but rather as a collection of molecules that move in a coherent fashion. In that respect, DPD can be understood as a *coarse-grained* version of the molecular dynamics method. The forces between dissipative particles can be loosely interpreted in this picture. The conservative forces oblige the fluid particles to be as evenly distributed in space as possible as a result of certain "pressure" among them, the friction forces represent viscous resistances between different parts of the fluid, whereas the stochastic forces represent degrees of freedom that have been eliminated from the description in the coarse graining process. One of the most attractive features of the model is its enormous versatility in order to construct simple models for complex fluids. In DPD the Newtonian fluid is made "complex" by adding additional interactions between the fluid particles. Just by changing the conservative interactions between the fluid particles, one can easily construct and model polymers, colloids, amphiphiles, and mixtures. For example, by joining consecutively sets of

particles with springs, one has a coarse grained model for actual molecules. These molecules can coexist with a solvent represented by other dissipative particles in order to model dilute surfactant and polymer solutions. Colloidal particles of arbitrary shape can be modeled by "freezing" dissipative particles within a region of space that moves as a rigid body. These solid objects coexist with solvent particles and strongly modify the rheology of the system. Introducing two types of particles that interact unequally allows to model mixtures and to study two phase decomposition and emulsification. Given the simplicity of modeling of mesostructures, DPD appears as a competitive technique in the field of complex fluids.

The aim of the present chapter is to give brief outline of the basics of DPD method, as well as some applications in the area of colloid science. Most of the applications, which are given here, are at a preliminary stage and additional investigation is needed for their completion. A complete study of a real system with DPD is given in the next chapter, where the results out of DPD simulation are compared with SCF theory predictions and in the chapter VI where DPD results are rescaled in order to model surface activity of real system.

IV.2. DPD Basics

IV.2.1. Interaction forces in DPD

In the DPD method fluids are represented by point particles. These particles are not regarded as the fluid molecules but rather as droplets or clusters of molecules. The particles (beads) interact through conservative, dissipative, and random forces, which are pair-vise additive, which means that the total impulse of the system is conserved. The total energy of the system is not conserved due to the presence of the dissipative forces, thus DPD restores NVT ensemble. There are also generalizations of the method, which allows energy conservations[60].

The conservation of total impulse and fulfillment of fluctuation dissipation theorem means that the equilibrium state of the system is not influenced by random and dissipative forces, and it is determined by the Boltzman distribution. The fluctuation and dissipation forces are governing how the system is reaching equilibrium, and determine the values of transport coefficients of the system, like viscosity and diffusion. This is a crucial point, which makes the technique suitable for simulating hydrodynamic processes because it implies that there

exists a transport equation for the hydrodynamic and concentration momentum density fields[59]. The method has been successfully used to study various problems, which are important for physical chemistry [60-70].

The dynamical evolution of the system is governed by Newton´s laws

$$\frac{d\mathbf{r}_i}{dt} = v_i, \qquad m_i \frac{d\mathbf{v}_i}{dt} = \mathbf{F}_i(t) \tag{4.1}$$

The force between each pair of particles is made up of a conservative F^C term, a dissipative F^D term, and a random F^R term. The effective force acting on particle ***i*** at time ***t***, $\boldsymbol{F_i}$, is given by

$$\mathbf{F}_i = \sum_{j \neq i} \mathbf{F}_{ij}^C + \sum_{i \neq j} \mathbf{F}_{ij}^D + \sum_{i \neq j} \mathbf{F}_{ij}^R \tag{4.2}$$

The dissipative and random force terms incorporate the effects of Brownian motion into the bigger length scales. The conservative component is taken to be linear up to a cut-off in particle separation r_c, and zero outside of this

$$\mathbf{F}_{ij}^C = \begin{cases} a_{km}(1 - r_{ij}/r_c)\hat{\mathbf{r}}_{ij} & (r_{ij} < r_c) \\ 0 & (r_{ij} > r_c) \end{cases} \tag{4.3}$$

where, $\boldsymbol{r}_{ij} = \boldsymbol{r}_i - \boldsymbol{r}_j$, $r_{ij} = |\boldsymbol{r}_{ij}|$, $\hat{\mathbf{r}}_{ij} = \boldsymbol{r}_{ij}/|r_{ij}|$, and a_{ij} is repulsion parameter, k and m are types of particle i and j. For the simplicity, all interactions are calculated with a cutoff radius r_c=1 and all the distances are reduced with respect to r_c and all particles have an equal mass of m=1. The dissipative force depends on the relative particle velocities $\boldsymbol{v}_{ij} = \boldsymbol{v}_i - \boldsymbol{v}_j$ and is

$$\mathbf{F}_{ij}^D = -\hat{\gamma}_{km}\omega^D(r_{ij})(\hat{r}_{ij} \cdot v_{ij})\hat{\mathbf{r}}_{ij} \tag{4.4}$$

The random force is

$$\mathbf{F}_{ij}^R = \hat{\sigma}_{km}\omega^R(r_{ij})\theta_{ij}\hat{\mathbf{r}}_{ij} \tag{4.5}$$

In these equations $\hat{\gamma}$ can be interpreted as the friction coefficient and $\hat{\sigma}$ the amplitude of noise. θ_{ij} is a random number sampled from a Gaussian distribution with zero mean and unit variance and is chosen independently for each pair of particles at each time step. Español and Warren[59] have shown that the system will sample the canonical ensemble and obey the fluctuation-dissipation theorem if following relation is fulfilled:

$$\hat{\gamma}_{km} = \frac{\hat{\sigma}_{km}^2}{2kT} \text{ and } \omega^D(r_{ij}) = \left[\omega^R(r_{ij})\right]^2 \tag{4.6}$$

where k is the Boltzman constant and T is thermodynamic temperature. As a simple choice for the weight functions we take for all simulations described below:

$$\omega^D(r) = [\omega^R(r)]^2 = \begin{cases} (1-r)^2 & r < 1 \\ 0 & r \geq 1 \end{cases} \tag{4.7}$$

In all the simulations presented in this chapter the overall DPD particle density ρ=M/V (M is total number of particles in the system, while V is total volume of the system) was set to 5. The frictions constant $\hat{\gamma}$, which physically governs the viscosity was set to 4.5, in according to ref 71. Provided that all force amplitudes are known explicitly, one could integrate the equations of motion of the system and study its evolution with time. The method used to integrate the equation of motion is a modified version of the velocity –Verlet algorithm[71]

$$\begin{aligned} &\mathbf{r}_i(t+\Delta t) = \mathbf{r}_i(t) + \Delta t \mathbf{v}_i(t) + 1/2(\Delta t)^2 \mathbf{F}_i(t), \\ &\tilde{\mathbf{v}}_i(t+\Delta t) = \mathbf{v}_i(t) + \lambda \Delta t \mathbf{F}_i(t), \\ &\mathbf{F}_i(t+\Delta t) = \mathbf{F}_i(r(t+\Delta t), \tilde{\mathbf{v}}_i(t+\Delta t)), \\ &\mathbf{v}_i(t+\Delta t) = \mathbf{v}_i(t) + 1/2 \Delta t (\mathbf{F}_i(t) + \mathbf{F}_i(t+\Delta t)). \end{aligned} \tag{4.8}$$

Where λ is integration empirical parameter. If λ is set to ½, integration scheme given with eq. 4.8 restores the original leap-frog version of the velocity Verlet algorithm. Groot and Warren[71] have studied the effect of alternative values for this factor and suggested values 0.65 as an optimal one. In our simulations the factor λ is set of 0.65 as well.

The choice of the time step in the dissipative particle dynamics is very important for the stability of the simulations, because the temperature depends strongly on the time step. The integration quality of the equations of motion, could be determined from the ratio between thermodynamic temperature, determined from eq. 4.6 (provided that the values of friction coefficients are known) and the moment value of temperature in the system, determined from the Maxwell – Boltzman distribution $kT_{mom} = \frac{1}{3M}\sum_i m_i \mathbf{v}_i^2$. The bigger the time step is the bigger is the difference between them, and they coincide only in the limit of zero time step.

Marsch and Yeomans[72] have obtained an analytic expression for the dependence of DPD temperature as a function of integration time step, which could be used for tuning the quality of DPD simulations. Throughout all the simulations in the present thesis the time step was set to $\Delta t=0.03$ (DPD-time units).

If only the equilibrium properties of the system are of interest, the amplitudes of dissipative forces, $\hat{\gamma}_{km}$, and random forces, $\hat{\sigma}_{km}$, could be set to a values, which are providing faster system equilibration and stable integration but allowing bigger time steps. Note that the fulfillment of fluctuation dissipation theorem is critical in this point, because it assures that the values of random and dissipative forces do not influence the equilibrium state of the system.

IV.2.2. Bridging the microscopic properties to DPD parameters of single component system

If the dynamic properties of the system are subject of interest one needs to use different values for the amplitudes of fluctuation and dissipation forces for different species into the system in order to capture the difference in the transport coefficients of real fluids, which species are representing. One possible way to do this is to tune the fluctuation and dissipation amplitudes in such a way so the ratios of the viscosities of species in real and DPD system are equal. For instance if one of the beads used in DPD is supposed to model a water and other bead is representing some type of oil, if the fluctuation amplitude is equal for both types of beads then in DPD both fluids will have one and the same viscosity, while the real fluids could have viscosities, which could differ several orders of magnitude. Thus DPD system will not properly represent the hydrodynamic motions of the mixing process of two fluids. So one needs to use different values for the fluctuation and the dissipation amplitudes for both types of beads to correctly model the dynamics of the real system.

Since the dynamical properties of the system are out of scope in all simulations in the thesis, we have assumed that the fluctuation and dissipation amplitudes are equal for all types of beads, and we have set $\sigma_{km}=3$. The dimension of energy was set so that in DPD $T=1$, thus all energies in DPD are in *kT* units. Then using eq. 4.6 the amplitude of the dissipative force is $\hat{\gamma}_{km}=4.5$, which provides stable integration and low temperature fluctuation in the system

(less than 3% of thermodynamic temperature for time step $\Delta t = 0.03$).

The only parameters, which have to be determined, are the values of conservative force amplitudes, a_{km}. If we have a system which consists of K different types of beads we have $K(K+1)/2$, different values of the conservative force amplitudes, because $a_{km} = a_{mk}$, which follows from the pair-vise additivity of the interaction forces. The principal values, a_{kk}, determinate the interaction between similar beads and therefore determine the thermodynamic properties of pure fluids, while the asymmetric values a_{km}, determine the thermodynamic properties of mixing two different types of fluids.

First we focus our attention how the symmetric constants a_{kk} could be obtained. By performing DPD simulations of homogeneous fluids Groot and Warren[71] have obtained the equation of state (EQS) of homogeneous DPD fluid. They show that even for very high DPD densities the equation of state remains purely quadratic

$$P = \rho + 0.101 a_{kk} \rho^2 \tag{4.9}$$

where, for simplicity we have set $kT = 1$, thus the value of a_{kk} is in kT units. P is thermodynamic pressure of the system, while ρ is the DPD density. The value of the numerical constant is obtained by fitting the pressure obtained in DPD with parabolic function. Thus the second virial coefficient, w, of DPD fluid is connected with the magnitude of the conservative forces as follows, $w = 0.101 a_{ii}$, while the third virial and higher coefficient are practically zero even for very high densities. In worth mentioning that similar numerical coefficient could be obtained using the van der Waals expression for the second viral coefficient

$$w = -2\pi \int_{R_c}^{\infty} u(r) r^2 dr \tag{4.10}$$

where, $u(r) = \frac{a_{kk}(1-r)^2}{2}\theta(1-r)$, is pair-vise potential of conservative force in DPD, $R_c = 0$ is the hardcore radius, and $\vartheta(x)$ is the Heavyside function which is one for positive values of argument and zero otherwise (we have set cut-off radius of DPD interactions, $r_c = 1$, thus all DPD length units are given in terms of r_c). Substituting the value of the potential into the

last equation one gets

$$w = 2\pi \int_0^1 \frac{a_{kk}(1-r)^2}{2} r^2 dr = \frac{\pi}{30} a_{kk} = 0.104 a_{kk} . \quad (4.11)$$

The use of the latter expression for the case of DPD was analyzed in details in the work of Pagonabarraga and Frenkel[73]. It was also commented in ref 73 that making DPD interactions non local (conservative forces start to depend from distance between the particles and weighted density around each of the particle), makes possible to change EQS of the DPD from pure quadratic to any initially required form. The problem of purely quadratic equation of state is that it models a super critical fluid and does not allow a liquid/gas coexistence for one component fluid. The generalization given in ref 73 avoids this problem and allows much broader range of application of DPD simulations.

By differentiating the DPD EQS given with eq. 4.9 one could determine the dimensionless compressibility of DPD fluid

$$\frac{1}{kT}\frac{\partial P}{\partial \rho} = 1 + 0.2 a_{kk} \rho . \quad (4.12)$$

Than this value could be matched to the dimensionless compressibility for real system[71]. The matching of the compressibility of real and DPD system also assures that the density fluctuations in both systems are similar. The density fluctuations are very important for the phase behavior, because they act as nucleation centers, wherefrom new the phase starts to grow. The dimensionless compressibility of water at room temperature is 16, thus if we would like to simulate water in DPD we could determine the interaction parameter between water like beads in DPD from the compressibility to be[71]

$$a_{ii} = 75 N_c / \rho \quad (4.13)$$

where, N_c is the number of water molecules which are combined to form one DPD bead. In the last equation it was assumed that if we combine N_c water molecules into a bead and the interaction between each molecules is $\tilde{a}_{kk}$ (in kT units), then for a cluster of N_c molecules, the interaction will be $N_c \tilde{a}_{kk}$. By matching the DPD fluid density with the density of water at room temperature (55M) one gets an expression for the DPD length scale of the system[71]

$$r_c = 3.1 (N_c \rho)^{1/3} \text{Å} . \quad (4.14)$$

Provided that the DPD length scale is known from some other matching conditions one could use eq. 4.13 or 4.14 to calculate back the value of N_c, which gives the degree of coarse graining in the system. The time scale in DPD then could be obtained by matching the diffusion coefficient of the fluid measured in DPD with the values of real system.

IV.2.3. Bridging the microscopic properties to DPD parameters of multi-component system

Now we will consider the multi-component systems. The values of symmetric amplitudes of the conservative repulsive forces could be obtained using the same procedure as described above for each of the components. But there are some bottlenecks, which should be carefully considered. The matching of the properties of real components into DPD should be done in a self-consistent way, which usurers that pressure time and length scales are similar for each of the components, when they are brought into contact. For instance consider that we would like to model in DPD the equilibrium behavior of two immiscible fluids (the latter is controlled by the value of unlike interactive parameter, which we will comment latter). When fluids are brought into contact the pressure in the system should be equal in equilibrium, thus if ρ_1 and ρ_2 are the bulk densities of each of the components in DPD we will have that

$$\rho_1 + 0.1 a_{11} \rho_1^2 = \rho_2 + 0.1 a_{22} \rho_2^2 = P . \tag{4.15}$$

Thus the one can see that equilibrium DPD density and like repulsion are not independent (see also figure 4.1 for more details and illustration example). From the other point we knew the density ratio of two real fluids, which means that the same ratio should apply for DPD i.e. we must have that,

$$N_{c,1}\rho_1 / N_{c,2}\rho_2 = \rho_1^R / \rho_2^R \tag{4.16}$$

where, $N_{c,i}$ is the number of molecules combined to form a single fluid bead, while ρ_i^R are real densities of those fluids. The latter equation also assures that the length scales determined from the real fluid density (see eq. 4.14) will be equal for both of the fluids. Thus the mapping of the properties of the each of the fluids should be done in a self-consistent

way, which assures that eq. 4.15 and eq. 4.16 are satisfied as well.

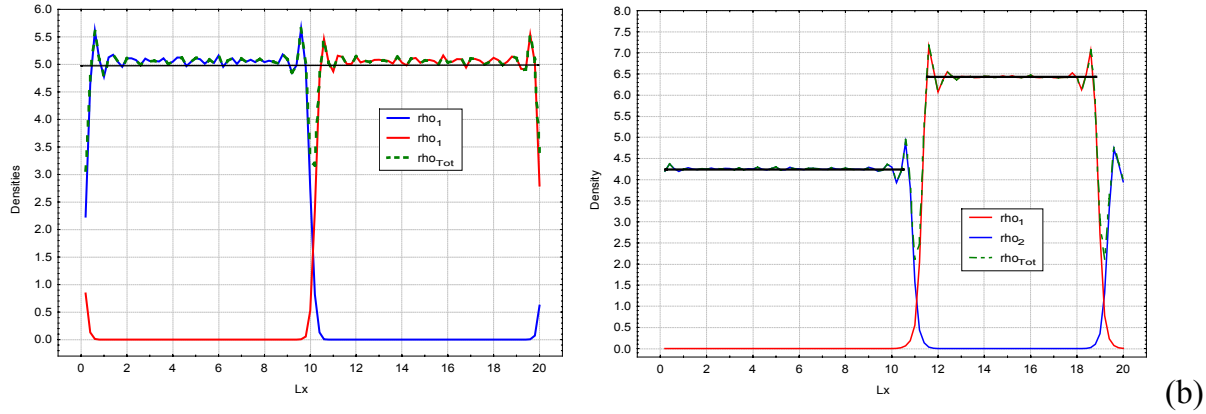

(a) (b)

Figure 4.1. Density distribution along x direction of simulation box of two component immiscible system obtained with the DPD method. In the case (a) the two fluids have equal repulsion between like beats, i.e. $a_{11} = a_{22} = 15$, while in the case (b) $a_{11} = 10$, $a_{22} = 25$. Total mean density in the system was set to 5, and the unlike repulsion between the beats was set to 75, which practically assures immiscibility of fluids. Half of the DPD beads are oftype 1, while the other half are of type 2. In the beginning of simulation there was a sharp slab in x direction of the simulation box, which divides two different fluids with equal density. Then DPD simulation was performed and the equilibrium density profiles are obtained. One can see that for the case (a) the density of two fluids remains equal, while for the case (b) the equilibrium densities of two fluids are different. In this case we have that $P_{sim} = 47$, wherefrom we could calculate using (eq. 4.12) that $\rho_1 + 0.1 a_{11} \rho_1^2 = \rho_2 + 0.1 a_{22} \rho_2^2 = P = 47$, and obtain $\rho_1 = 6.38$, $\rho_2 = 4.14$, which agrees well with observed mean density of the fluids $\rho_1 = 6.41$, $\rho_2 = 4.21$.

Note also that the above consideration is applicable when we have immiscible fluids like water and oil. When fluids are miscible like water and alcohols, then the situation is qualitatively different and one should match the partial pressures and molar fractions in the real and the model DPD system. Additional problem arises in this case if different coarse-graining is used for two types of fluids, i.e. when $N_{c,1} \neq N_{c,2}$ [†]. The problem in this case is that when we use different coarse-graining level for different beads we are changing local

[†] Typical example of this situation is when large molecules like surfactants and polymers dissolved in a solution are modeled with the DPD method, when part of a large molecule is represented with a single bead, while several solvent molecules are combined to form a solvent bead. The latter is done in order that all types of beads to have nearly one and the same real volume, because all conservative forces are assumed to have the same cut-off radius.

molar fraction (composition) in the system. The later is extremely important quantity, which determines that equilibrium behavior of mixture and is connected with the values of unlike repulsion parameters, which will be discussed shortly after. By changing the local molar fraction in the DPD system we are also chaining effectively the unlike interaction in our system, which means that the values of unlike parameters in DPD could become dependent of the molar fraction in the system. The latter is not a big problem when one has isotropic system, but becomes extremely important when anisotropic system is modeled. Typical example for this situation is when we model the phase behavior of the system (where concentration of one of the component is varied) with single set of DPD parameters, which are assumed to be independent of the composition. This problem is still unresolved and requires further detailed investigation. One way to solve it is to use different cut-off radii for different types of beads, which will allow incorporation of different length scales into the system. The latter approach allows using a different coarse graining without changing the local molar composition of the real and the DPD systems.

Here we consider the procedure for the determination of the interaction parameters between unlike beads[71]. Again, for the sake of simplicity we will illustrate the procedure working only with two beads, while the generalization for bigger number of beads is straightforward.

Since it has been shown both theoretically[73] and by simulations[71] that EQS of single component system in DPD is purely quadratic, one could assume that for the case of two-component system EQS will remain the same. The situation in this case is very close to the case of Van der Waals theory of real gasses and liquids or to the Flory-Huggins[74] mean field treatment of liquids and polymer melts, where up to the second virial coefficient one could write the EQS of two-component system *homogeneous* system as

$$P = (\rho_1 + \rho_2) + (w_{11}\rho_1^2 + 2w_{12}\rho_1\rho_2 + w_{22}\rho_2^2) = \rho + (w_{11}x_{0,1}^2 + 2w_{12}x_{0,1}x_{0,2} + w_{22}x_{0,2}^2)\rho^2 \quad (4.17)$$

where, we have assumed again that kT=1, while $x_{0,i} = \rho_i / \rho$, are *initial* the molar fractions of the components and $\rho = \rho_1 + \rho_2$, is the total particle density. Depending on the values of the viral coefficients w_{ij}, the system could either stay homogeneous or phase separate into two phases: one phase, rich in particles of type 1 and a second one rich in particles of type 2.

Which situation will be realized depends on the values of the free energy of the system, i.e. whether the two-phase system will have lower energy than the single-phase homogeneous system. The main parameter controlling the outcome is so called Flory-Huggins[74] parameter $\chi \propto 2w_{12} - w_{11} - w_{22}$. When the two components disfavor the contact between each other (the energy of 12 contact is higher than the energy of 11 or 22 contacts, i.e. $w_{12} > (w_{11} + w_{22})/2$), χ parameter is positive, while if they favor 12 over 11 or 22 contacts, χ is negative. If $\chi < 2$ the system will remain homogeneous, while if $\chi > 2$ the system always phase separate. In the purely symmetrical case, when $w_{11} = w_{22}$ and $\chi > 2$, the molar fraction of the component 1 in the phase rich of component 2 is given with

$$\chi = \frac{\ln(1 - 1/x_1)}{1 - 2x_1}. \tag{4.18}$$

The latter equation is determined from the requirement that pressure and chemical potential of each of the species are equal in both phases, when the system is in thermodynamic equilibrium. The last expression is very practical for both experimental and computational point of view, because it allows the value of Flory parameter only by measurement of the amount of phase 1 dissolved in phase 2 (which is called solubility).

The last relation given with eq. 4.18, was used by Groot and Warren[71] to bridge the values of unlike repulsive parameters of conservative force and Flory parameter χ. For the case of symmetric fluids ($a_{11} = a_{22} = a$) they have performed DPD simulations where "unlike" parameter a_{12} was varied. From the simulations, the amount, x_1, of fluid one dissolved into the second fluid was determined form the density profiles (see figure 4.1), wherefrom the Flory parameter was calculated using eq 4.18. The obtained value of χ was plotted against the unlike interaction excess, $\Delta a_{12} = a_{12} - a$, between the beads, which is supposed to be proportional to χ. They have found from simulations that

$$\chi = 0.286\Delta a \text{ for } \rho = 3$$

$$\chi = 0.689\Delta a \text{ for } \rho = 5. \tag{4.19}$$

The latter equations provide very useful practical relations, which allow mapping the values

of solubility or χ parameter to the DPD interaction potential. The values of χ or solubility could either be taken from experiments, or could be calculated using other molecular dynamic or Monte Carlo simulations, using a detailed interactive potential between all the atoms constructing molecules. One possible way to do this is to calculate pair-wise energies (where from cohesive energy and χ could be calculated), which are obtained by averaging a large number of molecule configurations generated by a Monte Carlo approach[74-77]. This approach was originally developed for calculation of the miscibility of different molecular blends and polymers. In this approach the constraints, associated with excluded volume are directly included, as well as all the electrostatic interactions. Thus though they are not included explicitly into the DPD interactive potentials, they are taken into account when the magnitudes of these potentials are bridged to the properties of real systems. For some of the results presented in the thesis, the solubility parameters are calculated using the above mentioned Monte Carlo (MC) approach. The force field, used in MC calculations was COMPASS (condensed-phase optimized molecular potentials for atomistic simulation studies)[77] that is especially parameterized for the modeling of fluids.

One should also to note that the mapping of asymmetric magnitudes of conservative potentials described above is done for the case of the purely symmetric case when the symmetric amplitudes are equal i.e. $a_{11} = a_{22}$. When the symmetric amplitudes are different than the equation 4.18 becomes much more complicated because the solubility of fluid 1 into fluid 2 is different from the solubility of 2 in 1. In this case, one needs to solve 3 equations (two for chemical potentials and one for pressure) together, in order to extract the solubility values. In this case the Van der Waals theory and Flory- Hugins theory will give a different functional expressions (they coincide only in the symmetric case), due to the fact the Van der Waals theory is off-lattice and atoms are not restricted on the sides of the lattice, which are distinguishable like it is in Flory and Brag-Williams theory. The later fact is manifested with different forms of partition function of both systems ($Q_{FH} = q_1^{N_1} q_1^{N_1} \frac{(N_1 + N_2)!}{N_1! N_2!}$ and $Q_{vdW} = q_1^{N_1} q_1^{N_1} \frac{1}{N_1! N_2!}$). Both theories are leading to similar expression for EQS, but the form of chemical potential is different. For the case of symmetric case the volume per fluid particle

is equal in both fluids and the difference is canceled out. Thus an additional investigation is required to check the asymmetric case, whether DPD system follows the predictions of Flory theory as it was assumed in ref 71 (described above) or it follows a Van der Waals theory. This is very important for many practical applications where the Flory parameters are difficult to calculate or measure, while there are many empirical combining rules which allow calculation of crossover Van der Waals parameters.

An additional problem arises when one wants to use equations 4.18 and 4.19. When the two fluids are soluble ($\chi < 2$), one can still use equation 4.19, as an empirical relation without a strict prove. In some cases for fluids that are highly soluble it could happen that the Flory parameter could have highly negative value. In this case excess of conservative interaction, Δa will be negative and when the absolute value of asymmetric interaction parameter is determined $a_{12} = a + \Delta a$, it could become negative. This case should be avoided by a proper rescale of all of the interaction parameters, because negative values of interaction parameters in DPD correspond to attraction. Providing that in DPD potential do not have hardcore a strong attraction in the system will lead either to collapse or pronounced instability during the simulation. In this case one could map the solubility at different temperature, where the fluids are immiscible, and then to extrapolate them to the required temperature[78].

Finally we will make an additional comment concerning the case when different coarse graining is used for different species in the system – i.e. different number of real molecules is combined to construct the beads of each of the fluids. As we have already discussed this leads to changes of local molar fraction corresponding to the DPD system and the real system. Now is clear from eq. 4.18 that if the local volume fraction is changed this will lead to changes in the solubility and the Flory parameters in the system. The problem is that eq. 4.18 is non-linear, which means also that the effective (rescaled) parameter will depend non-linearly on the local composition. As it was discussed this is not a problem for a homogeneous systems because this is a constant rescale, which is known a priory, but when the local molar fraction starts to vary this means that we should use different rescaling in different places of our system, which of coarse is not possible to be implemented in the standard DPD method. The latter problem could be avoided by making DPD potentials non-local as it is discussed in ref 73. Another possibility to tackle this problem is to use a systematic coarse-graining procedure

from "top to bottom" developed by Serrano et.al.[79] and independently by Flekkoy et. al.[80]. The latter approach gives a simulation technique very similar to DPD. The beads in this approach do not have fixed size and mass during the simulation like it is in DPD (where the system is coarse-grained once in the beginning, from where the interaction parameters are obtained and kept constant later on during the simulation), but they are defined as a Voroni cells of the tessellation of the simulation box. The Voroni tessellation of the simulation box could have arbitrary form and is updated at every simulation step. The latter allows adjusting the coarse-graining procedure at each time step and each point of the simulation box.

The molecules in DPD are constructed by connecting together several beads using the interaction spring force

$$\mathbf{F}_{ij}^{S} = \sum_{j} k_s (r_{ij} - r_0)\mathbf{r}_{ij} \tag{4.20}$$

The sum runs over all particles to which particle j is connected. The spring constant k_s and equilibrium spring distance r_0 are adjusted to have a proper length of the bonds connecting the beads. Usually it is achieved by using very high spring constant (above 160 in DPD units), while the equilibrium distance is set to have value equal to the ratio between the bond length of real molecule and DPD length scale.

IV.3. Some applications of DPD for modeling of colloidal systems

Practical colloidal systems, which are used in industry, are very complex and are very difficult to be investigated theoretically and experimentally, which is of key importance for the optimization of their performance. It is also quite natural to have a formulation, which consists of tens of different components, like surfactants, polymers, alcohols etc, each of them with an industrial grade purity (for instance industrial grade surfactant $C_{12}E_{20}$ is actually a mixture of surfactants of different E chain lengths.). In this case both theoretical and experimental investigation of the system are very complicated due to a huge amount of different factors, which are influencing the system behavior. From the other point of view computer modeling is providing a powerful tool for instigation of various properties of the

systems, because from the computational point of view there is practically no difference whether we have a system, which consists of pure surfactants or any composition of surfactants of different chain lengths. They are handled in one and the same way and require practically one and the same computational time for getting the final result. Mixtures of surfactants and polymers can be modeled in a similar way. One can even have system, which consists of polymers of a random monomer stricture (which is the case of many polymers and proteins, which are natural products). All these problems could be studied with a sufficient accuracy by modern mesoscale methods. One could also use a computer modeling methods for getting a better insight of the unknown systems in order to check basic physical reasoning and theories in some extreme cases, where the experiments could not be performed:

A) Checking the extremes of the theories: When one makes a new theory or model, usually it is checked whether or not the model behaves properly in some extreme cases where the result is known. For instance one could be interested in behavior of the system at very low or very high temperatures where the behavior is simple and well known. In reality this is very difficult to be performed, but from the point of view of computer modeling it does not matter whether the temperature of the system is 0, 300, 3000, 300000K. Usually the models are made for some idealized system, like being absolutely pure, absolutely monodisperse etc. In reality we never have an absolutely pure system, but in computer models one could construct it without any problem. One could never have an influence of only one factor to the system behavior, but in the computer modeling one could nearly achieve this by increasing the magnitude of the factor to very high values and setting the magnitudes of other factors to very low or zero values. All these aspects make a computer modeling a powerful tool for checking new theories (and in some cases the modeling is the ultimate single tool, which can check the validity of the theory).

B) Checking the basic physical reasoning: Even in the case when a detailed theory is not available one can still use some basic physical reasoning from which he could describe qualitatively the system behavior, predict and optimize the system and could also explain why the system fails in some cases to perform as it was expected, and what should be done in order to avoid this. This applies with a full strength to the industrial formulations, where their composition must be optimized in order to get a new, better product at low production cost. A

typical industrial formulation consists of tens (or even more) components and it is very difficult to investigate the system both from theoretical and experimental point of view in order see what is the effect and the influence of each of these components. The motivations used for making a specific formulation in the latter case are ether based on some “thumb” rules, same intuition and previous knowledge of the behavior of the other systems, which have similar components. In all these cases one applies some basic physical reasoning. This reasoning is in most cases sounds like: this is more hydrophilic or hydrophobic, this adsorbs here, this adsorbs there, these substances are making a complexes which are giving the performance boost, etc and etc. One can use the computer modeling in this cases to check this reasoning and to see whether they are true or not, whether they really lead to desired effect and what happens when something else is added. In this case the detailed computer model of the system is not needed and one can make a simple model systems, which capture this basic physical reasoning. For instance, one could make two substances to like very much each other (which models some hydrophilic or hydrophobic interaction) and do not like others. Then a simple computer modeling with this system could answer the question whether or not these substances will form complex and whether they interact in a way it is expected. One could vary the magnitude of the interaction to see what is chaining and whether it is chaining in a desired direction. One could also add other substances, again with model parameters, to see what will happen with the system. These simple simulations could be used as a very powerful tool for checking our considerations and could avoid a lot of extremely difficult time and money consuming experiments, which in some cases give quite questionable results. If the model system modeled in a computer does not behaves properly even with an unrealistic high interaction, one could expect that in reality this also will be the case and some other factors, explanation and models should be considered. The simulations could be analyzed in more details, in order to see what is the reason that even with a very high interaction the system behave differently form the initial expectations. The latter investigation could initiate many new ideas. Another example is when a scientist decides that a given experimentally measurable property is responsible for the “application” effect of the systems (for example values of contact angles or interfacial tension usually correlate quite well with the detergency performance). This decision is based usually on theories, which are

much more simple and hardly could apply to a complex system, or based on same experimental measurements and statistical correlations like QSAR (quantitative structure agreement relationships) or QSPR (quantitative structure property relations). So the scientist decides based on some experience that if he knows the experimental property under consideration he could predict outcome of the system. But in some case this correlation is working and in some not, and it is very difficult to understand why this happens. In this case the computer modeling also could help very much, one can construct the simple model system, which corresponds again to basic physical reasoning, and study directly the desired application effect and its relation with the corresponding property. For instance one could vary surface tension several orders of magnitudes (having even not realistic values), to see whether the effect goes to the desired direction. If not one could determine the reason for this behavior, directly from the model simulations and gain some idea why the correlation is working and why not. This could save huge amount of time because if the model system fails (even in some extreme cases), probably the real system will fail also. Thus there is no point to make a detailed computer-modeling picture of the real system, which measures a single physical property, supposed to be a measure for the industrial application of the system if the model simulations fail. This is a typical example when instead of doing a very complex computer modeling of some physical property one could make very simple simulations with model systems, which are modeling the whole process (or at least parts of it)!

In this part we give some examples how DPD could be used for modeling the behavior of colloidal systems. The following examples will be given:

- Surfactant phase behavior in static and dynamic (under shear) conditions;
- Interfacial tension modeling (more systematic results are given in chapters 5 and 6);
- Interaction between surfactant and polymer mixtures;
- Modeling of the phase behavior of very long random structure polymers;
- Modeling of spreading and wetting phenomenon of the oil on the solid interface;
- Modeling of oil droplet detachment from the solid substrate under shear;
- Oil drop elongation in a shear flow.

The results given here should be considered as preliminary (though some of them according

to our knowledge are original contribution) and more detailed investigation is needed. They are presented here in order to illustrate the power of DPD method and its possible applications for modeling different aspects of colloidal systems behavior. Most of the results are actually aimed to evaluate the applicability of DPD method to model the detergency process, but even from these preliminary results one could gain much better insight of what is going in the system.

IV.3.1. Modeling phase behavior of ethoxylated surfactants in dynamic and static conditions.

Modeling of the phase behavior of surfactant systems is of key importance for many industrial applications, like cleaning and washing (detergency), coating etc. At different surfactant concentration, different phases are formed into the solution, which have very different macroscopic properties, like viscosity and diffusion. The phase behavior could be strongly influenced also by an external hydrodynamics flow. The latter is very important for instance for the detergency, where the system is subjected to a strong shear flow, which could significantly influence the system performance.

In this paragraph we describe some preliminary results were the phase behavior of systems containing ethoxylated surfactant $C_{12}E_6$ (see figure 1.1b) was studied both in static[63,78] and dynamic conditions. The surfactant is represented in DPD model as C_4E_3, where C is bead, which corresponds to hydrophobic part of surfactant and combines 3 ($-CH_2-$) groups, while E is hydrophilic part of surfactant and combines 2 (OCH_2CH_2) groups, water is represented by a single W bead, which combines about 3 water molecules. The interactive parameters for the conservative forces are obtained as discussed by Groot et. al.[78]. Detailed study of the phase behavior of system which is very much like $C_{12}E_6$ could be found in ref 63, where a binary model of surfactant was used: one hydrophobic and one hydrophilic bead are connected to represent the surfactant molecule. The interaction parameters are taken without any matching to a real system, instead they were chosen from some general consideration of the sort: this part likes other, this part not, repulsion in the first case should be twice smaller than symmetric repulsion (tuned trough the water compressibility for all beads), while in other case it should be twice bigger etc. Nevertheless even with this very crude model in ref 63

they manage to restore quite successfully the phase diagram, which is very close to the one of $C_{12}E_6$. The latter again is manifestation of the fact that precise values of the interaction parameters in DPD are not so important for studying qualitatively the behavior of the system, but their relative magnitudes are important. One could model behavior of one and the same system, with different sets of parameters. This is quite typical for all coarse – grained computer and statistical models, where the detailed interaction potential is smeared out trough the coarse graining procedure, and some integrals of the potential are derived, which are matched with macroscopic properties.

(a) 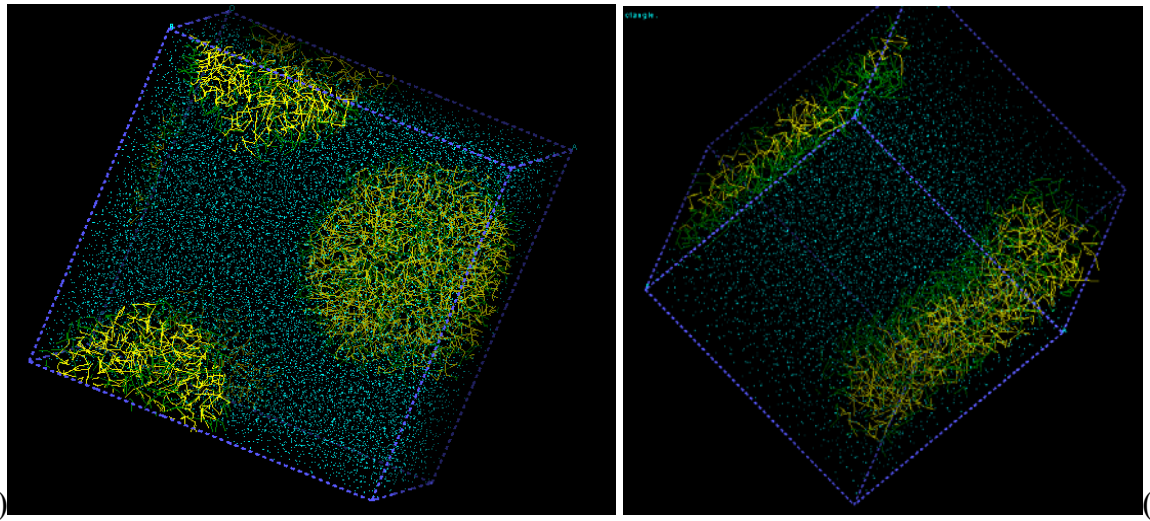 (b)

Figure 4.2. System containing $C_{12}E_6$ surfactant and water: (a) spherical and (b) cylindrical micelles. Green beads are hydrophilic part of surfactant, yellow beads represent the hydrophobic part, while blue are water beads. Surfactant is modeled as 3 hydrophilic and 4 hydrophobic beads, connected with a spring, while water is represented by single unconnected bead. DPD temperature was set to 1, which corresponds to a real temperature 30^{o} C. Box size was 10x10x10 DPD units. One length unit corresponds to about 6.8 Å . The DPD density was set to 5. In case (a) we have 120 surfactant molecules and the rest was filled with water, which responds to association number of 60 surfactant molecules per micelle.

In the beginning of our simulation, the surfactant and water molecules are randomly mixed into the box. Then equilibration was performed for about 100 000 time steps. In figure 4.2 we represent a snapshot of the simulation of rather small system where micellar behavior was studied. At low concentration we observe formation of spherical micelles in the system (case a), while increasing the concentration (case b) cylindrical micelles appear. By investigating the density profiles of surfactant beads in the micelles one could get a very valuable information about the structure of the micelle, how big hydrophobic core is, how the

surfactant tails are structured into the core etc.

By increasing surfactant concentration even further we observe the formation of a lamellar phase (figure 4.3a). At very high concentration (figure 4.3b) inverse micelles appear. We should point out that there might be a problem in a current representation of surfactant in DPD[78], because we did not observe a cubic phase though we have carefully looked for it.

Without Shear With Shear

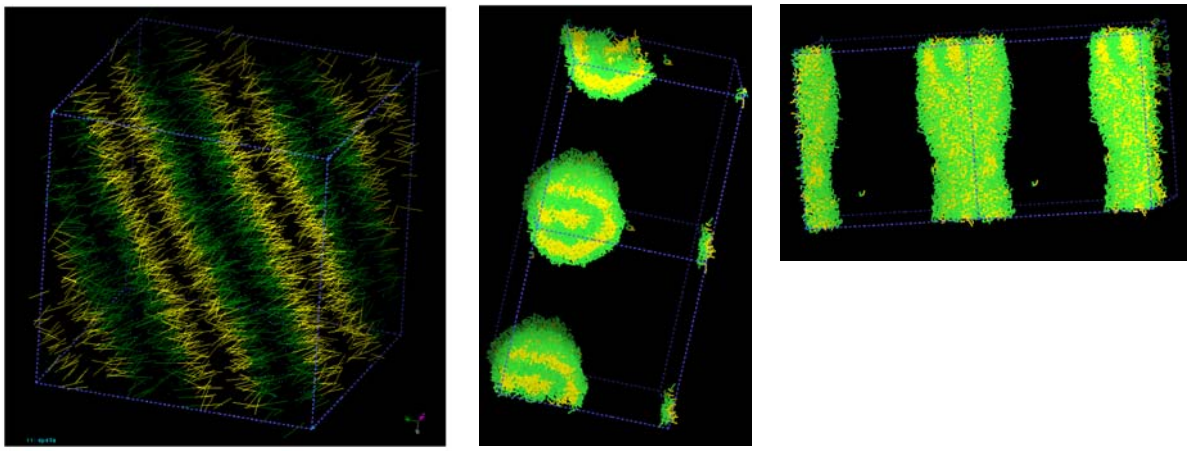

(a) Flow induced changes of the phase behavior: from lamellar to cylindrical vesicles

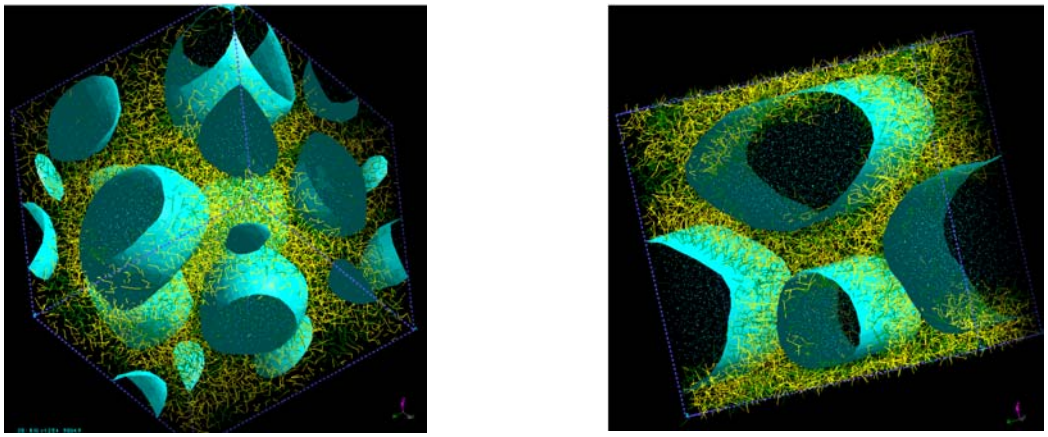

(b) Flow induced changes of the phase behavior: from inversed micelles to inversed hexagonal phase

Figure 4.3. Phase behavior of $C_{12}E_6$ in static and dynamic conditions.

Even a simulation performed with very big systems 40x40x40 which contain totally at about

320 000 beads, and running for 200 000 time steps did not show any profound formation of the phases under investigation. Same applies if we change surfactant type by adding or removing a beads from it, we did not observe a proper representation of phase behavior of $C_{3i}E_{2j}$ ethoxylated surfactants. This means that one should find a better mapping of the surfactant properties into DPD interactive parameters. Main problem for this type of surfactant comes from the fact that ethoxylated part is completely soluble in water and probably Flory parameter is not correctly mapped. Thus the results for this system should be considered, as a preliminary, and additional investigation is required.

In figure 4.3 on the right side we present a results after applying a shear to pre-equilibrated the simulation box. The shear was applied by using standard Lees-Edwards boundary conditions. The shear flow was applied to already equilibrated box (depicted at left side of figure 4.3) and simulation with shear was performed for additional 100 000 time step. After that the shear was switched off and additional simulation was performed for 100 000 time steps. One can see that sheared lamellar phase changes to onion like vesicles (both pictures in the top right of figure 4.3 show different views of the vesicle). This is in accordance with experimental observations given in ref 81. After the shear flow is stopped an additional simulation without shear restores back the system into its initial lamellar state.

Qualitatively different is the behavior of system, containing an inverse micellar phase. The blue surfaces drown in the bottom of figure 4.3 represent water isodensities. When a shear is applied to this system for 100 000 time steps, this leads to formation of long water channels which spread trough the simulation box, and form something like a inverse hexagonal phase. After the shear is stopped an additional 100 000 steps simulation (same time like the time system needs to order from complete disorder to a inverse micellar phase) did not change significantly the system, and inverse hexagonal phase remains. Thus this structure is very stable, which probably is due to the very high overall viscosity of the system. The latter result could be very important for many industrial applications, due to the different transport properties of species in the surfactant melt phase and water channels. Accounting to our knowledge this is the first simulation where inverse micellar and hexagonal phase are observed, and could be an original contribution.

Additional comment should be done, that the dynamical computer experiments are done

assuming that the dissipations and random amplitudes of DPD forces are equal for all types of beads, thus viscosities of all species are assumed to be equal. Latter is very rough assumption, and in the future, an additional simulations should be performed, where the dissipation coefficient are tuned in a way, which corresponds to the viscosities of real systems.

IV.3.2. Modeling surface tension of surfactant systems

In this part we give only initial information about modeling the surface tension of surfactant systems with DPD. Next chapter will be devoted to this case, and more details will be given there. In chapter 6, will be shown how the surface tension obtained from DPD model, could be mapped to the real experiments. An example for a system, where surface tension is studied is given in figure 4.4.

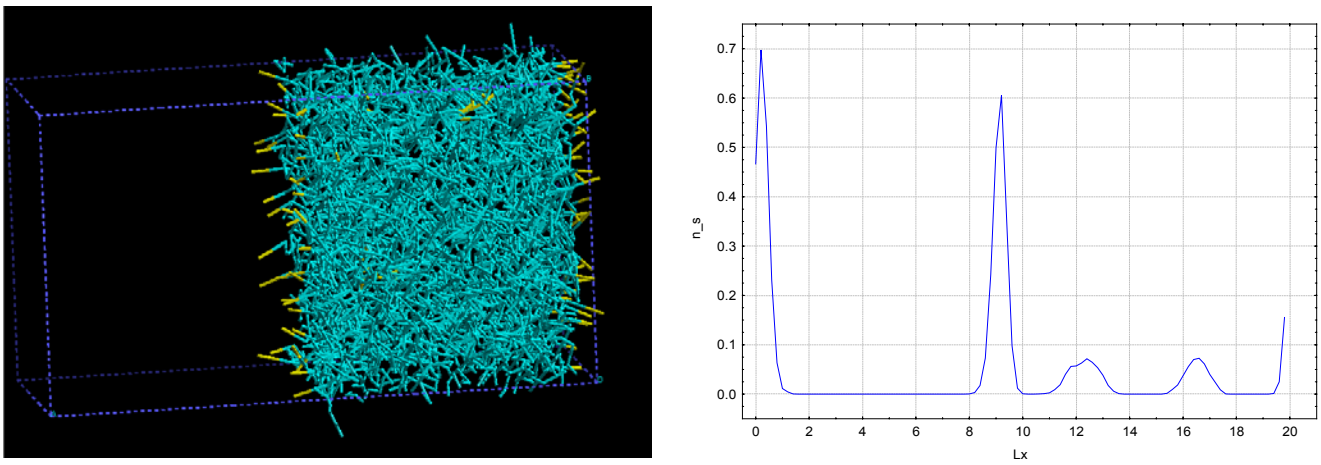

Figure 4.4. Snap shot of the simulation box (upper picture) and density distribution of surfactant head groups (bottom graph) for system containing "water" (which is hidden) and "oil" (blue) and oil soluble surfactant (yellow are surfactant head groups). In the beginning surfactant was randomly dissolved in the oil phase, while during the simulation most of it adsorbs at the interface (for more details see chapters V and VI).

There we show a snapshot and surfactant density distribution of non equilibrated simulation box. System contains oil and water like beads and oil soluble surfactant. In the beginning surfactant was dissolved into the oil phase. A sharp slab was also formed between oil and

water phases. The DPD simulation was performed and surfactant density distribution and surface tension were observed as a function of time. Such a simulation could give information not only for the equilibrium values of surface tension and adsorption, but as well as dynamical state information, which is very useful for many applications. Looking at the density distribution of surfactant one could see that even after very short time scales (snapshot was done after 5000 time steps) most of the surfactant is adsorbed at the interface. There is a small difference in the surfactant adsorption at both interfaces, which disappears after longer simulations. In the equilibrium (after 100 000 time steps) practically all of the surfactant adsorbs at the interface and only few molecules remain in the bulk oil phase. This is finite size effect of the simulation and it is commented in more details in chapter VI.

IV.3.3. Systems containing surfactants and long polymers

The simulation presented in this part are more or less illustrative for the power of DPD method. Detailed investigation of such system are presented in ref 82, where a model system containing a long polymer chain and surfactant with concentration bellow CMC was investigated. The main parameter, which was investigated was the end-to-end distance distribution of polymer chain as a function of surfactant concentration. Different polymers are considered: very hydrophilic or very hydrophobic ones. Depending on their hydrophobicity the water acts like a good or bad solvent, and even without surfactant the polymer conformation changes strongly. When the polymer is hydrophobic it does not like to contact with water and forms a small random globule. When it is hydrophilic it likes the water contact and has a “random walk” structure. When surfactant is added it additionally changes the conformation of the polymer, due to the adsorption of surfactant molecule on the chain of the polymer. Bellow CMC surfactant molecules adsorb at the polymer, but they are also tending to form complexes like micelles in order to minimize contact of the hydrophilic blocks with water. Latter leads to the decrease of the end–to-end distance of polymer as a function of the surfactant bulk concentration. Above CMC there are micelles and polymer chain tight several micelles together and form something like a necklace. In the latter case, the increase of the surfactant concentration increases the amount of micelles in the bulk,

which leads to effective increase of the end–to-end distance of polymer. As a result the end-to-end distance as a function surfactant concentration has a minimum, which is situated near CMC of the surfactant. The surfactant was modeled only with two beads hydrophilic and hydrophobic, water is modeled with one bead, and polymer is modeled as a homopolymer, which consists of 50, connected segments. An example of this system is given in figure 4.5.

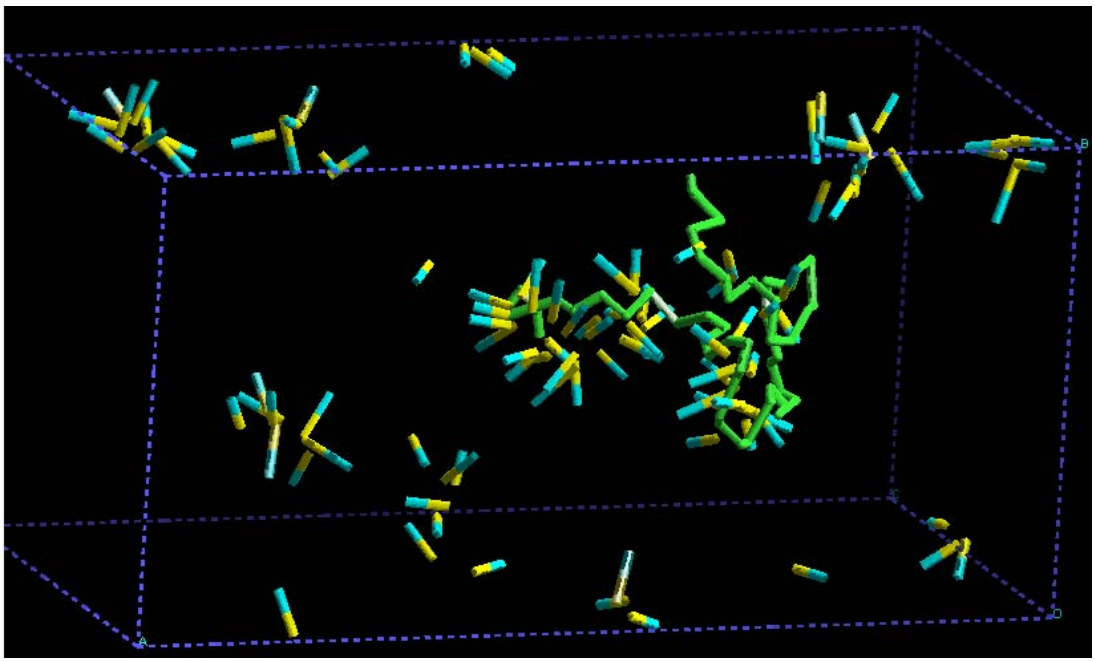

Figure 4.5. Hydrophobic polymer chain (green) in water (hidden) and surfactant (blue is hydrophilic block, yellow is hydrophobic block of surfactant) solution modeled with DPD. Surfactant concentration is bellow CMC. One could see a pronounced surfactant adsorption on the polymer chain.

The end–to-end distance of a polymer chain is very important for the steric interaction and stabilization of the systems containing polymers. The control of the end-to-end distance allows the control the magnitude of steric interaction, where from the system stability could be controlled. Although the simulations in this case are not connected with any specific system, whey could be considered as being of the type: checking conceptual ideas, and understanding the basic physics of the process. A lot could be learned from such type of simulation, and many properties of system could be studied and analyzed from the simulations.

IV.3.3. Systems containing polymers of "random-structure" in water solution

Here we present our results for the structure of long random sugar like polymer was investigated as a function of its bulk concentration. The simulation box was 30x30x30 DPD units and density was 5, which means that in the box we have 135 000 DPD beads. The recalculated (trough water density) box size is about 300Å. Each system is simulated for 10 000 DPD time steps (0.05 DPD units each). One DPD unit corresponds roughly to 200ps, thus one DPD time step is about 10 ps, i.e. total simulation time is about 100ns. Typical computational time on single PC (Athlon 1.4 Ghz with 521MB RAM, Windows 2K Server) for this system is 2.5 hours. This demonstrates the power of the DPD method, which could handle very large systems inexpensively from computational point of view.

The polymer consists of 2 types of segments, which we refer as W (hydrophilic) and G (hydrophoic). We used 50 segments connected in a single polymer chain, which are randomly distributed. Thus each polymer is unique and different from the others. From computational point of view, it does not matter whether molecules are different or are similar, they are handled similarly without increasing of the computational time as the variety of segments increases The random polymers are usually synthesized by nature. For example such polymers are sugar like polymers, like gluronats. Their properties and structure are very important for many biological processes.

In figure 4.6a we show a snapshot of simulation boxes having different number of polymer molecules. The first one consists of 540 Polymer molecules (35 wt%) (each molecule contains G:25 (green) W:25 (red)), there are 108 000 water beads which are hidden. The second picture consists of 100 polymer molecules (7.6 wt %), third from 50 (4 wt %) and the last one from 5 molecules.

One sees in figure 4.6a that there is not predominant structure in the system. The polymers are forming something like a randomly structured network, which is due to the random structure of polymer chains. If they are formed like di-block polymers, at the same conditions (concentration and interaction potentials) one could see a lamellar like structure at high concentrations (see figure 4.6b).

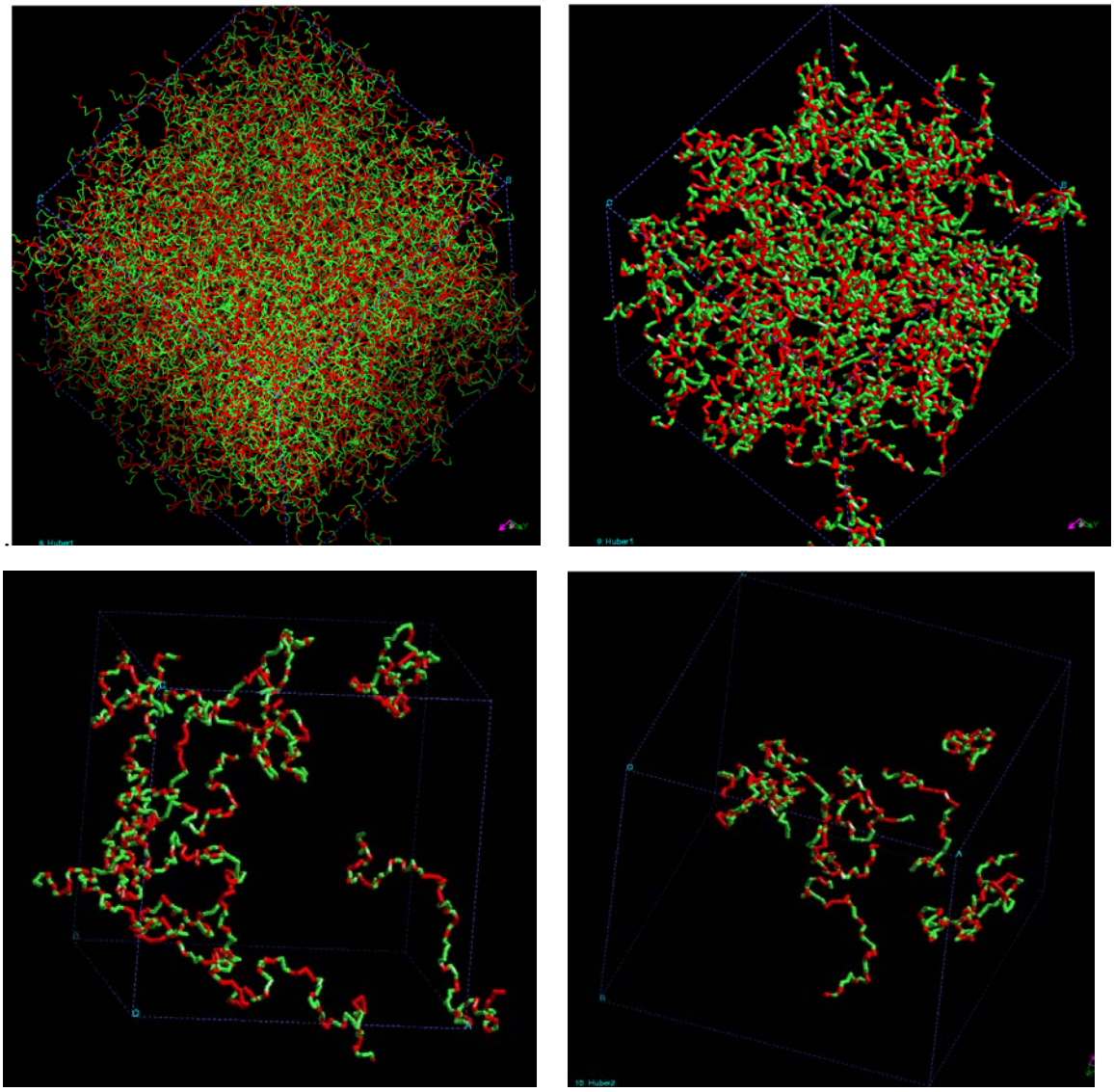

Figure 4.6a. DPD simulations of a system containing different amount of randomly structured sugar like polymer in water solution.

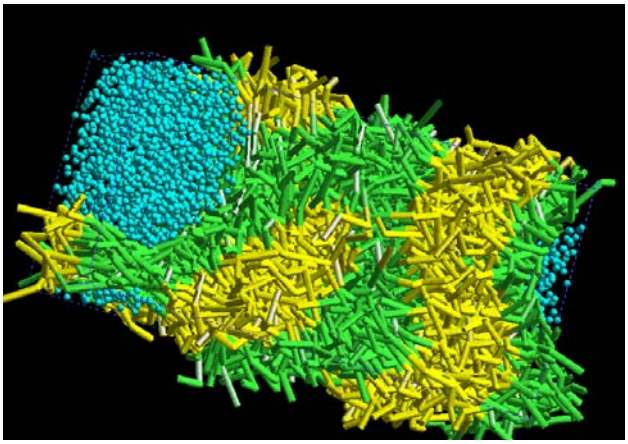

Figure 4.6b. DPD simulations of a system containing di-block sugar like polymers dissolved in water solution.

IV.3.4. Modeling of wetting phenomena- spreading of oil drops on a solid substrate.

Here we present DPD simulation results were we have modeled the equilibrium contact angle of oil drops situated on a solid interface. Example system is shown in figure 4.7. Similar simulations are performed in ref. 84.

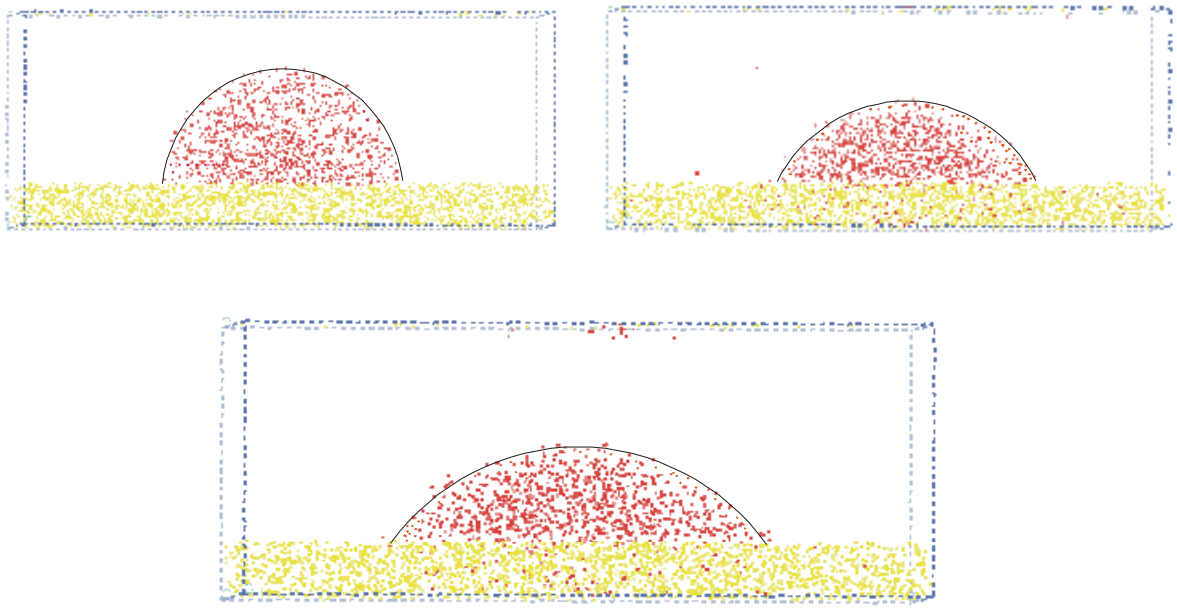

Figure 4.7. An oil drop wetting and spreading on a solid substrate modeled with DPD.

The oil and water were represented by single DPD beads. The solid wall is constructed by freezing a third type of beads into the bottom of box in BCC crystal structure. In the beginning oil was placed on the interface having hemi-spherical form. Then the DPD simulation is performed till the drop acquires its equilibrium form. Stages of the system evolution (oil spreading) are shown in figure 4.7 (first is initial configuration and the last picture is the final configuration). For the better determination of the contact angle one should use the density profiles of the oil beads (shown as a black line in the figure), or work with bigger system. By controlling the conservative interaction between the beads one controls the equilibrium contact angle in a wide range of values. In the present system the

repulsion between the oil and solid was decreased compared to the one between water and solid in order to decrease the contact angle. The latter leads to a limited penetration of the oil beads into the solid. In this case the system could be considered as a model of the spreading phenomenon on the paper or cotton like substrate. The penetration effect could be avoided ether by increasing the repulsion or by increasing the density of the wall. In this case due to higher repulsion a layer that is free of DPD particles appears near the wall (see 4.8a). The effect of the solid wall is also discussed in more details in the next chapter.

We would like to mention also that any type of wall can be used in DPD simulation. In the present case we have used a crystal wall – beads are frozen into BCC structure. But one can also use an amorphous wall, where beads have random position, or even a wall, which consists of several types of beads, like hydrophilic and hydrophobic domains. The latter could be also distributed in any desired way – like stripes or tails etc. This allows a huge range of wetting and spreading phenomena to be investigated. Wall could also have any non-planar shape or even we could have polymers grafted on the wall, and speeding over polymer brush to be investigated.

IV.3.5. Modeling droplet detachment from a solid wall in shear flow.

Here we present some DPD results where the detachment of an oil drop in shear flow was modeled. Similar system was described in the previous paragraph, which after the equilibration (contact angle was equilibrated) was subjected to a gradually increasing shear flow directed parallel to the wall (see figure 4.8a). The results of such simulation are presented in figure 4.8a. In figure 4.8b we present a video sequence of the real drop detachment to illustrate the similarity between simulation and reality. Similar simulation are also done performed in ref 83.

The first image in figure 4.8a represents a steady drop without shear, followed by a series of frames representing different stages of the detachment process. In the last image we present the stage of system after the shear was stopped and after the subsequent equilibration simulation without shear flow. Due to the sudden stop of the shear and due to the periodic boundary conditions, a strong hydrodynamic circulation appears, followed by a re-deposition

of the detached amount of oil drop back onto the surface, which forms second smaller drop (stage9). Looking at frames 1 and 9 one sees that both the initial and the final re-deposited drops have nearly the same contact angle. The latter is measure of the reproducibility of the simulation where equilibrium contact angle is determined in DPD, like it was described in previous paragraph.

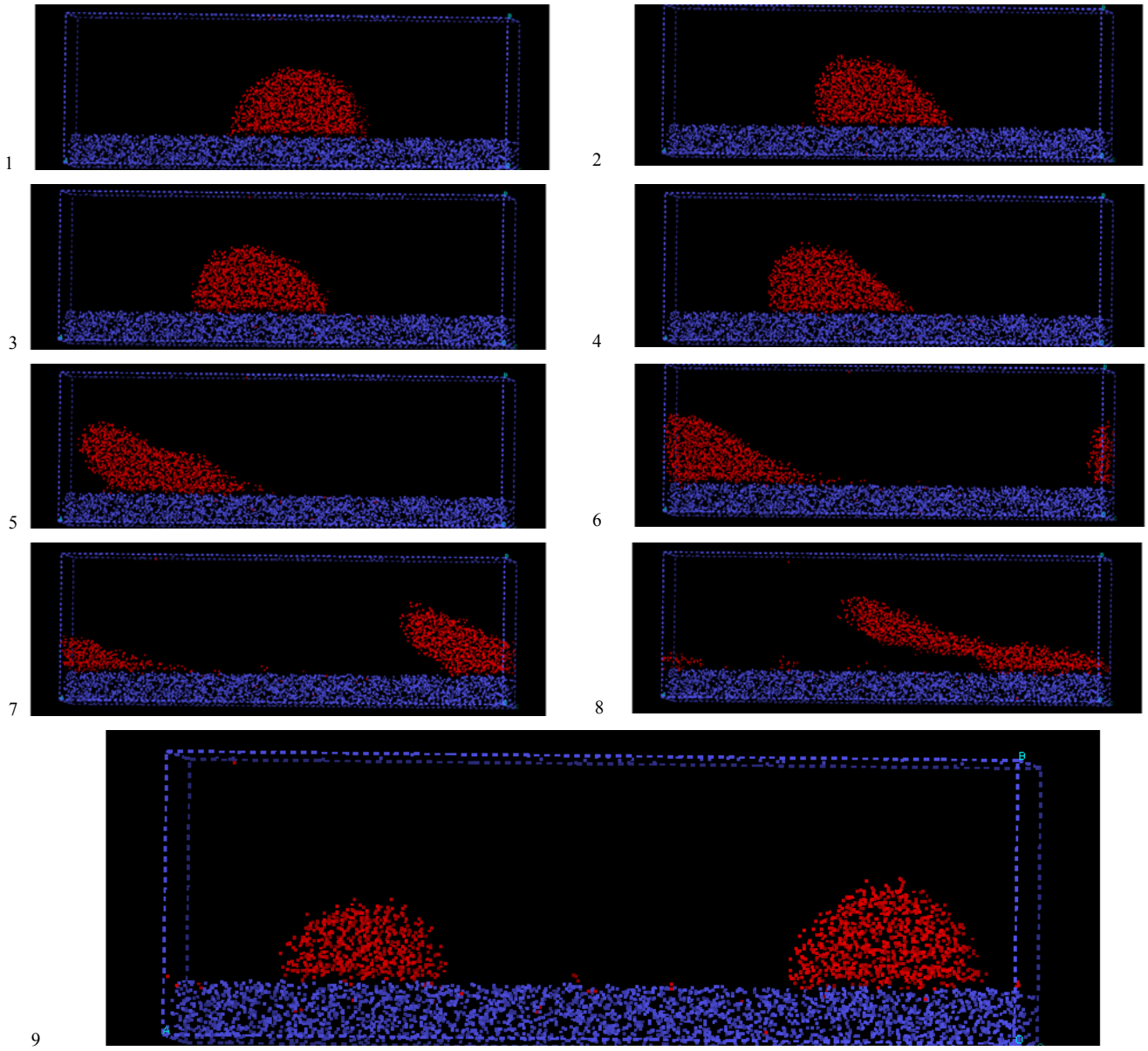

Figure 4.8a. Detachment stages of oil drop in shear flow modeled with DPD. Solid wall is blue, oil is red, and water fills the rest of the box, and is hidden. The wall is constructed by frozen (in the beginning of the simulation) DPD beads in amorphous structure. Due to the strong repulsion between the wall beads and other beads, there is a layer near the wall where beads are effectively expelled. Tuning the interaction between the wall, water and oil allows tuning equilibrium macroscopic three-phase contact angle of oil drop.

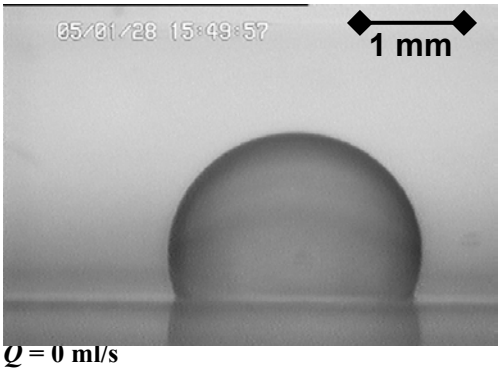

Q = 0 ml/s

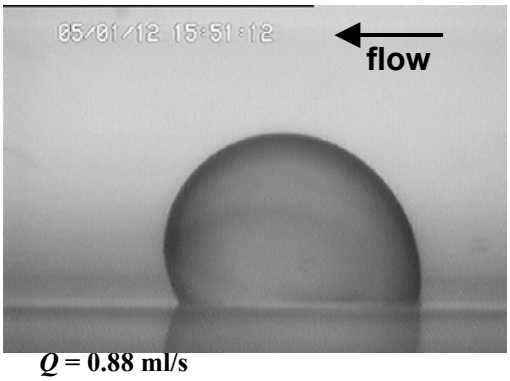

Q = 0.88 ml/s

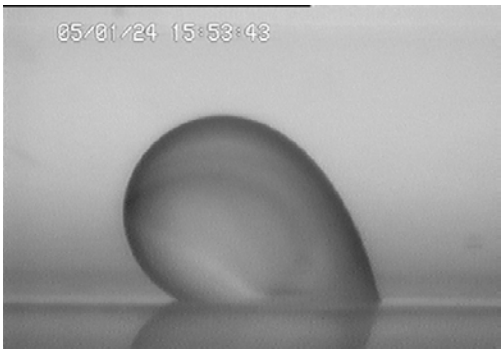

Q = 1.61 ml/s

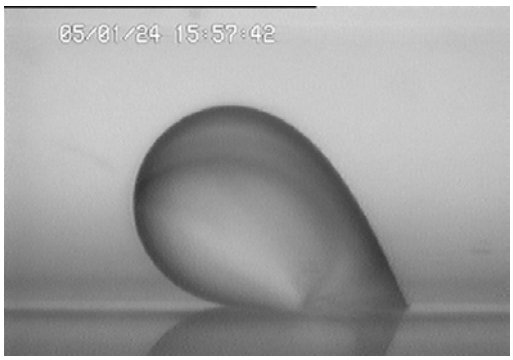

Q = 1.64 ml/s

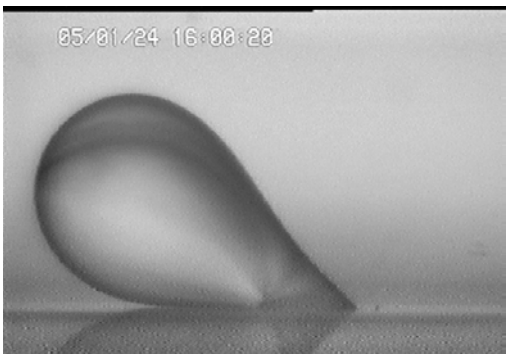

Q_{CR} = 1.76 ml/s (detachment- frame#1

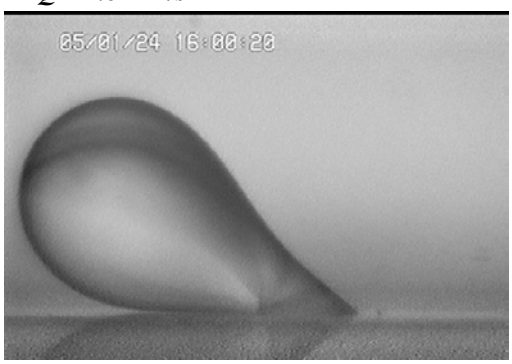

(detachment- frame #2)

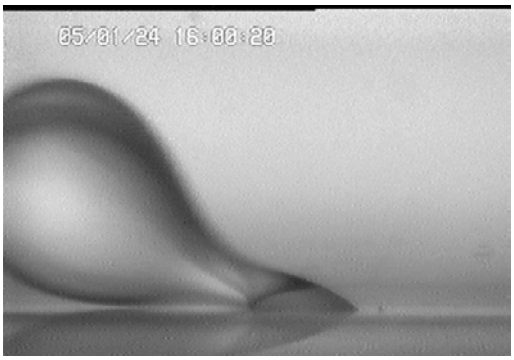

(detachment- frame #5)

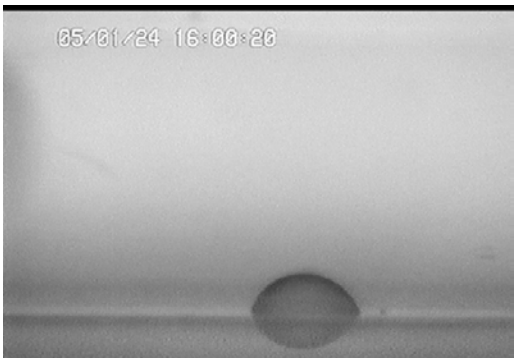

(detachment- frame #6)

Figure 4.8b. Detachment of an oil drop in shear flow of aqueous solution of surfactant. The shear channel dimensions are: height H_c = 5 mm and width W = 6 mm. Characteristic drop height H_d = 2 mm. The estimated critical Reynolds number is: Re ~ 138.

IV.3.4. Flow induced emulsification of oil drop

Here we show an example of elongation of the oil drop placed in the shear flow. Results of such a simulation are shown in figure 4.9.

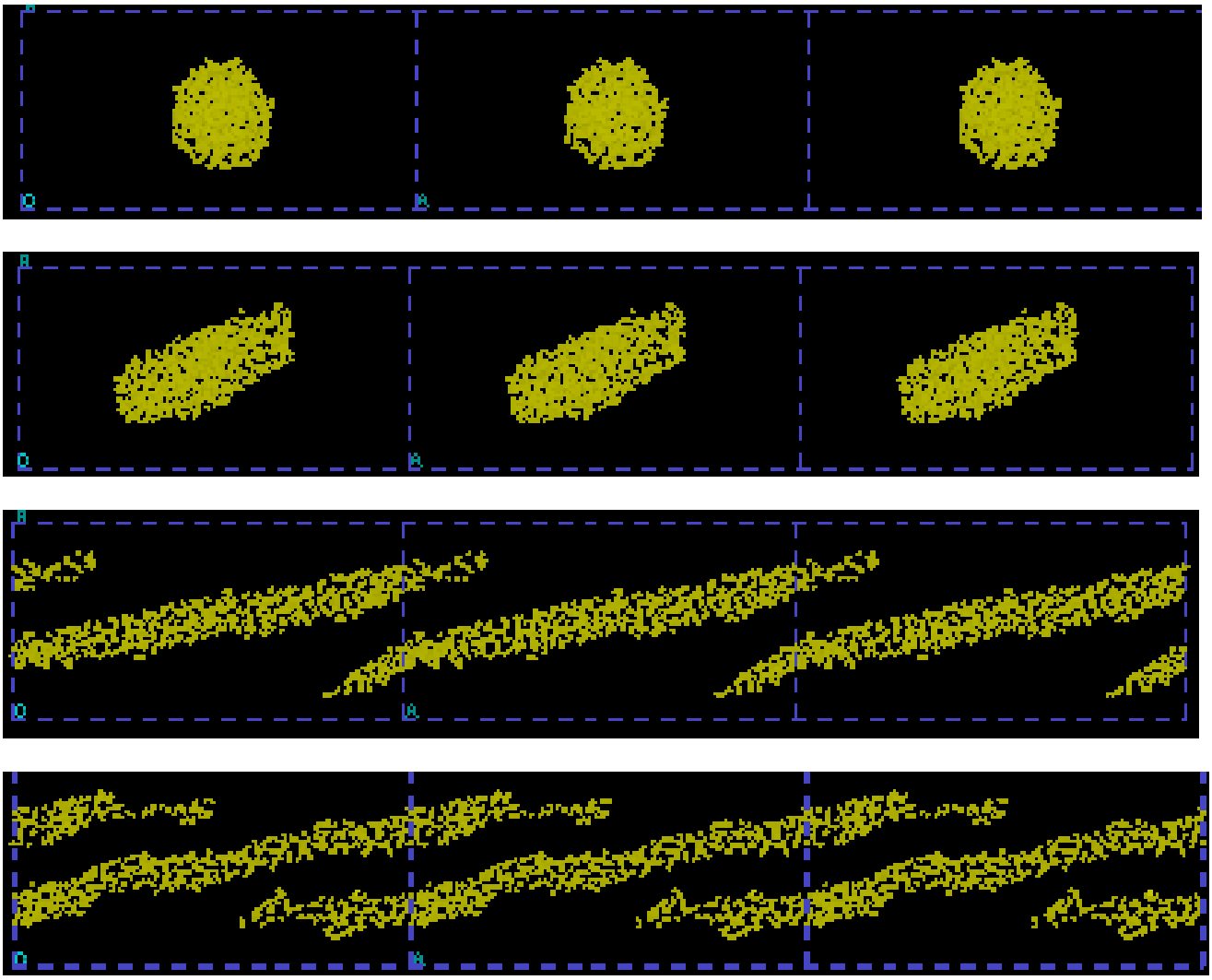

Figure 4.9. Oil (yellow) drop elongation in shear flow. The rest of the box is filled with water, which is not presented on the images. The three subsequent frames are shown in order to illustrate the droplet elongation.

Figure 4.9 shows the elongation of the droplet and the appearance of the instability of the droplet shape, which on the next frame (not shown here) leads to a droplet break up. The results presented in this paragraph could be used for modeling the process of emulsification of oil/water systems, subjected on strong shear flow, like stirring. Similar simulations have

been presented in ref. 84, where it has also been investigated (using DPD), the process of droplet formation (on the neck of a small capillary) and its break up due to the gravity. Both processes (drop in shear flow and drop in gravity field) are important for better understanding the process of mechanical detergency, which is of immense industrial importance[85-87].

We stress here that all results on dynamic behavior of different systems presented in this chapter are done using equal friction coefficients for all types of DPD beads, which means that phases are assumed to have equal viscosities. For more detailed investigation, the friction coefficients should be tuned in order to represent proper viscosities of the phases under investigation.

In the case when pure hydrodynamic effects are studied using the DPD method, there are no principle problems to match the simulations to real systems. This is due to the fact that provided that basic dimensionless hydrodynamic numbers in both systems (real and in the simulation) are matched on the scale of similarity theorems which ensures that both systems are equivalent from hydrodynamic point of view, but may have different dimensional scales.

IV.4. Conclusions

In this chapter we have outlined the basics of DPD method, and have shown several applications for modeling different properties and behavior of colloidal and surfactant systems. Most of the results have an illustrative purpose in order to show possible applications for modeling surfactant phase behavior and detergency. Some of them (phase behavior in dynamic conditions) according to our knowledge are original contributions, but additional investigation is required for their completion. In the next chapters we use the DPD simulation to model the surface activity of surfactants and we compare the results of the simulation with the predictions of the self-consistent field theory (SCF) outlined in previous chapters. There we will also describe a procedure, which allows rescaling the DPD simulation results into the real systems. The latter could be also considered as a new mapping procedure, which allows bridging the parameters of DPD to the surface activity of surfactant and polymer systems.

V. Polymers at Interfaces – Comparison Between Self Consistent Field Theory and Dissipative Particle Dynamics Computer Simulations

Abstract

To check the predictions of the SCF theory, discussed in the previous chapters, we have performed two types of Dissipative Particle Dynamics (DPD) computer simulations with long polymer brushes attached to an interface in good solvent. In the first type of simulation we have studied the density distribution of the chain monomers and the thickness of the homo-polymer brushes grafted at a solid interface. Very good agreement was observed between DPD results and the predictions of Self Consistent Theory (SCF): all segment density profiles obtained with DPD simulation nearly coincide with the curve predicted from SCF; we found that the brush thickness quantitatively follows the scaling law of SCF. In the second type of simulation we have constructed di-block polymer ("surfactant"), having a long hydrophobic chain, and hydrophilic head. Due to its very long hydrophobic chain the surfactant is highly amphiphilic and has high affinity to adsorb at the interface between oil and water. We have simulated the interfacial tension of this system and have compared the results from SCF – assuming that the main contribution to the surface tension comes mainly from the conformational energy of the surfactant tails. We observe that simulation results agree pretty well with the predictions of SCF theory.

V.1. Introduction

The properties of the systems containing surfactants and polymers are very important from both pure scientific and industrial point of view. Polymers grafted on solid surfaces have wide application in various polymer technologies and high-tech coatings. Grafted polymers have also been intensively studied theoretically since this model system plays an important role in understanding fundamental problems of polymeric materials. Di-block polymers composed of hydrophilic and hydrophobic blocks are widely used in many industrial systems as surfactants due to their high surface affinity. Understanding their surface properties plays is a key for performance optimization of commercially important formulations, like washing powders, shampoos and conditioners, household cleaners, etc. Both systems are subject to a great interest from both experimental, theoretical and computer simulation point of view. The scaling analysis of Alexander[24] and deGennes[25] and more sophisticated and detailed approach of Semonov[26], Milner et. al.[38], Skvortsov et. al.[37] reveal some important and fundamental properties of polymer systems. In their analysis Alexander and deGennes assume a stepwise distribution of the polymer segments near the interface

which captures well the scaling behavior of the brushes with the temperature and the numbers of segments but the numerical factors could not be predicted quantitatively based on their consideration. In the Self Consisted Mean Field (SCF) approach of Semonov[26], the non-uniform distribution of the polymer chain segments is taken into account by minimization of the corresponding density functional of the theory, which allows quantitative description of the properties of grafted polymer chains. The latter results are checked both experimentally[39] and numerically using a computer simulations[37,40]. In the work of Lay et. al.[27] a Monte Carlo computer simulation was performed using a fluctuation bond model. The chains of the polymer are confined on the lattice requiring self-avoidance. The results of the simulations show an excellent agreement with the predictions from SCF theory used with specific parameters of the Bond Fluctuation model[27]

Because the SCF theory of polymer brushes gives very simple analytical expressions it provides a very useful and powerful tool for checking and tuning of the parameters of computer simulations. The aim of the present chapter is to check the results from Dissipative Particle Dynamics[57-90] computer simulation against the predictions from SCF. For this reason we have done two types of simulations: (i) standard simulation of long polymer chains grafted on the solid interface where segment density profiles are compared with the predictions of the SCF theory and (ii) simulations of the interfacial tension of an oil-water interface, where a highly amphiphilic di-block polymer (having a very long hydrophobic block and a short hydrophilic block), adsorbs at oil/water interface. Here we assume that the main contribution to the interfacial tension (excess of the free energy of the system per unit area) comes from the free energy of the hydrophobic block of the polymer. The hydrophobic block at the oil/water interface is considered as a grafted polymer brush, with an additional correction, which takes into account that the polymers could adjust their area per molecule as that they are in equilibrium with a bulk solution. In this chapter we use one and the same theory to study and interpret the results from two completely different types of DPD simulations. This is an additional test that the DPD method correctly reproduces the SCF predictions and hence, could be used to calculate the system properties for cases when such the SCF model is difficult to resolve analytically.

This chapter is organized as follows: In section 2 we briefly outline the DPD method and the basis of the SCF theory. Special attention is paid to the relation of the parameters of the DPD

type of potential and those of the equation of state. In section 3 we describe computational details of the simulation, while in section 4 we compare the modeling results with the SCF theory.

V.2. Theoretical Background

The aim of the present paragraph is to outline briefly the basic of DPD and SCF in order to make the chapter self-consistent. SCF theory is discussed in more details in chapter II and III, while DPD method and some application are given in chapter IV.

V.2.1 DPD Method. Dissipative Particle Dynamics (DPD) is a comparatively new computational, coarse-grained method[57-90]. The main objects of DPD are called beads, which usually represent not single atoms or molecules but groups (clusters) or whole molecules. For instance: if we like to model a pure solvent, several solvent molecules could be combined in a single bead, which coordinates in DPD will represent a coordinates of the center of mass of the clustered molecules. Since the DPD is dealing with clusters of molecules rather than with single molecules, there is no need to use a hard-core repulsion between the beads, because there is no restriction preventing the overlap of the center of masses of groups of atoms or molecules. The latter is very important for the computational efficiency of the method and allows much larger times steps to be accesses during the calculation. For instance if the normal time step in a standard molecular dynamics is of order several femto seconds in DPD one could achieve values of order 1ns and even higher. The main differences between standard Molecular Dynamics (MD) and DPD are: (i) very simple interactive potentials and (ii) special Langevin type of thermostat used in DPD. The conservative force (acting between beads) in DPD is the simplest possible continuous force: it decreases linearly with the distance up to the cutoff radius, r_c, where it becomes zero, i.e. $\mathbf{F}_{ij} = -a_{ij}(1 - r_{ij}/r_c)\mathbf{e}_{ij}$, when $r_{ij} \le r_c$, and zero otherwise, a_{ij} is the magnitude of the conservative force (value at $r_{ij} = 0$), r_{ij} is the distance between the particles *i* and *j*, $\mathbf{e}_{ij}$ is the unit vector pointing from particle *j* to particle *i*. The conservative forces are always repulsive, which results in an equation of state (EQS), which is quadratic[71] and describes a super critical fluid. Thus, coexisting of liquid and gas in equilibrium cannot be modeled by using the standard type of the DPD conservative

forces. However, the DPD method is not restricted only to conservative force fields and one could in principle apply whatever force field he likes[73] – but the increase of the force complexity is paid with poorer computational efficiency of the method, which in the limiting case gives a standard MD with a special type of thermostat[71]. Generalization of the DPD method have been proposed, where the conservative forces acting between the DPD particles depend not only on the distance between them but also on a local weighted particle density around each particle[73]. This modification allows to change the EQS to a Van der Waals type, where one could simulate also a liquid-gas equilibrium, but the penalty is doubled (or more) computational time. By connecting several beads together with a spring (harmonic interactive potential) one could construct molecules (polymers in our case). In addition to the standard conservative forces in the DPD method, there are also two additional types of forces acting between the beads. These forces are called dissipation and random forces. The random force is a stochastic force, acting between each pair of beads, which depends on the distance between them and is pair-wise additive. Its magnitude of this force is multiplied by a random number chosen from Gaussian distribution, which must be uncorrelated for each pair and each time step. The second force (dissipative) is a deterministic force, which depends on the relative velocity between each bead pair and the distance between them and is also pair-wise additive. The magnitudes of dissipative and random forces are tuned in such a way that they obey the fluctuation dissipation theorem[59]. The latter means that they do not influence the final equilibrium state of the system, but their purpose is to keep the temperature constant throughout the simulation box, during the time of calculation. An important feature of the DPD method is that all forces acting between the beads are pair-wise additive, which means that the DPD preserves total impulse of the system. The thermodynamic ensemble simulated with standard DPD is NVT, though there is a generalization for the case of NVE.

DPD Units: For the sake of computational convenience the following units are used throughout the DPD calculations: $kT = 1$ (T is thermodynamic temperature of the system and k is the Boltzman constant)- which sets the unit for energy; $r_c = 1$ (the interaction between all type of beads is assumed to have one and the same cutoff radii) – which sets the unit for distance, and $m = 1$ (m is the mass of DPD beads), which sets the unit for mass. All beads are assumed to have one and the same mass, which is only done for convenience and is by no

means a restriction of the method. The exact value of the beads mass influences the dynamics of the process, but not the equilibrium state of the system, determined fully from the conservative inter-bead potentials. Here we are solely interested in equilibrium properties, which justifies this assumption. All other units could be derived from the above listed ones: for instance velocity unit could be extracted from the Boltzmann distribution $\sqrt{3kT/m}$, from where the time unit in DPD could be calculated: $\sqrt{m r_c^2 / 3kT}$. All results of the DPD simulations described in the text bellow are presented in "DPD units" – assuming that the corresponding physical units for given value should be used. For more details and comments how DPD units could be converted to the real one see chapter IV and chapter VI.4.2 as well.

V.2.2. Self Consistent Mean Field Theory. The Self Consistent Field Theory is discussed in details in chapter II of the thesis. Here we summarize only some main results of this theory, which we will need for the current discussion.

V.2.2.1. Grafted polymer chains. We will consider mono disperse chains grafted at the solid interface[24-27,37-40]. In the Self Consistent Mean Field theory (SCF)[26,37,38] the free energy of the system is written in terms of the density functional of the monomer concentration. For long grafted chains the free energy could be written as:

$$F = F_{osm} + F_{conf} + F_{solvent\_bulk}\,. \tag{5.1}$$

Here F_{osm} accounts for the purely osmotic contribution of the polymer segments, which does not account for the links between them in the polymer chain, F_{conf} accounts for the conformational entropy of the polymer chain and the $F_{solvent\_bulk}$ is the bulk free energy of the bulk solvent. The latter contribution will be omitted in our further discussion because it is of no interest for our considerations.

Using the mean field approach of Flory the osmotic term in eq 5.1 could be written as

$$F_{osm} = \frac{kTA}{v_0}\int_0^H Q(\varphi(x))dx \tag{5.2}$$

where, $\varphi(x)$ is the volume fraction of polymer segments, x is distance from solid the substrate, A is the total system area and v_0 is the volume of the monomer segment. Here

$Q(\varphi)$ is the corresponding free energy density. By definition, for free segments in a homogeneous solution of volume fraction φ_0, the osmotic pressure of the system can be calculated via Q as $P = \frac{kT}{v_0}\left(\varphi_0 \frac{\partial Q}{\partial \varphi_0} - Q\right)$. For simplicity, here we have explicitly assumed that the solvent and segments have one and the same volume molecular volume, i.e. segments are from one the same type like solvent molecules. The polymer chain is constructed by connecting several solvent molecules into a long chain. When the solvent molecules and the polymer segments have different volume, eq 5.2 should be corrected by factor of v_0 / v_w, where v_w is the volume per solvent molecule. The brush thickness, H, is defined as a point where the segment density is zero i.e. $\varphi(H) = 0$. In the text bellow we also use the term area per molecule, $\sigma = A/M$, while the adsorption is $\Gamma = 1/\sigma$.

We also assume that both solvent and polymer segments are uncompressible. Thus, one can write an additional equation for conserving of total volume of the polymer brush

$$\int_0^H \varphi(x)dx = Nv_0 / \sigma . \tag{5.3}$$

As it was shown in chapter II of the thesis the conformational free energy of long extended chains in a continuous limit could be written as

$$F_{conf} = \frac{kTAK_S}{v_0}\int_0^H \varphi(x)x^2 dx \tag{5.4}$$

where, $K_S = \frac{3\pi^2}{8N^2l^2}$ is the effective spring constant of the mean field potential of the chains – i.e. $K_s x^2/2$ is a mean potential of all surrounding chains that are acting on the specific segment of the polymer. The latter equation allows us to write the free energy of the system in the form of a density functional (DF) containing only the segment volume fraction.

The density of the osmotic part of the free energy could be expressed using the virial expansion (up to the quadratic term)

$$Q = \frac{w}{2}\varphi^2(x) + \chi\varphi(x)(1-\varphi(x)) \tag{5.5}$$

where w is the second virial coefficient of the pressure expansion (of like solvent and polymer segments) and χ is the Flory-Huggins parameter, which accounts for the interaction between the monomers and the solvent. Here we have explicitly separated the osmotic part

from the Flory-Huggins part. Usually both are combined together and one is working with a modified virial coefficient $B=(w-2\chi)$ (the linear term $\chi\varphi$ and ideal gas term in pressure expansion do not contribute due to the normalizing condition eq 5.3). For the case a "good" solvent (similar segments and solvent molecules) we have $\chi=0$. It has been shown by Groot et. al.[71] that for a DPD fluid the pressure has only a quadratic term even for very high concentrations, hence one can assume that the latter formula is exact for the case of DPD fluid considered in the simulation. The virial coefficient of DPD is $w\approx\frac{\pi}{30}a_{ii}\approx 0.1a$ [71,73], where, a_{ii}, is the conservative force amplitude determining the repulsion between like beads (solvent and segments). Since DPD uses soft potentials, both the segment and the solvent bead volume are $v_0=1/\rho$, where ρ is the density of the DPD system. Thus in the dissipative particle dynamic simulation one should expect that the corresponding density functional (DF) has the form

$$F/A=\int_0^H\Phi(\varphi(x))dx=\frac{kT}{v_0}\int_0^H\left\{\frac{w}{2}\varphi(x)^2+K_S\varphi(x)x^2\right\}dx. \qquad (5.6)$$

Note that eq 5.6 can also be used for systems where the second order virial expansion of the pressure is justified – i.e. cases for moderated surface coverage[26,37,38, 41].

In the SCF theory the functional 5.6 is minimized with respect of the segment volume fraction taking into account the normalizing condition eq 5.3 to give

$$kT\left(w\varphi(x)+K_Sx^2\right)=\mu_C=kTK_sH^2,\ \varphi(x)=\frac{K_SH^2}{w}(1-(x/H)^2) \qquad (5.7)$$

where, it has been used that the volume fraction vanishes at the x=H, and $\mu_C=v_0\frac{\delta\Phi}{\delta\varphi}$ is the chemical potential of the segment, which is independent of x. Substituting the last equation into the normalization condition for the volume fraction produces an expression for the brush thickness,

$$\left(\frac{H}{N}\right)^3=\frac{3wv_0}{2K_s\sigma}=\frac{4wv_0l^2}{\pi^2\sigma}. \qquad (5.8)$$

Substituting the solution for the brush thickness in the volume profile one can see that $\varphi(x)\sigma^{2/3}$ is a universal function of $x\sigma^{1/3}$, for any value of the area per polymer σ, thus all

density profiles should collapse onto one master curve[27] (when all other properties of the polymer are kept constant, while varying the surface coverage). One can also show that[26,27,37]

$$\langle x \rangle = \frac{\int_0^H \varphi(x) x dx}{\int_0^H \varphi(x) dx} = \frac{3}{8} H \,. \tag{5.9}$$

VI.2.2.2. Amphiphilic di-block copolymers at the "oil-water" interface. Here we consider the case of a highly amphiphilic di-block polymer (surfactant) adsorbed at the interface between two immiscible fluids. The first liquid we will call "water" (hydrophilic) and the second "oil" (hydrophobic). The polymer has two types of segments: one hydrophilic segment and N hydrophobic segments. This type of polymer is a model of a surfactant having a long chain: the water-like segment models the head of the surfactant molecule, while the hydrophobic segments represent the tail of the surfactant molecule. When the tail is long enough this surfactant is oil soluble, and also has high affinity to adsorb at the interface formed between two immiscible liquids. Using the SCF theory we will derive the relation between the surfactant adsorption, $\Gamma = 1/\sigma$, at the interface and the interfacial tension γ. For the case of a long hydrophobic block the main contribution to the interfacial tension comes from the free energy of the hydrophobic tails attached on the interface, which we will treat as a polymer brush. Thus the interfacial tension of the oil-water interface in the presence of surfactant can be represented as follows

$$\gamma = \gamma_0 + F / A + \Gamma \Delta\mu \tag{5.10}$$

where, γ_0, is the interfacial tension of the bare interface between oil and water, F is the polymer brush free energy given in chapter II, and the last term is the surfactant adsorption free energy, which takes into account that the surfactant at the interface is in chemical equilibrium with the surfactant in both liquid phases. $\Delta\mu$ is the difference between the chemical potential of the surfactant at the interface and in the bulk of the liquid. Since the bulk and the interface are in equilibrium, $\Delta\mu$ should be compensated by the change of the segments chemical potential due to their distribution near the interface,

$$\Delta\mu + N\mu_C = \Delta\mu + \frac{\sigma}{v_0}\int_0^H \mu_C \varphi(x) dx = 0 \tag{5.11}$$

Substituting the expression for the chemical potential of the segments one gets the closed form for the total interfacial tension

$$\gamma = \gamma_0 + \int_0^H \left[\Phi(\varphi(x)) - \frac{\delta\Phi}{\delta\varphi}\varphi(x) \right] dx = \gamma_0 - \frac{kTw}{2v_0}\int_0^H \varphi(x)^2 dx \,. \qquad (5.12)$$

Note that the last term in eq 5.12 is always negative, due to the spontaneous adsorption of the chains at the interface, i.e. it decreases the interfacial tension compared to the case of the pure oil-water interface. There is an exact analogy between this case and the case of free energy per unit area of spontaneous forming electric double layer (EDL)[92], where the energy of the electric field is always positive (energy of the chains in our case), while the chemical free energy of the adsorption is negative and the total contribution is negative. Substituting the solution for the volume fraction and the thickness of the brush from eq 5.7 and 5.8 into eq 5.12 we obtain:

$$\gamma = \gamma_0 - \frac{4kTK_s{}^2H^5}{15v_0w} = \gamma_0 - \frac{3kTN}{5\sigma^{5/3}}\left(\frac{\pi v_0 w}{2l}\right)^{2/3} = \gamma_0 - \alpha\Gamma^{5/3} \qquad (5.13)$$

where

$$\alpha = \frac{3kTN}{5}\left(\frac{\pi v_0 w}{2l}\right)^{2/3} .$$

The latter result is derived for the sake of comparison with the DPD system. For the case of real systems one should substitute $w \to \frac{v_0}{v_w}(1-2\chi)$ into eq 5.13.

$$\gamma = \gamma_0 - \frac{3kTN}{5\sigma^{5/3}}\left(\frac{\pi v_0^2(1-2\chi)}{2lv_w}\right)^{2/3} = \gamma_0 - \alpha\Gamma^{5/3}, \qquad \alpha = \frac{3kTN}{5}\left(\frac{\pi v_0^2(1-2\chi)}{2lv_w}\right)^{2/3} \qquad (5.13a)$$

Note that eq 5.13a is a new theoretical result, derived in this thesis, which provides a basis for a universal interfacial tension isotherm, as discussed latter in chapter VI.

V.3. Simulation Details

The dissipative particle dynamics simulation was performed to simulate properties of the long polymer chains. In the case of grafted chains we have performed simulation in a box with size 30x20x20 for a total DPD density 5, using 60000 similar DPD beads. Two walls were placed in the system at x=0 (where polymer chains are grafted) and x=30, as described bellow. Periodic boundary conditions were used in y and z directions. The repulsion parameter between the beads was fixed to $a_{ii} = 15$ and the masses of the beads were set to 1.

The polymer was construed by connecting the segment beads with a string with elastic constant $k = 160$ and equilibrium distance $l = 1$. We have connected $N = 20$ beads to form a polymer molecule, which was connected to an extra junction bead attached to the solid wall at $x = 0$. The temperature in all simulations was fixed to $kT = 1$. The integration step was $\Delta t = 0.03$, the dissipation magnitude was set to 4.5. The equations of motion are integrated using Verlet type of algorithm proposed by Groot et. al. with $\lambda = 0.65$.

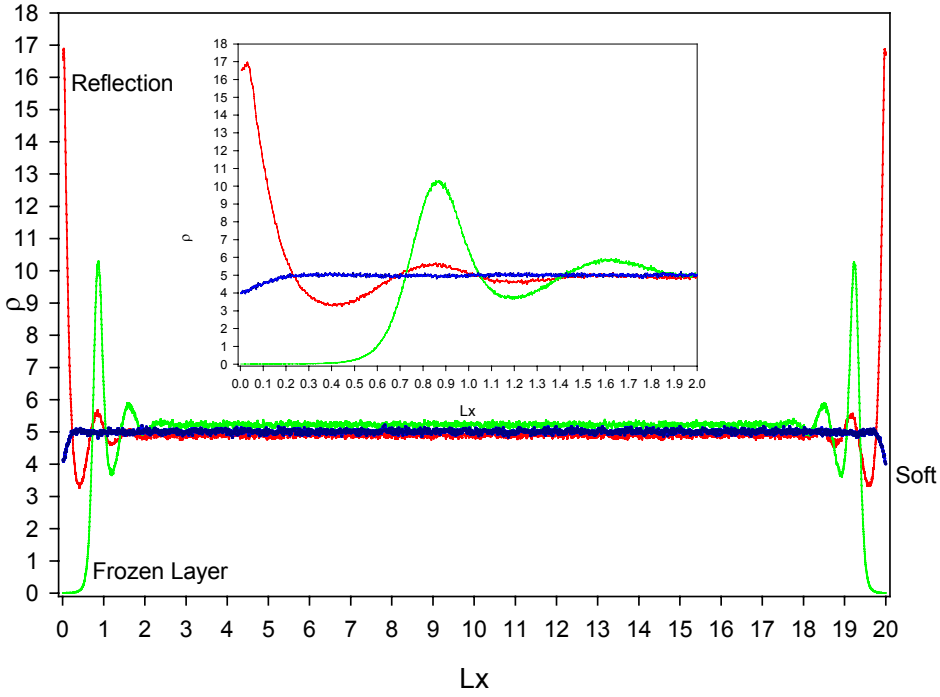

Figure 5.1. Density distribution along the simulation box for different types of walls: (a) wall constructed from a frozen layer of DPD particles; (b) reflecting wall – where no particles are used for the wall, but the beads are reflected back into solution when they hit the wall and (c) soft wall (explained later in the text and depicted in figure 5.2). The simulations were performed to illustrate the huge difference between the different types of walls near their vicinity (the intercepted plot shows close-up of the wall vicinity). All simulations were performed in a box with size 20x10x10 of total density 5, all the beads were similar (conservative repulsion was set to 15) and they are not connected. For the case of frozen layer part of the beads were fixed to form a wall with thickness 0.1 which contains 500 beads, which makes wall density equal to 50. One can clearly see that reflection wall effectively attracts the beads and density near the wall goes up to about 17 (compared to a mean density of 5 in the box), while the frozen wall is effectively repulsive and there is a layer close to the wall which is virtually free from DPD particles – wall thickness is 0.1 while the density is zero until distance at about 0.5. The soft wall makes very low distortion of the density profile in the close vicinity near it.

In order to avoid undesired fluctuations of the density near the solid walls[90] (see figure 5.1 for more details), we used a special type of "soft" wall as proposed in the work of Willemsen et. al.[89] (see figure 5.2a).

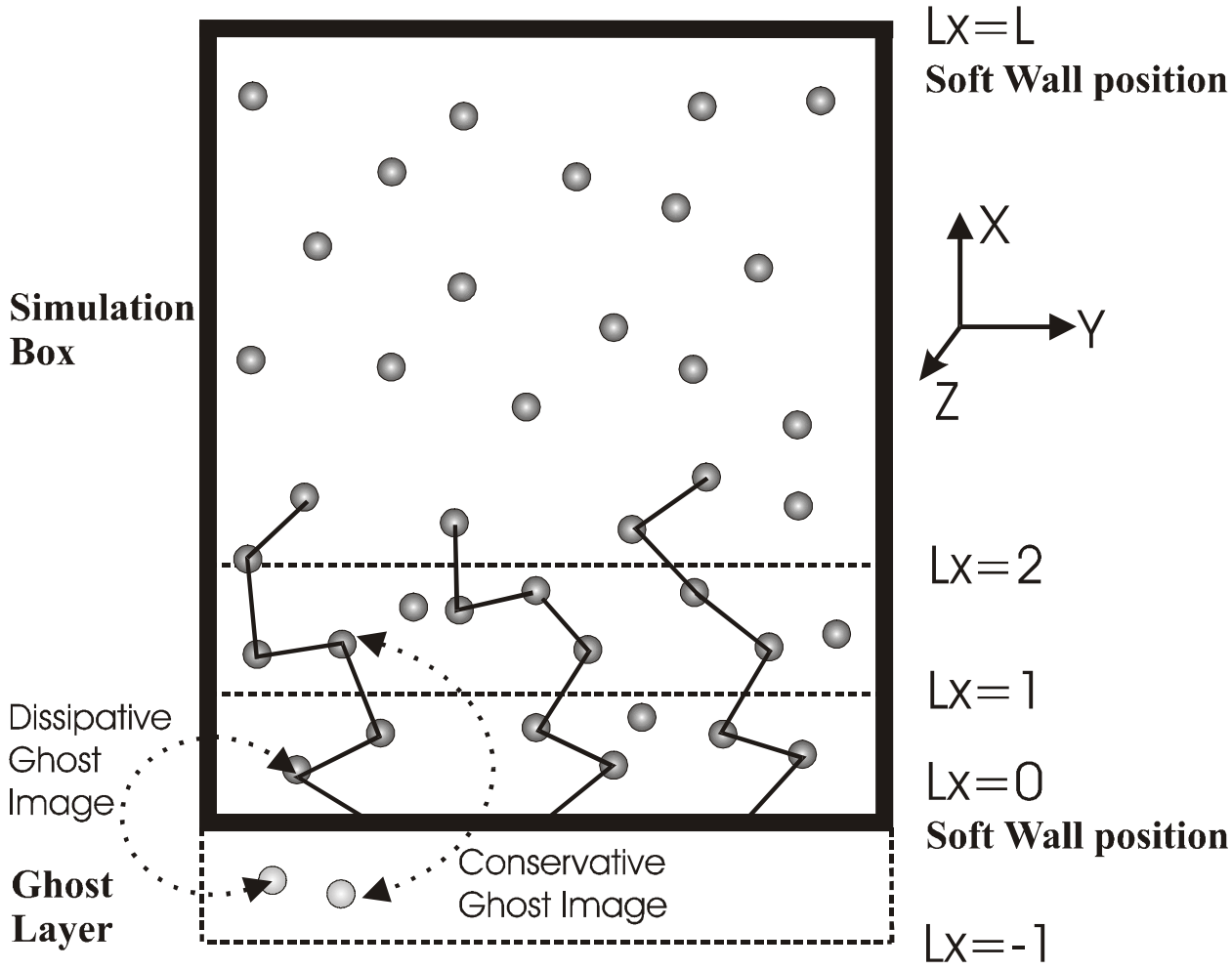

Figure 5.2a. Sketch of the simulation box and the implementation of the soft wall. Two walls are situated at the top and at the bottom of the box, while periodic boundary conditions in the other two directions are used. At the bottom of the box we have depicted the construction of "ghost" layer (the same applies at the top of the box). Beads connected with lines are part of polymer molecules. One of the polymer ends is permanently grafted at the wall at Lx=0. The other free beads form the solvent.

Willemsen et. al.[89] have proposed that the “”soft” wall must be represented by an extra layer, situated outside the box. The layer is filled with two types of “ghost” beads*. The first type of ghost particles contains images of real the DPD particles, which are within a distance of less than 1 DPD units from the walls as follows: for each particle a ghost has a tangential coordinates shifted by a random number between 0..1, while normal coordinate is obtained by a simple reflection with respect of the wall. The first type of ghost particles is used for calculation of the random and the dissipative forces. The second type of ghost particles contains images of the particles, which are within a distance between 1 and 2 DPD units from the wall. The coordinates of this particles are obtained from simple shift of their coordinates normal coordinates from interval [2,1] to interval [0,-1] (and [28,29] to [30,31] respectively). The sketch of the soft wall is given in figure 5.2a, while a snapshot of the simulation box is presented in figure 5.2b. The second type of ghost particles is used for calculation of the conservative forces. When a real DPD particle hits one of the walls it bounces back into the bulk.

This type of the wall is superior to the approach where the wall is simulated using a “frozen” layer of DPD particles because it gives much smoother density profiles near the wall (see figure 5.1). Another advantage of the soft wall is that it allows introducing a shear into the system, with is much better non-slip boundary condition. The latter could be used if one is interested of rheological properties of the polymer brush. Here, all our simulations are performed in a steady system without external shear rate. Initially the free (solvent) beads are randomly distributed within the box. The grafting beads are uniformly distributed along the wall (x=0) surface and the polymers are build one by one by adding a new beads having random coordinates requiring that the distance between consecutive beads is equal to the equilibrium distance of the chain spring. If the distance is much larger that the equilibrium one this leads to very high forces acting between the beads, which spoils the integration procedure and leads to higher temperature fluctuations in the beginning. Than, the equilibration is performed for 150 000 time steps, followed by 50 000 steps production run.

* In our case we have two walls in the system, one at the bottom of the box (x=0) and one at the top of the box (x=30). Each box has its own ghost layer, one of them situated at the bottom end of the wall [-1,0] and second at the top end [30,31]

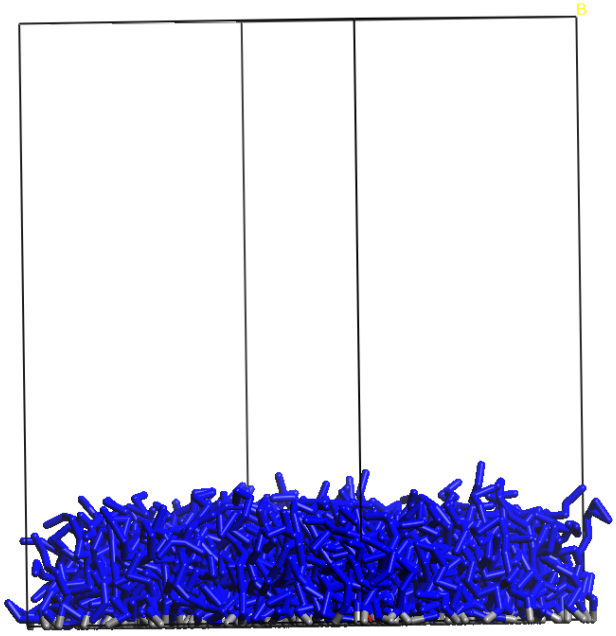

Figure 2b. Snapshot of the simulation box for the case of grafted polymer chains. The solvent beads are hidden. The soft wall is situated at the top and in the bottom of the box (see figure 2a). The box size is 30x20x20 DPD units and there are totally 60000 beads.

The total energy, the pressure and the temperature of the system were monitored in order to make sure that equilibrium is reached. The calculations are performed on a single CPU PC running under Windows 2000, with Athlon 1.4Ghz. The typical time for calculation of the single point is about 8h. The code uses sorted linked cell method, which gives computational time nearly linear with an increase of total number of the particles in our system. The parallel version of the code using Message Passing Interface (MPI) protocol running on Linux cluster (64 nodes, 1.4Ghz Athlon CPU each, situated in the University of Essen) gives a performance boost at about 20-30 times, but the results in this chapter are obtained using the serial version of the code.

In the second type of the simulation where the interfacial tension was studied the box size was 40x15x15 and the mean DPD density is 5, thus we have 45000 DPD particles. In this case, we have used periodic boundary conditions in all directions. The repulsion between similar beads was set to 15, while the repulsion between different beads was 30, 50, 75 or 150 in different type of simulations, described latter in the text. 30% of the beads were set to be water-like, while other 70% were used for oil and surfactant chain. *N* hydrophobic beads

were connected to one hydrophilic bead to form a surfactant. In the begging a sharp slab between oil and water beads was formed in x direction, and the higher values of repulsion between unlike beads support the immiscibility of both liquids during the simulation. The surfactant molecules were randomly spread in the oil phase. Then we perform a 200 000 time steps equilibration run, after which practically all the surfactant beads are adsorbed at the oil-water interface, then a production run of 75 000 steps is performed.

V.4. Results and Discussions

V.4.1 Grafted chains. In the work of Malfeyt et. al.[68] polymer chains grafted on two solid walls have been simulated and it qualitative agreement have been found between the DPD simulation results and the SCF theory predictions – the density profiles of the chain segments have been found to be nearly quadratic functions of the distance from the wall. At present we are not aware of another work with quantitative analysis and comparison of DPD simulation with the quantitative theory predictions. That is why here we perform more detailed quantitative analysis of this system.

In Figure 5.3, we show segment density profiles of the polymer brushes near the wall at different grafting density (100,200,300,400,500,600 polymers). Despite of the small fluctuations of the density near the wall and smooth decay near the end of the chains. The bigger part of the profiles is nearly quadratic[68], which is consistent with the prediction of SCF (see eq 5.11). In the Figure 5.4 we show the same profiles plotted in the special scale, were SCF theory predicts that they should collapse into one curve. One sees that they nearly collapse, a two curves which are deviating more strongly are the ones corresponding to very low surface coverage (100 and 200 polymers), where the assumption of strong stretching of the chains is no longer fulfilled. The profiles near the end of the brush are also deviating from the SCF quadratic profile, due to the fact that the theory fails to describe correctly the brush ends (there is a generalization of the profile near the end of the brush done by Milner[41]). The second source of the discrepancies is due to the fact that there is a difference between hard rod and very strong spring in the way the phase space is sampled in molecular dynamics[88] (although this usually gives a small correction).

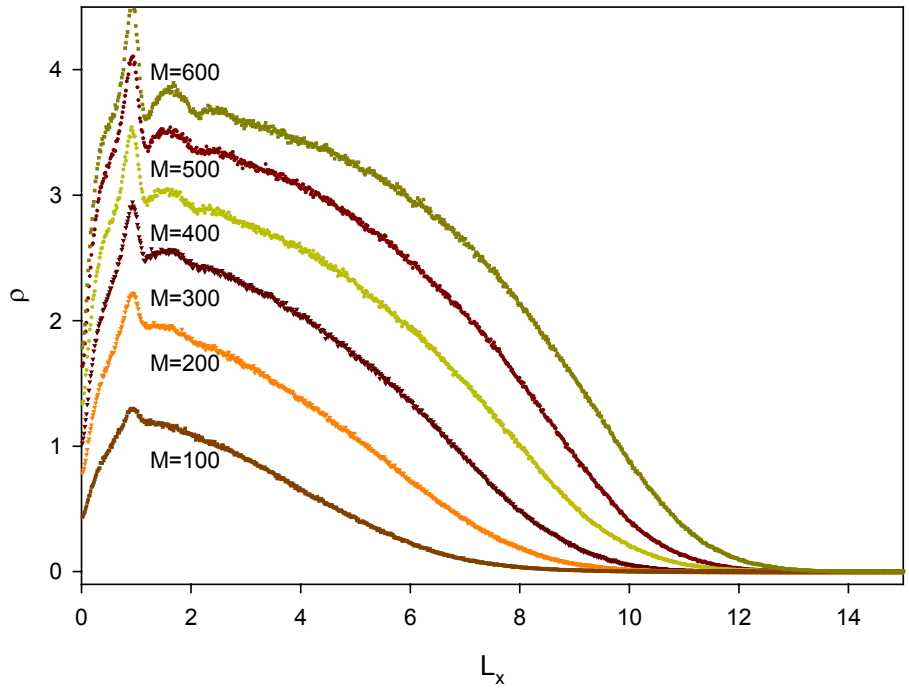

Figure 5.3. Segment density profiles vs. distance from the wall. The different curves correspond to different grafting density (different number *M* of molecules per unit area of the interface).

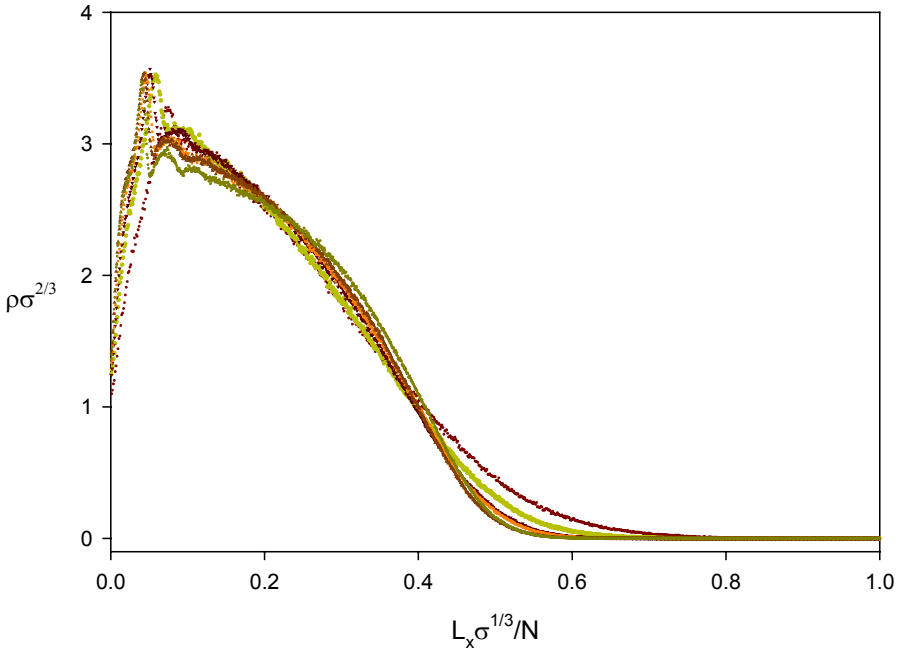

Figure 5.4. The same data as in figure 5.3, plotted in the SCF scale, where they should collapse into one "master" curve. Small deviations correspond to the case of very low grafting densities (*M*=100 and 200), where the SCF description is not correct.

From the DPD data we calculate the first moment of the segment density profiles. Because the profiles are calculated at equally spaced points the first moment is numerically given by the sum, $\langle x \rangle = \frac{\sum x_i \varphi(x_i)}{\sum \varphi(x_i)} = 3H/8$, which gives an estimate of the layer grafting thickness. Then, we calculate the brush thickness using eq 5.8 and compare the results with the SCF formulas. In Figure 5.5 we show the cubed brush thickness obtained from DPD as a function of area per molecule. One can see that all points lie on the straight line. The slope of the curve, from the best fit of the DPD data is 0.130 ± 0.003. We can compare this value with the prediction from SCF, $\frac{3wv_0}{2K_s\sigma} = \frac{4a_{ii}}{30\pi\rho}$, which for $\rho = 5$ and $a_{ii} = 15$ gives value 0.127. One sees that this compares remarkably well with the best fit for the slope.

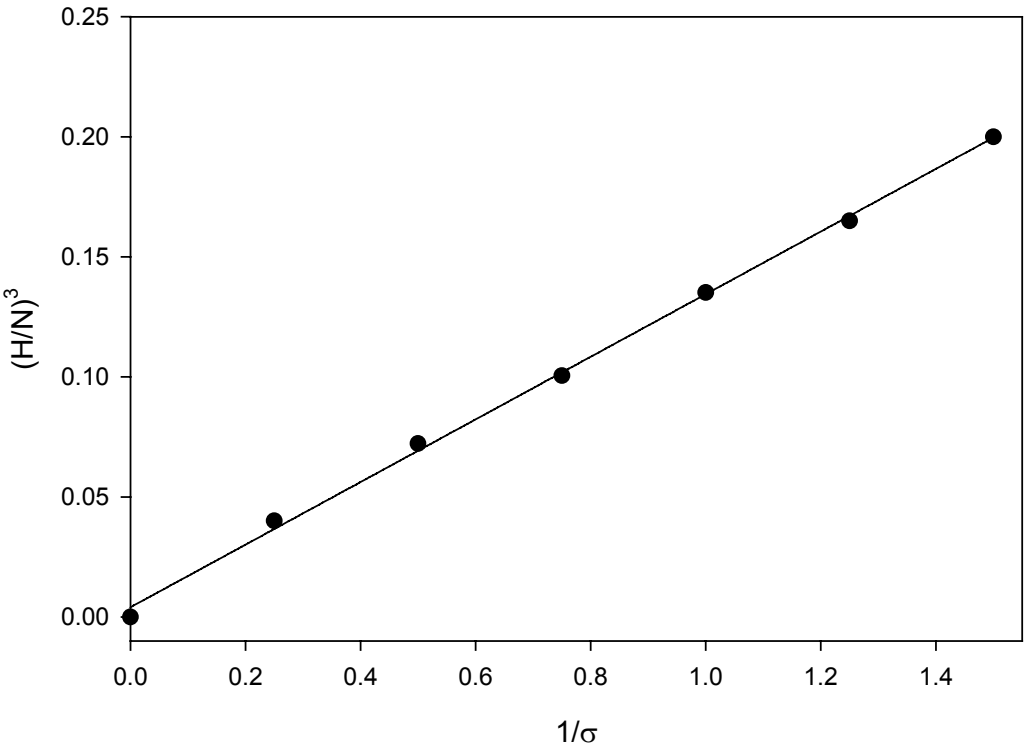

Figure 5.5. Thickness of the polymer brush grafted on the interface (obtained from the eq 5.8) as a function of area per polymer molecule. Slope of the line is 0.130 ± 0.003, while SCF value is $\frac{2}{5\pi} \approx 0.127$.

4.2 Interfacial Tension. First, we perform simulations of the pure oil-water interface using different values of the repulsion constant between unlike (oil and water) beads ($\delta a_{ij} = 15,\ 35, 60, 135$). In the work of Groot et. al.[71] there is an estimate of the interfacial tension of pure liquids formed from single beads (see ref 71, eq 36):

$$\gamma_0 = 0.75\rho kT\chi^{0.26}\left[1 - 2.36/\chi\right]^{3/2} \tag{5.14}$$

where, for the case $\rho = 5$, the Flory parameter is $\chi = 0.689\delta a_{ij}$. In Fig. 6.6 we show the comparison between our results and those obtained from eq 5.14. Additional control simulations were performed for the case of two-component polymer melt. In this case we used two immiscible DPD fluids, where every 5 similar beads were connected in a chain (all other parameters are the same as above). The slab between the two component polymer melts was formed, the interfacial tension was calculated from the simulation data and the result was compared with data available in the literature[71]. We observe very good agreement with the results of Groot (see ref 71, eq 33): for case of $\delta a_{ij} = 15$, the value of the interfacial tension obtained from our simulations was 6.96 ± 0.04, while Groot predicted 6.99, for the case of $\delta a_{ij} = 35$, our code gives 10.03 ± 0.07, while Groot predicted value 10.15. This very good agreement with literature data gives us a confidence that our code is error free. It worth mentioning t that the DPD module included in the software package Cerius^2 v4.2 from MSI (Accelrays) probably has a bug because it is failing to reproduce the results given in ref 71 (eqs 33 and 36). Thus, we have reason to believe that the aforementioned software will not be able to reproduce our results as well.

In the next part of this chapter we present our simulation results of the interfacial tension in the presence of surfactant at the interface between oil and water. Snapshots of the simulation box and the density profiles of a sample system are given in figure 5.7. One can see that the segment profiles of the surfactant tails are nearly symmetrical and that practically all surfactant molecules are adsorbed at the interface. The density of the surfactant heads is very sharp and they are situated very close to the interface. That is why it is appropriate to treat the surfactant molecules with the theory of the grafted chains.

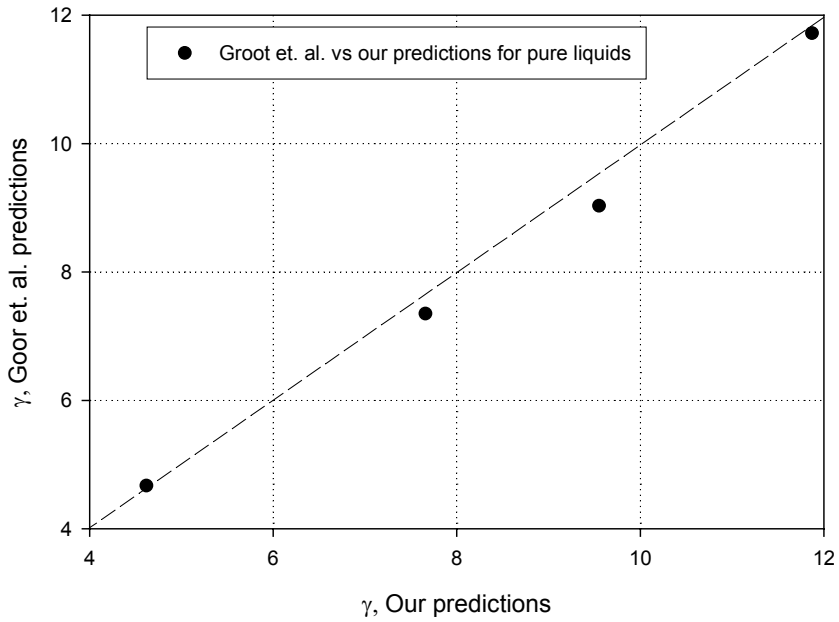

Figure 5.6. Check the accuracy of our code – comparison with the best-fit formula given by Groot et. al.[71] vs. our computational results.

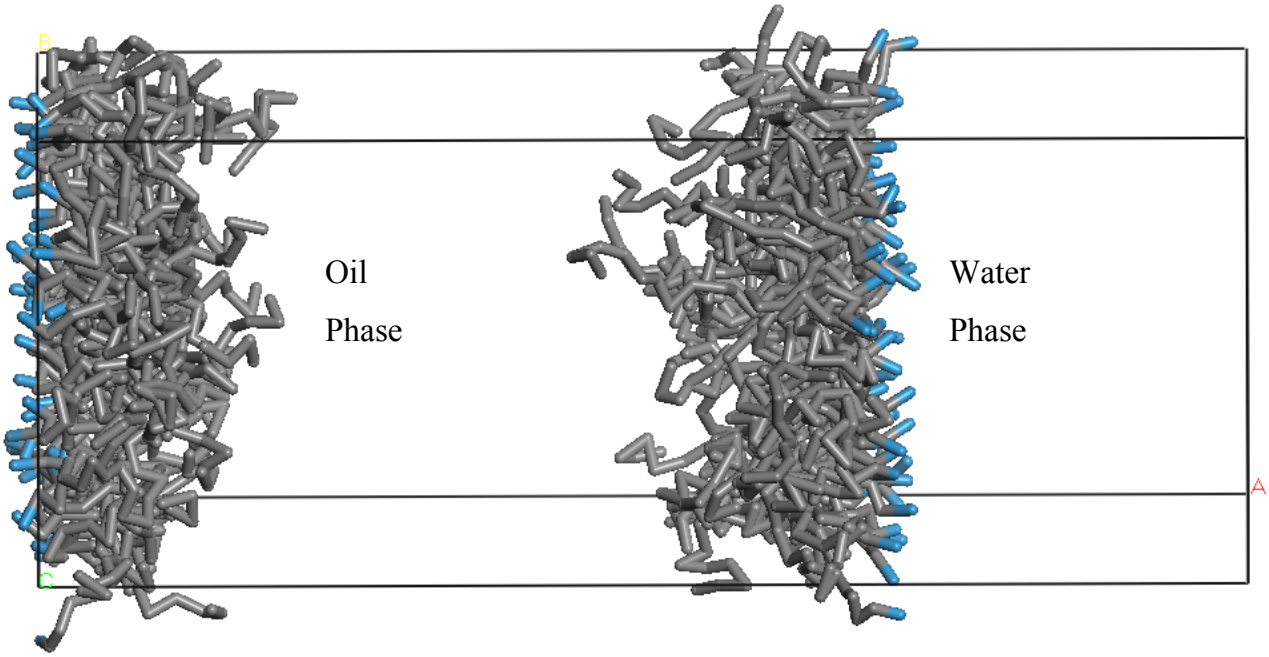

Figure 5.7a. Snapshot of the simulation box. Only the surfactant molecules are shown in the picture, while water and oil beads are hidden for clarity. The details are explained in the next figure caption, where the density distribution of the same system is shown. Due to the periodic boundary conditions two interfaces between oil and water are formed where surfactant molecules could adsorb.

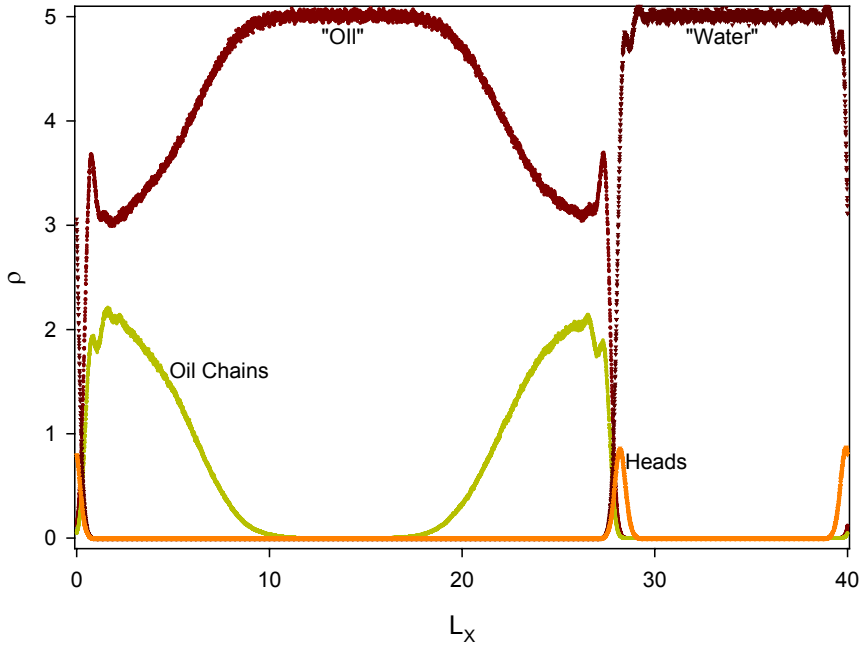

Figure 5.7b. Density profiles of the oil, water and surfactant segments. The total DPD density of the system is fixed to 5. The box size is 40x15x15 and the total number of beads is 45000.

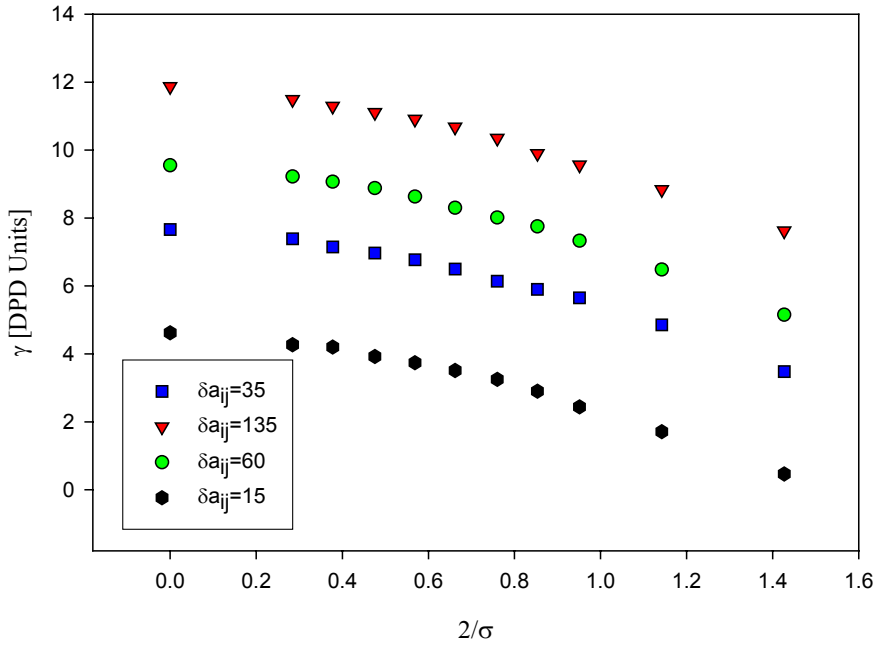

Figure 5.8. Interfacial tension as a function of area per molecule for different values of repulsion parameter between unlike beads (corresponding to a different interfacial tension of the pure interface. The repulsion parameter between like beads is fixed to 15 for all simulations).

The values of the interfacial tension as a function of the surfactant adsorption are presented in figure 5.8 for different values of the repulsion parameter between unlike beads (as outlined above).

From the other hand, the SCF formula for the interfacial tension (see eq 5.13) expressed in DPD units gives ($kT=1$, $l=1$, $w=\pi a_{ii}/30$, $v_0=1/\rho$)

$$\gamma=\gamma_0-N\left(\frac{\sqrt{3}\pi^2 a_{ii}}{400\sqrt{10}\rho}\right)^{2/3}\left(\frac{2}{\sigma}\right)^{5/3} \tag{5.15}$$

For the case, $N=20$, $a_{ii}=15$, $\rho=5$, we should have $\gamma=\gamma_0-2.36\left(\frac{2}{\sigma}\right)^{5/3}$.

We plot the interfacial tension in figure 5.8 as a function of $2/\sigma$ because of the periodic boundary conditions requiring two interfaces each of area equal to cross-section of the simulation box A, where totally M molecules are adsorbed (this is exactly what we know in the simulation: total area and total number of molecules, but we do not know exactly how they are distributed during the simulation), thus the real adsorption is $M/2A$, but we plot M/A which is twice higher.

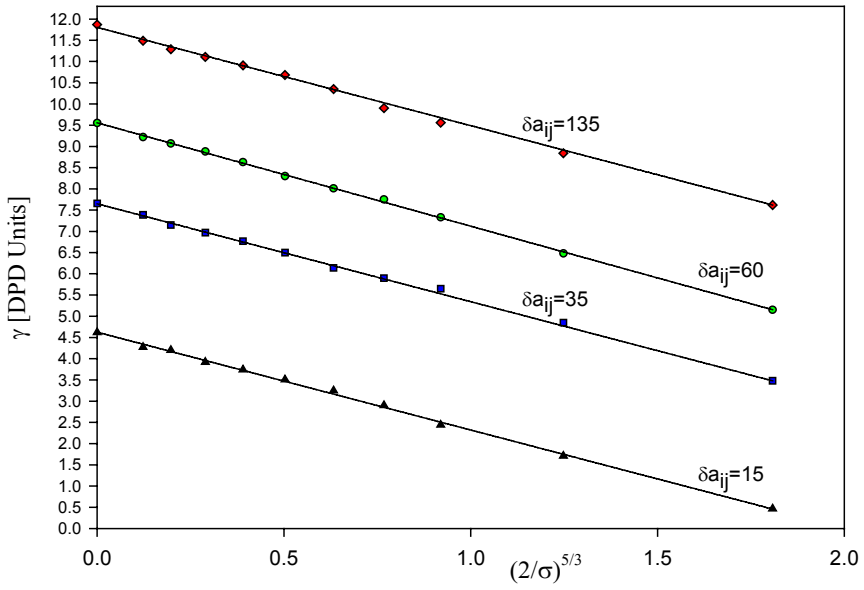

Figure 5.9. The same data as in Figure 5.8, plotted in the SCF scaling low. Different lines correspond to different values of the repulsion parameter between oil and water beads in the system. The SCF predicts that lines should be parallel. Slopes of the curves are (starting from bottom to top curve), -2.30 ± 0.03, -2.27 ± 0.03, -2.42 ± 0.02 and -2.31 ± 0.01 respectively. The mean slope of all four curves is -2.32 ± 0.06.

The interfacial tension during the simulation was calculated as an excess of normal over tangential component of the pressure tensor, along the direction perpendicular to the interface formed in the box. Due to the fact that we have two interfaces the excess of pressure is two times higher but the values reported next in the article are real interfacial tension i.e. the free energy excess is already divided by factor of two to account for the presence of two interfaces.

In figure 5.9 we have plotted the interfacial tension as a function of $\left(\frac{2}{\sigma}\right)^{5/3}$ and one can see that the interfacial tension really scales according to the prediction of the SCF theory.

Another interesting prediction from the theory is that the slope of the line should be independent of the properties of pure oil-water interface. In figure 5.9 one can see that all four lines are nearly parallel although the interfacial tension of bare interface was varied nearly 4 times. Slopes of the curves are (starting from bottom to top curve), -2.30 ± 0.03, -2.27 ± 0.03, -2.42 ± 0.02 and -2.31 ± 0.01 respectively. The mean slope of all four curves is -2.32 ± 0.06. Thus the slope of the curves is nearly constant and compares very well with SCF prediction, which is –2.36. The slopes as a function of the interfacial tension of the bare interface are plotted in Figure 5.10 and the SCF value is shown as a dotted line.

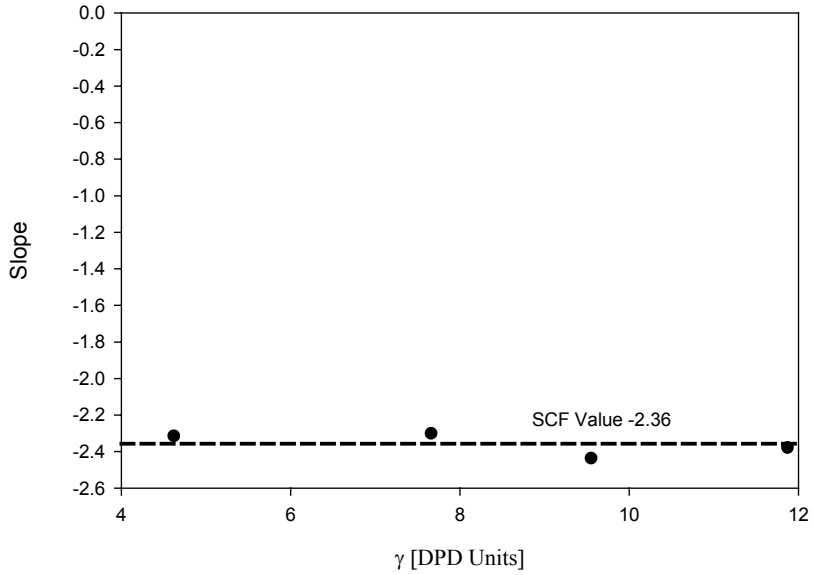

Figure 5.10. Slopes of the lines given in figure 5.9 as a function of the interfacial tension of the pure interface. The slopes (dots) are nearly constant, which agrees very well with the SCF prediction (dotted line): the mean slope from four points is -2.32 ± 0.06, while the SCF value is –2.36.

So we see that there is a very good agreement between the theoretical predictions of SCF and the simulation data from the DPD method.

Another prediction from SCF is that for a fixed surface coverage (surfactant adsorption) the interfacial tension should decrease linearly with the increase of the surfactant (hydrophobic) tail length. In figure 5.11 we show the simulation results for 4 different chains (N=15, 20, 25, 30) (the point N=0 – bare interface is added like as a control point, which was not taken into account into the linear fit), for the case of $\delta a_{ij} = 35$, $\sigma / 2 = 15^2 / 214 \approx 1.05$. One can see that the simulation results scale linearly with the increase of the chain length and that the slope of the curve (0.096 ± 0.002) compares very well with the SCF value 0.103.

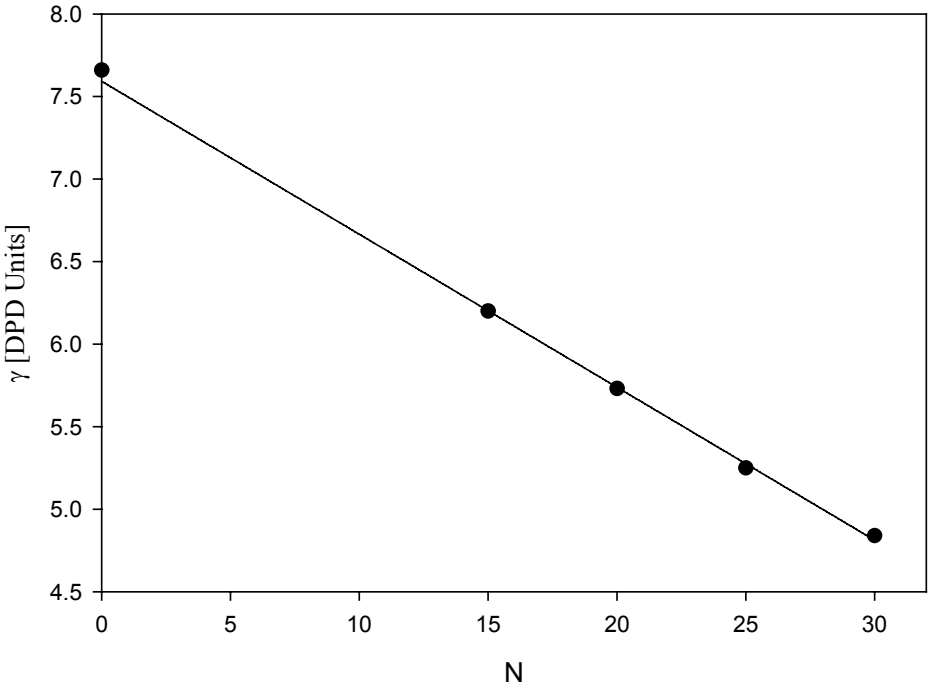

Figure 5.11. Interfacial tension as a function of the chain length (fixed area per molecule, $\delta a_{ij} = 35$, $\sigma / 2 = 15^2 / 214 \approx 1.05$). The point for N=0 is added as a control point (but is not used in the fit) because setting a chain zero length should effectively produce a pure interface, though there would still be some small correction due to presence of surfactant head group. The slope of the curve calculated from the best fit is 0.096 ± 0.002, while SCF predicts a value of 0.103.

V.5. Summary

We have performed two types of Dissipative Particle Dynamics (DPD) computer simulations of long polymer brushes grafted on an interface in contact with a good solvent. Two cases were considered. In the first one we have simulated homo polymers grafted on the solid interface and we have studied the density distribution of the chain segments and the equilibrium thickness of the polymer brush. We obtained pretty good agreement between the DPD data and the predictions of Self Consistent Field Theory (SCF): all profiles simulated with DPD nearly collapse onto the master curve predicted by the SCF theory, the thickness of the polymer brush also obeys the SCF scaling law, and its slope is also consistent with the theoretical predictions for DPD type of potential. In the second type of simulations we have constructed an amphiphilic di-block polymer ("surfactant"), which has a long hydrophobic chain, and hydrophilic head. This polymer adsorbs at "oil-water" interface since the water bead has the same properties like a surfactant head, while the oil beads are similar to the beads constructing the hydrophobic segment. Due to its very long hydrophobic chain the surfactant is oil soluble and has high affinity to adsorb at the interface between oil and water. We have simulated the interfacial tension of this system and have compared the results from SCF – assuming that the main contribution to the interfacial tension comes from the conformational energy of the tail of the surfactant and its adsorption free energy. We have derived a new theoretical relationship, which connects the interfacial tension and the surfactant adsorption. The latter is a basis of a new universal interfacial tension isotherm, as it will be discussed latter on chapter VI. We showed that the DPD Simulation results agree very well with the theoretical predictions.

It is also possible to simulate polydisperse brushes and to compare DPD results with the predictions of SCF theory. Our preliminary results in this direction proved to be quite promising and will be a subject of further studies beyond the scope of this thesis. Another extension of this work is to use similar type of approach for the case of dynamic processes like diffusion and shear flow into the system, where the SCF theory becomes much more complicated, but the DPD simulations remain the same and it would be possible to predict the properties of those systems.

VI. Self-Consistent Field Interfacial Tension Isotherm of surfactants: Comparison with experimental data

Abstract

Using the self-consistent field (SCF) theory we derive novel theoretical expression, which shows how the surface tension is scaling with the surfactant adsorption. By using latter relation and the Gibbs-Duhem equation a new theoretical isotherm accounting for the presence of surfactant was obtained. The scaling law of this surface tension isotherm was checked against various sets of experimental data available in the literature. We show that there is a very good agreement between the scaling predictions of the SCF-theory and experimental data for various types of surfactants: non-ionics, amphoterics and ionic ones, both on air/water and oil water/interface. For the case of non-ionics we have observed that the values of adsorption calculated from new surface tension isotherm, agree remarkably well with independent experimental data for adsorption obtained by ellipsometry and small angle neutron scattering (SANS).

VI.1. Introduction

VI.1.1. Surface tension of pure interfaces

Surface tension is a measure for the cohesive energy due to the existence of an interface between two phases of different properties. The molecules in the bulk of the two phases attract each other. The interactions of a molecule in the bulk of a liquid are balanced by equal attractive force in all directions. Molecules on the surface of a liquid experience an imbalance of forces as indicated below (see figure 6.1a).

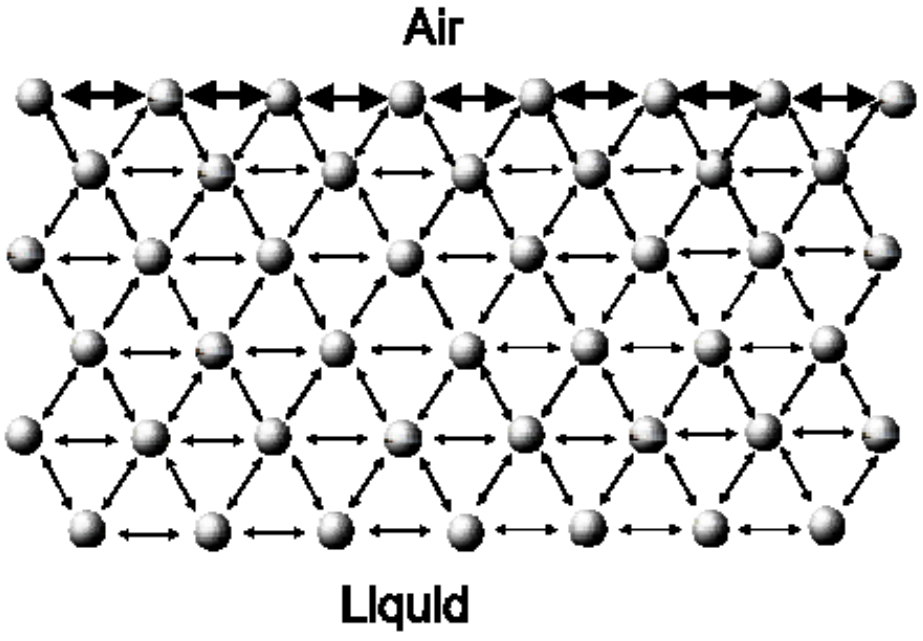

Figure 6.1a. Mechanical origin of the surface tension at pure liquid/gas interface.

The net effect of this uncompensated interaction is equivalent to an excess of free energy at the surface. This excess energy per unit area of the interface is called surface tension and has the meaning of a mechanical work to create a unit area of new interface. Though the latter picture is very rough representation of real system it gives a main idea for the molecular origin of the surface and interfacial tension.

Several approaches are used for calculation of the surface tension. The basic idea of the micro-mechanical treatment of non-uniform systems is to consider the bulk pressure as a non-isotropic tensor. Since the components of the pressure tensor are statistically averaged quantities, they are continuous functions of the position. They vary rapidly, but smoothly in the transition regions between the phases, which compose a given heterogeneous system. As pointed out by Irving and Kirkwood[93] the pressure tensor can be expressed through integrals over the intermolecular potentials and correlation functions (see e.g. Ono and Kondo[94]).

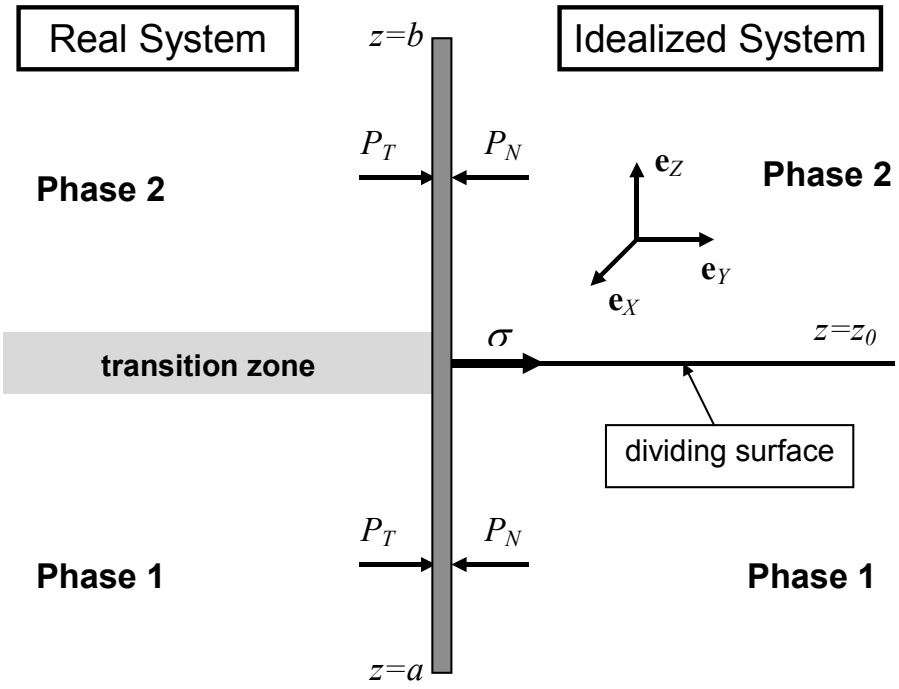

Figure 6.1b. Mechanical origin of the surface tension of pure interface according to Gibbs.

In the framework of the Gibbs formalism[95], the real non-homogeneous system (with transition regions with finite width) can be replaced by a suitably chosen idealized system (see picture 6.1b). The phases of the latter are treated as homogeneous and the transition

regions are replaced by sharp boundaries (surfaces) and the integrals over the pressure tensor are replaced by forces acting on the surfaces (e.g. surface tension). In order to ensure that the idealized system is mechanically equivalent to the real one, excesses of the system properties are also introduced. They are ascribed to the boundaries separating the respective homogeneous phases (e.g. to the surfaces separating the bulk phases). The position of the phase boundary in the model system is fixed by the conditions for the equivalence of the real and models systems, both mechanically and with respect to the extensive properties.

The well-known formula of Bakker[96] for the surface tension of a flat interface is a condition for the equivalence between the real and idealized systems with respect to the acting forces. This approach in the theory of the surface tension was further generalized for a planar interface by Kirkwood and Buff[97], Buff[98], Triezenberg and Zwanzig[99] (for more details see Evans[100]) and for curved interfaces by Buff[101-105], and Buff and Saltsburg[106]. The comprehensive review of many modern theories of surface and interfacial tension could be found in the books of Rowlinson[107] and Henderson[108].

The common units for surface tension are J/m^2 or mN/m, which are equivalent. By convention, the excess free energy a liquid and a vapor (gaseous) phase referred as surface tension. The same quantity for the interface between two condensed phases (liquid-liquid) or liquid-solid is referred as interfacial tension. Solids also may be described to have a surface free energy at their interfaces but direct measurement of its value is not possible through techniques used for liquids. The values of solid/liquid or solid/gas interfacial tension are important factors, controlling the wettability of solids by liquids. Polar liquids, such as water, have strong intermolecular interactions and hence high surface tensions. Any factor, which decreases the strength of this interaction, lowers the surface tension, such as the temperature increase or the presence of surface-active species, like surfactants or polymers.

VI.1.2. Surface tension of interfaces containing surfactants

When surfactants, e.g. long chain fatty alcohols or adsorbing polymers are present at the interface, they could significantly reduce the tension (γ). The excess with the respect of

homogeneous bulk phase of surfactant concentration at the interface is called adsorption (Γ), and it is a function of surfactant bulk concentration (c). There is a strong dependence of surface tension from temperature (T). The surface tension and the adsorption as functions of the bulk concentration of surfactant are called isotherms. When curve $\Gamma(c)$ is measured it is called adsorption isotherm, while when, $\gamma(c)$ is measured it is called surface tension isotherm. A common method to determine the equilibrium adsorption isotherm of a surfactant at the air-water surface is to measure the surface tension as a function of bulk concentration. Differentiation of the plot according to the Gibbs adsorption equation (see eq. 6.2.) yields the adsorption isotherm. Unfortunately, this method is rather imprecise since even small errors in the tension values may cause large errors in the derived surface excess concentrations. The result of this is that the choice of theoretical adsorption isotherms used to fit experimental surfactant adsorption isotherms remains controversial and is of prime importance.

Some of most commonly used isotherms for surfactants are shown in Table 6.1, those of Henry, Freundlich, Langmuir, Volmer[110], Frumkin[111] and van der Waals[109]. For $c \to 0$ all other isotherms (except that of Freundlich) reduce to the Henry isotherm. The physical difference between the Langmuir and Volmer isotherms is that the former corresponds to a physical model of localized adsorption, whereas the latter – to non-localized adsorption. The Frumkin and van der Waals isotherms generalize, respectively, the Langmuir and Volmer isotherms for the case, when there is interaction between the adsorbed molecules; β_1 is a parameter, which accounts for the interaction between surfactant chains. In the case of van der Waals interaction β_1 can be expressed in the form[112,113],

$$\beta_1 = -\pi kT \int_{r_0}^{\infty} \left[1 - \exp\left(-\frac{u(r)}{kT} \right) \right] \approx -\pi \int_{r_0}^{\infty} u(r) r dr$$

where $u(r)$ is the interaction energy between two adsorbed molecules and r_0 is the distance between the centers of the molecules at close contact. The comparison between theory and experiment shows that the interaction parameter β_1 is important for air-water interfaces, whereas for oil-water interfaces one can set β_1 to zero[113-115] (see also figure 6.1c).

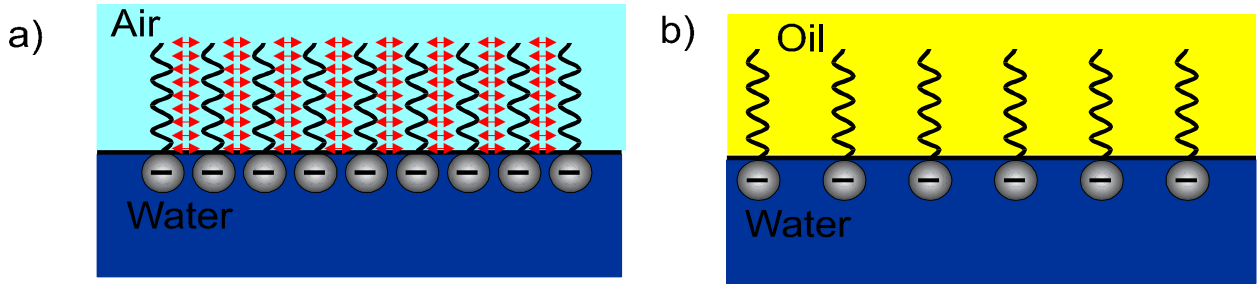

Figure 6.1c. There is a considerable interaction (denoted by red arrows) between the surfactant paraffin chains across air (a), whereas such an attraction is usually weak across oil (b).

Name	**Surfactant adsorption isotherms**	Surface tension isotherm, $\sigma = \sigma_0 - kTJ$
Henry	$Kc = \dfrac{\Gamma}{\Gamma_\infty}$	$J = \Gamma$
Freundlich	$Kc = \left(\dfrac{\Gamma}{\Gamma_F}\right)^{1/m}$	$J = \dfrac{\Gamma}{m}$
Langmuir	$Kc = \dfrac{\Gamma}{\Gamma_\infty - \Gamma}$	$J = -\Gamma_\infty \ln\left(1 - \dfrac{\Gamma}{\Gamma_\infty}\right)$
Volmer	$Kc = \dfrac{\Gamma}{\Gamma_\infty - \Gamma}\exp\left(\dfrac{\Gamma}{\Gamma_\infty - \Gamma}\right)$	$J = \dfrac{\Gamma_\infty \Gamma}{\Gamma_\infty - \Gamma}$
Frumkin	$Kc = \dfrac{\Gamma}{\Gamma_\infty - \Gamma}\exp\left(-\dfrac{2\beta\Gamma}{kT}\right)$	$J = -\Gamma_\infty \ln\left(1 - \dfrac{\Gamma}{\Gamma_\infty}\right) - \dfrac{\beta_1 \Gamma^2}{kT}$
van der Waals	$Kc = \dfrac{\Gamma}{\Gamma_\infty - \Gamma}\exp\left(\dfrac{\Gamma}{\Gamma_\infty - \Gamma} - \dfrac{2\beta\Gamma}{kT}\right)$	$J = \dfrac{\Gamma_\infty \Gamma}{\Gamma_\infty - \Gamma} - \dfrac{\beta_1 \Gamma^2}{kT}$

Table 6.1. The most popular surfactant adsorption isotherms and the respective surface tension isotherms.

β_1 takes into account the van der Waals attraction between the hydrocarbon tails of the adsorbed surfactant molecules across air (which corresponds to $\beta_1 > 0$). Such attraction is very weak when the hydrophobic phase is oil, which is in consonance with $\beta_1 \approx 0$.

The situation is more complicated for ionic surfactants. In this case, due to the charge of surfactant molecules, the interface also caries a charge, which results in the formation of an

electric double layer (EDL) near the interface. The latter has an important consequence because it brings non-homogeneity of the surfactant concentration near the interface, which must also be taken into account when surface excess of surfactant (adsorption) is calculated. The EDL could also have a significant electrostatic free energy, which must be considered, when surface tension is calculated. An additional complication also comes from the fact that there is a secondary adsorption of counter ions of surfactant to the interface (counterion condensation), which gives a contribution to the Gibbs-Duhem relation. A modern treatment of the ionic surfactant adsorption problem could be found in the work of Kralchevsky et. al.[115] and Warszynski et. al.[116].

Experimentally, surface and interfacial tension is measured by a tensiometer. This instrument is based on force measurements of the interaction of a probe with the surface of interface of two fluids. The forces experienced by the balance as the probe interacts with the surface of the liquid can be used to calculate surface tension. The forces present in this situation depend on the following factors; size and shape of the probe, contact angle of the liquid-solid interaction and the surface tension of the liquid. The size and shape of the probe are easily controlled. The contact angle is assumed to be zero (complete wetting). This is achieved by using probes made of a platinum/iridium alloy, which ensures both complete wetting and easy and reliable cleaning. The mathematical interpretation of the force measurements depends on the shape of the probe used. Two types of probes are commonly used, the DuNouy Ring and the Wilhelmy Plate. There are also other modern experimental methods for determination of the surface tension, such as drop maximum volume method, drop shape analysis, stopped or oscillating jet etc[11].

The surfactant adsorption at the interface is much more difficult to measure and usually indirect model-dependent methods are used, such as ellipsometry, small angle neutron scattering (SANS) or radiometry. Detailed review on these experimental methods could be found in the review of Lu et. al.[117]. Theories and methods for measurements of surface tensions of polymer melts are described in the review of Dee[118].

In the previous chapter we derived a connection between the interfacial tension of liquid/liquid interface and the surfactant adsorption. The main assumption allowing us to obtain the result was that the main contribution comes from the conformational energy of the polymer chain. In the present chapter we check the predictions of the SCF obtained in the

previous section against experimental data for the surface tension of various types of surfactant systems. As it was already discussed in the thesis introduction, most of the surfactants are not long enough to be considered as polymers, but from other point of view they are too long to be considered as having only two blocks – hydrophilic and hydrophobic. Most of the theoretical and semi-empirical surface and interfacial tension isotherms are considering the surfactants as a solid discs adsorbed at the interface, thus ignoring the internal structure and degrees of freedom in the surfactant chain. As we will show in this chapter this is an importation contribution and should not be neglected. By artificially extending the surfactant chain (i.e. by assuming extra degrees of freedom in the chain) we assume that the surfactant behaves like a polymer chain, thus one could estimate the conformation of the surfactant chain using the SCF theory predictions described in the previous chapter. This gives a new scaling law of the interfacial tension of the surfactant. In this chapter we check this scaling law against a large variety of experimental data for the surface (interfacial) tension of various types of surfactants.

VI.2. SCF Surface Tension Isotherm for a nonionic surfactant

In the previous chapter we showed that for brushes adsorbed at the liquid-liquid interface, the interfacial tension, γ, is function of the adsorption, Γ. Using SCF arguments we obtained that (see eq. 5.13):

$$\gamma = \gamma_p - \alpha\Gamma^{5/3} \tag{6.1}$$

where,

$$\alpha = \frac{3kTN}{5}\left(\frac{\pi v_0^2(1-2\chi)w}{2lv_w}\right)^{2/3}$$

v_0 is the volume of the segment of the chain, l defines the distance of between the segments, v_w desribes the volume of the solvent molecule, N is the number of segments in the chain, so that the whole length of chain is Nl. χ desribes the Flory-Huggins parameter accounting for

the interaction between the solvent molecules and segments of the chain, while γ_p is the value of the surface tension for the case of pure interface ($\Gamma = 0$).

In Chapter III we showed that the same form of surface energy remains also valid for an amphiphilic di-block polymers, adsorbed at the liquid/liquid interface. Here we will assume that our surfactants have the same behavior like the polymer brushes at liquid-liquid interface and we will use the above equation for predicting the liquid-liquid interfacial tension in the presence of surfactant. The main problem with the expression given with eq. 6.1 is that for practical applications one knows the interfacial tension as a function of the bulk concentration. Adsorption properties are much more difficult to be measured (compared to the bulk concentration) and this requires additional experiments like ellipsometry, SANS[117] etc. On the other hand, one can express the SCF isotherm in terms of the bulk concentration of surfactant by using the Gibbs- Duhem equation:

$$d\gamma = -\Gamma d\mu_s = -\Gamma d\mu_b \approx -kT\Gamma d\ln c \tag{6.2}$$

where, μ_b and μ_s are surface and bulk chemical potentials of the surfactant, which are equal in equilibrium. For low bulk concentrations of surfactant we assume that the activity coefficient of the surfactant in the bulk to be equal to 1. After differentiation of eq 6.1 and substitution of the result into eq 6.2 we obtain the relation between the surfactant adsorption and its bulk concentration (adsorption isotherm of surfactant)

$$\ln(c/c_0) = \frac{5\alpha}{2kT}\left(\Gamma^{2/3} - \Gamma_0^{2/3}\right) \tag{6.3}$$

where, c_0 is chosen as a reference bulk concentration where the equilibrium adsorption is Γ_0. Both parameters are connected with $\gamma_0 = \gamma_p - \alpha\Gamma_0^{5/3}$ (see eq. 6.1). We need a reference point in this case in order to determine the integration constant. The reason why we could not use the obvious reference point, $\Gamma_0 = 0$ is that in this case $c_0 = 0$ and the logarithmic term in eq 6.3 is divergent. Note that eq 6.3 is not applicable for extremely low (close to zero) concentration of surfactant. Eliminating the adsorption in eq 6.3 and substituting back into eq 6.1 we obtain

$$\gamma = \gamma_p - \left[\frac{2kT}{5\alpha^{3/5}}\ln(c/c_0) + \left(\gamma_p - \gamma_0\right)^{2/5}\right]^{5/2} \quad \text{or}$$

$$(\Pi)^{2/5} - (\Pi_0)^{2/5} = \beta \ln(c/c_0)\,. \qquad (6.4)$$

Here we have introduced surface pressure instead of surface/interfacial tension

$$\Pi = \gamma_p - \gamma \text{ and } \Pi_0 = \gamma_p - \gamma_0, \qquad \beta = \frac{2kT}{5\alpha^{3/5}}.$$

The latter equation in 6.4 is also called two-dimensional equation of state, because it gives the connection between the two-dimensional pressure and the two-dimensional analogue of concentration (adsorption). If the reference concentration, c_0 is chosen to be close to a critical micelle concentration (CMC) one can express the value of adsorption, Γ_∞, close to CMC (by assuming that the limiting surfactant adsorption is very close to the value at CMC), as $\Gamma_\infty = \left(\frac{\gamma_p - \gamma_{CMC}}{\alpha}\right)^{3/5}$. We could also evaluate the slope, α, of SCF isotherm provided that the value of Γ_∞ is known

$$\alpha = (\gamma_p - \gamma_{CMC})/\Gamma_\infty^{5/3}\,. \qquad (6.5)$$

For a surfactant composed of two long hydrophilic and hydrophobic chains (di-block polymer) one can derive a similar expression for the interfacial tension isotherm with $\alpha = \alpha_{hydrophobic} + \alpha_{hydropilic}$, (see chapter III for more details).

When we have a surfactant adsorbed at an air/water interface with a very long hydrophobic chain directed towards the air we could also derive a similar expression like eq 6.4. Again by speculating that the main contribution to the surface tension comes through the conformation of the hydrophobic chains in the air and assuming that second virial coefficient is fully determined by the van der Walls interaction between the oil segments in the air, which is the same assumption which is done in the Frumkin[111] and van der Waals isotherms[109] (see figure 6.1b also).

The isotherm given with eq 6.4 (which we will call later on β - plot) is by no means trivial. Looking back at the way it was derived one could see that it is supposed to be valid for the case of liquid/liquid interface for a non-ionic surfactants having very long chain and small head. Thus the application of eq 6.4 for the case of short chain surfactant is by no-means strictly justified from the theoretical point of view. The application of eq 6.4 for the case of ionic surfactant is even more hazardous because all the electrostatic contributions to the

surface tension are not taken into account[115-116]. Nevertheless we will show that the scaling law given by eq 6.4, is valid for a variety of real systems and many types of surfactants. In this case, the parameter of the isotherm given with eq 6.4 should be considered like an empirical one with the value determined from the best fit of the experimental data. More detailed investigation why SCF scaling low is working for so large variety of systems is currently in progress.

VI.3. Practical application of the SCF adsorption isotherm

Let us consider a set of experimental data for the surface or the interfacial tension γ, as a function of bulk concentration *c*, of surfactant. In order to represent the data in SCF- plot given by eq 6.4 one needs to know the surface tension of the surfactant free interface γ_p, to calculate the surface pressure $\Pi = \gamma_p - \gamma$ for each concentration point. It is a matter of convenience whether to use a reference point with concentration c_0 (surface tension γ_0 and surface pressure $\Pi_0 = \gamma_p - \gamma_0$) or not. For a given reference point (which could be any point of the isotherm) we plot the function

$$y = \tilde{\beta} x \tag{6.6}$$

where,

$$y = (\Pi)^{2/5} - (\Pi_0)^{2/5} \text{ and } x = \tilde{\beta} \log_{10}(c / c_0).$$

In this case *x* denotes a dimensionless quantity while the dimension of *y* (e.g. of $\tilde{\beta}$) is $(mN/m)^{2/5}$. For the sake of convenience we use a decimal logarithm instead of a natural one, because looking at the graph one could very easy calculate the powers of 10, while it is much more difficult to calculate powers of *e*. Because of that we redefine the constant $\tilde{\beta} = \beta \ln(10)$. If the experimental data for the surface tension isotherm are plotted in this SCF scale we expect that if the theory scaling is correct the data points would lay on a straight line starting from moderately low concentrations up to the CMC. Above CMC interfacial tension flats of and it definitely does not follows SCF scaling law. It is possible that deviations for the case of very small concentrations can be observed, where the surface tension is very close to the value of the pure interface. The reasons for such a deviation could be:

a) For very low values of adsorption (i.e. bulk concentration) the surfactant tails are not stretched and the strong stretching approximation, which is one of the key assumptions in the SCF is not fulfilled.

b) For very low concentrations the value of surface tension is very close to that of the pure interface and the system may need a very long time to reach equilibrium. During this long equilibration period any drifts in the experimental apparatus or small changes of conditions, like temperature fluctuations or external contaminations, could give the effect comparable to the effect of surfactant. Thus the experimental accuracy could not be sufficient for very low concentrations.

In this case the *y*–values in the SCF-plot are practically constant while x values due to the log term could change very much, thus points could significantly deviate from the straight line.

If there is significant deviation for small concentrations we exclude those points from the plot. We use linear regression to fit the experimental points and find a value for $\tilde{\beta}$. An additional indication for the validity of the fit is to use an adjustable intercept. If eq 6.6 correctly describes our experimental data, then the intercept should be very close to zero, or at least very small compared to the value of $\Pi_0^{2/5}$. Using the value of the fit parameter, $\tilde{\beta}$, one can calculate back the surface tension in the normal scale $\gamma(\log_{10} c)$ using the equation

$$\gamma(\log_{10} c) = \gamma_p - \left[\tilde{\beta}\log_{10}(c/c_0) + \Pi_0^{2/5}\right]^{5/2}. \tag{6.7}$$

If a reference point is not used one can plot the experimental data

$$y = \tilde{\beta}x + \delta \tag{6.8}$$

where, $y = (\Pi)^{2/5}$ and $x = \log_{10}(c)$. After the constants $\tilde{\beta}$ and δ are determined by linear regression in this scale (SCF), the interfacial tension can be presented as follows

$$\gamma(\log_{10} c) = \gamma_p - \left[\tilde{\beta}\log_{10}(c) + \delta\right]^{5/2}. \tag{6.9}$$

We expect that if the SCF model is consistent with the experimental data, there should not be a big deference between values of $\tilde{\beta}$ obtained with or without reference point, because the choice of a reference point simply shifts the straight line along its axis in the SCF scale.

The value of $\tilde{\beta}$ obtained from the fit of experimental data for the interfacial tension isotherm in SCF scale can be used to estimate the surfactant adsorption at the interface by using eq. 6.1

$$\Gamma = \frac{\Pi^{3/5}}{\alpha^{3/5}} = \frac{5\Pi^{3/5}\beta}{2kT} = \frac{5\tilde{\beta}\Pi^{3/5}}{2\ln(10)kT}. \qquad (6.10)$$

The surface pressure Π in the last equation can be calculated either from the experimental data or it can be derived from eq 6.7 or eq. 6.9. Provided that the value of $\tilde{\beta}$ is obtained from the fit in SCF plot, one could calculate the occupied area per surfactant molecule from

$$\frac{1}{\Gamma}[\text{Å}^2/molecule] \approx \frac{1.272T}{\Pi^{3/5}\tilde{\beta}} \qquad (6.11)$$

where, $\Pi = \gamma_p - \gamma$ is measured in mN/m, $\tilde{\beta}$ is measured in $(mN/m)^{2/5}$ (and is the value obtained from SCF fit), while *T is the absolute temperature*. Note that in the SCF fit we have chosen for convenience to plot $\log_{10} c$ (decimal log), instead of $\ln c$ (natural log).

The values of the adsorption or the area per molecule calculated from eq 6.11 will be compared with those (where available) obtained from independent experiments like ellipsometry[119] or SANS[117,119], or alternatively, using those data one could estimate $\tilde{\beta}$ and compare the prediction of the SCF theory for the interfacial tension isotherm.

For the case of ionic surfactant one could take into account the effect of counter ion adsorption by multiplying the Gibbs-Duhem equation (eq 6.2) by factor of 2. The arguments for this approximation are following[115-117]: if we have electrical neutrality in the bulk and at the interface and we have 100% dissociation of surfactant in both places, than the bulk concentration and adsorption of surfactant and counter ions should be equal. Due to the equilibrium (between surfactant and counter ions) and full dissociation, the chemical potentials of counter ions and surfactant should be also equal. From the other point of view counter ions at the interface are statistically independent object and their contribution to the surface tension should be counted also in the Gibbs-Duhem equation. Due to equality of adsorption and chemical potential of surfactant and counter ions, the net contribution of the ionic surfactant to the Gibbs - Duhem equation should be twice the contribution of non-ionic surfactant. If this is the case the values of area per molecule obtained from eq. 6.11 should be multiplied by factor of two also. Note that the above arguments have only approximate

validity and could be quite incorrect and misleading. The reason is due to the fact that when we have ionic surfactant the surface dissociation is never 100% and also the interface is charged. The latter leads to several important consequences: (i) adsorption of counter ions and surfactant are different and (ii) due to the surface charge there is electric double layer near the interface, whose electrostatic energy also contributes to the values of interfacial tension. For more details on the subject one could see work of Kralchevsky et. al.[115].

According to ref 115, the expected values of area per molecule for ionic surfactants should be between 1 and 2 times the value predicted from eq. 6.11.

VI.4. Comparison of the SCF theory predictions with experimental data

VI.4.1. Surface and interfacial tension of non-ionic surfactants

VI.4.1.1. Surface tension of $C_{12}E_5$

For this system experimental data are available in the literature for both the surface tension† isotherm and the adsorption isotherm (Binks et. al[119]). The adsorption isotherm on air-water interface has been obtained from independent ellipsometrical and SANS measurements.

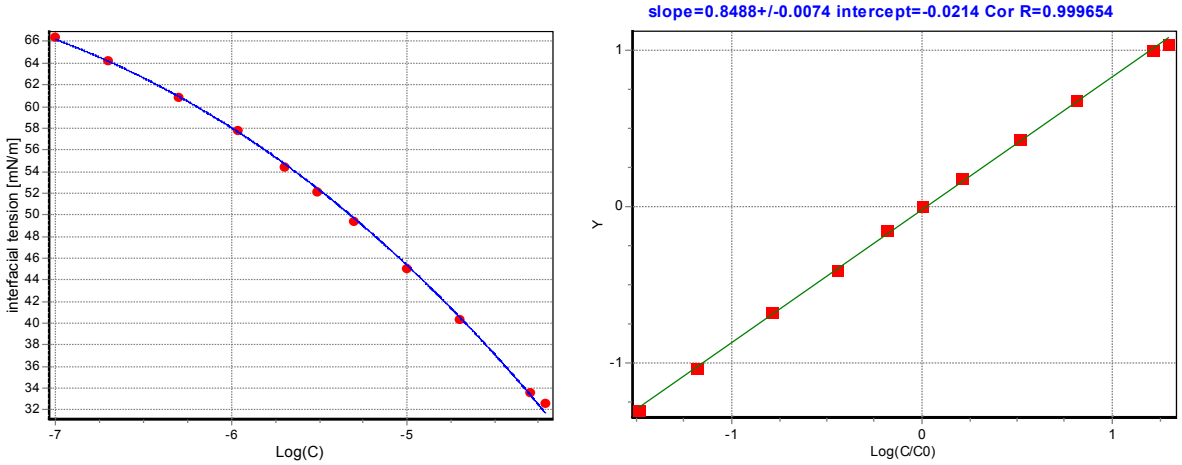

Figure 6.2a. Experimental data for the surface tension isotherm of $C_{12}E_5$ (left plot) – dots are the experimental values[119] while solid curve is obtained from the best fit in SCF scale (right plot). The last data point on the plot corresponds to the surfactant CMC. The solid line is the fit with the SCF theory. One could see that experimental isotherm is in excellent agreement with SCF scale (the plot at the right-hand side).

† In all cases throughout the text the surfactant concentration is given in mol per liter, *M*, while surface/interfacial tension is measured in mN/m.

Here we fit the experimental data for the surface tension in SCF scale and compare the predictions of the SCF theory for the surfactant adsorption with the experimental values. The results are presented in figure 6.2a and 6.2b. Looking at figure 6.2a one sees that the experimental values of surface tension lie on a straight line in the SCF plot with correlation coefficient of linear regression R=0.9996. In figure 6.2b we compare the values of area per molecule of surfactant obtained from the independent experiments with values calculated from the SCF fit of surfactant isotherm and eq 6.11.

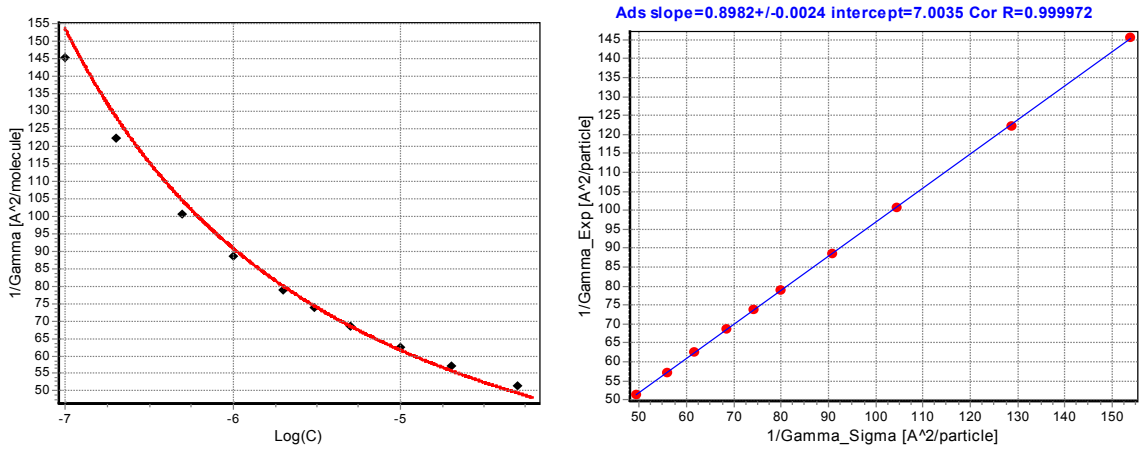

Figure 6.2b. Experimental adsorption isotherm of $C_{12}E_5$ (left plot) – dots are the experimental ellipsometry and SANS values[119], while solid curve is obtained from the fit of surface tension data. On the right plot we have compare the experimental and predicted (from surface tension fit eq. 6.10) values of area per molecule.

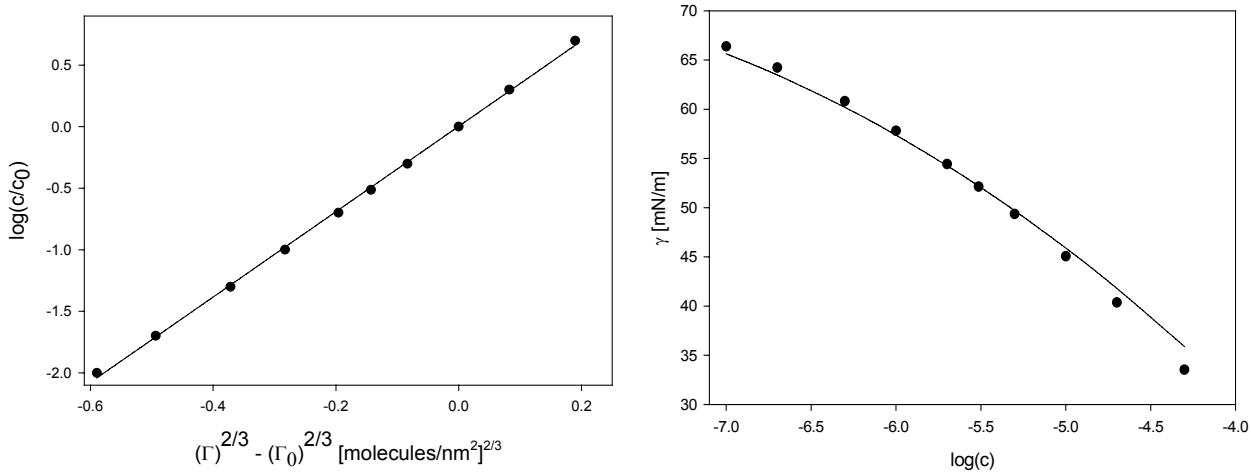

Figure 6.2c. Experimental adsorption isotherm of $C_{12}E_5$ plotted according to eq 6.3 (left plot). In the plot on right-hand side we show comparison between the experimental surface tension isotherm (dots) and the predicted one obtained from SCF fit of the independent adsorption data (left-hand side plot).

The agreement between both is remarkably good and the differences for the case of very small concentrations are within the limit of the accuracy of the ellipsometry and the SANS experiment[117,119].

An additional test of SCF scaling prediction is presented in figure 6.2c where the adsorption data are plotted in the scale according to eq. 6.3, i.e. we also have compared the adsorption isotherm from the experiment with the SCF given with eq 6.3. Note that the latter plot should be considered as completely independent check of SCF scaling because the experimental data for adsorption are independent from the surface tension measurements. Nevertheless one sees that in both cases we find an excellent agreement between the scaling laws of SCF theory and those followed by the experimental data. Using the slope of the adsorption data plotted in SCF scale one could calculate back the surface tension. The comparison was shown also in left plot in 6.2c. The agreement is also quite good, which means that the surface tension and adsorption isotherm are fitted self-consistently with similar values of the parameter α. The difference between the values of α obtained form surface tension isotherm and adsorption isotherm is less then 10%, which is within the experimental accuracy of the ellipsometry and the SANS data [117,119].

One should also note that in order to calculate the adsorption from the ellipsometry data one needs a model of the surfactant layer at the interface. In the ellipsometry the measured parameter is the product of layer thickness times the refractive index of the layer, which gives the optical length in the optically active media. In order to calculate the thickness of the layer one needs an estimate of the refractive index and vice versa. The problem is that both of them are dependent from the local concentration of "matter", as well as from the total amount in the layer is subject of determination. Thus one needs to speculate about how the matter is distributed into the optically active layer (which will give an estimation of the refractive index) and what is the layer thickness, and how it depends on the total amount of matter in the layer.

> "*In this context, it is important to note that ellipsometry essentially yields only a single measured parameter (the ellipsometry angle* Δ*) reflecting the adsorbed film structure, which can reliably yield only a single unknown,* Γ*. Thus, although ellipsometric data is precise, it is information poor*"[119].

For the case of amphiphilic di-block polymer or surfactant instead of one layer at the interface, one has at least two. One optically isotropic slab consisting of surfactant hydrophilic headgroups mixed with water plus a second, optically isotropic slab consisting of surfactant hydrophobic tail-groups in air. In ref 119 it was assumed that the surfactant hydrophobic layer has constant thickness, *H*, independent from the adsorption, equal to 80% of the length of the extended surfactant tail. The same applies for the hydrophilic layer. The segments are assumed to be distributed homogeneously in the layer, with a volume fraction equal to $\varphi = \Gamma v / H$, where v is the volume of hydrophilic or hydrophobic part of surfactant. The refractive index of corresponding layer was calculated assuming a linear dependence from volume fraction: $n = \varphi n_{tails} + (1-\varphi) n_{pure}$.

The SCF theory can provide an alternative model for the surfactant layers, which can be used to interpret data from ellipsometry. Since the SCF scaling works well for both surface tension and adsorption isotherms, one can speculate that also it could be applied for constructing more realistic layer model of the surfactant adsorption at the interface. For example SCF predicts that the layer thickness is not a constant, but it depends on the adsorption as $H \sim \Gamma^{1/3}$. Second we knew that the volume fraction of chain segments is not constant in this layer and has nearly parabolic profile given with $\varphi \sim (1 - x^2 / H^2)$. In addition, those quantities are connected to with the parameters of adsorption and surface tension isotherm (α and β). All this additional information could be used to constrict more realistic and self-consistent models for the interpretation of the ellipsometry data for surfactant adsorption at a liquid/fluid interface. This topic will be a subject of more detailed study in the future.

VI.4.1.2. Surface tension of $C_{10}E_6$

Here we show comparison between experimental data for the surface tension[120] and the SCF scaling predictions for the case of another nonionic surfactant $C_{10}E_6$. Again there is a remarkably good agreement between experimental data and scaling law of SCF. The correlation coefficient of the straight line in this case is again 0.9996 (see figure 6.3).

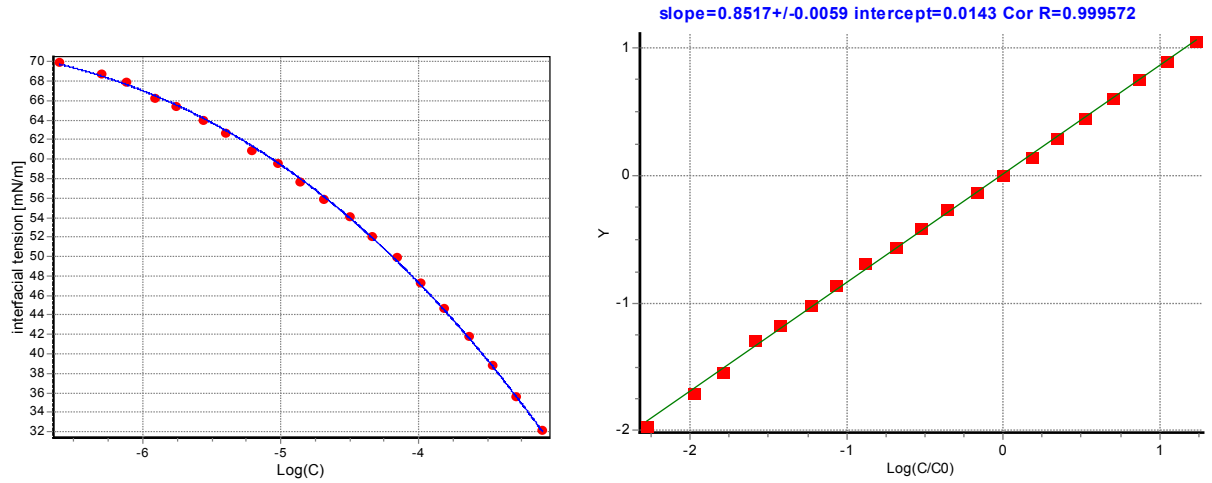

Figure 6.3. Experimental data for the surface tension isotherm[120] of $C_{10}E_6$ (left) – dots are the experimental values, while the solid curve is obtained from the best fit in SCF scale (right). The last data point corresponds to the CMC of the surfactant. One could see that the experimental isotherm is in excellent agreement with the SCF predictions.

VI.4.1.3. Surface tension of $C_{12}E_6$

Here we show comparison between experimental data for the surface tension[120] and SCF scaling predictions for another nonionic surfactant $C_{12}E_6$ (see figure 6.4).

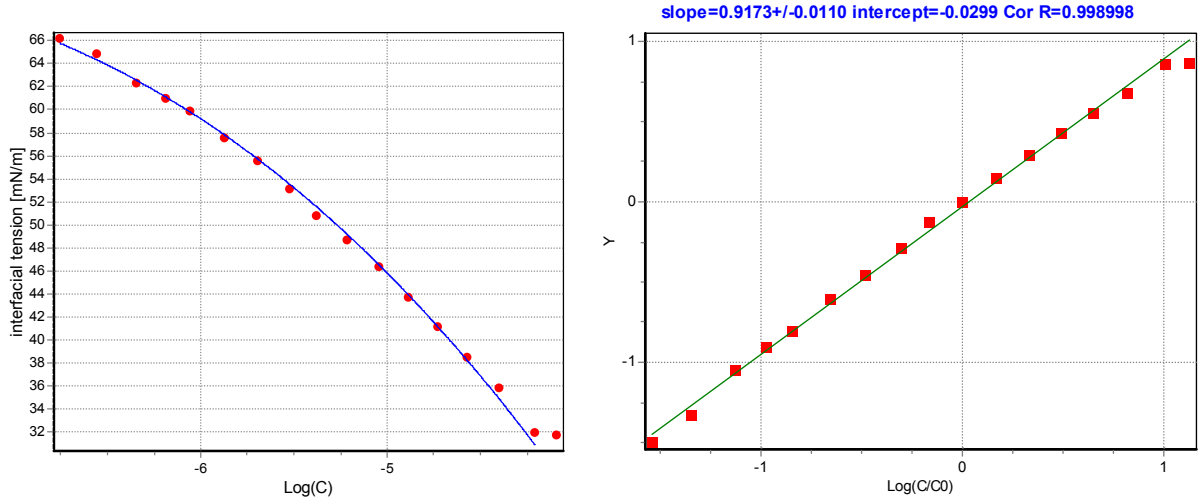

Figure 6.4. Surface tension isotherm[120] of $C_{12}E_6$.The last point in the surface tension isotherm is above CMC. One clearly sees that it also deviates from the straight line in SCF plot. All points below CMC are included into the fit and lie on a straight line.

VI.4.1.4. Surface tension of Sulfobetaine

In this case we compare the SCF scaling predictions for the case of amphoteric surfactant Sulfobetaine[121]. The results are shown in figure 6.5. In this case we have more points above CMC. In two lines on the SCF plot (right) correspond to data below and above CMC.

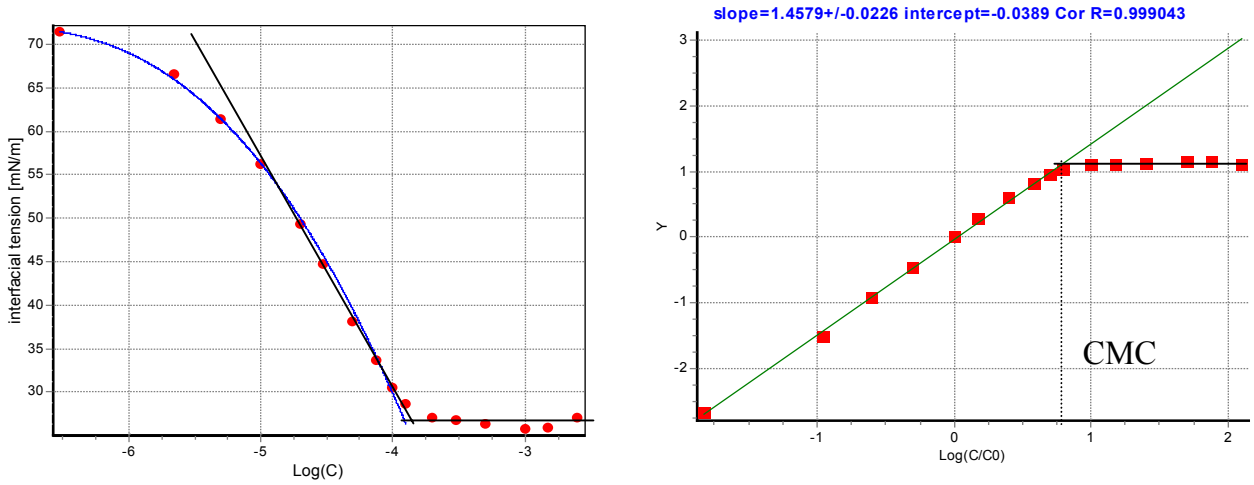

Figure 6.5. Surface tension of zwitterionic surfactant Sulfobetaine (n-Dodecyldimethyl(3-sulfopropyl)-ammonium hydroxide from Tokyo Kasei Chemical Co).

The intersection point of the two lines gives the surfactant CMC. In this specific example we have used a reference point to obtain SCF graph, $c_0 = 2\times10^{-5} M$; the CMC obtained from the intercept of two graphs in SCF plot is $1.3\times10^{-4} M$. On the left-hand side of figure 6.5 we have illustrated the standard method for calculation of CMC. This method assumes that in the vicinity of CMC adsorption is nearly constant, equal to limiting value Γ_∞ . The Gibbs-Duhem equation (eq 6.2) in this case predicts $d\gamma = -kT\Gamma_\infty \ln c$. Thus, in close vicinity of CMC the changes of surface tension should be linear with respect of $\ln c$. Then CMC is defined as an intercept between two lines: a straight line which is passing trough the experimental data in the regime bellow CMC determined from Gibbs-Duhem equation and a second line, which is passing trough the data above CMC, assuming that they level off above the CMC. The main problem using the standard method is that near the vicinity of CMC only a few points are laying in the linear region. As it is demonstrated in the right part of figure 6.5, when using a SCF plot one could use the whole experimental data range for the determination of CMC, because all data below CMC lie on one line and all data above on the second, both which are quite distinct.

VI.4.1.5. Surface tension of a mixture of amphoteric surfactant Sulfobetaine with 5wt% SDS

In this case we have compared the experimental data[121] for a mixture of Sulfobetaine with 5wt% SDS. So we have a mixed monolayer at the interface containing two surfactants. Again one could argue that the SCF scale is not correct for a mixed monolayer, due to the fact that we didn't use a theory for the mixture of surfactants (or polymer brushes). The probable explanation in this case is that both surfactants have and the same length of the tails, thus the layer containing hydrophobic tails is nearly identical and one could treat it with the theory of single-component brushes. If the two surfactants have different chain length, then the hydrophobic layer will consists of brushes of different length and the structure will be different. The latter case is treated in the SCF theory and can also be incorporated in a similar treatment.

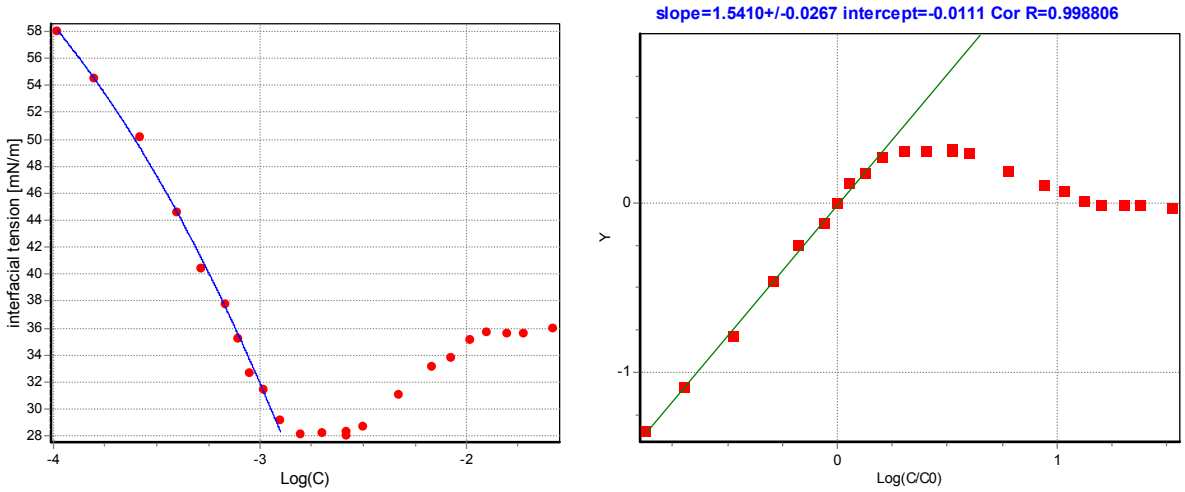

Figure 6.6. Surface tension of mixture of amphoteric surfactant Sulfobetaine and 5wt% SDS[121].

All data below CMC lay on a straight line when plotted in SCF scale. In addition, the data up-to the isotherm minimum (which typically appears in mixtures of surfactants, or when the surfactant sample contains contaminations) are on the line, which is also quite interesting and should be analyzed in more details. It is also worth mentioning that the standard method for determination of CMC fails due to the broad minimum, which spreads from $10^{-3}M$ to $10^{-2}M$. This case was analyzed in details in the work of Lin et. al.[122], where they claim that CMC of surfactant is the point after the minimum of isotherm where data flats off. Hence

CMC according to the method proposed in ref 122 is at about 10^{-2}M (in the beginning of the plateau), and is quite different from the value obtained by using the standard method (10^{-3}M). One sees that in this case this difference is about one order of magnitude and cannot be neglected.

Conclusions of Lin et. al.[122] were based on the comparison of conductivity (for ionic surfactants) and surface tension data of the solution. The conductivity of the surfactant solution changes when micelles appear in to the solution due to the different charges of surfactant monomers and micelles.

In another interpretation[122] method, it was assumed that CMC is at the minimum of the surface tension isotherm. Looking at SCF plot one sees that all data starting from very low concentration, up to the minimum of SCF plot are on the straight line. Thus one could say that up-to this point the surfactant behavior is qualitatively the same and this point could really be taken as a definition of CMC.

VI.4.1.6. Surface tension of amphoteric surfactant LADA

In this case we compared the experimental data of the amphoteric surfactant LADA[121] against the scaling predictions of SCF (see figure 6.7).

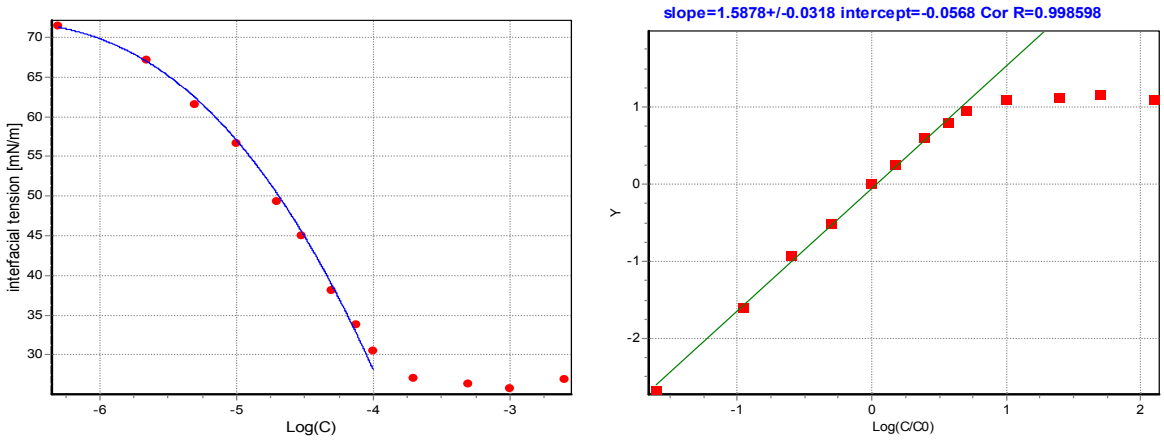

Figure 6.7. Surface tension of amphoteric surfactant LADA[121] (Lauric Acid Diethanol Amide), commercial-grade products of Kao Co., Tokyo, Japan. The data are presented in both normal and SCF scale up to the CMC of the surfactant.

Very good agreement is obtained below CMC and the position of the CMC of the surfactant from the SCF plot can be clearly distinguished. Amphoteric surfactants are used in many industrial formulations due to the their strong synergistic effects (interaction) with non-ionics. When mixed with non-ionics (even at very low concentration) they aim to form dimer complexes, which are much more surface-active than each of the two surfactants alone. Those surfactant complexes are more surface active, have better foamability and are better emulsifiers, which gives significant performance improvement (boost) of the product. This is the reason why in some cases they are called also boosters.

VI.4.1.7. Interfacial tension of the amphoteric surfactant DDAO at the water/hexane interface

In figure 6.8 we show experimental data (the measurements are performed in University of Essen) for the interfacial (water/hexane) tension of another type of Aminoxide surfactant. This amphoteric surfactant is positively charged at low pH and neutral at high pH. Again we see that there is very good agreement between the theoretical predictions and the experiment.

Note that results presented up to now were for the surface tension isotherms (air-water interface), while in this case the experimental data represent an interfacial (water/hexane) tension measurements. This example demonstrates that the SCF isotherm works and fits equally well both surface and interfacial tension isotherms.

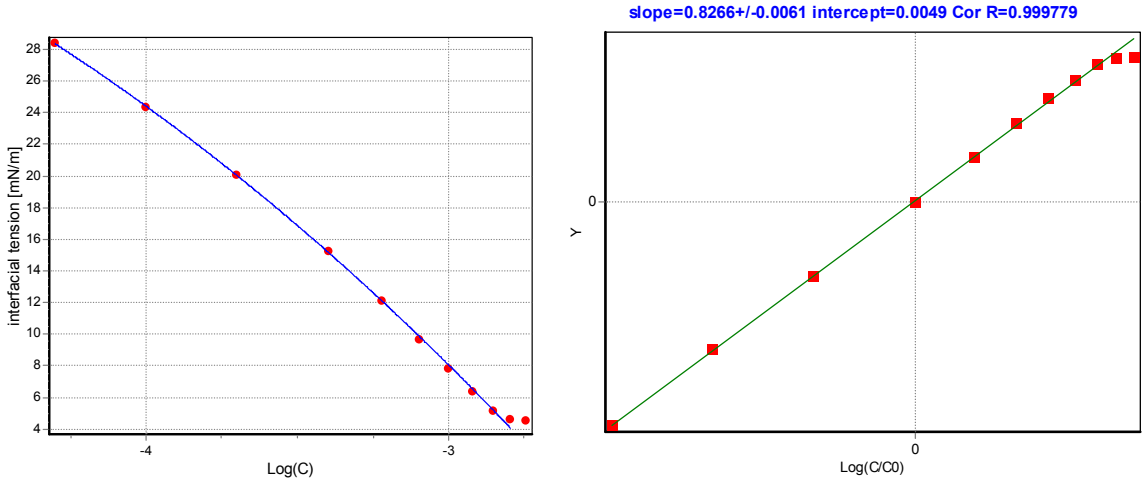

Figure 6.8. Interfacial (water/hexane) tension of amphoteric surfactant DDAO (Dodecyl dimethyl-amin-oxide). The data are taken from ref 123. It is worth to mention that the SCF scaling fits air-water and oil-water interfacial tension isotherms as well.

In summary, we my state that for many types of non-ionic and amphoteric surfactants the scaling predictions of the SCF-isotherm are fulfilled remarkably well, both at air-water and oil-water interfaces. The predicted values of the adsorption for the case of $C_{10}E_5$, agree very well with the adsorption isotherm measurements obtained by an independent experiments. So one could expect that there will also be a pretty good agreement for other non-ionics. This assumption will be a subject of additional studies.

It is also instructive to compare different SCF-slopes for various surfactant systems and to perform a qualitative analysis of the data and to compare them with theoretical predictions of the model.

VI.4.2. Comparison between SCF theory, experimental isotherm and DPD simulation of interfacial (water/hexane) tension of amphoteric surfactant DDAO

Here we compare the results obtained with DPD simulation method with the experimental findings (discussed in previous paragraph) for the case of interfacial tension (water/hexane) of DDAO. The DPD simulation was performed by Ryjkina[123] and the simulation details are entirely described in ref 123. Our aim here is to rescale the simulation results in order to be directly comparable with experimental one, using SCF theory. In the referenced study the surfactant oil and water are represented by 3 different types of beads, connected with springs in order to form molecules, which is summarized in figure 6.9a.

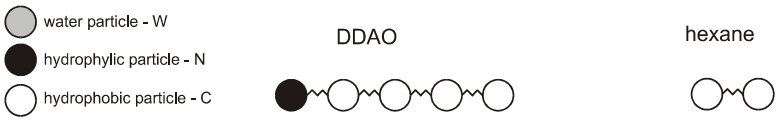

Figure 6.9a. DPD representation of DDAO surfactant, water and hexan molecule.

The repulsion parameters for the different DPD-particles were calculated explicitly from the Flory-Huggins interaction parameter χ as it was proposed by Groot et. al[71]. For the calculation of the χ parameter, a Monte Carlo approach, which includes the constraints,

associated with excluded volume[71,74,75,123] was used. The latter approach allows estimation of pair wise interaction energies with a significant accuracy. For all calculations of the pair-wise energies the force field COMPASS (condensed-phase optimized molecular potentials for atomistic simulation studies)[77] was used. The latter is especially parameterized for modeling of condensed phases. The size of simulation box was 20x10x10 DPD units. The simulation used to calculate the surface tension was performed by using the same procedure like in Chapter V and the same computer code.

The obtained curve of the interfacial tension as function of the surfactant adsorption is shown in figure 6.9b. The interfacial tension of the pure (water/hexane) interface is 8.9 DPD units while the corresponding experimental value is 48.23 mN/m. Thus the conversion factor for the surface tension from DPD units to the real one is 48.23/8.9=5.41 mN/m. An additional check of this simple rescaling procedure was performed, also in ref 123. In this case the interfacial tensions of different hydrocarbons obtained from DPD were matched to the experimental values (see for more details ref 123).

It is naturally to ask why the surface tension was calculated as a function of the surfactant adsorption, and not as a function of the bulk concentration. The reason is that in the simulation the equilibrium bulk concentration corresponding to the respective adsorption is very low. Consequently the number of surfactants molecules, which are in the simulation box and are not adsorbed at the interface is very low. So this caused by the finite size of the simulation box, which could be partially improved by using larger geometries.

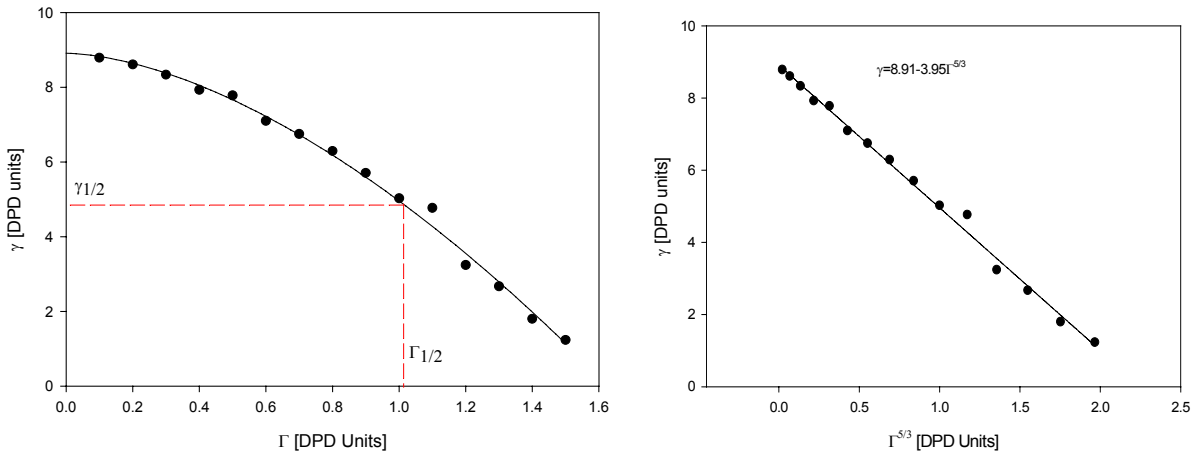

Figure 6.9b. DPD simulation results[123]. The value of the adsorption, $\Gamma_{1/2}$, corresponding to surface tension equal to ½ of the value for a surfactant-free interface is 1.07 DPD units.

We will show bellow that 1 DPD unit corresponds to 8.5Å, and hence the total volume of the simulation box (20x10x10 DPD units) corresponds to a bulk phase with volume at about 1000 nm^3. For a typical bulk concentration of surfactant 10^{-3}M, which is near CMC one could calculate that in such a box we could find about 1-2 particles! Thus if an interface is present, practically all surfactant molecules will be adsorbed there and only a few molecules will remain in the bulk. Thus there will be a huge error (fluctuations) in the bulk concentration of surfactant (simulated in above mentioned box), while the adsorption could be still estimated with a sufficient accuracy. Much bigger simulation box would be required for an accurate estimation of the bulk concentration. But the increase of the box size also increases the number of particles, which finally increases the computational time.

It is also instructive to compare the slope of the line in the SCF plot (eq. 6.1) with the formula, which we derived in the previous part for the DPD simulation (eq. 5.15). This formula assumes that the effect comes from the conformation of the long tails of the surfactant at the interface. That is why in previous section we performed simulations for relatively long chains (20 monomers). In this case, however, we have only 4 beads in our surfactant chain and from the SCF point of view this system is away from the scope of the validity of SCF theory. Nevertheless we see that even for this system the SCF scale works quite well, so it is interesting to compare also the values of the slope obtained from simulation and the one calculated from eq 5.15. In the simulation the DPD density was 5, while repulsion between oil beads was set to be 54kT. By substituting those values into eq. 5.15 for a distance between the beads $l=1$ and N=4, we obtain the following relation between the interfacial tension and adsorption $\gamma = \gamma_p - 3.5\Gamma^{5/3}$. While the slope of the line in Figure 6.9b is -3.9 ± 0.2. This is a remarkably good result if one bears in mind that the SCF theory is applied for the case where it is expected not to be strictly valid.

In order to compare the DPD values of the surface tension vs. the surfactant adsorption we recalculated the experimental values of the surface tension vs. the surfactant concentration in terms of surface tension vs. adsorption. Using the fitting parameters from the SCF plot we calculated the adsorption by using eq. 6.11. The result of this calculation is shown in figures 6.9c, and 6.9d. In figure 6.9c we show the adsorption vs. the bulk concentration (adsorption isotherm), while in figure 6.9d we present the surface tension vs.

the adsorption, which appears to be the same type of curve, which was obtained with from the DPD simulation.

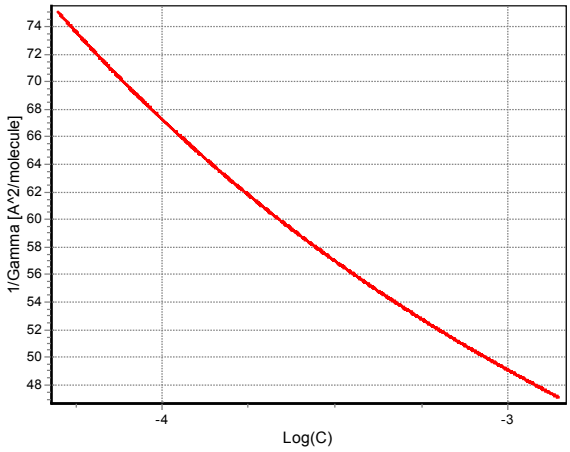

Figure 6.9c. Adsorption of DDAO at the water-hexane interface vs. the surfactant bulk concentration, obtained from the SCF fit of the surface tension isotherm (see figure 6.8).

Now we rescale the DPD data in dimensional form. The surface tension scaling was discussed above (through the value for the surfactant-free interface) by factor 5.41 mN/m. The adsorption can be scaled by adjusting the values of adsorption in DPD and real units by matching the point where the interfacial tension is half of the value of the pure hexane-water interface for both for real system and DPD simulation (see figure 6.9b).

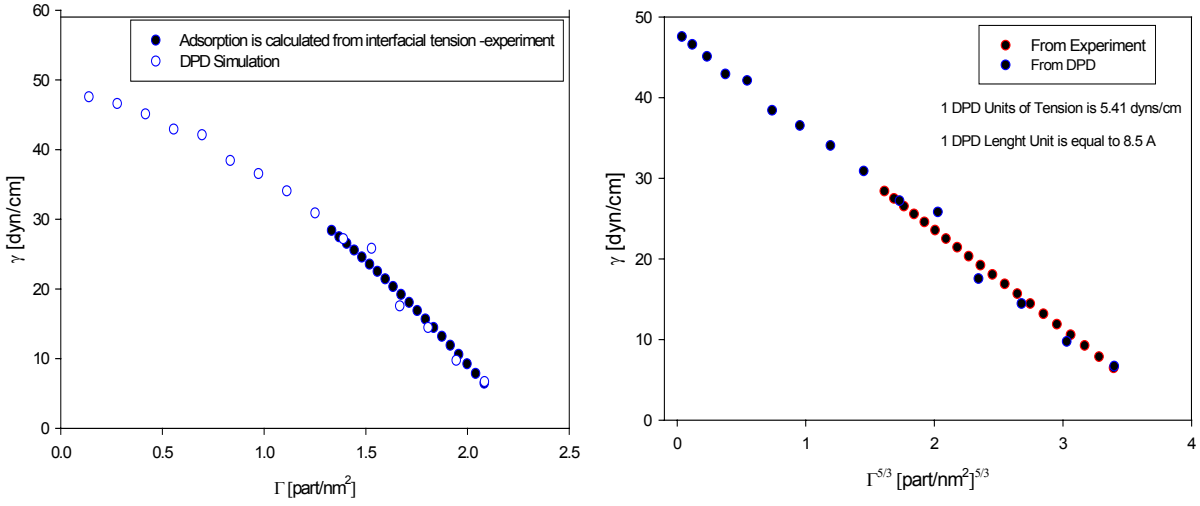

Figure 6.9d. Comparison between rescaled DPD simulation values of the adsorption vs. the surface tension with the experimental data. The right-hand side plot present the data in the expected SCF scale (linear).

For the experimental value (see figure 6.9d) we find that the $1/\Gamma_{1/2} = 67\,\text{Å}^2/molecule$, while for DPD we have $1/\Gamma_{1/2} = 1.07\,r_c^2/molecule$ (r_c is the cutoff radius in DPD, which was set to correspond 1 in DPD length unit), from where one gets the length scale in DPD, $r_c = 8.5\text{Å}$. This enables us to rescale the DPD adsorption values to the real ones and to compare the rescaled DPD values with the experimental one as shown in figure 6.9c. One could see that there is an excellent agreement between both sets of data.

This result is not surprising because of the fact that both the DPD system and the real system obey the scaling law of SCF theory. By mapping the values of the surface tension of the pure hexane-water interface between DPD and experiment we actually have fixed the intercept of the scale (see eq. 6.1). By adjusting the reference point $\Gamma_{1/2}$ (which determines the dimensional scale factor) we adjust the slope of both curves to correspond to $\alpha = \gamma_p/(2\Gamma_{1/2}^{5/3})$. So if both the experiment and the DPD results follow the SCF scale, the two data sets would coincide with each other. But they would deviate from each other if there is a strong deviation from the SCF predictions. By adjusting the values of the interfacial tension for the real system and the DPD simulations one can calculate directly the real length scale in the DPD simulation, which can be compared with data obtained from independent considerations. Close agreement between those values is an indication that the DPD system really matches the behavior of the real system. In this case by mapping the compressibility of water of the real and the DPD system it was estimated that the length scale of DPD is about 8Å, while mapping the surface tension of real and DPD system we obtain that the scale is 8.5Å, which is a rather good agreement taking into account that the mapping of compressibility gives rather rough estimation of the length scale (for more details see reference 123).

The main reason why a huge set of properties calculated by DPD cannot be mapped to the properties of the real system is that DPD uses a very small set of initial parameters to describe the system. For example, in this case we have assumed that only 6 interactive parameters are enough to represent differences in interaction between different types of species in our system. These are the interactive parameters between the hydrophilic bead, the water bead and the bead representing the head of surfactant and like interactions. But in the real system the picture is much more complicated which requires more information to be

mapped on a molecular level. One cannot expect that by mapping only a few parameters in the DPD simulation it will be sufficient to describe all physical properties of the real system. Thus a deviation of order of 5-10%, should are considered as a good agreement in most cases. This is common for all coarse-grained methods – where some information at a lower level is not used for the sake of simplicity. Depending on the specific application of the computer modeling methods one is mapping the properties of prime interested, so that the simulation results have sufficient accuracy. For instance if the compressibility of the fluid is of prime interest, one could use one length scale, but if the surface properties are have prime importance one could use different length scale. The closer these two values are the higher is the confidence that the system is modeled properly by the method.

We would like also to point out that the mapping between real and DPD systems could be used for estimation of the interactive parameters of the surfactant (see eq 5.15), provided that the length scale is known a priory from independent considerations (like matching distance between the beads with the bond length between the segments of surfactant molecule).

VI.4.3. Surface and interfacial tension of ionic surfactants

Here we compare the SCF theory predictions and the experimental observation for the case of some commonly used ionic surfactants[124-127]. As it was already discussed in the introduction there are no strict theoretical arguments why SCF scale should work for such systems, but nevertheless we will demonstrate the event for this case the SCF-isotherm performs remarkably well.

VI.4.3.1. Surface tension of SDS solutions

For the case of the ionic surfactant Sodium Dodecyl Sulfate (SDS) we have compared two isotherms: with (figure 6.11) and without background electrolyte (salt) (figure 6.10).

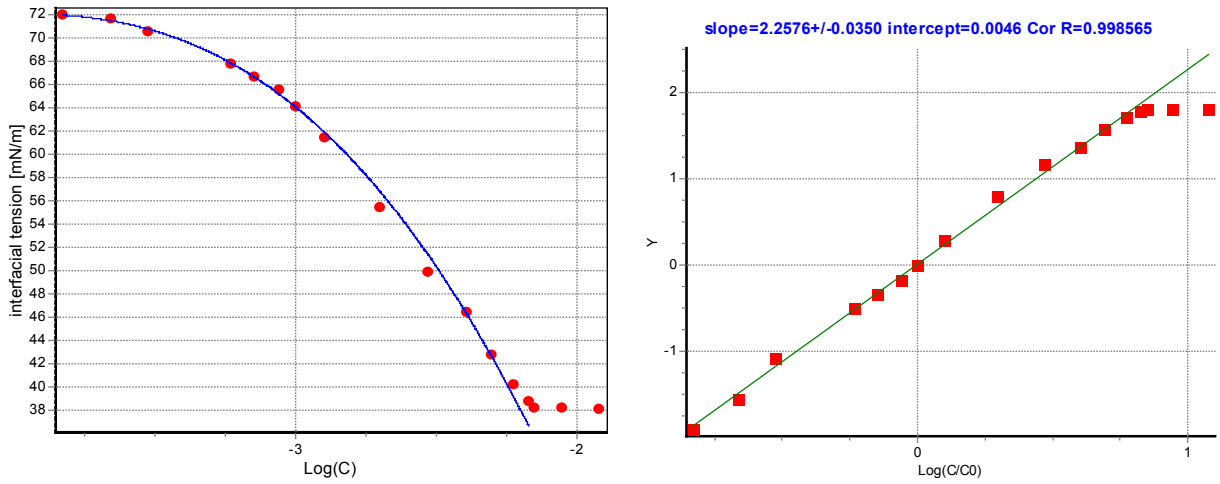

Figure 6.10. Surface tension of pure SDS no salt (Tadjima[125]).

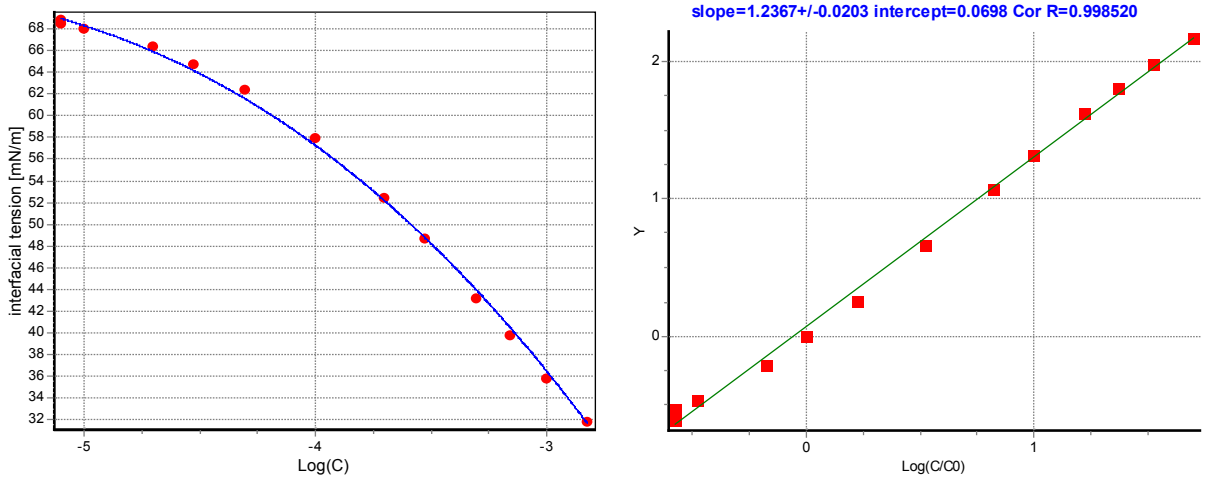

Figure 6.11. Surface tension of SDS with 115mM NaCl (Tadjima[126]).

One could see that in both cases the experimental data, when plotted in SCF scale, follow the straight line. The agreement for the case with salt is slightly better than the one without salt, because higher salt concentration corresponds to smaller electrostatic contributions, which are neglected in the SCF theory outlined here. Note that the slope of the curves in SCF scale is different – thus somehow the slope takes effectively into account the electrostatic contributions. This is by no means trivial, because one could expect that the electrostatics will change not only the slope of the SCF scale, but it will change the scale completely! This is a very interesting finding and requires additional attention, which will be subject of future investigations. The same approach like the one described in the work of Kralchevsky et. al.[115] could be used to account for how the electrostatic effects interfere with the conformation

effects of the surfactant tail. In this case one could still use eq. 5.1, but one should take into account:

- The adsorption of counter ions – which will modify Gibbs-Duhem equation (eq. 5.2).
- The electrostatic contribution to the surface free energy.
- The surfactant activity coefficient is different from 1 - due to the electrostatics in the bulk.

VI.4.3.2. Surface tension of pure SDP_3S

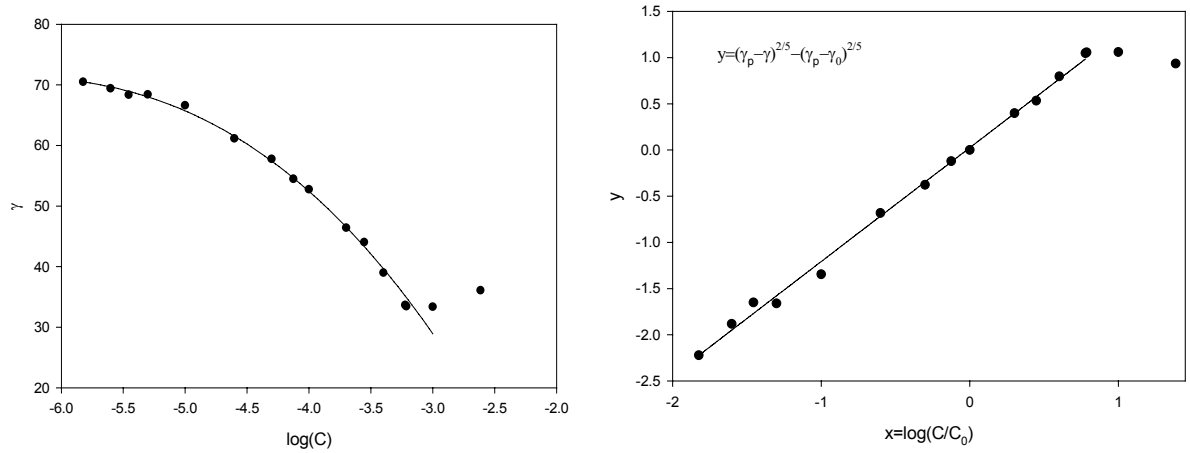

Figure 6.12. Surface tension[121] of sodium dodecyl polyoxyethylene-3 sulfate (SDP_3S) (industrial grade surfactant from Kao Co), $\tilde{\beta} = 1.23$.

In figure 6.12 we show comparison between SCF theory and the experiment data for another ionic surfactant, sodium dodecyl polyoxyethylene-3 sulfate (SDP_3S), taken from ref 121a. This surfactant has a hydrocarbon tail similar to that of SDS, but the head-group is different due to the presence of hydrophilic ethoxy groups. If the main contribution to the surface tension comes from the interaction between the hydrocarbon tails of the surfactant molecules, the SCF-slope of this isotherm should be very similar to the one for SDS. Looking for the data for SDS in previous section, we see that the slope of the SCF plot (1.24) for SDS with electrolyte (115mM NaCl) is nearly the same with the value for SDP_3S solution (1.23), which is in consonance with our predictions theoretical expectations.

VI.4.3.4. Surface tension of pure C_{10}TAB

In the last few sections we will give some results for the homology of C_kTAB cationic surfactants. The data are taken from the work of Bergeron[124].

For the first one, C_{10}TAB, the results are shown in figure 13a. We see that there is a good agreement between SCF-scale and experimental observations. In his work Bergeron[124] gives also an experimental values of surfactant adsorption obtained by Thomas et al.[117] using SANS, which we also compare with the adsorption values obtained from SCF-fit of the surface tension.

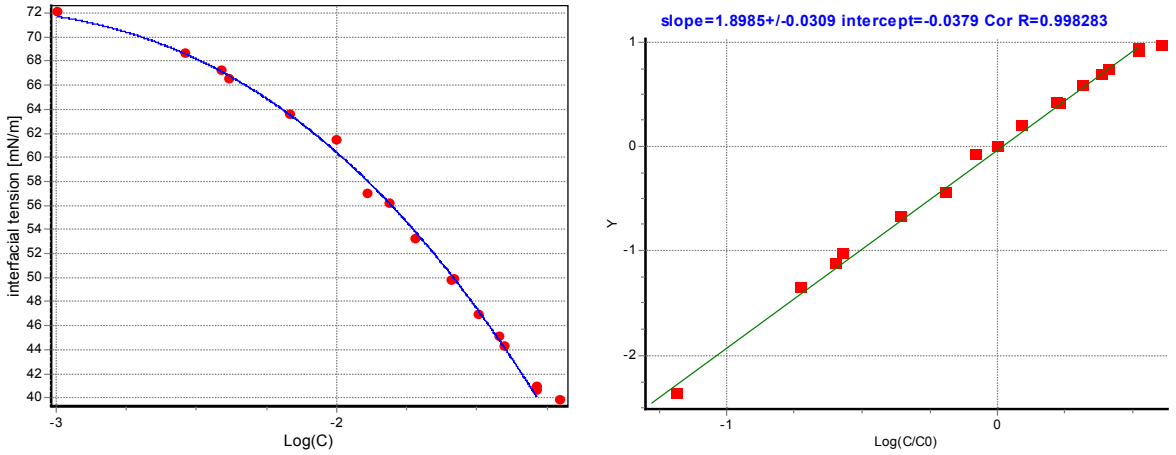

Figure 6.13a. Surface tension[124] isotherm of C_{10}TAB.

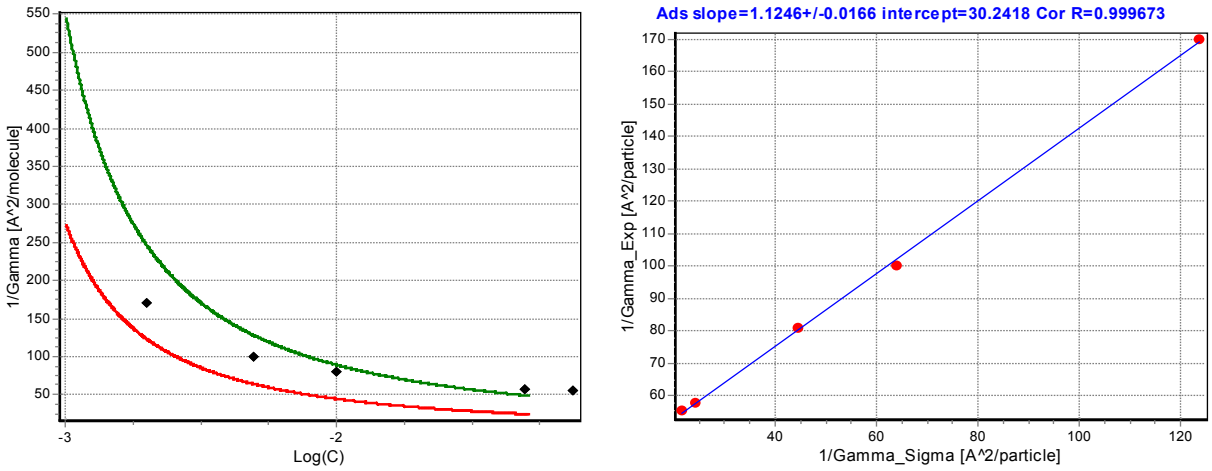

Figure 6.13b. Air/water adsorption isotherm of C_{10}TAB (Sigma, ref. Thomas et al[117]). In the left hand side diagram the dots represent independent experimental data obtained from SANS, while solid line are obtained from the fit of surface tension (red is obtained using eq. 5.11, while green is line corresponds to a Gibbs – Duhem equation is multiplied by factor of 2). In the right-hand side plot the comparison with SANS data and the fit of the surface tension data (eq 5.11, and red curve on the left plot) is presented.

We also compare the adsorption obtained using the SCF isotherm and the values obtained from SANS[117]. The results of this comparison are given in figure 13b. On the left-hand side plot the solid lines represent the adsorption values obtained from the SCF isotherm, with and without using factor 2 in front of Gibbs – Duhem equation, while the dots are SANS values. One sees that the experimental values are in the region between two solid curves, though for small concentrations the Gibbs-Duhem equation with factor two seams to give better results. Bergeron[124] has arrived at the same conclusion by using polynomial fit of surface tension isotherm, with consecutive use of Gibbs-Duhem equation with factor of 2.

In order to estimate the pre-factor in front of the Gibbs-Duhem equation, we plot the area per molecule obtained from the experiment as a function of the area per molecule obtained from the SCF fit of surface tension data (with a factor one in the Gibbs equation). Our initial expectations were that it must be a straight line with very small intercept and with slope, which corresponds to the true pre-factor in the Gibbs-Duhem equation. The right-hand side plot in figure 6.13b gives the results of this fit. One can see that the experimental vs. predicted values really produces a straight line. However, the slope is about 1.12, but the intercept is rather high and is about 30Å^2/molecule. Thus its looks like that the pre factor is close to 1 (1.12 corresponds to 12% surface dissociation of surfactant, which agrees well with literature data[115]), but due to some reasons all values of the adsorption are shifted with a constant. At present, it is not clear why this occurs, and what is the physical explanation for such a shift. We obtain the same result with C_{14}TAB.

Thus, based on the observations so far we could say that the systems containing ionic surfactants:

- follow the scaling law of SCF with a sufficient accuracy
- the SCF slope is function of the ionic strength of the bulk solution
- the adsorption values calculated from SCF fit of isotherm with factor 1 and 2 in front of Gibbs-Duhem equation reproduces correctly the range of the experimental values
- The exact values of the adsorption compared with those from the SCF fit show a significant shift.

We believe that with the use of the theory for ionic surfactants developed in the work of Kralchevsky et. al.[115] we would be able to clarify the points, given here in a future study.

VI.4.3.5. Surface and interfacial tension of pure C_{12}TAB

Here we compare both surface and interfacial (water/silicon oil with 5cs viscosity product of KAO Co.) tensions of C_{12}TAB with the SCF theory scaling predictions. Again, we observe a good agreement between the SCF theory and the experimental data (see figure 6.14 and 6.15). The small deviation for the case of low concentrations in figure 6.14 could be due to poor experimental accuracy - one could see that the experimental point are rather scattered in this region.

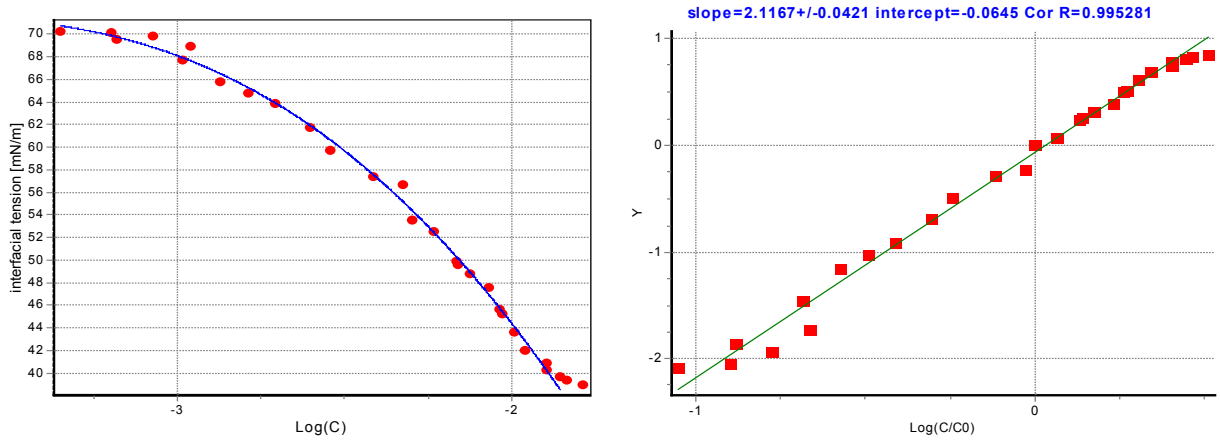

Figure 6.14. Surface tension[124] isotherm of C_{12}TAB.

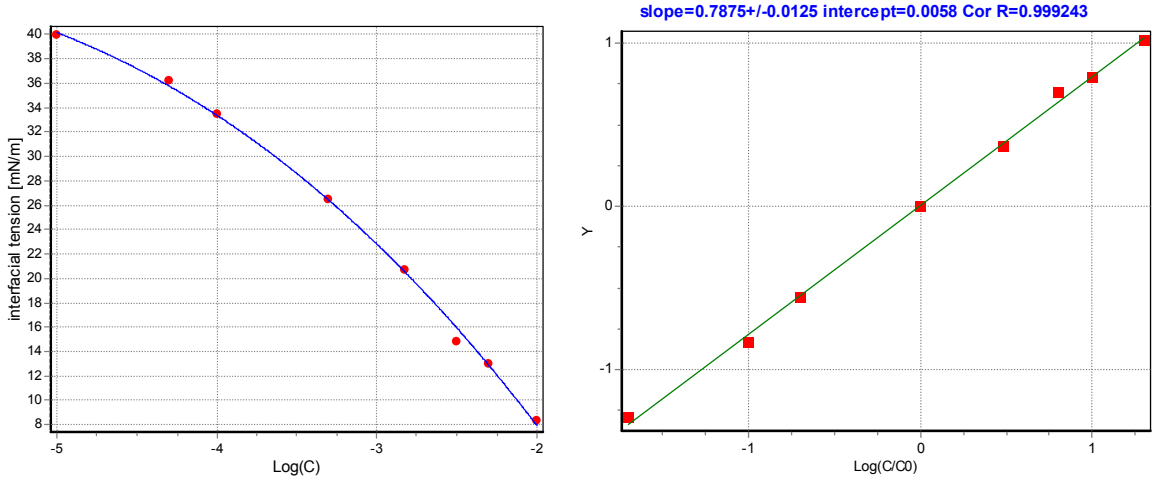

Figure 6.15. Interfacial (water-silicone oil) tension isotherm[121] of C_{12}TAB (from Sigma).

Note that the last figure (6.15) presents data for the interfacial tension isotherm for the water-silicone oil interface. It is worthwhile to mention that even for ionic surfactants the SCF-scale is working well for both surface and interfacial tension measurements. Another interesting

observation is that for pure C_{12}TAB and SDS (no additional salt in both cases) the slopes of the SCF scale are very close, which is also in agreement with the SCF predictions. Both surfactants have similar tails and different headgroups (even with opposite charges), thus if the main contribution to the surface tension comes from the hydrocarbon tails, they should have a close slopes in the SCF scale.

VI.4.3.5. Surface tension of pure C_{14}TAB

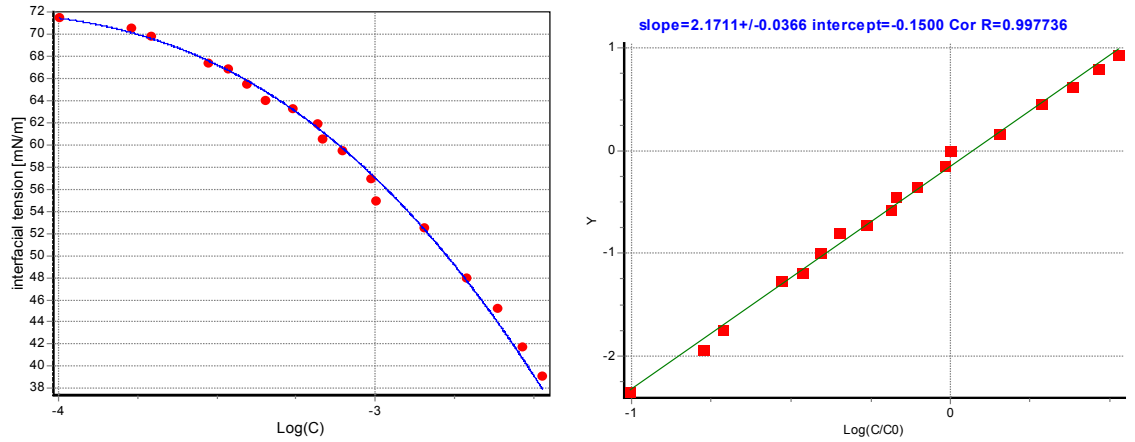

Figure 6.16a. Surface tension isotherm of C_{14}TAB[124].

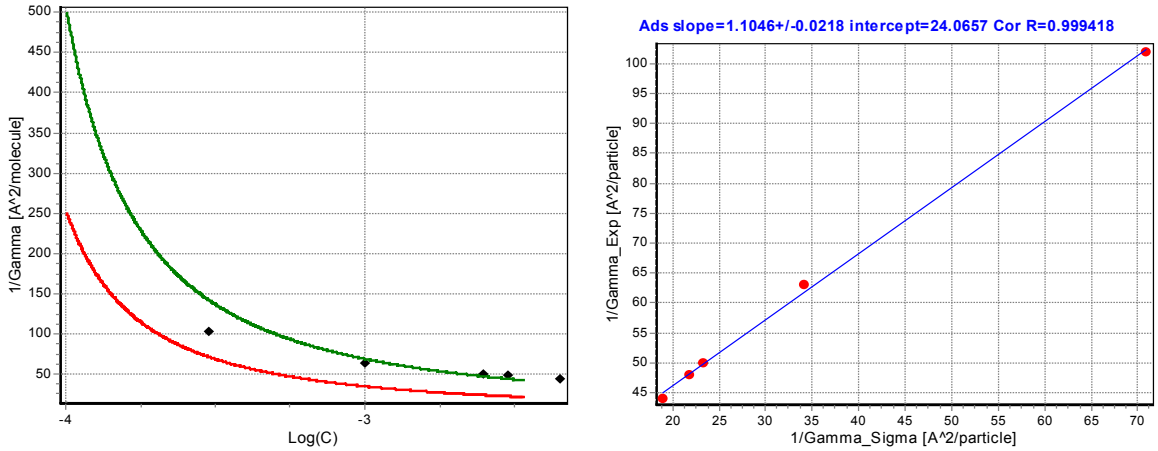

Figure 6.16b. Air/water adsorption isotherm[124] of C_{14}TAB. In the left-hand-side plot, the dots represent independent experimental data obtained from SANS, while solid lines are obtained from the best fit of surface tension (red is obtained using eq. 5.11, while green is lines corresponds to a doubled area per molecule – Gibbs – Duhem equation is multiplied by a factor of 2). In the right-hand side plot the comparison between the experimental data and the data obtained from fit of surface tension (eq 5.11, and red curve on the left plot) is presented.

It is easy to recognize that the SCF scale works well (see fig 6.16a) for this system as well. Again when we plot the experimental data for the surfactant adsorption against the values predicted using SCF-fit of the surface tension we observe that they are in a straight line, but there is a significant shift of the area per molecule (see figure 6.16b) as it was discussed for the case of C_{12}TAB.

VI.4.3.6. Surface tension of pure C_{16}TAB

We finish our considerations with surface tension of C_{16}TAB again taken from ref 124. The results are presented in figure 6.18. Again good agreement between SCF-scale predictions and experimental data is observed.

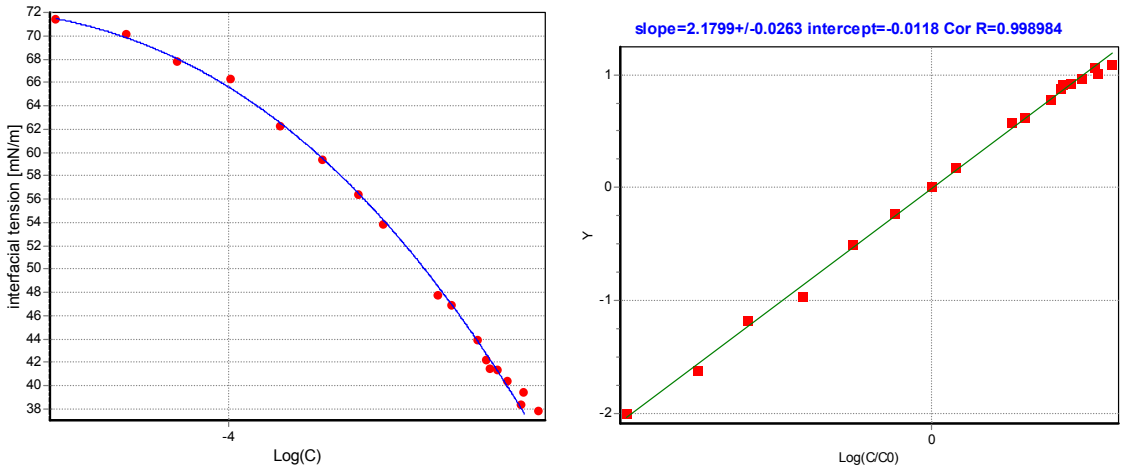

Figure 6.18. Interfacial (water/silicone oil) tension isotherm of C_{16}TAB. Data are taken again from ref 124.

Looking at the SCF slopes of all C_kTAB, one could see that they increase with and an increase of the surfactant chain length, in accordance with the expectations. When chain length increases this makes the surfactant is more surface active i.e. the effect on the surface tension is stronger, which means higher values of the SCF-slopes. Latter is also in agreement with eq. 5.13. But the increase of the surface activity is not monotonic as it could be expected and the SCF slopes of C_{14}TAB and C_{16}TAB appear to be very close.

VI.5 Conclusions

By using self-consistent field theory we have obtained a new theoretical relation between the surface tension and surfactant adsorption. Combining the last relation and Gibbs- Duhem equation we have obtained a new theoretical surface tension isotherm. The scaling law of this isotherm was checked against excessive amount of experimental data. We show that there is a very good agreement between the scaling predictions of the SCF theory and experiments for numerous types of surfactants: non-ionics, amphoterics and ionic ones, measured on air-water and oil-water interfaces. For the case of non-ionic surfactants the values of adsorption calculated from surface tension isotherm, agree pretty well with an independent experimental data for surfactant adsorption obtained by ellipsometry and small angle neutron scattering (SANS). Proving the applicability of this isotherm opens a door for very broad range of practical and theoretical applications:

- One gets very precise expressions for the estimation of the surfactant adsorption using experimental surface tension isotherm.
- New scaling law of isotherm gives more precise method for determining CMC of the surfactant system.

Providing that many surfactant systems follow the scaling behavior of SCF, means that other predictions of the theory could also be brought into play. One of them is that the density profile of chain segments is nearly parabolic. This could be very important for many indirect methods for determinations of the adsorption of the surfactant systems (like ellipsometry), where the exact profile of the surfactant chains near the interface is of critical importance for the interpretation of the experimental results.

We have also demonstrated a new method, which allows bridging the surface tension results obtained from DPD to real systems. We would like to point also that the mapping between real and DPD system could be used for estimation of the DPD interactive parameters of the surfactant system, providing that DPD length scale is known a priory from other considerations.

VII.1. General Conclusions

The main results of the present thesis are summarized in chapters III, V, VI.

In Chapter III we present a general method for calculation of surface elastic properties of the mono and di-block polymers and surfactants. We succeeded in deriving a general formula for the calculation of bending elasticity constants of polymer brushes and surfactant monolayers at liquid interface, which is the main and new result in this chapter. The formulas obtained in this chapter expresses the elastic constants in terms of the flat solution of the density profile, and does not require the solutions in other spherical or cylindrical interfaces. The formula is derived in a general form, which holds for any local density functional and is not restricted only for the case of SCF theory of polymer brushes.

The main breakthrough here is the observation that for a certain class of density functional theories (the self-consistent theory of polymer brushes also belongs to this class) the curvature expansion of the free energy could be performed in analytical form without necessity to know a specific solution of the problem for the chain segment distribution. This is rather different from previous results, known in the literature where the elastic constants are given in terms of the "flat" solution and its curvature expansion for the case of spherical or cylindrical interface. For the specific class of local density functional (DF), we have demonstrated that one could make a curvature expansion of the solution in a closed analytical form, which allows a direct calculation of the bending constants and the spontaneous curvature of surfactant (or grafted polymer) monolayers. We demonstrated that this method works well and can directly reproduce known results obtained previously by other authors. This approach is also useful for the case when it is difficult to obtain analytic solution of the problem, but a numerical one can be found.

Several different cases of brushes and solvents are considered and the elastic constants are calculated for each of these systems. Combination of those results for the case of di-block polymers and surfactants allows determination of a large variety of new practical relations, which could be useful in describing the phase behavior of oil, water and surfactant ternary mixtures and in modeling microemulsions.

In Chapter IV we describe the Dissipative Particle Dynamics (DPD) computational method and its application for the case of surfactant systems. One of the results, which is presented there and which could be considered, as an original contribution is the modeling of the phase behavior of non-ionic surfactants both in static and dynamic conditions. Plans for future work in this area are also discussed.

In Chapter V we have performed two types of Dissipative Particle Dynamics (DPD) computer simulations with long polymer brushes in good solvent grafted at an interface. In the first type of simulations homo-polymers are grafted on the solid interface and we have studied the density distribution of the chain monomers and the thickness of the polymer brush. We observed very good agreement between the DPD results and the predictions of Self Consistent Theory (SCF): all profiles simulated with DPD nearly collapse on the master curve predicted by SCF; the thickness of the polymer brush was found to obey the scaling law of SCF; its slope is also in agreement with the theoretical predictions for a DPD type of potential. In the second type of simulation we have constructed an amphiphilic di-block polymers ("surfactant"), having a long hydrophobic chain, and a hydrophilic head. These polymers adsorb at the "oil"/"water" interface (the water beads have the same properties like surfactant headgroups, while the oil beads is the same as the chain beads). Due to its very long hydrophobic chain, the surfactant is oil soluble and is highly surface active, i.e. it adsorbs predominantly at the interface between oil and water. We have simulated the interfacial tension of this system and have compared the results from SCF – assuming that the main contribution to the surface tension comes mainly from the conformational energy of the surfactant tails. We have found that the simulation results agree remarkably well with the theoretical predictions.

In Chapter VI we derive a new surface tension isotherm based on the SCF theory considerations. We show the comparison between the SCF theory and surface tension experiments for various surfactant systems. It turns out that a huge variety of surfactant systems follow the scaling behavior of this isotherm starting from very low concentrations up to the critical micelle concentration (CMC). According to our knowledge this is one of the best performing apparently universal isotherm, which works equally well for non-ionic, ionic

and amphoteric surfactants both for air/water and oil/water interfaces. This should be considered as the main practical result of the thesis. This isotherm opens a door for a very broad range of practical and theoretical applications:

- One can obtain very precise expressions for estimation of the surfactant adsorption using experimental surface tension isotherm. We show that there is an excellent agreement for the case of ethoxylated surfactants, where the predicted adsorption values are compared with independent SANS and ellipsometry data
- New scaling law of this isotherm gives more precise method for determination of the CMC of the surfactant systems
- Providing that many surfactant systems follow the scaling behavior of the SCF theory, means that other predictions of the theory could also be used. One of them is that the density profile of chain segments is nearly parabolic. This could be very important for many indirect methods for determinations of the adsorption of the surfactant systems (like ellipsometry), where the exact profile of the surfactant chains near the interface is of critical importance for the interpretation of the experimental results.

In this chapter, we have also developed a new method, which allows bridging of the surface tension results obtained from DPD to those for real systems. The interfacial tension mapping procedure between real and DPD systems could be used for an estimation of the DPD interactive parameters as well.

The results of chapter III, V, VI, are submitted as three separate publications:

- Chapter 3 – Physical Review Letters.
- Chapter 5 – Macromolecules.
- Chapter 6 – Langmuir.

VII.2. Zusammenfassung

Die Hauptergebnisse dieser Doktorarbeit sind in den Kapiteln III, V, VI beschrieben.

Im Kapitel III wurde die allgemeine Methode für die Berechnungen der oberflächen-elastischer Eigenschaften von Mono- und Diblockpolymeren sowie von Tensiden dargestellt. Das hauptsächlich neue Ergebnis in diesem Kapitel stellt die abgeleitete allgemeine Gleichung zur Berechnung der Biegungselastizitätskonstanten für Polymerbürsten und Tensidmonofilme an der flüssigen Grenzflächen im Sinne von Lösungen der SCF für flache Oberflächen dar. Der Hauptdurchbruch ist die Beobachtung, dass für eine bestimmte Klasse von Dichte-Funktional Theorien (die Self-Consistent Theorie für Polymerbürsten gehört auch zu dieser Klasse) die Krümmungsausdehnung in analytischer Form angegeben werden kann, ohne Kenntnis über die Verteilung von Kettensegmenten zu haben. Dieses Ergebnis unterscheidet sich von den aus der Literatur bekannten Resultaten, in welchen die Elastizitätskonstanten in Ausdrücken für „flache“ Lösungen und deren Krümmungsausdehnung in Termen für die sphärischen oder zylindrischen Grenzflächen gegeben sind. Für diese bestimmte Klasse von Dichte-Funktional (DF) wurde gezeigt, dass die Krümmungsausdehnung der Lösung in geschlossener analytischen Form berechnet werden kann. Dies erlaubt die direkte Berechnung der Biegungskonstanten sowie die Berechnung der spontanen Krümmung der Tensid- oder aufgepfropften Polymermonofilmen. Es wurde gezeigt dass diese Methode sehr gut funktioniert und auch bekannte Ergebnisse direkt reproduziert werden können. Diese Methode kann ebenfalls für den Fall eingesetzt werden, dass für ein Poblem keine analytische Lösung zu finden ist sondern eine numerische Lösung gefunden werden kann. Unterschiedliche Arten von Bürsten und Lösungsmitteln wurden betrachtet und die Elastizitätskonstanten für jedes dieser Systeme berechnet. Die Kombination der Ergebnisse für den Fall der Diblockpolymere und der Tenside erlaubt die Bestimmung einer Vielzahl von neuen praktischen Zusammenhängen die in der Beschreibung des Phasenverhaltens von Öl/Wasser/Tensid ternären Mischungen und im Modellierung von Mikroemulsionen von großer Bedeutung sein könnten.

Im Kapitel IV wurde die Computersimulationsmethode Dissipative Partikel Dynamik (DPD) und deren Anwendung auf Tensid-Systeme beschrieben. Eines der in Kapitel IV vorgestellten Ergebnisse ist die Modellierung des Phasenverhaltes von nichtionischen Tensiden unter statischen und dynamischen Bedingungen. Pläne für die zukünftige Arbeit in diesem Forschungsgebiet sind bereits diskutiert.

Im Kapitel V wurden zwei Arten von Dissipativen Partikel Dynamik (DPD) Computer-simulationen mit langen Polymerbürsten durchgeführt die in geeignetem Lösungsmittel gut an der Grenzfläche anhafteten. Beim ersten Simulationstyp wurden die Homopolymere auf die feste Grenzfläche aufgepfropft und die Dichtenverteilung der Kettenmonomere sowie die Dicke der Polymerbürste ausführlich untersucht. Es zeigte sich eine sehr gute Übereinstimmung zwischen den DPD Ergebnissen und den Vorhersagen von **Self-Consist** Theorie (SCF): alle mit DPD simulierten Profile zeigten keine Übereinstimmung mit der durch die SCF vorhergesagter Masterkurve; die ermittelte Dicke der Polymerbürsten lässt sich durch das Skalierungsgesetz von SCF beschreiben, die Neigung der Polymerbürsten steht auch in Übereinstimmung mit den Vorhersagen für DPD Potentialarten.
Beim zweiten Simulationstyp wurde ein amphiphiler Dieblockpolymer („Tensid“) bestehend aus einer langen hydrophoben Kette und einem hydrophilen Kopf gebildet. Dieses Polymer adsorbierte an der Öl/Wasser-Grenzfläche (die Wasser-Partikel hatten die gleichen Eigenschaften wie die Tensid-Kopf-Partikeln, während die Öl-Partikel die gleichen Eigenschaften wie die hydrophobe Partikel von Polymerketten hatten). Aufgrund der langen hydrophoben Kette war das Tensind öllöslich und hoch Grenzflächenaktiv und adsorbierte überwiegend auf der Grenzfläche zwischen Öl und Wasser. Wir haben die Grenzflächen-spannungen für diese Systeme berechnet und die Resultate mit der SCF verglichen. Dabei wurde angenommen, dass der Hauptbeitrag zur Grenzflächenspannung vorwiegend durch die Änderung der konformationellen Energie der hydrophoben Kette der Tenside erfolgt. Die Simulationsresultate zeigten eine bemerkenswerte Übereinstimmung mit den theoretischen Vorhersagen, sowie mit den Resultaten vorheriger Berechnungen (aufgepfropfte Ketten).

Im Kapitel VI wurde eine neue Oberflächenspannungsisotherme basierend auf der SCF abgeleitet und ein Vergleich zwischen der SCF Theorie und Oberflächenspannungs-experementen für verschiedene Tensidsysteme durchgeführt. Es stellte sich heraus, dass ein großes Spektrum von Tensidsystemen dem Skalierungsverhalten dieser Isotherme, angefangen von sehr niedrigen Konzentrationen bis zu kritischer Mizellbildungs-konzentration (CMC), folgt. Userem Wissen nach ist dies eine der besten Ableitungen der offenbar universellen Isotherme, welche für nichtionische, ionische und amphotere Tenside sowie für Wasser/Luft als auch für Öl/Wasser Grenzflächen verwendet werden kann.
Diese Erkenntnis stellt damit auch das praktische Hauptergebnis dieser Arbeit dar.
Diese Isotherme eröffnet ein breites Spektrum an theoretischen wie praktischen Anwendungsgebieten:

- Durch die Anwendung der experimentellen Oberflächenspannungsisotermen kann man sehr precise Ausdrücke für die Bestimmung von Tensid-Adsorptionen erhalten. Für den Fall der ethoxilierten Tensiden ergibt sich eine sehr genaue Übereinstimmung, wobei die vorhergesagten Adsorptionswerte mit unabhängigen SANS- und Ellipsomertriedaten verglichen wurden.
- Durch eine neue Skalierungsgesetzmäßigkeit der Isotherme erhält man eine viel genauere Methode für die CMC Bestimmung der Tensidlösungen.
- Wenn viele Tensidsysteme dem Skallierungsverhalten der SCF Theorie folgen, so kann man auch andere Vorhersagen der Theorie verwenden. Eine dieser Vorhersagen ist, dass die Dichteprofile der Kettensegmente beinahe parabolisch verlaufen. Das kann für viele indirekte Methoden der Adsorptionsbestimmung (wie Ellipsometrie) in den Tensidsytemen, in denen die exakte Profile der Tensidketten in der Nähe der Grenzfläche von der kritischen Bedeutung für die Interpretierung der experimentellen Ergebnisse sind, sehr wichtig sein.

In dieser Doktorarbeit haben wir auch eine neue Methode entwickelt, die es erlaubt die DPD Simulationsergebnisse für Oberflächenspannung mit denen für reale Systeme zu verbinden. Wir möchten besonderes betonen, dass die Anpassung zwischen realen und DPD Systemen für die Einschätzung der Wechselwirkungsparameter in den hydrophoben Tensidteilen angewandt werden kann. Dabei wird vorausgesetzt dass die reale Längeskalen bekannt sind.

List of References

1. Israelachvili, J.N., in "*Intermolecular and Surface Forces*", Academic Press, London, **1992**.
2. Rosen, M. J. in "*Surfactants and Interfacial Phenomena*", 2nd ed.; Wiley-Interscience Publication: New York, **1989**.
3. Adamson, A. W.; Gast, A. in "*Physical Chemistry of Surfaces*", 6th ed.; Wiley-nterscience Publication: New York, 1997.
4. Mysels, K.J.; Shinoda, K.; and Frankel, S.; in "*Soap Films, Studies of Their Thinning and a Bibliography*", Pergamon Press, N.Y., **1959**.
5. Mitchell, D.J.; Tiddy, G. J. T.; Waring, L.; Bostock, T.; McDonald, M.P.; *J. Chem. Soc., Faraday Trans.*, **1983**, *79*, 975.
6. Derjaguin, B. V.; Churaev, N. V.; Muller, V. M.; in "*Surface Forces*"; Nauka: Moscow, 1986; [in Russian].
7. Lomax, E. G., Ed. "*Amphoteric Surfactants*"; Surfactant Science Series, Vol. 59; Marcel Dekker: New York, 1996.
8. Alargova, I. Y. Vakarelsky, V. N. Paunov, S. D. Stoyanov, P. A. Kralchevsky, A. Mehreteab and G. Broze*, Langmuir***, 1998,** *14*, 1996.
9. Hunter, R. J. in "*Zeta Potential in Colloid Science*"; Academic Press: New York, 1981.
10. Exerowa, D.; Kruglyakov, P. M. in "*Foams and Foam Films*"; Elsevier: Amsterdam, 1998;
11. Joost, P. in "*Dynamic Surface Phenomena*"; VSP BV: Zeist, The Netherlands, 1999.
12. Levich, V.G., in "*Physicochemical Hydrodynamics*", Prentice-Hall, Englewood, NJ, **1962**.
13. Ivanov, I. B., Ed. *Thin Liquid Films*; Marcel Dekker: New York, 1988.
14. Edwards, D. A.; Brenner, H.; Wasan, D. T. in "*Interfacial Transport Processes and Rheology*"; Butterworth Heinemann: Oxford, 1991.
15. S. Stoyanov, N. Denkov, *Langmuir*, **2001**, *17*,1150.
16. Marinova, K.G; Denkov, N.D.; *Langmuir*, **2001**,*17,* 2426.

17. Engels, Th.; Rybinski, W. von; Schmiedel, P.; Prog. Colloid Polymer Sci., **1998**, *111*, 117.
18. Rybczynski, W., Bull. Int. Acad. Cracovie (Acad. Pol. Sci.), 40 (1911).
19. Hadamar, J. S., *C. R. Acad. Sci. Paris* **152,** 1735 (1911).
20. Grosberg, A..Y.; Khoklov, A.R., Statistical Physics of Macromolecules, AIP Press, New York, 1994.
21. de Gennes, P.-G. in "*Scaling Concepts in Polymer Physics*", Cornell University Press, Ithaca, **1979**.
22. Flory P.J. in "*Statistical Mechanics of Chain Molecules, Hansen Publishers*", New York, **1969**. Flory P.J. in "*Principles of Polymer Chains*", Cornell University Press, Ithaca, NY, **1953**.
23. Hiemenz P.C. in "*Polymer Chemistry - The Basic Concepts*", Marcel Dekker, New York, **1984**.
24. Alexander, S. J. *J. Phys. France* **1977**, *38*, 983.
25. de Gennes, P. G. *Macromolecules* **1980**, *13*, 1069.
26. Semonov, A. N. *Zh. Exp. Theoret. Phiz.* **1985**, *88*, 1242.
27. Lai, P. -Y.; Zhulina E. B. *Macromolecules* **1992**, *25*, 5201.
28. Safran, S.A. *Advances in Physics*, **1999**, *48*, 395.
29. Paunov, V.N.; Sandler, S.; Kaler, E.W.; Langmuir, **2000**, *16*, 8917.
30. Milner, S.T.; Witten, T.A.; *J.Phys., Paris*, **1988**, *49*, 1951.
31. Milner, S.T.; Wang, Z. –G.; Witten T. A. *Macromolecules*, **1989**, *22*, 498.
32. Wang, Z. –G.; Safran, S.A.; *J. Chem. Phys*, **1991**, *94*, 679.
33. Clement, F.; Joanny, J.-F.; *J. Phys. II*, **1997**, *7*, 973.
34. Biokhuis, E.M.; Lekkerkerker, H.N.W.; Szleifer, I. *J.*; *Chem. Phys.*, **2000**, *112*, 6023.
35. Fleer, G. J.; Cohen Stuart, M.A.; Scheutjens, J.M.H.M.; Cosgrove, B.; Vincent, B. in "*Polymers at interfaces*", Chapman & Hall; London, **1993**.
36. Currie, E.P.K; Fleer, G.J.; Cohen Stuart, M.A.; Borisov, O.V.; *Eur. Phys. J. E.*, **2000**, *1*, 27.
37. Skvortsov A. M.; Gorbunov A. A.; Pavlushkov I. V.; Zhulina E. B.; Priamitsyn V. A. *Polym. Sci. U.S.S.R.* **1988**, *30*, 1706.
38. Milner, S.; Witten, T.; Cates, M. *Macromolecules* **1988**, *21*, 2610.

39. Auroy, P.; Auvray, L.; *Phys. Rev Lett*. **1991**, *66*, 719.
40. Paul, W.; Binder K.; Heermann D. W.; Kremer K. *J. Phys II* **1991**, *1*, 37.
41. Milner, S. T. *Science*, **1991**, *251*, 905.
42. Winsor, P.A. *Solvent Properties of Amphiphilic Compounds*, Butterworth, London, 1954.
43. Helfrich, W., *Z. Naturfrsch*, C, **1973**, *28,* 693.
44. Petrov, A.G.; Bivas, I.; *Prog. Surf. Sci.* , **1984**, *16,* 389.
45. Petrov, A.G.; Mitov, M.D.; Derzhanski, A.; *Phys. Lett. A*, **1978**, *65,* 374.
46. Huh, C.; J. Soc. Pet. Eng. **1983**, *23*, 829.
47. Meier, D.J., *Phys.Chem.* **1967**, *71***,** 1861.
48. Hesselink, F.Th., *J. Phys.Chem.* **1969**, *73,* 3488.
49. Dolan, A.K.; Edwards, S.F.; *Proc. R. Soc. Lond.* A **1974**, *337,* 509.
50. Ben-Shaul, A.; Szleifer, I.; Gelbart, W.M., *Proc.Nat.Acad. S U.S.A.* **1984,** *81*, 4601.
51. Szleifer, I.; Ben-Shaul, A.; Gelbart, W.M.; *J. Phys. Chem.*, **1990**, *94,* 5081.
52. Szleifer, I.; Kramer, D.; Ben-Shaul, A.; *J. Chem. Phys.*, **1990**, *92,* 6800.
53. Barneveld, P.A.; Scheutjens, J.M.H.M.; Lyklema, J.; *Langmuir*, **1992**, *8*, 3122.
54. Barneveld, P.A.; Hesselink, D.E.; Leermakers, F.A.M.; Lyklema, J.; Scheutjens, J.M.H.M.; *Langmuir*, **1994**, *10*, 1084.
55. Leermakers, F.A.M.; van Noort, J.; Oversteegen, S.M.; Barneveld, P.A.; Lyklema, J.; *FaradayDiscuss.*, **1996**, *104***,** 317**.**
56. Scheutjens, J.M.H.M.; Fleer, G.J.; *J. Phys. Chem.*, **1979**, *63,* 1619.
57. Hoogerbrugge, P.; Koelman, J. *Europhys. Lett.* **1992**, *19*, 155-160.
58. Koelman, J.; Hoogerbrugge, P. *Europhys. Lett.* **1993**, *21*, 363-368.
59. Español, P.; Warren, P. *Europhys. Lett*. **1995**, *30*, 191.
60. Coveney, P.; Novik, K. *Phys. Rev. E.* **1996,** *54*, 5134.
61. Groot, R.; Madden, T., *J. Chem. Phys*.**1998**,*108*, 8713.
62. Boek, E.; Coveney, P.; Lekkerkerker, H. *J. Phys.: Condens. Matter* **1996,** *8*, 9509.
63. Jury, S.; Bladon, P.; Cates, M.; Krishna, S.; Hagen, M.; Ruddock, N.; Warren, P. *Phys. Chem. Chem. Phys.* **1999**, *1*, 2051.
64. Dzwinel, W.; Yuen, D. A. *Int. J. Mod. Phys. C* **2000**, *11*, 1.
65. Dzwinel, W.; Yuen, D. A. *J.Colloid Interface Sci.* **2000**, *225*, 179.
66. Gibson, J. B.; Chen, K. S. *J. Colloid Interface Sci.* **1998,** *206*, 464.

67. Zhang, K.; Manke, C. W. *Mol. Simul.* **2000,** *25*, 157.
68. Malfreyt, P.; Tildesley, D. J. *Langmuir* **2000,** *16*, 4732.
69. Groot, R. D.; Madden, T. J.; Tildesley D.J. *J. Chem. Phys.* **1999,** *110*, 9739.
70. Ryjkina, E. ; Kuhn, H. ; Rehage, H.; Müller, F.; Peggau, J. *Ang. Chem.Int. Ed.*, **2002**, *41*(6), 983.
71. Groot, R.; Warren, P. *J. Chem. Phys.* **1997,** *107*, 4423.
72. Marsch, C.; Yeomans, J. *Europhys. Lett.*, **1997**, *37*, 511.
73. Pagonabarraga I.; Frenkel D. *J. Chem. Phys.* **2001**, *115*, 5015.
74. Flory, P. in "*Principles of Polymer Chemistry*", Cornell University Press, Ithaca, New York; **1953**.
75. Fan, C.; Olafson, B.; Blanco, M.; Hsu, S. *Macromolecules* **1992**, *25*, 3667.
76. Blanko, M. *J. Comput. Chem.* **1991**, *12*, 237.
77. Sun, H. *J. Phys. Chem.* **1998**, *102*, 7338.
78. Groot, R.D.; Rabone, K.L.; *Biophysical Journal*, **2001**. *81*(2), 725.
79. Serrano, M.; Espanol, P.; Zuniga, I.; *Computer Physics Communications*, **1999**, *122*, 306.
80. Flekkoy, E.G.; Coveney, P.V.; Fabritiis, G. De; *Physical Review E*, **2000**. *62*(2), 2140.
81. Soubiran,L.;Staples, E.; Tucker,I.; Penfold, J.; Creeth, A.; *Langmuir*, **2001**, *17*, 7988.
82. Groot, R.D.; *Langmuir*, **2000**, *16*, 7493.
83. Jones, J.L.; Lal, M.; Ruddock, J.N.; Soenley N.A.; *Faraday Transactions*, **1999**, *112*, 129.
84. Clark, A.T.; Lal, M.; Ruddock, Warren, P.B.; *Langmuir*, **2000**, *16*, 6342.
85. Carroll, B.; Marinov, G.; Stoyanov, S.; Ivanov, I. B.; Danov, K.; Garrett, P.; *Ind. Eng. Chem. Res.* **2002** – in press.
86. Stoyanov, S.; Ivanov, I. B.; Marinov, G.; Danov, K.; Carroll, B.; *Ind. Eng. Chem. Res.* **2002** – in press.
87. Danov, K.; Stoyanov, S.; Ivanov, I. B.; Carroll, B.; Garrett, P.; *Ind. Eng. Chem. Res.* **2002** – in press.
88. Frenkel, D.; Smit B. In *Undestanding Molecular Simulation: From Algorithms to Applications*; Academic Press: New York, 1998.

89. Willemsen, S. M.; Hoefsloot, H. C.; Iedema, P. D. *Int. J. Mod. Phys.* **2000**, *11*, 881.

90. Kong, Y.; Manke, C. W.; Madden, W.G.; Schlijper, A. G. *Int. J. Thermophys*, **1994**, *15*, 1093.

91. Allen M. P. and Tildesley D. J. in "*Computer Simulation of Liquids",* Clarendon Press, **1987**.

92. Overbeek, J. T. *Colloid and Interfaces*, **1990**, *51*, 61.

93. Irving, J. H.; Kirkwood, J. G.; *J. Chem, Phys.*, **1950**, *18*, 817.

94. Ono, S.; Kondo, S.; "*Molecular theory of surface tension of liquids*" in "*Handbuch der Physik*", vol 10, Springer, Berlin; **1960**.

95. Gibbs, J. W.; "*The Scientific papers of J. Willard Gibbs*", vol. I, p219; Dover, New York; **1961**.

96. Bakker, G.; "*Kapillariat und Oberfkachenspannung*" in "*Wien-Harms Handbuch der Experimental Physik*", vol VI, Leipzig; **1962**.

97. Kirkwood, J. G.; Buff, F. P.; *J. Chem. Phys.*, **1949**, *17*, 338.

98. Buff, F. P.; *Z. Elektrochem.*, **1952**, *56*, 311.

99. Triezenberg, D. G.; Zwanzig R.; *Phys. Rev Lett.*, **1972**, *28*, 1183.

100. Evans, R.; *Advan. Phys.*, **1979**, *28*, 143.

101. Buff, F. P.; *J. Chem. Phys.*, **1951**, *19*, 1591.

102. Buff, F. P.; *J. Chem. Phys*, **1955**, 23, 419.

103. Buff, F. P.; *J. Chem. Phys.*, **1956**, 25, 146.

104. Buff, F. P.; "*Theory of capillarity*" in "*Handbuch der Physik*", vol 10, Springer, Berlin; **1960**.

105. Buff, F. P.; *Discuss. Faraday Soc.*, **1960**, 30, 52.

106. Buff, F. P.; Saltsburg , H.; *Chem. Phys.*, **1957**, 26, 23.

107. Rowlinson, J.S.; Widom, B.; in "*Molecular theory of Capillarity*"; Clarendon Press, Oxford; **1982**.

108. Henderson, D. Ed. in "*Fundamentals of Inhomogenious Fluids*", Marcel Decker, New York; **1992**.

109. T.L. Hill, in "*An Introduction to Statistical Thermodynamics*", Addison-Wesley, Reading, MA; **1962**.

110. M. Volmer, *Z. Physikal. Chem.*, **1925**, *115*, 253.

111. Frumkin; *Z. Physikal. Chem.*, **1925**, *116*, 466.

112. Landau, L.D.; Lifshitz, E.M.; in "Statistical Physics, Part 1", Pergamon Press, Oxford; **1980**.

113. Gurkov, T.D.; Kralchevsky, P.A.; Nagayama, K.; *Colloid Polym. Sci.*, **1996**, *274,* 227.

114. E.H. Lucassen-Reynders, J. Phys. Chem. 70 (1966) 1777.

115. Kralchevsky, P. A.; Danov, K. D.; Broze, G.; Mehreteab, A.; *Langmuir*, **1999,** *15,* 2351.

116. Warszynski, P.; Lunkenheimer, K.; Czichocki, G.; *Langmuir*, **2002**, *18*, 2506.

117. Lu, J.R.; Thomas, R.K.; Penfold, J.; *Adv. Colloid Interface Sci.*, **2000**, *84*, 304.

118. Dee, G. T.; Sauer, B.B.; *Adv. Phys.*, **1998**, *47*, 161.

119. Binks, B. P.; Fletcher, P. D. I.; Paunov, V. N.; Segal, D.; *Langmuir*, **2000**,*16*, 8926.

120. Zhmud, B. V.; Tiberg, F.; Kizling, J.; *Langmuir*, **2000,** 16, 2557.

121. (a) Basheva, E. S.; Ganchev, D.; Denkov, N.D.; Kasuga, K.; Satoh, N; Tsujii, K.; *Langmuir,* **2000**, *16,*1000.

(b) http://chemical.kao.co.jp/e/ProductInformation/catalog/surfactant(e)/ESurfactantNonion-5.htm

(c) Internal industrial report to KAO Co Japan, done by Laboratory of Chemical-Physics and Engineering, University Sofia, Bulgaria.

122. Lin, S.-Y.; Lin, Y.-Y.; Chen, E.-M.; Hsu, C.-T.; Kwan C.-C.; *Langmuir*, **1999,** *15*, 4370.

123. Ryjkina, E. Ph.D. *Thesis, Uni-Essen*, Germany, **2002**.

124. Bergeron, V. ; *Langmuir*, **1997**, *13*, 3474.

125. Tajima, K.; Muramatsu, M.; Sasaki, T. *Bull. Chem. Soc. Jpn.***1970**, *43*, 1991.

126. Tajima, K. *Bull. Chem. Soc. Jpn.* **1970**, *43*, 3063.

127. Tajima, K. *Bull. Chem. Soc. Jpn.* **1971**, *44*, 1767.

Curriculum Vitae

Simeon Dobrev Stoyanov

Personal Information

Date of Birth: April 20, 1970
Place of Birth: Sofia, Bulgaria
Citizenship: Bulgarian
Present home address: 11 Gustav- Hicking Str., 45127 Essen, Germany
Telephones: +49 172 2430486 (mob), +49 201 1055756 (home), +49 211 7976616 (office)

Education

1. 1988 - National High School of Mathematics and Natural Sciences, Sofia, Bulgaria, /top 1% score/.
2. 1993 - M.Sc. in Faculty of Physics, University of Sofia, Bulgaria , /top 1% score/, Theoretical Physics Department, Major: Physic of Nuclei and Elementary Particles; M.Sc. Thesis: "Direct interaction between relativistic particles. Newtonian Formalism" - /top 1% overall score/.
3. 1993-1997 Undergraduate Student in Mathematical Faculty, University of Sofia, Bulgaria.
4. 1995 - M.Sc. in Physical Chemistry – (Tempus Project Specialization on "Waste Water Treatment") in Laboratory of Thermodynamics and Physicochemical Hydrodynamics, Faculty of Chemistry, University of Sofia, Bulgaria, Thesis: "Motion of the Front between Thick and Thin Film: Hydrodynamic Theory and Experiment with Vertical Foam Films".

Awards

1. 1987 Golden Medal from the National Science and Technology Youth Organization of Bulgaria for the patent "Mechanical Monochromator of Neutrons".
2. 1987 Second Place at the National Physics Olympiad, Stara Zagora, Bulgaria.
3. 1987 Diploma of Merit at the 18th International Physics Olympiad, Jena, Germany.
4. 1987 Third Prize at the Second Balkan Physics Olympiad, Bucharest, Rumania.
5. 1988 Third Place at the National Physics Olympiad, Stara Zagora, Bulgaria.
6. 1988 Third Prize at the 19th International Physics Olympiad, Bad Ishl, Austria.
7. 1988 Gold Medal from the National High School of Mathematics and Natural Sciences, Sofia, Bulgaria.
8. 1989 Second Prize at the University Students Physics Olympiad, Sofia, Bulgaria.
9. 1990 First Prize at the National Students Physics Olympiad, Sofia, Bulgaria.
10. 1993 Best Student of the Year of the University of Sofia, Bulgaria.

Academic Experience

1. June - December 1994: Tempus Specialization in the Laboratoire de Physique Statistique, Ecole Normale Supérieure, 24 rue Lhomond, 75231 Paris Cedex 05, France.
2. January - April 1996: Visiting Scientist in the Lehrstuhl für Strömungsmechanik, Technische Fakultät, Friedrich-Alexander Universität Erlangen-Nürnberg, Cauerstraße 4, D-91058 Erlangen, Germany.
3. 1995- 2000 Research Associate in the Laboratory of Thermodynamics and Physico-Chemical Hydrodynamics (LTPH), Faculty of Chemistry, University of Sofia, Bulgaria.
4. 1996 -2000 Ph.D. Student in the Laboratory of Thermodynamics and Physico-Chemical Hydrodynamics (LTPH), Faculty of Chemistry, University of Sofia, Bulgaria.
5. 2000 - Marie Currie Industry Host Fellow – Henkel KGaA, Düsseldorf, Germany and University of Essen, Germany.

Participation in International Conferences and Symposia

1. 7th International Symposium on Ionic Implantation, June 10-15, 1992, Elenite, Bulgaria (poster).
2. 9th International Conference on Surface and Colloid Science, July 6-12, 1997, Sofia, Bulgaria (Two Posters).
3. 3th Eurofoam conference, June 4-8, 2000, Delft, Netherlands (poster).
4. IACIS 2000, Bristol UK, 2000 (poster).
5. Bunzen Tagum 2001 – coauthor of the lecture hold by H. Kuhn.
6. ECIS 2001, Coimbra Portugal – (poster)
7. Detergency and Cosmetics, 10-12 April, 2002, Barcelona, Spain, – poster.

List of Publications

Articles

1. "**Mechanical Monochromator of Neutrons**", S. Stoyanov, Certificate for a patent: number 43501 signature G 01 T5 /00, Bulgarian National Invention Institute, Sofia 1987.

2. "**Selected Optical Problems**", B.Karadjov, M.Maksimov, S.Stoyanov, *Ministry of Education Publishing* House, Sofia 1988.

3. **"Motion of the Front between Thick and Thin Film: Hydrodynamic Theory and Experiment with Vertical Foam Films"**, *Langmuir*, **13**(6), (**1997**) 1400-1407, Stoyanov, S.D., Paunov, V.N., Basheva, E., Ivanov, I.B., Broze, G., and Mehreteab, A.

4. **"Stability of Evaporating Two-Layered Liquid Film in the Presence of Surfactant. II. Linear Stability Analysis"**, *Chem.Eng.Sci.*, **53**, 2823-2837 (**1998**) - Danov, K.D., Paunov, V.N., Stoyanov, S.D., Alleborn, N., Raszcilier, H., Durst, F.

5. "**Properties of Amphoteric Surfactants Studied by z -potential Measurements**", *Langmuir***,** **14**(8), (***1998***)***,*** p. 1996-2004, *Alargova, I. Y. Vakarelsky, V. N. Paunov, S. D. Stoyanov, P. A. Kralchevsky, A. Mehreteab and G. Broze.*

6. "**Effect of the Rheology on Foam Drainage"**, *Langmuir*, **14**(16), ***(1998)****,p 4463-4465, S. Stoyanov, C. Duskin, D. Langevin, D. Weaire, G. Verbist.*

7. **" Hydrodynamic Theory and Experiments for the Motion of the Front between the Thick and Thin Regions in a Foam Films "**, Stoyanov, S.D., Paunov, V.N., Basheva, E., Ivanov, I.B., Broze, G., and Mehreteab, A. in *"3th Eurofoam conference on Foams, emulsions and application*", ed. P. Zitha, J. Banhart and G. Verbiyst, *Verlag Metall Inovation Technologie*, Bremen, Germany (**2000**), p 274- 281.

8. "**A study of oil drop removal in axisymmetric flow - comparison between experiment and theory**", *proceedings of IACIS 2000, Bristol UK* (**2000**), S. Stoyanov, G. Marinov, K. Danov , I. Ivanov, B. Carroll.

9. **"Role of Surface Diffusion for the Drainage and Hydrodynamic Stability of Thin Liquid Films",** S. Stoyanov, N. Denkov, *Langmuir*, **17**(4), (**2001**), p. 1150-1156.

10. **"Foam Boosting by Amphiphilic Molecules in the Presence of Silicone Oil",** E. Basheva, S. Stoyanov, N. Denkov, K. Kasuga, N. Satoh, K. Tsujii, *Langmuir*,**17**(4), (**2001**), p. 969-979.

11."**Experimental and Theoretical Study of Drop Detachment in Axisymmetric Flow Field. Part I. Experimental Study**." Carroll, B. ; Marinov, G.; Stoyanov, S.; Ivanov, I. B.; Danov, K.; Garrett, P. , *Ind. Eng. Chem. Res.* **2002** – accepted.

12."**Experimental and Theoretical Study of Drop Detachment in Axisymmetric Flow Field. Part II. Theoretical Model for Drop Detachment – Comparison with the Experiments**.", Stoyanov, S.; Ivanov, I. B.; Marinov, G.; Danov, K.; Carroll, B. , *Ind. Eng. Chem. Res.* **2002** – accepted.

13."**Experimental and Theoretical Study of Drop Detachment in Axisymmetric Flow Field. Part III. Hydrodynamic Modeling of Flow Pattern in Radial Symmetric Removal Apparatus.",** Danov, K.; Stoyanov, S.; Ivanov, I. B.; Carroll, B.; Garrett, P. , *Ind. Eng. Chem. Res.* **2002** – accepted.

Patents

1. "**Mechanical Monochromator of Neutrons**", S. Stoyanov, Certificate for a patent: number 43501 signature G 01 T5 /00, Bulgarian National Invention Institute, Sofia 1987.

Books

1. "**Selected Optical Problems**", B.Karadjov, M.Maksimov, S.Stoyanov, *Ministry of Education Publishing* House, Sofia 1988.

Research Interests

1. Thin Liquid Films Stability;
2. Non DLVO Surface Forces;
8. Stability and Drainage (creaming) of Foams and Emulsions;
9. Anti-foaming;
4. Dynamics of Wetting and Spreading;
5. Soil oil removal – theoretical modeling of the droplet stability and detergency;
6. Computer modeling of the physico-chemical processes using various methods: MD, MC, DPD, CA;
7. Density Functional Theories of inhomogeneous fluids and colloid systems .

Teaching Activities

1. Mathematical Methods in Chemistry and Physics – Seminars and Lectures
2. Transport Phenomenon- Seminars
3. Computer Modeling and Programming- Seminars and Lectures

Outline of previous research activities

1. Motion of the Front between Thick and Thin Film: Hydrodynamic Theory and Experiment with Vertical Foam Films.

The motion of the front between thick and thin foam film formed in a vertical frame is studied both experimentally and theoretically. The rate of motion of the front turns out to be constant for a given electrolyte concentration. Another important quantities that are measured are the thickness of the black film and the jump of the film tension, when the front reaches the bottom meniscus. The rate of the front turns out to be proportional to the jump of the film tension irrespective of the amount of added electrolyte. The theoretical model we developed allows quantitative interpretation of the experimental data. It is demonstrated that the motion of the front "thick-thin" film is accompanied with the formation of microscopic steady capillary waves in the transition zone. We show that the energy dissipation in the film is concentrated mainly into the latter part of the transition zone.

Citations:

1. Chattopadhyay A, Time-dependent changes in a shampoo bubble, J CHEM EDUC 77: (10) 1339-1342 OCT 2000;
2. Du XZ, Liang YQ, Spectroscopic study of the self-assembly behavior of a vertical soap film stabilized with cetyltrimethylammonium bromide and Thiazole Yellow, PHYS CHEM CHEM PHYS 2: (7) 1515-1518 2000
3. Chattopadhyay A, Molecules in a thin bubble membrane, LANGMUIR 15: (23) 7881-7885 NOV 9 1999
4. Prins A, van Kalsbeek HK, Foaming behaviour and dynamic surface properties of liquids, CURR OPIN COLLOID IN 3: (6) 639-642 DEC 1998
5. Du XZ, Lu YQ, Liang YQ, FTIR and UV-Vis spectroscopic studies of black soap film, J COLLOID INTERF SCI 207: (1) 106-112 NOV 1 1998
6. Kabalnov A, Thermodynamic and theoretical aspects of emulsions and their stability, CURR OPIN COLLOID IN 3: (3) 270-275 JUN 1998

2. Stability of Evaporating Two-Layered Liquid Film in the Presence of Surfactant. II. Linear Stability Analysis.

We performed a linear analysis of the stability of two-layered liquid film which is evaporating upon a horizontal solid substrate. The film contains surfactant that is soluble in both liquid phases. The governing equations for the film thickness and the surfactant concentration derived there are treated by using linear analysis in the present study. The resulting system of ordinary differential equations describes the evolution of small long-wave disturbances of the film shape and the surfactant distribution during the film evaporation. The model allows one to investigate the role of different factors on the film stability. The limiting cases of pure liquids and tangentially immobile surfaces, as well as the general case are

studied numerically. Both cases when a low- and a high-molecular weight surfactants present into the film are investigated.

3. Properties of Amphoteric Surfactants Studied by zeta-potential Measurements.

The electric properties of adsorption monolayers of an amphoteric surfactant (LDAO) where studied. We measured the zeta-potential of latex particles covered with this surfactant. The influence of pH, ionic strength and surfactant concentration on the electric properties of the adsorption monolayer has been examined. We propose a theoretical model, which describes the dependence of zeta-potential on both pH and the ionic strength. The model accounts for the adsorption of H+, Na+ and Cl- ions on the amphoteric surfactant head-groups. Very good agreement between theory and experiment is achieved. The zeta-potential measurements, coupled with the theoretical model, can be considered as a method for quantitative characterization of the ionization properties of amphoteric surfactants in adsorption layers.

Citations:

1. Huang YX, Tan RC, Li YL, et al., Effect of salts on the formation of C-8-lecithin micelles in aqueous solution, J COLLOID INTERF SCI 236: (1) 28-34 APR 1 2001.
2. Garamus V, Kameyama K, Kakehashi R, et al., Neutron scattering and electrophoresis of dodecyldimethylamine oxide micelles, COLLOID POLYM SCI 277: (9) 868-874 SEP 1999

4. Effect of the Bulk Rheology on Foam Drainage.

The velocity of drainage of foam has been measured in a type of experiment where there is a liquid front propagating without deformation. The velocity was found to be independent of the surfactant layer properties (surface tension, Gibbs elasticity) and to be inversely proportional to the square root of the bulk liquid viscosity, as predicted by the theory.

Citations:

1. Stein HN, Laven J, On the validity of the foam drainage equation, J COLLOID INTERF SCI 244 (2): 436-438 DEC 15 2001
2. Safouane M, Durand M, Saint Jalmes A, et al., Aqueous foam drainage. Role of the rheology of the foaming fluid, J PHYS IV 11 (PR6): 275-280 OCT 2001
3. Cox SJ, Bradley G, Hutzler S, et al., Vertex corrections in the theory of foam drainage, J PHYS-CONDENS MAT 13: (21) 4863-4869 MAY 28 2001
4. Schwartz LW, Roy RV, Modeling draining flow in mobile and immobile soap films, J COLLOID INTERF SCI 218: (1) 309-323 OCT 1 1999

5. A study of oil drop removal in axisymmetric flow - comparison between experiment ant theory.

The detachment of oil drops from a solid plane surface under the action of an axisymmetric extensional flow in the surrounding aqueous phase is considered both theoretically and experimentally. Theoretically, the main hypotheses are: (i) the pressure distribution around the drop is a linear function of the vertical distance from the substrate, i.e. the flow creates an effective body force as sensed by the drop; (ii) the droplet detaches at a constant contact angle boundary condition. The critical detachment condition is the value of the maximum (critical) dimensionless droplet volume (a function only of the droplet contact angle).

Experimentally, removal was studied for millimetre-sized drops deposited on glass surfaces having different degrees of hydrophobisation and also on polyester (polyethylene terephthalate) film. This produced a broad range of contact angles. The oil-water interfacial tension was also varied by the addition of sodium dodecyl sulphate. From images of the oil droplets taken at rest and at critical (detachment) flow rate, dimensionless volumes could be extracted and compared with the predictions from theory. In addition, calculations performed for the hydrodynamic flow velocity and pressure distribution around the droplet allowed an independent determination of the effective body force sensed by the droplet. A further approach utilized drop-shape image processing of the deformed droplets to estimate the experimental suction pressure. Good agreement between theoretical calculations (carried out with several independent procedures) and experimental findings was found.

6. Role of Surface Diffusion for the Drainage and Hydrodynamic Stability of Thin Liquid Films.

The dynamics of thin liquid films is analyzed taking into account the dependence of the surface diffusion coefficient of the adsorbed surfactant molecules on the density of the adsorption layer. The analysis shows that the Gibbs elasticity disappears from the final equations describing the drainage and hydrodynamic stability of thin liquid films. Thus from theoretical viewpoint, no correlation between the Gibbs elasticity and the dynamic properties of the thin foam and emulsion films is expected. This conclusion is valid also for a variety of other dynamic processes (in a quasi-stationary regime) where the concentration Marangoni effect is important, such as the motion of drops and bubbles in a liquid medium, and rheology of foams and emulsions. The theory predicts that the main factors governing these processes are: (i) the density of the adsorption layer, and (ii) the surface friction coefficient of the adsorbed molecules.

Citations:

1. Valkovska DS, Danov KD, Influence of ionic surfactants on the drainage velocity of thin liquid films, J COLLOID INTERF SCI 241 (2): 400-412 SEP 15 2001.

7. Foam Boosting by Amphiphilic Molecules in the Presence of Silicone Oil.

The effect of several surface active additives (called for brevity "foam boosters") on the foaming properties of solutions of the anionic surfactant sodium dodecyl polyoxyethylene-3 sulfate (SDP3S) is studied in the presence of silicone oil. As foam boosters we study betaine, lauryl acid diethanolamide (LADA), lauryl alcohol (LA), and a short-chain nonionic surfactant (denoted as Booster A). All these substances are used, or have a potential to be used as commercial foam boosters in different formulations. The silicone oil is pre-dispersed in the foaming solution in the form of micrometer-sized droplets, which act as foam breaking entities (antifoams). A set of several experimental methods is employed to clarify the main characteristics that are affected by the boosters. Foam tests show that LADA and Booster A enhance mainly the foaminess of the solutions, LA improves mainly the foam stability, whereas the betaine increases both. The enhanced foam stability in the presence of betaine and LA correlates well with the higher barriers to oil drop entry, measured by the Film Trapping Technique (FTT). No correlation of the film stability with the so called entry, E, spreading, S, and bridging, B**,** coefficients of the silicone oil is observed. Optical observations of foam films show that the boosting effect cannot be explained by a reduced rate of the foam film thinning. Only the addition of LA leads to deceleration of the final stage of the film thinning process. The obtained results demonstrate that the various boosters affect different characteristics of the foaming solution, and which of the additives is appropriate for a particular application depends strongly on the time-scale of interest.